MOLYBDENUM AND TUNGSTEN CARBIDE CATALYSTS

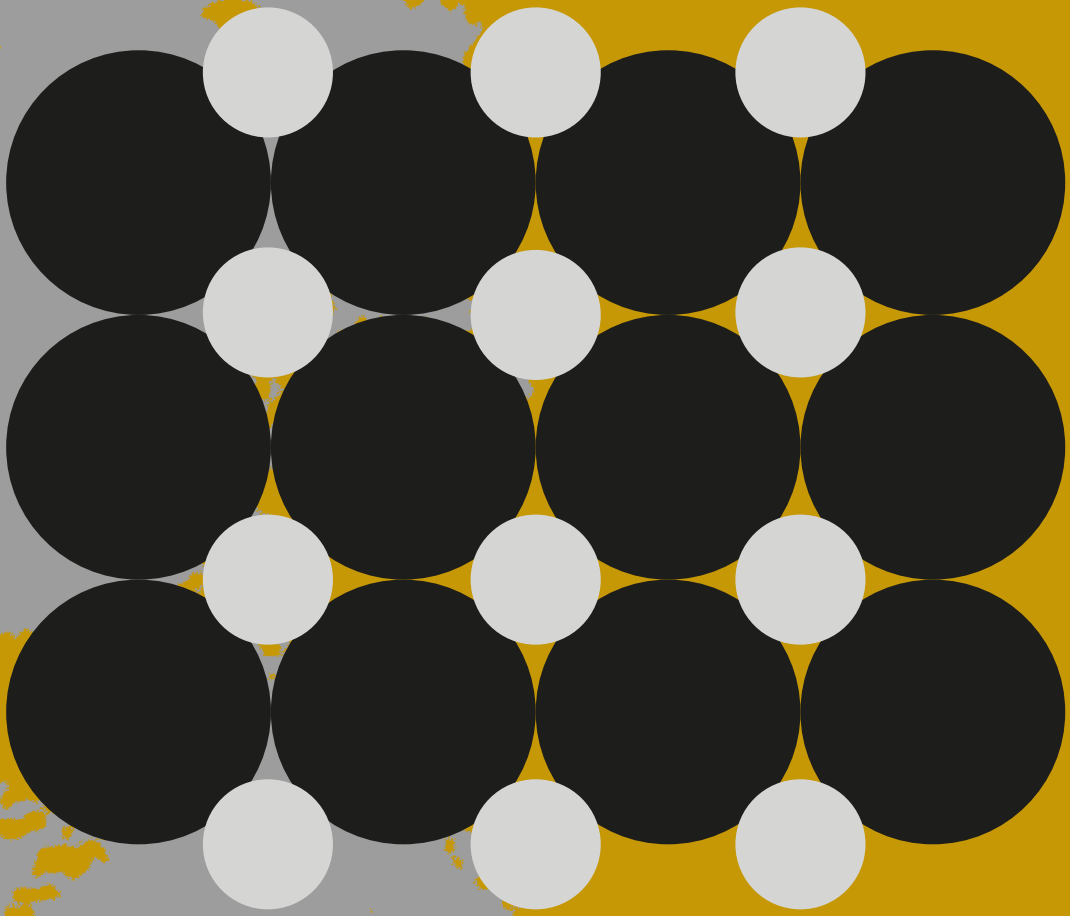

AN APPROACH TOWARDS SUSTAINABLE CONVERSIONS

MARLENE FÜHRER

Propositions

1. Developing operando characterization techniques of carbide catalysts are needed to fully understand their catalytic behaviour.
   (this thesis)

2. In the future transition metal carbides will shine too.
   (this thesis)

3. Unbiased science requires the publication of negative or non-surprising results to prevent wasted efforts.

4. Luck is a factor in the peer-reviewing process of academic papers.

5. Other countries need to take example from the Dutch biking culture.

6. Being honest and transparent about the knowledge limitations of science increases public trust.

Propositions belonging to the thesis, entitled

"Mo and W carbide catalysts – An approach towards sustainable conversions"

Führer, M.

Wageningen, 26 April 2023

Mo and W carbide catalysts – An approach towards sustainable conversions

Marlene Führer

Thesis committee

Promotor

Prof. Dr JH (Harry) Bitter

Professor of Biobased Chemistry & Technology

Wageningen University & Research

Co-promotor

Dr T (Tomas) van Haasterecht

Researcher, Biobased Chemistry & Technology Group

Wageningen University & Research

Other members

Prof. Dr AH (Aldrik) Velders, Wageningen University & Research

Prof. Dr S (Sophie) Hermans, Université catholique de Louvain, BE

Prof. Dr M (Martin) Muhler, Ruhr Universität Bochum, DE

Prof. Dr E.T.C. (Eelco) Vogt, Utrecht University, NL

This research was conducted under the auspices of the VLAG Graduate School (Biobased, Chemical, Food, and Nutrition sciences)

Mo and W carbide catalysts – An approach towards sustainable conversions

Marlene Führer

Thesis

submitted in fulfilment of the requirements for the degree of doctor at Wageningen University by the authority of the Rector Magnificus, Prof. Dr A.P.J. Mol, in the presence of the Thesis

Committee appointed by the Academic Board to be defended in public on Wednesday 26 April 2023 at 4 p.m. in the Omnia Auditorium.

Marlene Führer

Mo and W carbide catalysts – An approach towards sustainable conversions,
210 pages.

PhD thesis, Wageningen University, Wageningen, the Netherlands (2023)

With references, with summary in English

ISBN 8-94-6447-628-6

DOI https://doi.org/10.18174/589697

„Das Gleiche lässt uns in Ruhe, aber der Widerspruch ist es, der uns produktiv macht."

Johann Wolfgang von Goethe

Mo and W carbide catalysts – An approach towards sustainable conversions

1

Chapter 1

General Introduction

In order to achieve sustainability in producing future materials, chemicals and fuels, twelve principles of green chemistry are put forward (Figure 1.1).[1] One of these principles is the use of catalysis, with the main goal of reducing the amount of waste often generated when using stoichiometric reagents and of increasing the energy efficiency of the reaction. In this respect it is crucial to find effective, selective, stable catalysts, preferably based on abundant elements. Catalysts will also play an important role in the shift from a fossil-based chemical industry to a more sustainable, bio-based industry by using renewable biomass as raw material, which is another noble goal of green chemistry. This thesis focuses on the production of new catalysts based on abundant materials (principle 9) for the conversion of bio-based feedstocks (principle 7). The catalysts proposed here are based on (mixed) molybdenum/tungsten (Mo/W) carbides as alternatives for noble-metal-based catalysts (Figure 1.2).

Figure 1.1 The 12 Principles of Green Chemistry provide a framework for chemists and chemical engineers contributing to the broad scope of global sustainability.[1,3]

Figure 1.2 Transition metal carbides as alternative catalysts for biomass upgrading.

Noble metals are effective heterogeneous catalysts for biomass conversions, e.g., deoxygenations and hydrogenations.[4] Nevertheless, the limited availability of noble metals on earth has motivated the search for alternative catalysts that are less expensive and more abundant. Since the 1970s it has been clear that transition-metal carbides, such as Mo and W carbides, are catalysts for reactions that involve hydrogen activation and, as such, are promising and less costly replacements for precious noble metals (Figure 1.2).[5] Mo carbides and W carbides are studied with respect to isomerization, hydrodesulfurization and hydrodenitrogenation reactions, electrocatalysis in fuel cells and syngas conversion.[6-10] Moreover, Mo carbide and W carbide catalysts have been used in biomass conversion reactions as well. They have been shown to be excellent catalysts for (hydro-) deoxygenation and dehydration (Scheme 1.1A), removing the oxygen of biomass for the further production of chemicals and biofuels.[7,11-13] In addition, the carbides are active for hydrogenations.[14-19] The latter offers the possibility to study the hydrogenation of cinnamaldehyde, which is an interesting model reaction for studying the chemoselectivity of hydrogenation catalysts. (Scheme 1.1B).

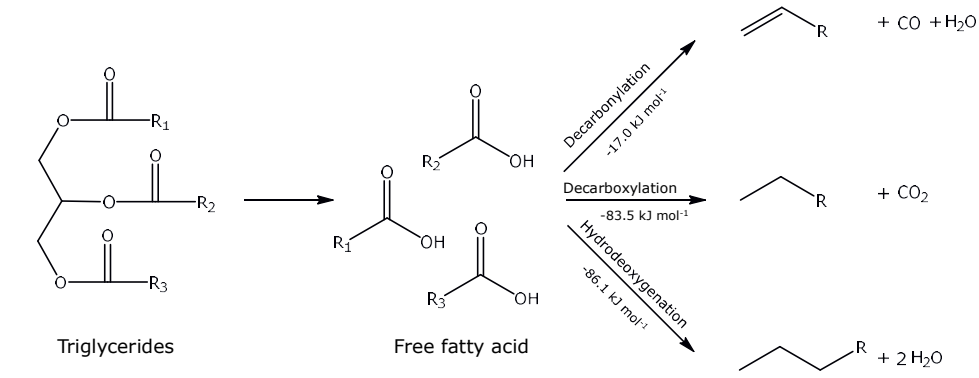

A Possible (hydro-) deoxygenation and dehydration pathways

B Cinnamaldehyde hydrogenation reaction route

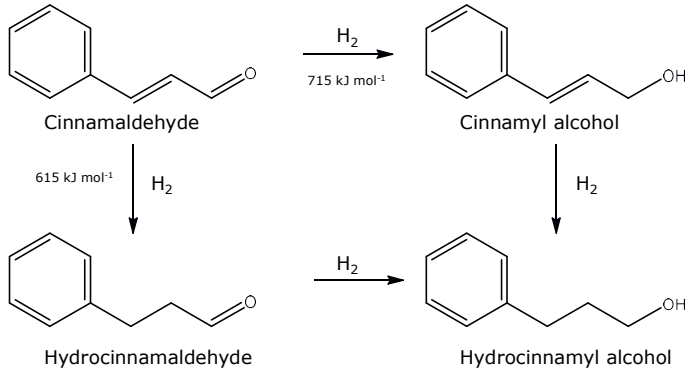

Scheme 1.1 Reactions studied in this thesis: (A) Possible (hydro-) deoxygenation and dehydration pathways with $\Delta G_{300^{\circ}C}$ [20] and (B) cinnamaldehyde hydrogenation reaction routes. [21]

Noble metals versus non-noble metals

Figure 1.3 shows the abundance and the CO_2 production during mining and processing of different metal precursors. It is evident that noble metals such as Pt and Pd are scarce. This results in higher prices and usually also higher CO_2 production footprints. From an abundance perspective, metals such as Co, Ni and Cu are the preferred choice, as these are more abundant than Mo and W. However, not all catalytic conversions can be performed with these elements.

Apart from considering an element's abundance on earth, it is also important to consider the amount of effort associated with the element's accessibility, recovery, purification and processing. Molybdenum, for instance, is on the European Union's list of critical raw materials.[22] This is not because of its limited abundance on earth but due to its (currently) limited accessibility. This accessibility can be limited by, for example, geopolitical circumstances.

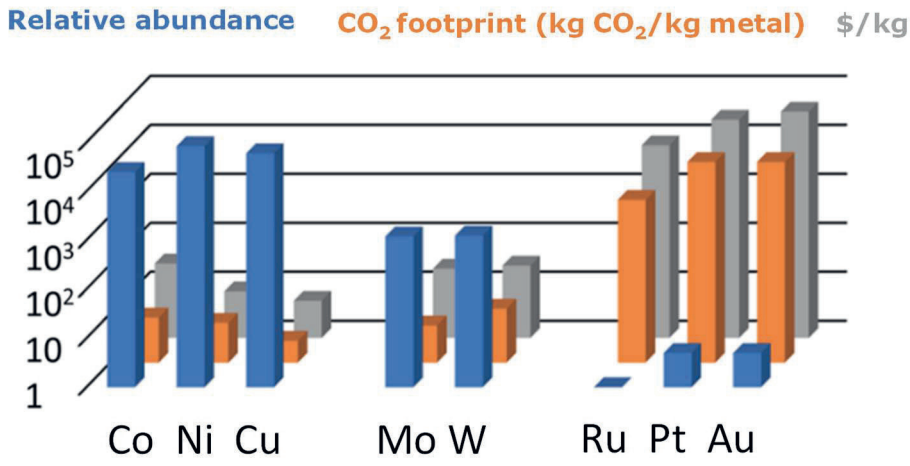

Figure 1.3 Relative abundance, CO_2 production and cost ($/kg) of mining and purification of different

Nevertheless, in terms of abundance and CO_2 footprint the transition metals molybdenum and tungsten lie between noble metals and non-noble metals, while their price is comparable to that of non-noble metals. Therefore, they should be further explored as alternatives to noble metals.

Although Mo and W metal carbides often show "Pt like behaviour," especially in terms of activity, their selectivity behaviour can differ significantly from that of noble-metal-based catalysts. Carbide catalysts are known to selectively cleave carbon-oxygen bonds without carbon-carbon scission.[23] For example, in the hydrodeoxygenation of stearic acid, Pd and Pt catalysts primarily yield heptadecane (C17) via the decarboxylation pathway (carbon-carbon scission).[24] In contrast, the conversion of stearic acid over supported Mo and W carbides occurs via the hydrodeoxygenation pathway, resulting in hydrocarbons with the same chain length as the starting material. Interestingly, when comparing the two carbide catalysts, the W carbide catalysts are selective (>50%) towards highly valued alkenes (C18) at the intermediate conversion level, while supported Mo carbides are selective towards C-18 oxygenate formation (octadecanol and octadecanal).[25] The cleavage of the C-O bond is attributed to potentially present of acidic sites on the carbide catalyst through the formation of (surface) acid sites. The advantage of these acidic sites has been described more often for carbide based materials in different types of reactions, such as dehydration and isomerization.[11,26]

In addition to their higher abundance and good performance, Mo carbides and W carbides have another advantage over noble metals: their tolerance to N and S impurities.[2] These impurities are often present when processing crude oil or renewable feedstocks.[27,28] In the presence of S and N

impurities, carbide catalysts have the ability to change the nature of their active site from carbide to sulphide or nitride, respectively. Interestingly, they can remain catalytically active, since the sulphide and nitride phases also possess activity for the same type of reactions.[13,29,30] This distinguishes them from noble-metal catalysts, which are quickly deactivated in the presence of compounds containing sulphur or nitrogen.

As can be seen, transition-metal carbides such as those of Mo and W have many advantages over noble metal catalysts, such as high abundance, good catalytic performance (selective/active), and tolerance to N and S impurities. Nevertheless, transition-metal carbides make up only a small group of catalysts. This is mainly due to the limited stability of carbides in liquid-phase reactions, the cumbersome preparation, and the lack of understanding of the relationship between the catalysts' properties and their performance. Therefore, these carbides are the topic of study in this thesis.

Carbide catalysts: preparation and characterization

In this thesis the focus is on carbon supported Mo and W carbide catalysts, which are prepared by incipient wetness impregnation of a carbon support with a solution of the desired metal salt precursors and dried afterwards. The subsequent carburization process produces the catalytically active metal carbide. In this thesis two major synthesis routes have been used to prepare supported metal carbides: temperature-programmed reduction (TPR)[31] and carbothermal reduction (CR).[32-35] In CR synthesis an oxidic precursor is loaded onto a carbon support and then heated up to a high temperature, here 900 °C. The resulting reaction between a fraction of the carbon and the oxide forms the carbide. During TPR synthesis the oxidic precursor is carburized at lower temperatures, between 300 °C and 650 °C, in the presence of an external carbon source such as CO,[36] methane,[37-39] or other hydrocarbons.[40-42] The TPR can be used for bulk as well as for supported catalysts. Information on the effect these carburization methods have on the physicochemical properties of the resulting carbide materials in relation to their catalytic behaviour is lacking.

Though impregnation and carburization is often used to prepare metal carbides, other methods are available if needed. These methods include the so-called "solution methods,"[43,44] the ultra-high vacuum (UHV) synthesis[7] and the sol-gel synthesis.[45-47] In the "solution methods," the bulk carbide is formed by the decomposition of a salt precursor and a carbon source. Common carbon sources are urea[48] or sugars.[43,49] One challenge of these methods is to find the right ratio between the metal and the carbon. An excess of carbon will lead to surface contamination with carbon.[50] The UHV synthesis occurs via ethylene carburization of clean Mo[51,52] and W[53-55] foils. This method leads to phase-pure carbide foils, as demonstrated by Chen et al.,[54] which allows fundamental

surface studies, such as XPS, AES, high-resolution electron energy loss spectroscopy (HREELS) and UHV temperature-programmed desorption, of the carbide. Other developed but less used carbide synthesis methods are the pyrolysis of a metal complex,[56,57] gas-phase reaction of volatile metal compounds[58] and solid-state metathesis.[59]

For the impregnated catalysts investigated in this thesis, the carburization (activation) of the catalysts is a crucial step that can influence the metal-to-carbon ratio,[41] the nanoparticle dispersion,[36] the nanoparticle size[60] and the crystal structure.[61] These in turn are important characteristics that affect the catalytic performance. For example, Macedo et al. showed that CR synthesis in an inert atmosphere results in hexagonal β-Mo_2C, while TPR synthesis in a carbon containing atmosphere yields cubic α-MoC_{1-x}.[38] This affects the intrinsic activity of the catalysts. TPR-synthesized cubic α-MoC_{1-x} exhibits a better catalytic activity than β-Mo_2C, which is attributed to the lower site density of the cubic structure. Thus, it is essential to understand and characterize the structure, morphology and other fundamental physiochemical properties of carbides in order to improve their catalytic performance.

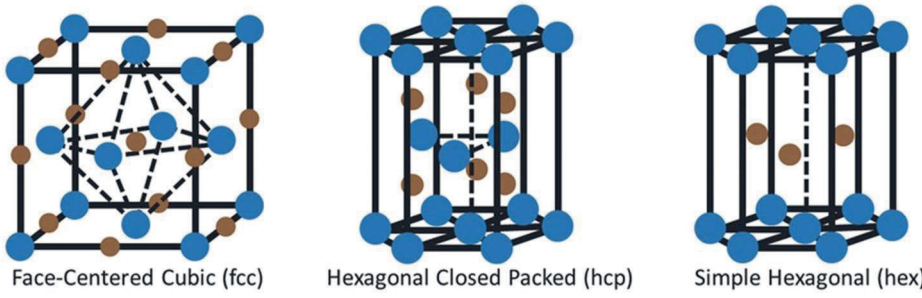

Figure 1.4 Common crystal structures of transition-metal carbides: in blue are the metal atoms and in brown the carbon atoms (adopted from Zhong et al. [62]).

Various analytical and spectroscopic techniques do exist to determine structure-performance relationships and to ultimately design an active, selective and robust catalyst.[63] X-ray diffraction (XRD) is a key technique used to obtain information on crystalline structures. This technique allows phase identification, quantification of the crystalline fraction, and monitoring structural changes in the catalysts.[64,65] The most prominent carbide phases are hexagonal β-Mo_2C, cubic α-MoC_{1-x} and hexagonal MoC for molybdenum based carbides and hexagonal α-WC, hexagonal β-W_2C and cubic y-WC_{1-x} for tungsten carbide, see Figure 1.4. For carbide characterization, XRD is the main technique to determine or confirm the crystalline phase after the carburization. During the carburization process (e.g., TPR or CR synthesis) many intermediate phases are formed, including MeO_3 (Me=metal) and the suboxide MeO_2, finally resulting in the carbide phase,

which can be different depending on the synthesis method, as discussed above. However, also metallic Mo or W and/or oxycarbides have been identified during the synthesis process, or even mixtures of different phases can co-exist.[38,66] For this reason it is crucial to study the carburization process and the resulting material. Other techniques to follow the carburization are thermogravimetric analysis (TGA), temperature-programmed desorption mass spectrometry (TPD-MS), X-ray photoelectron spectroscopy (XPS) and X-ray absorption near edge structure (XANES or NEXAFS).[41,67-76]

In addition to XRD, XANES has been utilized to correlate the chemical reactivity of the catalysts with their electronic and structural properties. Surprisingly, while some XANES measurements have been carried out on molybdenum carbide,[77-87] only five XANES studies on tungsten carbide have been reported so far.[88-92] One of those five is the study of Lee et al.,[91] who measured XANES of Mo (on K-edge and L_{III}-edge) and W (on L_{III}-edge) carbides and their parent metals to understand the differences in their electronic and structural properties. The authors observed a positive shift in edge position and an increase in the white line areas (on the L_{III}-edges) after the formation of the carbide. Although these results have yielded a wealth of information on electronic and chemical on carbides, it was stated that the theoretical basis for the interpretation of these features needs to be greatly refined before this information helps us to understand the carbide materials. Even rarer than XANES studies on carbide samples is the use of extended X-ray absorption fine structure (EXAFS) for these materials. The work of Ingham et al.[90] is one example investigating W carbides. In that study, passivated WC samples were compared with WO_2, WC and W metal standards. The passivation treatment significantly increased the oxide proportion in comparison with the original material. It was assumed that a W oxide was formed around the WC core. Although not many XANES and EXAFS studies have been done, these findings highlight that important information can be obtained that is needed to understand these carbide materials.

Bimetallic carbides

Recently, bimetallic carbide catalysts, for example, CoMo carbide,[93-95] MoNi carbide[96-99] and NiW carbide,[98,100] have also attracted attention. It has been observed that the addition of a second metal, such as nickel, cobalt or iron, can enhance the activity, improve the stability, or modify the selectivity of monometallic carbides, such as those of Mo and W.[96-103] Smirnov et al.[99] developed a nickel molybdenum carbide alloy with enhanced hydrogenation abilities for the anisole conversion compared with molybdenum carbide. The addition of Co to a Mo carbide increases the stability of the furfural hydrodeoxygenation.[94] In addition, mixtures of Mo and W carbides have recently been shown to exhibit a similar or better catalytic performance in comparison with

the respective monometallic carbides.[104-106] Tran et al. reported a synergistic effect between Mo and W carbides in the guaiacol hydrodeoxygenation to hydrocarbons. The mixed MoW carbide catalysts exhibit superior catalytic activity, which was ascribed to the presence of H_2 activating sites and oxophilic sites in the same catalyst. The H_2 activating sites arise from the interaction between Mo and W atoms, while the presence of (metallic) W introduces oxophilicity.

However, for bimetallic carbides the influence of catalyst preparation method on the final catalysts (e.g., their crystal structures and compositions) and the catalytic performance is not yet fully understood, as also Mehdad et al. stated in 2019.[70] Some studies have offered preliminary suggestions for the property-performance relationships of supported mixed carbides. For instance, Fu et al.[104] synthesized a series of mixed MoW carbide catalysts, supported on carbon nanotubes, via carbothermal reduction, which were used for hydrogen evolution reactions. Based on XRD and TEM-EDX analyses, the authors concluded that an orthorhombic MoW phase had formed in which Mo and W were atomically mixed. Leclercq et al. [64,107] attempted to determine the surface composition of bulk MoW materials with XPS analysis. It was found that a molybdenum enrichment occurred on the surface. However, the exact composition and structure of the mixed MoW carbide were not disclosed.[64,107] Ideas based on STEM-EDX,[104] XRD[105] or TGA[70] have been proposed for the optimal preparation of homogeneously mixed MoW carbides. However, the unambiguous determination of the structure of supported, mixed MoW carbide catalysts requires the use of a combination of characterization techniques.

Choice of hydrogenation reactor and the investigation of carbide stability

The choice of reactor is very important for any reaction since it influences activity, selectivity and stability of a catalyst.[108] The purpose of a hydrogenation (or hydrodeoxygenation) reactor is to bring three phases into contact: the hydrogen, the catalyst and the reactant, all in the absence of air. In order to provide contact between the reactant and the catalyst and to control the rate of diffusion, some sort of mixing is needed.[109] There exist several reactor types for the hydrogenation, such as batch, slurry reactor and packed-bed bubble reactor. In the laboratory the heterogenous hydrogenation is mostly executed in batch reactors,[108] but also plug-flow, fixed-bed reactors, in general operating under continuous flow, are often used. In the following the advantages and disadvantages to use these reactor types with carbide catalysts in hydrogenation and hydrodeoxygenation reactions of bio-based molecules are discussed briefly.

As mentioned above, batch reactors are often used on a lab-scale level for almost any feasible hydrogenation reaction. However, the batch reactor has a number of disadvantages, in particular when operating on a large scale. The use of hydrogen gas requires a dedicated high-pressure-resistant reactor, autoclave conditions and special safety precautions, which leads to operational

hazard.[110,111] Hydrogenations are usually very exothermic and performed at high temperature, which necessitates effective heat removal. In addition, batch reactors are restricted with respect to the quantities that can be produced, and the process scale-up is challenging due to the changes in heat and mass transfer.

The continuous plug-flow reactor has the advantage that, in contrast to a batch reactor, it only requires one startup and one shutdown during the production of one product. Since reactant and product are continuously introduced into and removed from the reactor, the reaction space of a continuous reactor is smaller. This makes it easier to control process variables such as temperature and hydrogen flow.[111] In summary, operating a continuous reactor is more efficient and safer. However, one challenge of using a plug-flow reactor for hydrogenation reactions of bio-based molecules is to bring the three phases (hydrogen, catalysts and reactant) into contact well enough. The fixed-bed, three-phase, trickle-flow reactor has been designed for this kind of reactions. Bio-derived molecules are mostly large molecules and are not liquid at room temperature; therefore, model compounds that have a shorter carbon chain and are liquid at room temperature are often used for the hydrogenation or hydrodeoxygenation.[112]

The main benefit of the plug-flow reactor over the batch reactor is that it offers the possibility to investigate the catalyst's stability. Due to the nature of the batch reactor, catalyst deactivation cannot be observed separately from one run of experiment. Hence, to investigate catalytic stability the catalyst needs to be recycled, and multiple subsequent experiments need to be run. After each batch the vessel needs to be emptied and cleaned, which implies that the catalyst falls dry. If the carbide catalyst is no longer protected by the solvent, it is prone to oxidation under atmospheric conditions. Moreover, reactant and products remaining in the pores are known to deteriorate via unwanted side reactions and can also deactivate the catalyst. An additional regeneration step after each run would thus be required; however, this would affect the catalytic active site and make it very challenging to reproduce the reaction. As a result, a batch reactor cannot provide sufficient information on the stability of catalysts. Hence, to study the deactivation of (carbide) catalysts, a continuous plug-flow reactor is preferred.[113,114]

Investigation and understanding of the deactivation of carbide catalysts during reaction are of great importance in order to improve the catalytic performance. Carbide catalysts are known to suffer from deactivation, especially in liquid-phase reactions.[112,115-118] The mini review by Macedo and co-workers summarizes the main deactivation mechanisms of carbide catalysts, which are leaching, coke formation, oxidation and particle growth.[119] The nature of the catalyst support can affect the catalyst deactivation by coke formation[118] and leaching.[120] In this thesis a carbon support is considered to be stable with respect to coke formation for biomass-based

conversions.[119] However, a strong interaction between the carbon support and the metal carbides is not guaranteed, which can lead to metal leaching.[120] Deactivation by oxidation is a frequently found mechanism for carbide materials used in biomass conversions.[112,120] For instance, Mortensen et al. evaluated the hydrodeoxygenation of 1-octanol over ZrO_2 supported Mo_2C catalysts, with an emphasis on stability. After 76 h of operation in a fixed-bed, three-phase, trickle-flow reactor, 1-octanol conversion had decreased from 70% to 37%. The deactivation of the catalyst was attributed to the oxidation of the carbide by water, which was produced during the reaction.

Research scope and outline

Despite the great potential of transition metal carbides, they are still not widely used in commercial applications. More knowledge needs to be gained about the nature of the active site, the evolution of the morphology, the surface structure and composition, and the stability during long-term reactions. To achieve this, the effects of the carburization on (mixed) metal carbides are investigated and their chemical and electronic properties are characterized in this thesis, using a combination of techniques (e.g., TGA, chemisorption, XANES). In addition, the catalysts are tested for decarboxylation/decarboxylation and hydrodeoxygenation of stearic acid to produce aldehydes, alcohols, alkenes and alkanes.[121,122] Furthermore, a fixed-bed, three-phase flow reactor is built for investigating the stability of Mo carbide during long-term hydrogenation reactions of cinnamaldehyde as an α,β-unsaturated compound.

The thesis is divided into three parts. The first part consists of Chapters 2–3 and focuses on the synthesis, structural properties and performance of bimetallic metal carbides. The second part (Chapters 4-5) describes the hydrogenation of cinnamaldehyde over Mo carbide catalysts and their stability in batch and plug-flow reactors. The last part, Chapter 6, deals with the overlooked properties of transition metal carbides. In the following the chapters are discussed in more detail:

In **Chapter 2**, the synthesis and characterization of carbon nanofiber supported mixed MoW carbides is described. The challenge here is to synthesise a single phase mixed metal carbide and to define the exact composition and structure of these materials. We chose to prepare mixed MoW carbides via co-impregnation by dissolving the Mo and W salts in water and carburising them via the TPR and CR synthesis route. We used a combination of characterization techniques (TPD-MS, TPR-MS, TGA, XRD, XANES, EXAFS and STEM-EDX) to evaluate the physicochemical characterizes of these materials. The catalysts were tested for their performance in the hydrodeoxygenation of fatty acid (batch reactor, 350 °C, 30 bar of H_2).

Monometallic Mo and W carbide catalysts are active for the conversion of stearic (and oleic acid) into alkenes, oxygenates and alkanes following the hydrodeoxygenation pathway. Interestingly, when comparing carbon supported Mo-carbides to W-carbides catalysts, the former ones were more selective towards oxygenates, while the W-carbides were more selective towards alkenes. In **Chapter 3**, we establish to which extent we can combine the properties of both W-carbide and Mo-carbide by using carbon nanofiber supported mixed MoW-carbides. We examined how the catalytic performance of mixed MoW carbides depends on the Mo:W ratio. The supported bimetallic carbide catalysts were prepared by the CR method and the hydrodeoxygenation of stearic acid was performed in a batch reactor (350 °C, 30 bar of H_2).

Though the Mo and W carbides have been shown to be catalytic active for hydrogenation, their potential for chemoselective hydrogenations has not been studied. These selective hydrogenations are often exemplified by cinnamaldehyde towards either unsaturated alcohols or saturated aldehydes. In **Chapter 4** we show the potential of Mo and W carbide nanoparticles supported on carbon nanofibers to replace Pt for the HYN of cinnamaldehyde (batch, 200 °C, 20 bar of H_2).

Catalytic hydrogenation of cinnmalaldeyhde has often been conducted in batch reactors. However, to investigate the stability a plug flow reactors is more beneficial, as explained above. In **Chapter 5** the stability of Mo carbide catalysts is investigated in a plug flow reactor (90-170 °C, 20 bar of H_2). For this two Mo carbide catalysts with different particle size are prepared (4-5 nm and 5-6 nm) and tested.

In **Chapter 6** we discuss the potential of Mo and W carbides as an alternative for noble metal catalysts for use in the conversion of traditional fossil feedstocks, heavier fossil feedstocks and renewable biomass feedstocks. We point out the tolerance of transition metal carbides with respect to N and S impurities and the ability to (partially) convert the carbides to their respective nitrides or sulphides**.** The availability and catalytic activity of these carbide catalysts have both been mentioned before, but their relative stability in the presence of such impurities barely has.

Chapter 7 aims to place the obtained results in a broader context, and provides recommendations for further research.

Figure 1.5 presents a schematic overview of this thesis with the main subjects studied in each chapter.

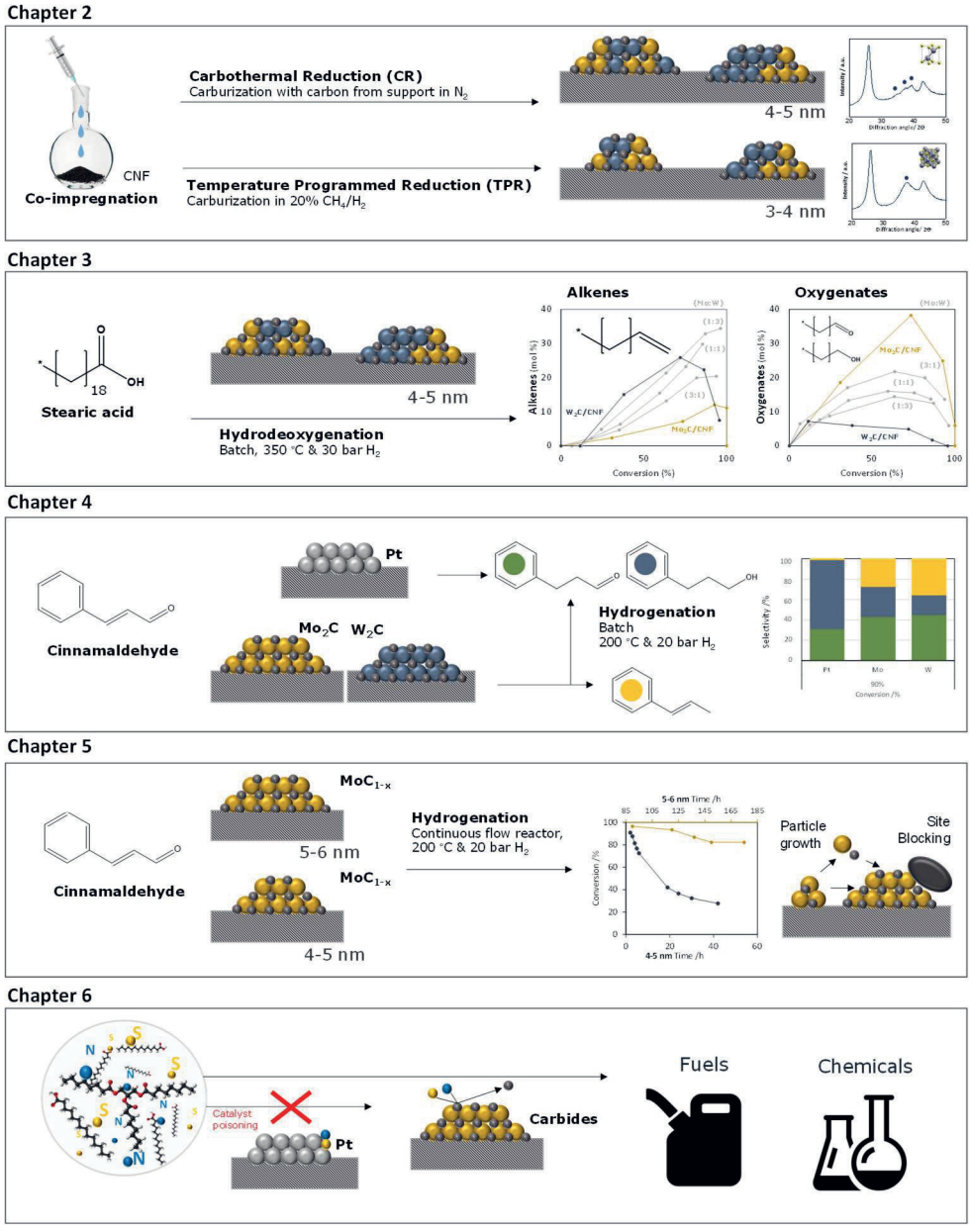

Figure 1.5 Schematic overview of this thesis.

References

(1) Anastas, P. T.; Warner, J. C. *Green Chemistry: Theory and Practice*; Oxford University Press, 1998.

(2) Führer, M.; van Haasterecht, T.; Bitter, J. Molybdenum and tungsten carbides can shine too. *Catalysis Science & Technology* **2020**.

(3) Ganesh, K. N.; Zhang, D.; Miller, S. J.; Rossen, K.; Chirik, P. J.; Kozlowski, M. C.; Zimmerman, J. B.; Brooks, B. W.; Savage, P. E.; Allen, D. T.; ACS Publications, 2021; Vol. 55.

(4) Gosselink, R. W.; Hollak, S. A.; Chang, S. W.; van Haveren, J.; de Jong, K. P.; Bitter, J. H.; van Es, D. S. Reaction pathways for the deoxygenation of vegetable oils and related model compounds. *ChemSusChem* **2013,** *6* (9), 1576.

(5) Levy, R. B.; Boudart, M. Platinum-Like Behavior of Tungsten Carbide in Surface Catalysis. *Science* **1973,** *181* (4099), 547.

(6) Furimsky, E. Metal carbides and nitrides as potential catalysts for hydroprocessing. *Applied Catalysis A: General* **2003,** *240* (1–2), 1.

(7) Sullivan, M. M.; Chen, C. J.; Bhan, A. Catalytic deoxygenation on transition metal carbide catalysts. *Catalysis Science and Technology* **2016,** *6* (3), 602.

(8) Iglesia, E.; Baumgartner, J. E.; Ribeiro, F. H.; Boudart, M. Bifunctional Reactions of Alkanes on Tungsten Carbides Modified by Chemisorbed Oxygen. *Journal of Catalysis* **1991,** *131* (2), 523.

(9) Szymanska-Kolasa, A.; Lewandowski, M.; Sayag, C.; Brodzki, D.; Djega-Mariadassou, G. Comparison between tungsten carbide and molybdenum carbide for the hydrodenitrogenation of carbazole. *Catal Today* **2007,** *119* (1-4), 35.

(10) Wang, H.; Liu, S.; Smith, K. J. Understanding selectivity changes during hydrodesulfurization of dibenzothiophene on Mo2C/carbon catalysts. *Journal of Catalysis* **2019,** *369*, 427.

(11) Chan-Thaw, C. E.; Villa, A. Metal carbides for biomass valorization. *Applied Sciences (Switzerland)* **2018,** *8* (2).

(12) Robinson, A. M.; Hensley, J. E.; Medlin, J. W. Bifunctional Catalysts for Upgrading of Biomass-Derived Oxygenates: A Review. *Acs Catalysis* **2016,** *6* (8), 5026.

(13) Smith, K. J. Metal carbides, phosphides, and nitrides for biomass conversion. *Current Opinion in Green and Sustainable Chemistry* **2020,** *22*, 47.

(14) Mamède, A.; Giraudon, J.-M.; Löfberg, A.; Leclercq, L.; Leclercq, G. Hydrogenation of toluene over ß-Mo2C in the presence of thiophene. *Applied Catalysis A: General* **2002,** *227* (1-2), 73.

(15) Da Costa, P.; Lemberton, J.-L.; Potvin, C.; Manoli, J.-M.; Perot, G.; Breysse, M.; Djega-Mariadassou, G. Tetralin hydrogenation catalyzed by Mo2C/Al2O3 and WC/Al2O3 in the presence of H2S. *Catal Today* **2001,** *65* (2–4), 195.

(16) Dhandapani, B.; Clair, T. S.; Oyama, S. Simultaneous hydrodesulfurization, hydrodeoxygenation, and hydrogenation with molybdenum carbide. *Applied Catalysis A: General* **1998,** *168* (2), 219.

(17) Deng, Y. C.; Gao, R.; Lin, L. L.; Liu, T.; Wen, X. D.; Wang, S.; Ma, D. Solvent Tunes the Selectivity of Hydrogenation Reaction over alpha-MoC Catalyst. *J Am Chem Soc* **2018,** *140* (43), 14481.

(18) Kim, H. G.; Lee, K. H.; Lee, J. S. Carbon monoxide hydrogenation over molybdenum carbide catalysts. *Research on Chemical Intermediates* **2000,** *26* (5), 427.

(19) Akopyan, A. V.; Polikarpova, P. D.; Forofontova, O. I.; Levin, I. S.; Mnatsakanyan, R. A.; Davtyan, D. A.; Zurnachyan, A. R.; Anisimov, A. V.; Karakhanov, E. A. Hydrogenation of Alkenes on Molybdenum and Tungsten Carbides. *Theor. Found. Chem. Eng.* **2020,** *54* (5), 1045.

(20) Gosselink, R. W.; Hollak, S. A. W.; Chang, S. W.; Van Haveren, J.; De Jong, K. P.; Bitter, J. H.; Van Es, D. S. Reaction pathways for the deoxygenation of vegetable oils and related model compounds. *ChemSusChem* **2013,** *6* (9), 1576.

(21) Wu, T.; Han, M. Vapor-phase hydrothermal construction of defective MoS 2 for highly selective electrocatalytic hydrogenation of cinnamaldehyde. *Materials Advances* **2022**.

(22) EU Commission - Deloitte Sustainability, B. G. S., Bureau de Recherches Géologiques et Minières, Netherlands Organisation for Applied Scientific Research. Study on the review of the list of Critical Raw Materials. **2017**.

(23) Lin, Z.; Chen, R.; Qu, Z.; Chen, J. G. Hydrodeoxygenation of biomass-derived oxygenates over metal carbides: from model surfaces to powder catalysts. *Green chemistry* **2018,** *20* (12), 2679.

(24) Snåre, M.; Kubic˘kova, I.; Mäki-Arvela, P.; Eränen, K.; Murzin, D. Y. Heterogeneous catalytic deoxygenation of stearic acid for production of biodiesel. *Ind Eng Chem Res* **2006,** *45* (16), 5708.

(25) Stellwagen, D. R.; Bitter, J. H. Structure–performance relations of molybdenum-and tungsten carbide catalysts for deoxygenation. *Green Chemistry* **2015,** *17* (1), 582.

(26) Serrano-Ruiz, J. C.; West, R. M.; Dumesic, J. A. Catalytic conversion of renewable biomass resources to fuels and chemicals. *Annual review of chemical and biomolecular engineering* **2010,** *1*, 79.

(27) He, B.; Van Gerpen, J.; Thompson, J. Sulfur content in selected oils and fats and their corresponding methyl esters. *Applied engineering in agriculture* **2009,** *25* (2), 223.

(28) Bandosz, T. J.; Buczek, B.; Grzybek, T.; Jagiello, J. The determination of surface changes in active carbons by potentiometric titration and water vapour adsorption. *Fuel* **1997,** *76* (14-15), 1409.

(29) Hargreaves, J. Heterogeneous catalysis with metal nitrides. *Coordination Chemistry Reviews* **2013,** *257* (13-14), 2015.

(30) Grilc, M.; Veryasov, G.; Likozar, B.; Jesih, A.; Levec, J. Hydrodeoxygenation of solvolysed lignocellulosic biomass by unsupported MoS2, MoO2, Mo2C and WS2 catalysts. *Applied Catalysis B: Environmental* **2015,** *163*, 467.

(31) Oyama, S. Preparation and catalytic properties of transition metal carbides and nitrides. *Catal Today* **1992,** *15* (2), 179.

(32) Li, X.; Ma, D.; Chen, L.; Bao, X. Fabrication of molybdenum carbide catalysts over multi-walled carbon nanotubes by carbothermal hydrogen reduction. *Catalysis Letters* **2007,** *116* (1-2), 63.

(33) Wu, K.; Yang, C.; Zhu, Y.; Wang, J.; Wang, X.; Liu, C.; Liu, Y.; Lu, H.; Liang, B.; Li, Y. Synthesis-controlled α-and ß-molybdenum carbide for base-promoted transfer hydrogenation of lignin to aromatic monomers in ethanol. *Ind Eng Chem Res* **2019,** *58* (44), 20270.

(34) Alaba, P. A.; Abbas, A.; Huang, J.; Daud, W. M. A. W. Molybdenum carbide nanoparticle: Understanding the surface properties and reaction mechanism for energy production towards a sustainable future. *Renewable and Sustainable Energy Reviews* **2018,** *91*, 287.

(35) Frank, B.; Friedel Ortega, K.; Girgsdies, F.; Huang, X.; Schlögl, R.; Trunschke, A. CNT supported MoxC catalysts: Impact of loading and carburization parameters. *ChemCatChem* **2013,** *5* (8), 2296.

(36) Lemaître, J.; Vidick, B.; Delmon, B. Control of the catalytic activity of tungsten carbides: I. Preparation of highly dispersed tungsten carbides. *Journal of Catalysis* **1986,** *99* (2), 415.

(37) Oshikawa, K.; Nagai, M.; Omi, S. Characterization of molybdenum carbides for methane reforming by TPR, XRD, and XPS. *J Phys Chem B* **2001,** *105* (38), 9124.

(38) Macedo, L. S.; Oliveira, R. R.; van Haasterecht, T.; Teixeira da Silva, V.; Bitter, H. Influence of synthesis method on molybdenum carbide crystal structure and catalytic performance in stearic acid hydrodeoxygenation. *Applied Catalysis B: Environmental* **2019,** *241*, 81.

(39) Löfberg, A.; Seyfried, L.; Blehen, P.; Decker, S.; Bastin, J. M.; Frennet, A. Pore structure of bulk tungsten carbide powder catalysts. *Catalysis letters* **1995,** *33* (1), 165.

(40) Nguyen, T. H.; Adesina, A. A.; Yue, E. M. T.; Lee, Y. J.; Khodakov, A.; Brungs, M. P. Synthesis of Mo-W carbide via propane carburization of the precursor sulfide: Kinetic analysis. *J Chem Technol Biot* **2004,** *79* (3), 286.

(41) Decker, S.; Lofberg, A.; Bastin, J. M.; Frennet, A. Study of the preparation of bulk tungsten carbide catalysts with C2H6/H-2 and C2H4/H-2 carburizing mixtures. *Catalysis Letters* **1997,** *44* (3-4), 229.

(42) Wu, Y.; Dang, J.; Lv, Z.; Zhang, S.; Lv, X.; Bai, C. In *Minerals, Metals and Materials Series*, 2018; Vol. Part F12.

(43) Patel, M.; Subrahmanyam, J. Synthesis of nanocrystalline molybdenum carbide (Mo2C) by solution route. *Materials Research Bulletin* **2008,** *43* (8-9), 2036.

(44) Preiss, H.; Meyer, B.; Olschewski, C. Preparation of molybdenum and tungsten carbides from solution derived precursors. *Journal of materials science* **1998,** *33* (3), 713.

(45) Hudson, M. J.; Peckett, J. W.; Harris, P. J. Low-temperature sol− gel preparation of ordered nanoparticles of tungsten carbide/oxide. *Ind Eng Chem Res* **2005,** *44* (15), 5575.

(46) Rasaki, S. A.; Zhang, B.; Anbalgam, K.; Thomas, T.; Yang, M. Synthesis and application of nano-structured metal nitrides and carbides: A review. *Progress in Solid State Chemistry* **2018,** *50*, 1.

(47) Giordano, C.; Antonietti, M. Synthesis of crystalline metal nitride and metal carbide nanostructures by sol–gel chemistry. *Nano Today* **2011,** *6* (4), 366.

(48) Giordano, C.; Erpen, C.; Yao, W.; Antonietti, M. Synthesis of Mo and W carbide and nitride nanoparticles via a simple "urea glass" route. *Nano letters* **2008,** *8* (12), 4659.

(49) Vitale, G.; Guzmán, H.; Frauwallner, M. L.; Scott, C. E.; Pereira-Almao, P. Synthesis of nanocrystalline molybdenum carbide materials and their characterization. *Catal Today* **2015,** *250*, 123.

(50) Mehdad, A. Mixed metal carbides: understanding the synthesis, surface properties and catalytic activities. **2015**.

(51) Frühberger, B.; Chen, J. Reaction of ethylene with clean and carbide-modified Mo (110): Converting surface reactivities of molybdenum to Pt-group metals. *J Am Chem Soc* **1996,** *118* (46), 11599.

(52) Kelly, T. G.; Chen, J. G. Controlling C–O, C–C and C–H bond scission for deoxygenation, reforming, and dehydrogenation of ethanol using metal-modified molybdenum carbide surfaces. *Green Chemistry* **2014,** *16* (2), 777.

(53) Humbert, M. P.; Menning, C. A.; Chen, J. G. Replacing bulk Pt in Pt–Ni–Pt bimetallic structures with tungsten monocarbide (WC): Hydrogen adsorption and cyclohexene hydrogenation on Pt–Ni–WC. *Journal of Catalysis* **2010,** *271* (1), 132.

(54) Ren, H.; Chen, Y.; Huang, Y. L.; Deng, W. H.; Vlachos, D. G.; Chen, J. G. G. Tungsten carbides as selective deoxygenation catalysts: experimental and computational studies of converting C3 oxygenates to propene. *Green Chemistry* **2014,** *16* (2), 761.

(55) Liu, N.; Rykov, S.; Chen, J. A comparative surface science study of carbide and oxycarbide: the effect of oxygen modification on the surface reactivity of C/W (1 1 1). *Surf Sci* **2001,** *487* (1-3), 107.

(56) Giraudon, J.-M.; Leclercq, L.; Leclercq, G.; Lofberg, A.; Frennet, A. Organometallic route to dimolybdenum carbide via a low-temperature pyrolysis of a dimolybdenum alkyne complex. *Journal of materials science* **1993,** *28* (9), 2449.

(57) Li, X. L.; Li, Y. D. Synthesis of Scroll-Type Composite Microtubes of Mo2C/MoCO by Controlled Pyrolysis of Mo (CO) 6. *Chemistry–A European Journal* **2004,** *10* (2), 433.

(58) Ledoux, M. J.; Huu, C. P.; Guille, J.; Dunlop, H. Compared activities of platinum and high specific surface area Mo<inf>2</inf>C and WC catalysts for reforming reactions. I. Catalyst activation and stabilization: Reaction of n-hexane. *Journal of Catalysis* **1992,** *134* (2), 383.

(59) Nartowski, A.; Parkin, I.; Craven, A. Solid state metathesis routes to transition metal carbides. *J Mater Chem* **1999,** *9* (6), 1275.

(60) Ochoa, E.; Torres, D.; Pinilla, J. L.; Suelves, I. Influence of carburization time on the activity of Mo2C/CNF catalysts for the HDO of guaiacol. *Catal Today* **2019**.

(61) Chen, X. Z.; Chen, X.; Qi, J.; Liang, C. H. Self-assembly synthesis of lamellar molybdenum carbides with controllable phases for hydrodeoxygenation of diphenyl ether. *MOLECULAR CATALYSIS* **2020,** *492*.
(62) Zhong, Y.; Xia, X.; Shi, F.; Zhan, J.; Tu, J.; Fan, H. J. Transition metal carbides and nitrides in energy storage and conversion. *Advanced science* **2016,** *3* (5), 1500286.
(63) Hanefeld, U.; Lefferts, L. *Catalysis: An integrated textbook for students*; John Wiley & Sons, 2018.
(64) Leclercq, L.; Provost, M.; Pastor, H.; Grimblot, J.; Hardy, A. M.; Gengembre, L.; Leclercq, G. Catalytic properties of transition metal carbides: I. Preparation and physical characterization of bulk mixed carbides of molybdenum and tungsten. *Journal of Catalysis* **1989,** *117* (2), 371.
(65) Pielaszek, J.; Mierzwa, B.; Medjahdi, G.; Marêché, J. F.; Puricelli, S.; Celzard, A.; Furdin, G. Molybdenum carbide catalyst formation from precursors deposited on active carbons: XRD studies. *Applied Catalysis A: General* **2005,** *296* (2), 232.
(66) Bouchy, C.; Derouane-Abd Hamid, S. B.; Derouane, E. G. A new route to the metastable FCC molybdenum carbide α-MoC(1-x). *Chem Commun* **2000**, DOI:10.1039/a907534h 10.1039/a907534h(2), 125.
(67) Bastos, L. C. A.; Monteiro, W. R.; Zacharia, M. A.; da Cruz, G. M.; Rodrigues, J. A. J. Preparation and characterization of Mo/W bimetallic carbides by using different synthesis methods. *Catalysis Letters* **2008,** *120* (1-2), 48.
(68) Sebakhy, K. O.; Vitale, G.; Hassan, A.; Pereira-Almao, P. New Insights into the Kinetics of Structural Transformation and Hydrogenation Activity of Nano-crystalline Molybdenum Carbide. *Catalysis Letters* **2018,** *148* (3), 904.
(69) Carrales-Alvarado, D.; Dongil, A.; Fernández-Morales, J.; Fernández-García, M.; Guerrero-Ruiz, A.; Rodríguez-Ramos, I. Selective hydrogen production from formic acid decomposition over Mo carbides supported on carbon materials. *Catalysis Science & Technology* **2020,** *10* (20), 6790.
(70) Mehdad, A.; Jentoft, R. E.; Jentoft, F. C. Single-phase mixed molybdenum-tungsten carbides: Synthesis, characterization and catalytic activity for toluene conversion. *Catal Today* **2019,** *323*, 112.
(71) Cotter, T.; Frank, B.; Zhang, W.; Schlögl, R.; Trunschke, A. The Impact of V Doping on the Carbothermal Synthesis of Mesoporous Mo Carbides. *Chemistry of Materials* **2013,** *25* (15), 3124.
(72) Hanif, A.; Xiao, T. C.; York, A. P. E.; Sloan, J.; Green, M. L. H. Study on the structure and formation mechanism of molybdenum carbides. *Chemistry of Materials* **2002,** *14* (3), 1009.
(73) Liang, C.; Ying, P.; Li, C. Nanostructured ß-Mo2C prepared by carbothermal hydrogen reduction on ultrahigh surface area carbon material. *Chemistry of materials* **2002,** *14* (7), 3148.
(74) Choi, J.-S.; Bugli, G.; Djéga-Mariadassou, G. Influence of the Degree of Carburization on the Density of Sites and Hydrogenating Activity of Molybdenum Carbides. *Journal of Catalysis* **2000,** *193* (2), 238.
(75) Bkour, Q.; Cuba-Torres, C. M.; Marin-Flores, O. G.; Tripathi, S.; Ravishankar, N.; Norton, M. G.; Ha, S. Mechanistic study of the reduction of MoO2 Mo2C under methane pulse conditions. *Journal of Materials Science* **2018,** *53* (18), 12816.
(76) Xiao, T.; Hanif, A.; York, A. P.; Sloan, J.; Green, M. L. Study on preparation of high surface area tungsten carbides and phase transition during the carburisation. *Physical Chemistry Chemical Physics* **2002,** *4* (14), 3522.
(77) Shou, H.; Ferrari, D.; Barton, D. G.; Jones, C. W.; Davis, R. J. Influence of passivation on the reactivity of unpromoted and Rb-promoted Mo2C nanoparticles for CO hydrogenation. *ACS Catalysis* **2012,** *2* (7), 1408.
(78) Youn, D. H.; Han, S.; Kim, J. Y.; Kim, J. Y.; Park, H.; Choi, S. H.; Lee, J. S. Highly Active and Stable Hydrogen Evolution Electrocatalysts Based on Molybdenum Compounds on Carbon Nanotube–Graphene Hybrid Support. *ACS Nano* **2014,** *8* (5), 5164.
(79) Porosoff, M. D.; Yang, X.; Boscoboinik, J. A.; Chen, J. G. Molybdenum carbide as alternative catalysts to precious metals for highly selective reduction of CO<inf>2</inf>to CO. *Angewandte Chemie - International Edition* **2014,** *53* (26), 6705.
(80) Lee, J. S.; Boudart, M. In situ carburization of metallic molybdenum during catalytic reactions of carbon-containing gases. *Catalysis Letters* **1993,** *20* (1-2), 97.
(81) Liu, S.; Wang, L.; Ohnishi, R.; Ichikawa, M. Bifunctional catalysis of Mo/HZSM-5 in the dehydroaromatization of methane to benzene and naphthalene XAFS/TG/DTA/ MASS/FTIR characterization and supporting effects. *Journal of Catalysis* **1999,** *181* (2), 175.
(82) Shou, H.; Davis, R. J. Reactivity and in situ X-ray absorption spectroscopy of Rb-promoted Mo 2C/MgO catalysts for higher alcohol synthesis. *Journal of Catalysis* **2011,** *282* (1), 83.
(83) Shou, H.; Li, L.; Ferrari, D.; Sholl, D. S.; Davis, R. J. Use of infrared spectroscopy and density functional theory to study the influence of rubidium on alumina-supported molybdenum carbide catalyst for higher alcohol synthesis from syngas. *Journal of Catalysis* **2013,** *299*, 150.
(84) Ding, W.; Li, S.; D Meitzner, G.; Iglesia, E. Methane Conversion to Aromatics on Mo/H-ZSM5: Structure of Molybdenum Species in Working Catalysts. *The Journal of Physical Chemistry B* **2001,** *105* (2), 506.
(85) Rocha, A. S.; Da Silva, V. T.; Eon, J. G.; De Menezes, S. M. C.; Faro Jr, A. C.; Rocha, A. B. Characterization by27Al NMR, X-ray absorption spectroscopy, and density functional theory techniques of the species responsible for benzene hydrogenation in Y zeolite-supported carburized molybdenum catalysts. *J Phys Chem B* **2006,** *110* (32), 15803.
(86) Chen, J. G. NEXAFS investigations of transition metal oxides, nitrides, carbides, sulfides and other interstitial compounds. *Surface Science Reports* **1997,** *30* (1-3), 1.
(87) Oyama, S.; Clark, P.; Teixeira da Silva, V.; Lede, E.; Requejo, F. XAFS characterization of highly active alumina-supported molybdenum phosphide catalysts (MoP/Al2O3) for hydrotreating. *The Journal of Physical Chemistry B* **2001,** *105* (21), 4961.

(88) Gong, Q.; Wang, Y.; Hu, Q.; Zhou, J.; Feng, R.; Duchesne, P. N.; Zhang, P.; Chen, F.; Han, N.; Li, Y.et al. Ultrasmall and phase-pure W2C nanoparticles for efficient electrocatalytic and photoelectrochemical hydrogen evolution. *Nature Communications* **2016,** *7*.

(89) Hunt, S. T.; Kokumai, T. M.; Zanchet, D.; Román-Leshkov, Y. Alloying tungsten carbide nanoparticles with tantalum: Impact on electrochemical oxidation resistance and hydrogen evolution activity. *The Journal of Physical Chemistry C* **2015,** *119* (24), 13691.

(90) Ingham, B.; Brady, C. D. A.; Burnstein, G. T.; Ryan, M. P. EXAFS Analysis of Electrocatalytic WC Materials. *J. Phys. Chem.* **2009,** *113* (40), 17407.

(91) Lee, J. S.; Yie, J. E. An XANES study of carbides of molybdenum and tungsten. *Korean Journal of Chemical Engineering* **1991,** *8* (3), 164.

(92) Uo, M.; Asakura, K.; Watanabe, K.; Watari, F. XAFS analysis of the bronchoalveolar lavage fluid of a tungsten carbide pneumoconiosis patient. *Chemistry letters* **2010,** *39* (8), 852.

(93) Al-Megren, H. A.; Xiao, T.; Gonzalez-Cortes, S. L.; Al-Khowaiter, S. H.; Green, M. L. Comparison of bulk CoMo bimetallic carbide, oxide, nitride and sulfide catalysts for pyridine hydrodenitrogenation. *Journal of Molecular Catalysis A: Chemical* **2005,** *225* (2), 143.

(94) Lin, Z.; Wan, W.; Yao, S.; Chen, J. G. Cobalt-modified molybdenum carbide as a selective catalyst for hydrodeoxygenation of furfural. *Applied Catalysis B: Environmental* **2018,** *233*, 160.

(95) Zhao, Z.; Yang, H.; Li, Y.; Guo, X. Cobalt-modified molybdenum carbide as an efficient catalyst for chemoselective reduction of aromatic nitro compounds. *Green Chemistry* **2014,** *16* (3), 1274.

(96) Masoumi, S.; Dalai, A. K. NiMo carbide supported on algal derived activated carbon for hydrodeoxygenation of algal biocrude oil. *Energy Conversion and Management* **2021,** *231*, 113834.

(97) Chen, H.; Wang, Q.; Zhang, X.; Wang, L. Effect of support on the NiMo phase and its catalytic hydrodeoxygenation of triglycerides. *Fuel* **2015,** *159*, 430.

(98) Zhang, H.; Chen, G.; Bai, L.; Chang, N.; Wang, Y. Selective hydrogenation of aromatics in coal-derived liquids over novel NiW and NiMo carbide catalysts. *Fuel* **2019,** *244*, 359.

(99) Smirnov, A. A.; Geng, Z.; Khromova, S. A.; Zavarukhin, S. G.; Bulavchenko, O. A.; Saraev, A. A.; Kaichev, V. V.; Ermakov, D. Y.; Yakovlev, V. A. Nickel molybdenum carbides: Synthesis, characterization, and catalytic activity in hydrodeoxygenation of anisole and ethyl caprate. *Journal of Catalysis* **2017,** *354*, 61.

(100) Xiao, T.; Wang, H.; York, A. P.; Williams, V. C.; Green, M. L. Preparation of nickel–tungsten bimetallic carbide catalysts. *Journal of Catalysis* **2002,** *209* (2), 318.

(101) Al-Megren, H. A.; González-Cortés, S. L.; Xiao, T.; Green, M. L. A comparative study of the catalytic performance of Co-Mo and Co (Ni)-W carbide catalysts in the hydrodenitrogenation (HDN) reaction of pyridine. *Applied Catalysis A: General* **2007,** *329*, 36.

(102) Gao, S.; Chen, H.; Liu, Y.; Li, G.-D.; Gao, R.; Zou, X. Surface-clean, phase-pure multi-metallic carbides for efficient electrocatalytic hydrogen evolution reaction. *Inorganic Chemistry Frontiers* **2019,** *6* (4), 940.

(103) Puello-Polo, E.; Brito, J. L. Effect of the type of precursor and the synthesis method on thiophene hydrodesulfurization activity of activated carbon supported Fe-Mo, Co-Mo and Ni-Mo carbides. *Journal of Molecular Catalysis A: Chemical* **2008,** *281* (1-2), 85.

(104) Fu, Q.; Peng, B. X.; Masa, J.; Chen, Y. T.; Xia, W.; Schuhmann, W.; Muhler, M. Synergistic Effect of Molybdenum and Tungsten in Highly Mixed Carbide Nanoparticles as Effective Catalysts in the Hydrogen Evolution Reaction under Alkaline and Acidic Conditions. *Chemelectrochem* **2020,** *7* (4), 983.

(105) Tran, C. C.; Hang, Y. L.; Garcia-Perez, M.; Kaliaguine, S. Synergistic effect of Mo-W carbides on selective hydrodeoxygenation of guaiacol to oxygen-free aromatic hydrocarbons. *Catalysis Science & Technology* **2019,** *9* (6), 1387.

(106) Zhao, Z.; Zhu, Z.; Wang, F.; Li, S.; Bao, X.; Zhang, L.; Lin, S.; Yang, Y. Bimetallic carbides embedded in heteroatom-doped carbon nanotubes for efficient electrocatalytic hydrogen evolution reaction and high-performance lithium storage. *Chemical Engineering Journal* **2021,** *415*, 128885.

(107) Leclercq, L.; Provost, M.; Pastor, H.; Leclercq, G. Catalytic Properties of Transition-Metal Carbides .2. Activity of Bulk Mixed Carbides of Molybdenum and Tungsten in Hydrocarbon Conversion. *Journal of Catalysis* **1989,** *117* (2), 384.

(108) Westerterp, K.; Molga, E.; Van Gelder, K. Catalytic hydrogenation reactors for the fine chemicals industries. Their design and operation. *Chemical engineering and processing: process intensification* **1997,** *36* (1), 17.

(109) Rylander, P. *Catalytic hydrogenation over platinum metals*; Elsevier, 2012.

(110) Nishimura, S. *Handbook of heterogeneous catalytic hydrogenation for organic synthesis*; Wiley New York, 2001.

(111) Irfan, M.; Glasnov, T. N.; Kappe, C. O. Heterogeneous Catalytic Hydrogenation Reactions in Continuous-Flow Reactors. *ChemSusChem* **2011,** *4* (3), 300.

(112) Mortensen, P. M.; de Carvalho, H. W. P.; Grunwaldt, J.-D.; Jensen, P. A.; Jensen, A. D. Activity and stability of Mo2C/ZrO2 as catalyst for hydrodeoxygenation of mixtures of phenol and 1-octanol. *Journal of Catalysis* **2015,** *328*, 208.

(113) De Vylder, A.; Lauwaert, J.; Van Auwenis, S.; De Clercq, J.; Thybaut, J. W. Catalyst stability assessment in a lab-scale liquid-solid (LS) ^{2} plug-flow reactor. *Catalysts* **2019,** *9* (9), 755.

(114) Van Der Klis, F.; Gootjes, L.; Van Haveren, J.; Van Es, D.; Bitter, J. From batch to continuous: Au-catalysed oxidation of d-galacturonic acid in a packed bed plug flow reactor under alkaline conditions. *Reaction Chemistry & Engineering* **2018,** *3* (4), 540.

(115) Liu, X.; Smith, K. J. Acidity and deactivation of Mo2C/HY catalysts used for the hydrogenation and ring opening of naphthalene. *Applied Catalysis A: General* **2008,** *335* (2), 230.

(116) Zaikovskii, V. I.; Vosmerikov, A. V.; Anufrienko, V. F.; Korobitsyna, L. L.; Kodenev, E. G.; Echevskii, G. V.; Vasenin, N. T.; Zhuravkov, S. P.; Matus, E. V.; Ismagilov, Z. R.et al. Properties and deactivation of the active sites of an MoZSM-5 catalyst for methane dehydroaromatization: Electron microscopic and EPR studies. *Kinet Catal+* **2006,** *47* (3), 389.

(117) Jongerius, A. L.; Gosselink, R. W.; Dijkstra, J.; Bitter, J. H.; Bruijnincx, P. C. A.; Weckhuysen, B. M. Carbon Nanofiber Supported Transition-Metal Carbide Catalysts for the Hydrodeoxygenation of Guaiacol. *ChemCatChem* **2013,** *5* (10), 2964.

(118) Pham-Huu, C.; York, A. P. E.; Benaissa, M.; Gallo, P. D.; Ledoux, M. J. Reactions of n-Heptane and Methylcyclopentane over an Oxygen-Modified Molybdenum Carbide Catalyst. Study of Coke Formation, Catalyst Deactivation, and Regeneration. *Industrial and Engineering Chemistry Research* **1995,** *34* (4), 1107.

(119) Macedo, L. S.; Stellwagen, D. R.; da Silva, V. T.; Bitter, J. H. Stability of Transition-metal Carbides in Liquid Phase Reactions Relevant for Biomass-Based Conversion. *Chemcatchem* **2015,** *7* (18), 2816.

(120) Li, C.; Zheng, M.; Wang, A.; Zhang, T. One-pot catalytic hydrocracking of raw woody biomass into chemicals over supported carbide catalysts: simultaneous conversion of cellulose, hemicellulose and lignin. *Energy & Environmental Science* **2012,** *5* (4), 6383.

(121) Hollak, S. A. W.; Gosselink, R. W.; van Es, D. S.; Bitter, J. H. Comparison of Tungsten and Molybdenum Carbide Catalysts for the Hydrodeoxygenation of Oleic Acid. *Acs Catalysis* **2013,** *3* (12), 2837.

(122) Gosselink, R. W.; Stellwagen, D. R.; Bitter, J. H. Tungsten-Based Catalysts for Selective Deoxygenation. *Carbohydrate research* **2013,** *52* (19), 5089.

2

Chapter 2

Synthesis and Characterization of Supported Mixed MoW Carbide Catalysts

This Chapter is based on: M. Führer, T. van Haasterecht, E.J.J. de Boed, P. E. de Jongh and J. H. Bitter Synthesis and Characterization of Supported Mixed MoW Carbide Catalysts. *Submitted (under review, 2022)*

Here an additional X-Ray absorption study is added which was in collaboration with E. Schreuder, S. Parry and M. Tromp

Abstract

Mixed MoW carbide catalysts are of interest because of their reported synergetic effects in hydrogenation reactions. However, the characterization of these materials needs further attention; the exact structure and composition of these mixed carbides have not been unambiguously established. We synthesized a series of these catalysts with different Mo and W ratios via two different synthesis methods e.g., temperature-programmed reduction and carbothermal reduction, and found that both synthesis methods resulted in mixed bimetallic (MoW) carbide phases. Irrespective of the synthesis method, all bimetallic catalysts (Mo:W bulk ratios of 1:3, 1:1 and 3:1) show compositions on the nanoscale level that are close to those of the bulk ratios. Furthermore, the crystal structures of the produced phases and the nanoparticle size differ depending on the synthesis method. A cubic carbide (MeC_{1-x}) phase with 3-4 nm nanoparticles was obtained when using TPR method while a hexagonal phase (Me_2C) with 4-5 nm nanoparticles was found when using the CR method. The TPR-synthesized carbides showed higher activity for the hydrodeoxygenation of fatty acids. This higher activity of the TPR samples was tentatively related to the cubic crystal structure, particle size or a combination of those two effects. These results highlight that the crystal structure and/or the particle size have more impact on the catalytic performance than the composition of the mixed metal carbides.

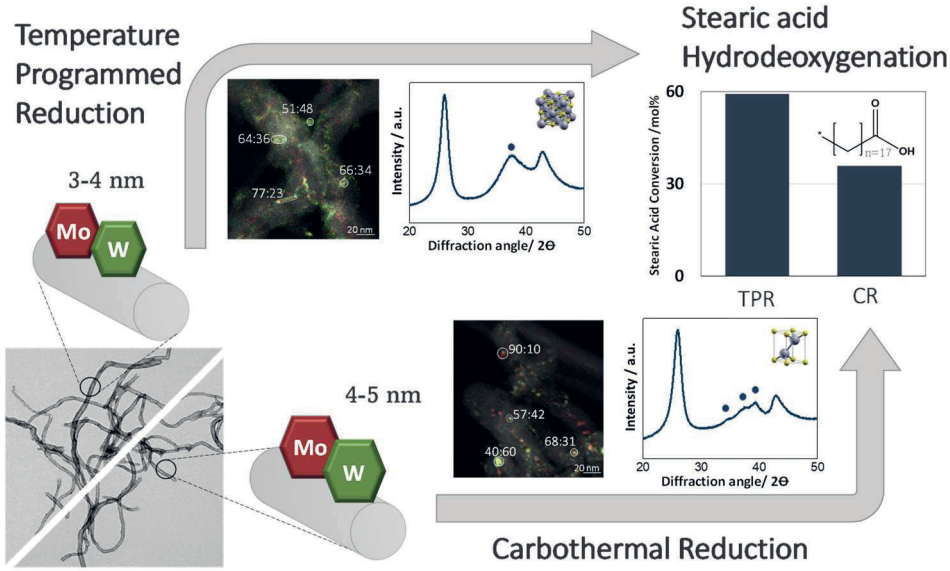

Introduction

Combining two metals in one catalyst can result in a synergetic catalytic performance with respect to activity, selectivity and stability compared with monometallic catalysts.[1-3] Prime examples are the addition of non-noble metals to noble metals such as Pt, Au and Pd for use in hydrogenation[3], hydrodeoxygenation[4], Fischer-Tropsch synthesis[5] and aqueous-phase reforming.[6,7] For instance for the conversion of biobased feedstocks, the addition of Ni, Co or Fe to Pt decreases the adsorption energy of CO and H on the Pt surface which results in a threefold increase of the activity for aqueous-phase reforming of ethylene glycol.[6,7] Although the performance of noble-metal catalysts and their bimetallic forms is excellent, the limited availability and often high costs of these metals spurred a quest for alternatives.[8,9]

Transition metal carbides like Mo and W carbides are catalysts for reactions that involve hydrogen activation and are as such interesting alternatives for noble metals.[10,11] Recently, also (bulk) bimetallic MoW carbide catalysts have attracted attention.[12-23] For example, Tran et al. observed a synergistic effect between Mo and W carbides in the hydrodeoxygenation of guaiacol to hydrocarbons[18]. These mixed-carbide catalysts exhibited superior catalytic activity due to the presence of H_2-activating sites and oxophilic sites in the same catalyst; the H_2-activating sites were created by the interaction between Mo and W atoms while the presence of (metallic) W introduced oxophilicity. Mehdad and co-workers synthesized and characterized single-phase mixed MoW carbides with different Mo-to-W ratios for toluene hydrogenation.[21] In their work, they observed that increasing W content led to decreasing activity relative to monometallic Mo carbides, but the selectivity towards the more desired products such as benzene and xylene increased. Wang et al. used a bimetallic carbide catalyst consisting of Mo_2C and WC for the electrochemical hydrogen evolution reaction.[23] They found that electrochemical activation can partially remove surface carbon which in turn changes the surface hydrophilicity. The contribution of the residual carbon was claimed to protect the carbide from oxidation and helps maintain the high performance and stability of the catalyst.[23]

Though these examples highlight the relevance of Mo/W mixed carbides, the relationship between synthesis history, catalyst characteristics and catalytic performance of supported metal-carbides has only been scarcely investigated.[14,17,22,24] For supported metal-carbides, two major synthesis routes have been developed, i.e. temperature-programmed reduction (TPR)[11] and carbothermal reduction (CR)[25]. Information about the effect of these carburization methods on the physicochemical properties of these bimetallic materials in relation to their catalytic behavior is lacking, as also stated by Mehdad et al. in 2019.[19]

Both the CR and the TPR method are widely used for preparing catalysts.[26-28] In CR synthesis, an oxidic precursor is loaded onto a carbon support, followed by heating up to high temperature e.g., 900 °C, resulting in the reaction of a fraction of the carbon with the oxide to form the carbide. During TPR synthesis, the loaded oxidic precursor is carburized at lower temperatures i.e., between 300 °C and 650 °C in the presence of an external carbon source such as CO[29], methane[8,30,31] or other hydrocarbons[32-34]. However, certainly for bimetallic carbides, the influence of parameters such as temperature ramp, nature of the precursor and the carburizing atmosphere is not fully understood yet. Depending on the synthesis method and conditions, the morphology, e.g. crystal structure[35] or particle size[36] of the (mixed) carbide can be different and this, in turn, can influence the activity and selectivity of catalyst. For instance, Macedo et al. showed that carbothermal reduction synthesis in an inert atmosphere results in hexagonal β-Mo_2C, while TPR synthesis in a carbon-containing atmosphere yields cubic α-MoC_{1-x}; these materials do not only show differences in crystallinity, but also in their intrinsic activity.[8] TPR-synthesized cubic α-MoC_{1-x} exhibits a better catalytic performance than β-Mo_2C. This was attributed to the lower site density of the cubic structure, which makes the Mo atoms more accessible for the reactant.

Some studies have offered suggestions for the composition and structure of supported mixed carbides. Fu et al.[17] synthesized a series of mixed MoW carbide catalysts supported on carbon nanotubes via carbothermal reduction, which were used for hydrogen evolution reactions. Based on XRD and TEM-EDS analysis, these researchers concluded that an orthorhombic MoW phase formed in which Mo and W were atomically mixed. Leclercq and co-workers[37,38] used XPS analysis to explore the surface composition of bulk MoW materials and found Mo enrichment on the surface; however, they did not establish the exact composition and structure of the mixed MoW carbides. Techniques to study the preparation of homogeneously mixed MoW carbides involve either STEM-EDX[17], XRD[18] or TGA[19], but the unambiguous determination of the structure of supported mixed MoW carbide catalysts requires the use of a combination of characterization techniques.

In this paper, we report on carbon nanofiber-supported mixed MoW carbides, which we synthesized via both the TPR and the CR method. We used TPD-MS, TPR-MS, TGA, XRD, XANES, EXAFS and STEM-EDX to investigate the influence of the synthesis method on the physicochemical characteristics of these catalysts. Finally, we attempted to relate their activity for the hydrodeoxygenation of stearic acid to the characteristics of the catalysts especially to their particle size and crystal phase.

The CR synthesis pathway of monometallic Mo carbides with the use of a carbon-supported ammonium heptamolybdate (AHM) precursor has been studied previously[8,25,39-42], but we were able to find only a few studies[39,43] on the synthesis of W carbides from ammonium metatungstate, while no reports at all were available for the supported synthesis of mixed MoW carbides. The TPR synthesis of both W carbides and Mo carbides has been previously studied, but with different materials such as $MoCl_5$/WCl_6[16] and ammonium tungsten oxide hydrate[14].

Material and Methods

Carbide Catalyst Synthesis

Carbon nanofibers (CNF) were grown from a mixture of hydrogen (102 ml/min), nitrogen (450 ml/min) and carbon monoxide (260 ml/min) at 550 °C and 3 barg for 24 h over a reduced 5 wt.% Ni/SiO_2 catalyst (3 g), as reported previously.[1] To remove SiO_2 after growth, the mixture (CNF+Ni+SiO_2) was refluxed three times in 1 M KOH for 1 h with intermediate decanting and washing with 1 M KOH. Next, the CNF was treated by refluxing in 65% concentrated nitric acid for 1.5 h to remove the remaining Ni and introduce oxygen groups on the CNF surface. Finally, the CNF was washed with demineralized water to neutral pH and ground to a 90-120 μm fraction.

The CNF-supported catalysts were synthesized by incipient wetness impregnation (pore volume support 0.7 ml/g). We used aqueous solutions of ammonium heptamolybdate (AHM; Sigma-Aldrich, 99.98% trace metals basis, pH 5), ammonium metatungstate (AMT; Sigma-Aldrich, 99.98% trace metals basis, pH 3) or a mixture of both salts (molar ratio of Mo:W = 1:3, 1:1 and 3:1). All catalysts contained the same total metal loading of 0.9 mmol/$g_{catalyst}$. After impregnation, the catalysts were dried overnight at 110 °C in static air and stored for further use.

The impregnated catalyst precursors (impregnated CNF) were carburized either via the temperature-programmed reduction method or the carbothermal reduction method in a tubular plug reactor. In the TPR method, the precursor (250 mg) was exposed to 20% CH_4/H_2 (total flow of 100 min^{-1}) for 2 h at 650 °C (β = 5 °C/min). For the carbothermal reduction, the samples were carburized in N_2 flow (50 ml/min) and heated from room temperature (RT) to 900 °C (β = 5 °C/min). To avoid contact with air, the carburized catalysts were directly transferred from the carburization reactor to a (N_2 atmosphere) glove box without exposure to air.

Characterization

We followed the development of the sample during both synthesis methods by thermogravimetric analysis (TGA), Temperature Programmed Desorption coupled with Mass Spectrometry in inert (TPD-MS, see below) and Temperature Programmed Reaction coupled

with Mass Spectrometry in CH_4/H_2 (TPR-MS, see below). The catalysts were further characterized by STEM-EDX and XRD. A physical mixture of the monometallic carbides and bare CNF were included for comparison.

For the CR method, CO evolution, e.g. measured by TPD-MS, is a good proxy for following the carburization process.[8,39,44-46] In general, up to 600 ˚C, the precursor decomposes/reduces while the actual carburization occurs above 600 ˚C with the concomitant release of CO resulting from the simultaneous reduction and carburization of the metal oxide to the carbide.[45,46] Since the support is the carbon source for the CR method, clear weight changes are expected. Therefore, TGA is a suitable technique to investigate at which temperature the carburization takes place.

Temperature-programmed desorption (TPD-MS) and temperature-programmed reduction (TPR-MS) mass spectrometry analyses were performed with a Micromeritics AutoChem II 2920 coupled to a Pfeiffer Vacuum ThermoStar™ mass spectrometer. To study the carburization process during CR, the precursors (100 mg) were heated to 900 °C at 10 °C/min under helium (total flow of 20 min^{-1}) for the TPD-MS method. For the TPR method, the samples (100 mg) were exposed to 20% CH_4/H_2 (total flow of 100 min^{-1}) while heated to 750 °C at 5 °C /min. The gas phase was then evaluated via MS.

Thermogravimetric analysis (TGA) was performed in 150 μl alumina crucibles (Mettler-Toledo) using a Mettler-Toledo TGA/DSC 1 apparatus. During the CR method, the precursors (40 mg) were heated to 1000 °C at 10 °C/min under nitrogen (100 ml/min). To study the TPR method with TGA, the precursors (40 mg) were exposed to 20% CH_4/H_2 (total flow of 100 ml/min) while heating to 750 °C at 5 °C /min.

HAADF-STEM images and EDX analyses were acquired using an FEI Talos™ F200X transmission electron microscope operating in scanning transmission mode at 200 kV and equipped with a high-brightness field emission gun (X-FEG) and a Super-X G2 EDX detector, with the aid of the Velox™ software. For these analyses, the samples were ground and drop-casted from an ethanolic dispersion onto a lacey carbon-coated 300 mesh copper grid.

The XRD patterns were recorded on a Bruker D8 Advance with an Lynxeye-XE-T PSD detector equipped with a Cu-K$\alpha_{1,2}$ tube generating X-rays with λ = 1.542 Å. The measurements were taken in the 2θ range of 20° to 80° with a step size of 0.05° at 1 sec^{-1}.

N_2 physisorption isotherms were recorded with a Micromeritics, Tristar II Plus at liquid nitrogen temperature (-195.8 °C). 100 mg of sample was degassed at 200 °C for 2h using a Micromeritics

VacPrep 061. The pore volume and surface area of the samples were determined using the BET theory.

Extended X-ray adsorption fine structure (EXAFS) and X-ray absorption near edge spectroscopy (XANES) at Mo K-edge (20000 eV) and W L_3-edge (10207 eV) were recorded at the B18 beamline of the Diamond Light Source, UK, using Si (1 1 1) double crystal monochromator. The measurements were performed in fluorescence mode. Mo foil and W foil spectra were simultaneously collected to samples and standards to enable the energy calibration.

The powders were capped in a cutout sample holder with Kapton tape on each side and afterwards shrink wrapped in foil to avoid any contact with air. The reference materials Mo, MoO_2, Mo_2C, W, WO_2 WC and WC_2 pressed into pellets. For the data analysis of the XAFS spectra and the EXAFS spectra, the program Athena and Artemis were used, respectively. The averaging, background subtraction and normalization procedures were performed using standard routines. The data were fitted in R-space with k1, k2, and k3 weightings simultaneously.

Hydrodeoxygenation

The hydrodeoxygenation (HDO) reaction was performed in a 100 mL stainless-steel Parr 4598 Micro Batch stirred reactor system. Typically, the reactor was filled with 250 mg catalyst, 2 g stearic acid (Sigma-Aldrich, ≥95%, FCC, FG), 1 g tetradecane as internal standard (Sigma-Aldrich, ≥99%), and 50 mL dodecane (Sigma-Aldrich, ReagentPlus ®, ≥99%). Next, the loaded reactor was twice purged with 30 bar Ar and afterwards flushed with H_2. Subsequently, the reactor was pressurized to 30 bar H_2, heated to 350 °C while stirring at 800 rpm. The reaction was performed for 4 h. Liquid samples from the reactor were taken at regular time intervals to investigate the product distribution. From the taken reaction solutions, sample two separate samples were diluted with CH_2Cl_2:MeOH (2:1 v/v%) and analyzed by gas chromatogram (with a FID detector). The two values were averaged and reported, the deviation from the average will be indicated by error bars.

The catalyst stability was tested by subsequent experiments with one batch of carbide catalysts. Between the runs, the remaining reaction medium was decanted, and then the catalysts were washed/decanted with 100 ml dodecane before adding the fresh reaction medium.

Results and Discussion

CR synthesis

The synthesis pathway of the carbides with the use of a carbon-supported precursor takes place via several steps including precursor decomposition, oxide formation/reduction, and carburization.[8,39,44-46] The Supplementary Information provides a detailed analysis of the CR synthesis; Figures S2.1 and S2.2 show the evolution of all gases in our experiments. The weight changes and phase transitions can be found in Figure S2.3 and Figure S2.4, respectively. Scheme S2.1 and Table S2.1 show the results for the carbide samples, including a discussion of the synthesis pathways. Based on those results, we concluded that the CO evolution and weight rate changes are indicative for the carburization process and are suitable for determining the carburization temperature of the CR synthesis. To prove that the CO evolution does not result from the degradation of the CNF, TPD-MS and TGA results for the pristine CNF support without any precursors were conducted under the CR treatment conditions (Figure S2.1). The results show that the CO release and the weight loss are significantly less than for the samples with metal precursors.

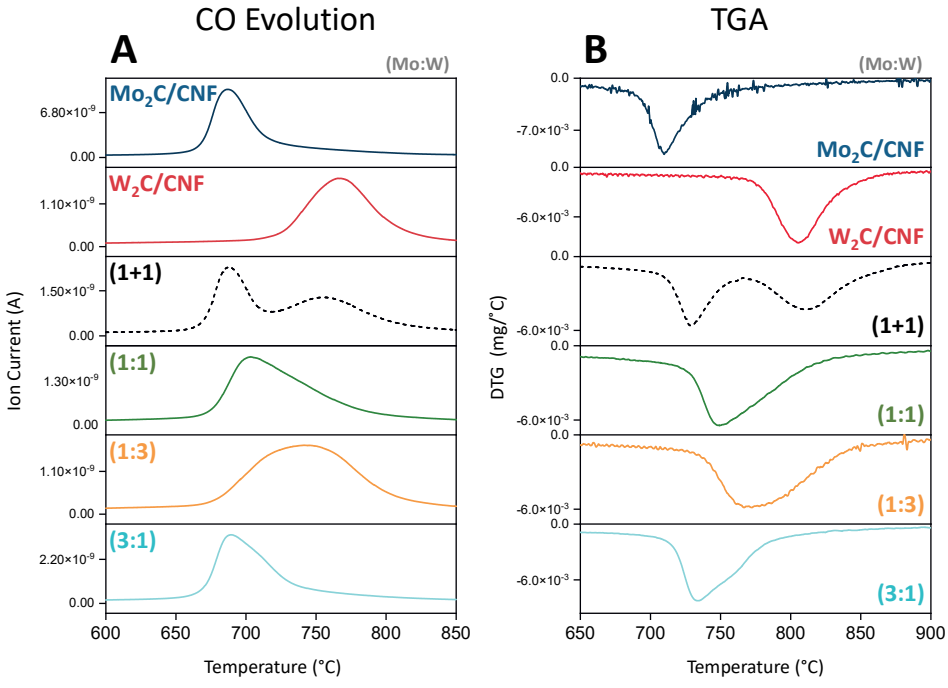

Figure 2.1 A: CO evolution during CR synthesis of monometallic and mixed-metal carbides. B: Comparison of weight change rates during CR synthesis.

Figure 2.1 A (TPD-MS) displays the CO evolution as a function of temperature for the monometallic carbides, the mixed carbides and a 1:1 physical mixture during the CR synthesis. For the monometallic samples, Figure 2.1 A clearly displays one CO evolution peak at 680 °C for Mo on CNF and one CO evolution peak at 770 °C for W on CNF, indicating that for monometallic samples the carburization occurs in one step. The physical mixture (indicated as the 1+1 sample in Figure 2.1A) shows two CO evolution peaks at the temperature representative for Mo and W which indicates that the two carburization processes are independent of each other in a physical mixture.

Mixed Mo:W carbide samples show CO evolution temperatures i.e., carburization temperatures in between those of Mo and W carbides; the maximum shifts toward higher temperatures with increasing W content. These carburizations cause only one CO peak, which indicates that the carburization of the Mo and W occurs simultaneously in a single step. This indicates that a single mixed MoW phase is formed. However, the peaks, especially for samples with higher W contents, are broad and asymmetric. This suggests some heterogeneity with respect to size and/or composition of the nanoparticles.

Figure 2.1 B displays the weight loss rates (DTG) based on TGA for the same samples, during the CR carburization step for the different monometallic, bimetallic and physical mixed samples. A similar trend of higher carburization temperature for samples containing more W as in the TPD-MS measurements (Figure 2.1 A) is visible. In addition, the physical mixture again shows the two separate peaks for Mo and W carburization.

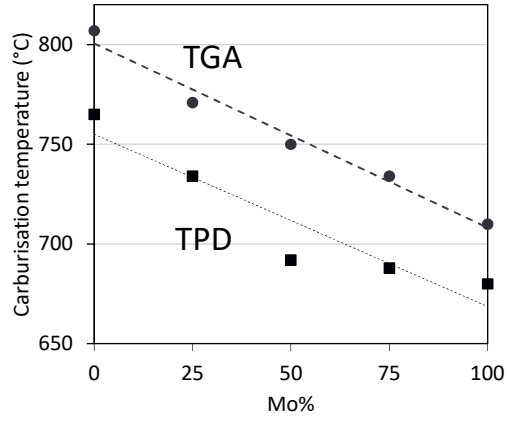

Figure 2.2 Comparison of TGA and TPD carburization temperatures as a function of Mo content in monometallic and bimetallic Mo/W-carbides.

In Figure 2.2, the carburization temperatures obtained from TPD-MS (Figure 2.1 A) and TGA (Figure 2.1 B) are plotted as a function of the metal composition of the samples (represented by the Mo fraction). Clearly, the TPD and TGA analyses show the same trends for the carburization temperature although the absolute temperatures are lower in the TPD analysis. We attribute this to experimental differences. The TPD-MS is performed in a plug-flow reactor while for TGA the gases are flown over the sample in a cup resulting in less intense contact between gas and catalyst particles. Thus in turn might result in a less effective heat transfer and as a consequence differences in carburization temperature were found.

Overall, we conclude that in CR, the carburization of bimetallic samples occurs in between the carburization temperatures of each of the two individual monometallic carbides, possibly in a single step, indicating the formation of a mixed MoW carbide phase.

TPR synthesis

TPR synthesis of the carbides was followed by using both TPR-MS and TGA and was found to occur in several steps. We discuss this further in the Supplementary Information. Figures S2.5 and S2.6 show the results for the CO, CO_2 and CH_4 gas evolution, Figure S2.7 shows the weight

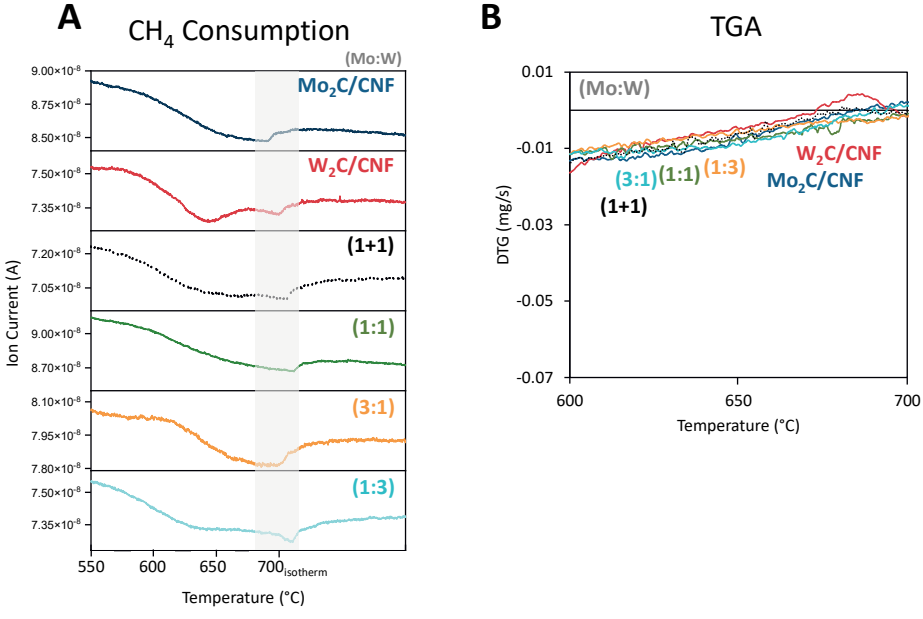

Figure 2.3 A: CH_4 consumption during TPR synthesis of monometallic and mixed metal carbides. B: Comparison of weight change rates during TPR synthesis.

changes and the phase transformations are shown in Figure S2.8. In Figure S2.9 the thermal effects during the carburization are discussed.

To summarize these results, similar as for the CR, we observed that the TPR synthesis for the Mo occurs via the oxide phase. In contrast, we observed that the reduction of the W oxide takes only place via first the formation of metallic W. During the formation of the metallic W CO is released. Next the carburization of the metallic W phase occurs, where CH_4 is consumed but no CO is released. Hence, the TPR carburization can best be followed by studying the consumption of CH_4. Figure 2.3 A displays the CH_4 consumption during TPR synthesis. For monometallic W, there are two CH_4 consumption peaks; the first one results from the reduction of WO_2 to W at 640 °C and the second one, near 700 °C, corresponds to the carburization of the metal. For Mo, only one broad peak in the range of 620 to 700 °C is visible, with a maximum at 700 °C, indicating the carburization of the MoO_2 species to the Mo carbide. Thus, for both monometallic samples, the carbide formation is complete around 700 °C. The carburization of the physical mixture and the bimetallic carbides also occurs at this temperature, indicated by the grey area in Figure 2.3 A.

In contrast to the CR method, the carburization step of the TPR synthesis cannot be observed with TGA. This is because the overall conversion of the metal oxides to the metal carbides does not induce a significant weight change, as can be seen Figure 2.3 B. The carbon replacing the oxygen, in the case of the TPR methods, originates from an external source (as opposed to CR where weight change originates due to the consumption of the carbon support while forming gaseous products) and does not lead to a weight change of the sample. Nevertheless, based on the observed CH_4 consumption shown in TPR-MS data and XRD (Figure S2.8), it is clear that a carbide phase formed during synthesis via the TPR method.

The techniques described above indicate (indirectly) the formation of mixed MoW carbides for the CR prepared samples, not however for the TPR samples. Additionally, no inside have gained on the potential interaction between W and Mo after the formation of the mixed metal carbides. To obtain those insight of the (CR and TPR) prepared samples, we performed HAADF-STEM, EDX, XRD, XANES and EXAFS analyses.

HAADF-STEM EDX

Figure 2.4 and 2.5 show representative HAADF-STEM images and EDX images of CNF-supported MoW carbide samples prepared by CR and TPR (with Mo:W 1:1), respectively. The images and analysis for samples with the other two Mo:W ratios (1:3 and 3:1) can be found in the Supplementary Information (Figures S2.10 and S2.11).

For the CR-prepared sample (BET surface area = 114 m^2/g, total pore volume = 0.3 $*10^{-6}$ ml/g), the HAADF-STEM image clearly shows the metal-containing particles as bright spots on the CNF support (BET surface area = 194 m^2/g, total pore volume = 0.4 $*10^{-6}$ ml/g). These particles have sizes of 4 to 5 nm. The elemental analysis indicates that W and Mo are well distributed over the support and analysis of this whole image yields an average Mo:W ratio of 55:45, which corresponds well to the bulk ratio of the prepared catalyst (i.e. 50:50 Mo:W). At the single-particle level, Mo:W ratios vary, showing that an inhomogeneous mixed phase had formed (e.g. Mo:W with 1:1 ratio shows ratios of 40:60, 57:43, 90:10 and 69:31). No monometallic particles were observed for any of the CR-synthesized samples.

Similar observations can be made in Figure 2.5 for a TPR-prepared sample (BET = 151 m^2/g, total pore volume = 0.3 $*10^{-6}$ ml/g). The particle size seems to be marginally smaller (3-4 nm) in comparison with samples prepared by the CR method. Again, the Mo:W bulk ratio (50:50) is

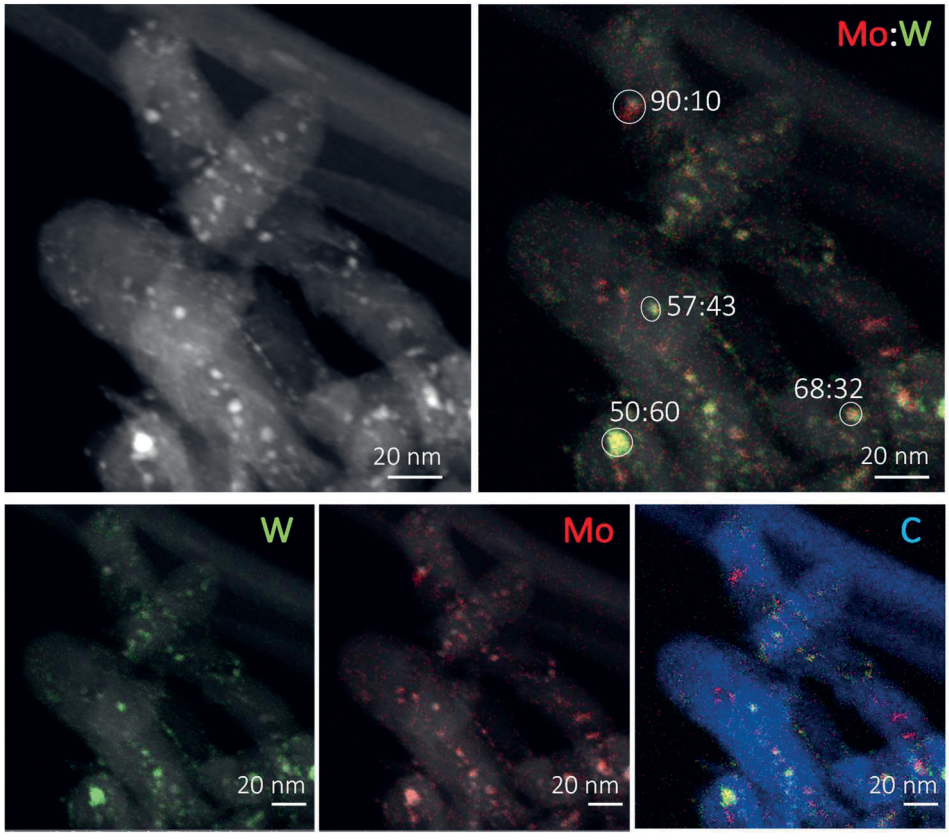

Figure 2.4 HAADF-STEM image with EDX map overlays of the CR-prepared CNF-supported MoW carbide sample with a Mo:W ratio of 1:1 showing tungsten in green, molybdenum in red and carbon in blue. The depicted ratios indicate the Mo:W ratio in the individual particles. Scale bar: 20 nm.

similar to the ratios in the whole image. The single-nanoparticle analysis yielded variable Mo:W ratios, which are distributed around the bulk ratio (52:48, 64:36, 77:23 and 66:34), similar as for the sample prepared by the CR method, indicating the formation of a mixed metal carbide phase.

From these HAADF-STEM and EDX analyses, we can conclude that a mixed phase formed on a single particle level, irrespective of the synthesis method. For samples prepared by the CR method, this is in agreement with the TGA and TPD-MS results. Also, the variation in the Mo:W ratios of the individual nanoparticles found with EDX explains the broad peak observed during the TGA and TPD-MS analyses and the absence of two isolated carburization peaks representative of Mo and W. In addition, we observed that the TPR synthesized particles are ~1nm smaller than the CR carburized samples (see particle size distribution in Figure S2.12).

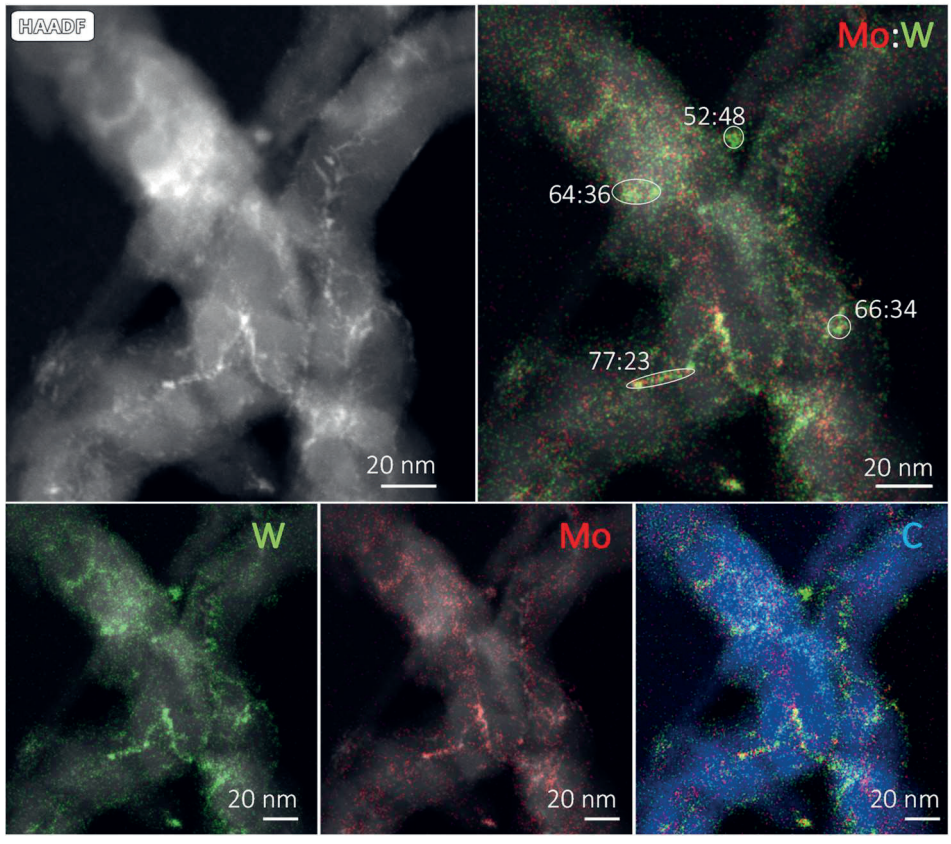

Figure 2.5 HAADF-STEM image with EDX map overlays of the TPR-prepared CNF-supported MoW carbide sample with a Mo:W ratio of 1:1 showing tungsten in green, molybdenum in red and carbon in blue. The depicted ratios indicate the Mo:W ratio in the individual particles. Scale bar: 20 nm.

XRD

After having established that synthesis via CR and TPR both resulted in mixed-metal particles (though with varying Mo:W ratios on single nanoparticles and slightly different particle sizes), we used XRD to establish which crystal phases have formed in these materials. Figure 2.6 shows the XRD patterns of all carbide samples. The signals at 2θ=28° and 2θ=43° represent the (002) and (101) reflections of the CNF.[47] All XRD patterns of CR-prepared carbides show a similar pattern with diffractions at 2θ values of 34.4°, 37.7°, 39.4°, 61.5°, 69.2° and 74.7°, indicated by the yellow squares. These reflections correspond to the hexagonal phase of β-Mo_2C or β-W_2C.[11,48,14,17] It has previously been suggested that Vegard's law[17] can be used to prove the formation of a MoW mixed-metal carbides phase. We, however, did not observe a systematic shift in peak position with increasing Mo content. The difference between β-Mo_2C and β-W_2C is intrinsically small (0.1 2θ) and hence the difference do not show up in the very broad diffraction peaks for these mixed-metal nanoparticles (see Figure S2.13 (CR) and Figure S2.14 (TPR) in the Supplementary Information for more details).

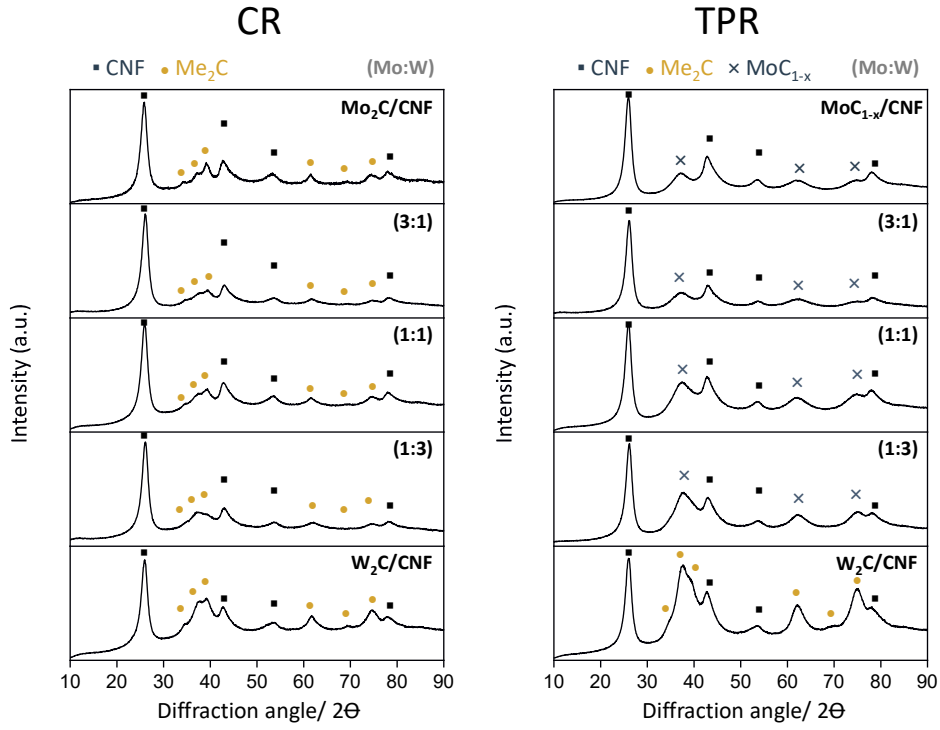

Figure 2.6 XRD pattern of monometallic carbide catalyst samples and bimetallic carbide catalyst samples, synthesized via TPR under 20% CH_4/H_2 (left) and via CR in N_2 (right).

For the carbide catalysts prepared via TPR, different crystal structures were found for the Mo and W carbides (Figure 2.6, right). The Mo sample prepared via TPR shows a broad reflection at a 2θ of 39°. This reflection represents the cubic α-MoC_{1-x} phase (less stable than the hexagonal form[49]), here indicated by the blue crosses.[8,27,50,51] The W carbide prepared via TPR displays reflections at 2θ values of 34.4°, 37.7°, 39.4° similar as seen for the CR prepared carbides. However, the peak at 37.7° is much sharper and higher in intensity which makes it difficult to conclude that this carbide phase consists exclusively of a hexagonal W_2C phase. The bimetallic carbides show a broad peak at a 2θ value of 39°, which can be attributed to the cubic carbide phase. However, since peaks are broad it cannot be excluded that the hexagonal structure is also present.

To conclude, the formed crystal structure is depending on the synthesis method. CR carburization leads to the formation of thermodynamic more stable hexagonal carbides[49,52,53] probably due to the higher carburization temperature, whereas TPR-carburized carbides display a pure cubic crystalline structure for Mo carbide and a mixture of crystal structures for the mixed-metal carbides.

XANES

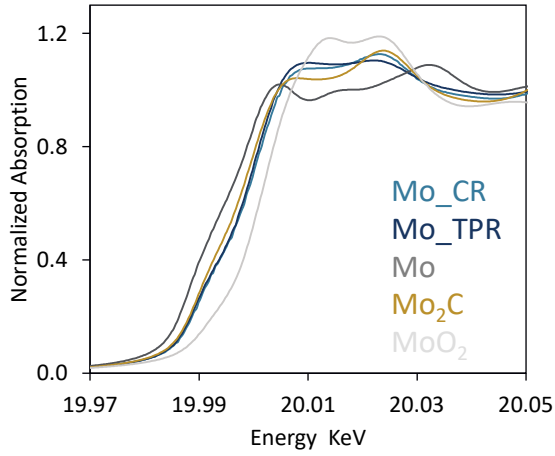

Figure 2.7 Mo K-edge of the monometallic samples prepared via CR and TPR in comparison to the references Mo, MoO_2 and Mo_2C

Preliminary X-ray absorption spectroscopy experiments on the Mo K-edge have been performed to investigate the viability of that technique for the mixed carbides and to get further insights on the characteristics of the catalysts.[54]

The X-ray absorption near edge structure (XANES) at the Mo K-edge for Mo, MoO_2, Mo_2C, and the mono metallic carbides prepared by TPR and CR are shown in Figure 2.7. The spectra of standards are in line with those described literature.[55] The edge position of our CR and TPR samples coincide with that or Mo_2C indicating that both samples were in the carbide phase (which is in line with XRD, TPD-MS and TGA as discussed above). However, some difference in the edge features just above the edge at 20007.0 eV and 20023.4 eV are different for the Mo_2C and the supported samples. This indicates that the (electronic) properties of the supported carbides are not the same as those of bulk Mo_2C. The reason for this is currently under investigation.

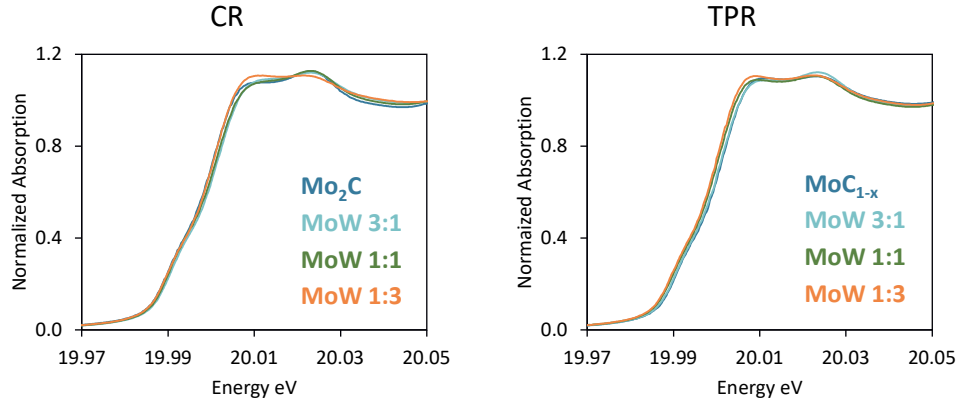

Figure 2. 8 Mo K-edge XANES spectra at room temperature Mo_2C and bimetallic MoW carbide (3:1, 1:1 and 1:3) samples.

The XANES spectra at the Mo K-edge of the monometallic Mo carbide and the bimetallic MoW carbides prepared by CR and TPR are shown in Figure 2.8. Since all samples display the same edge position which is representative for Mo_2C (Figure 2.7) we conclude that all bimetallic samples are fully carburized (within experimental error). Interestingly, the spectra of the bimetallic have a different intensity just above the main edge in comparison to the monometallic carbide for both synthesis methods. The most clearly visible difference was observed for the 1:3 (Mo:W) sample irrespective of the synthesis method. Thus, the addition of W into a Mo-carbide cluster affects the structural (and electronic) parameters of the material. Nevertheless a full understanding needs further (theoretical) investigation.

EXAFS

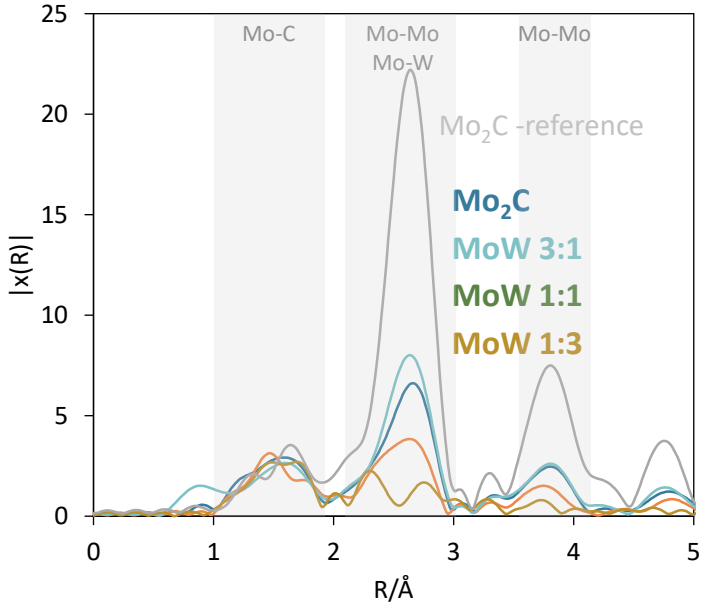

Figure 2. 9 Fourier transform (no phase shift correction) of k^3- weighted Mo EXAFS: Mo-ref, MoCNF, and mixed MoW with the ratio of 1:3, 1:1 and 3:1 (Mo:W)

We further studied the Mo carbide catalysts prepared via CR by EXAFS. The Fourier Transformations (FT) of the CR carburized samples and Mo_2C standards are plotted in Figure 2.9. Clearly three regions can be observed a small peak around 2.1 Å, a larger second peak around 2.9 Å and one around 4.2 Å. Compared the Mo_2C reference the intensity of the Mo-Mo contribution decreased indicating a decrease in Mo-Mo coordination number (for bulk Mo_2C 3 Mo-C at 2.1 Å, 12 Mo-Mo at 2.9 Å and 4.2 Å Mo-Mo at 2)[56] are expected for the supported nanoparticles. In addition the Mo-Mo contribution varies between the mixed samples indicating that Mo and W are indeed mixed in these sample. The virtual absence of a Mo-Mo contribution in the 1:3 and 3:1 sample indicate that destructive interference of the separate contributions to the overall EXAFS must have occurred (which will significantly complicate data fitting). The get a feeling of the fit quality Figure 2.10 show the fitting in k and R space for the 1:1 sample (the fit of the monometallic Mo carbide is given in Figure S2.15). The overall fitting results are shown in Table 2.1. The simulation may be considered satisfactory, since the parameters indicative of the quality of the fits, namely, R_{factor}, E^0, and σ^2 are in an acceptable range.[56]

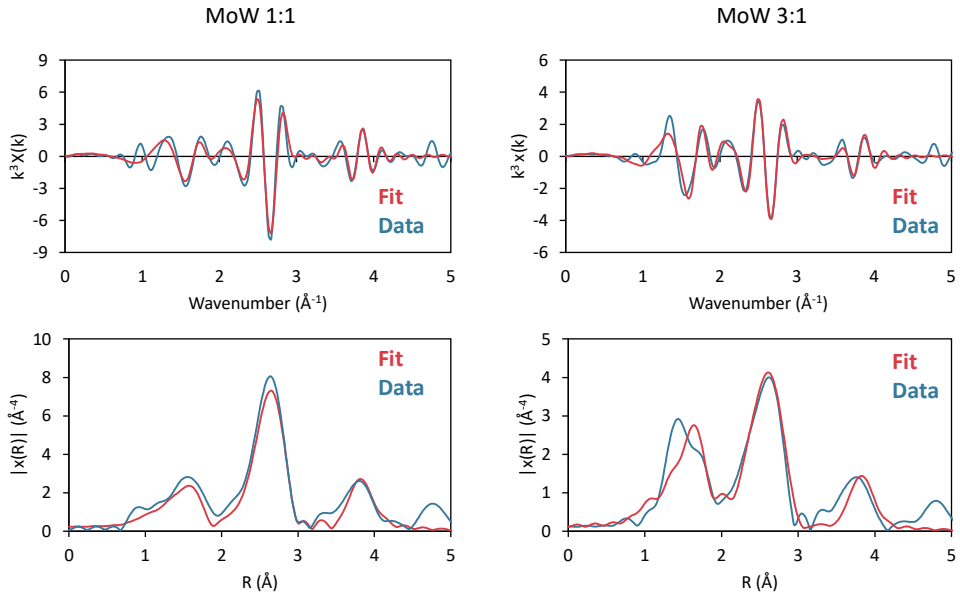

Figure 2.10 EXAFS oscillations (top) and k^3-weighted Fourier-transformed spectra (bottom) for the carburized MoW catalysts with 1:1 and 3:1 ratio

The coordination number of the monometallic Mo carbide nanoparticles is 3.8 for the first Mo-Mo shell and thus much smaller than that of the bulk Mo carbide reference (12.0 for the Mo-Mo shell) as expected. When adding W to the Mo carbide, the coordination number does decrease even more which is to be expected when part of the Mo is replaced by W. Nevertheless the coordination numbers cannot be fully explained yet. The coordination number of Mo-W for the mixed sample with a 3:1 and 1:1 is both around 1 which does not match the bulk value. Therefore some inhomogeneity is the samples can be expected though more simulations are needed to fully explain these coordination numbers. For the 1:3 sample no sensible fits could be obtained since (due to anti phase behavior) the Mo-Mo region does not contain any signals while the XANES does indicate that Mo and W are present. Nevertheless, these results indicate (again) that a mixed MoW phase on nanoscale level are formed and that EXAFS/XANES can be used to study these samples in detail.

Table 2.1 Preliminary fitting parameters of the CR carburized samples

	Samples	Scatterer	CN	Δ E_0 (eV)	R (Å)	Δσ² (Å²)	k-range	R-range	R-factor
CR	Mo	C	2.4 ± 0.5	-2 ± 1	2.11 ±0.00	0.003 ± 0.002	3.0 - 16.0	1.20 - 4.50	7%
		Mo	3.8 ± 0.8		2.95 ±0.03	0.007 ±0.001			
		Mo	1.4 ± 1.1		4.21 ±0.04	0.004 ± 0.004			
	MoW 3:1	C	2.3 ±0.4	-5 ± 1	2.10 ±0.01	0.004 ±0.002	3.0 - 16.0	1.25 - 4.50	6%
		Mo	1.0 ±0.3		2.96 ±0.01	0.002 ±0.001			
		W	0.9 ±0.3		2.94 ±0.02	0.003 ±0.004			
		Mo	1.0 ±0.8		4.19 ±0.02	0.004 ±0.003			
	MoW 1:1	C	2.1 ±0.6	-4 ± 1	2.09 ±0.01	0.003 ±0.003	3.0 - 16.0	1.35 - 4.50	4%
		Mo	2.2 ±0.4		2.94 ±0.01	0.003 ±0.001			
		W	1.0 ±0.3		2.93 ±0.01	0.004 ±0.002			
		Mo	1.6 ±0.9		4.17 ±0.02	0.004 ±0.003			

k^1-k^2-k^3-weigthed fit, S_0^2=1.0 (Fixed).

Catalytic performance

The catalytic performance of the prepared catalysts was evaluated for stearic acid conversion in a batch reactor (350 °C and 30 bar H_2), after 1 h. Please note that we found that above the used stirring rate of 800 rpm the reaction rate become independent of the stirring rate thus H_2 mass transfer did not play a significant role (see Figure S2.16). In addition mass transfer limitations due to differences in textual properties of the carbide catalysts (after the synthesis) were excused as we did not observe significant differences in textual properties, shown in Table S2.3.

Figure 2.11 displays the activities of the CR and TPR samples as function of composition. For the monometallic catalysts the Mo carbide catalysts (75 mol% (CR) or 85 mol% (TPR) conversion) exhibited superior activity compared to the W carbide catalysts (35 mol% (CR) 45 mol% (TPR) conversion) irrespective of the synthesis method. This is in line with activities reported by Gosselink et al. and Stellwagen et al.[39,57]

The bimetallic carbides are also active for fatty acid conversion. For the CR samples, their activity resembles that of W carbide. While for the TPR-synthesized mixed carbides the activity is more between that of the monometallic catalysts. Unlike what was previously reported,[17,18] we observed no enhanced catalytic activity for the bimetallic carbide catalysts. To exclude experimental issues these results were reproducible over repeated synthesis of these catalysts (see Supporting Information Figure S2.17).

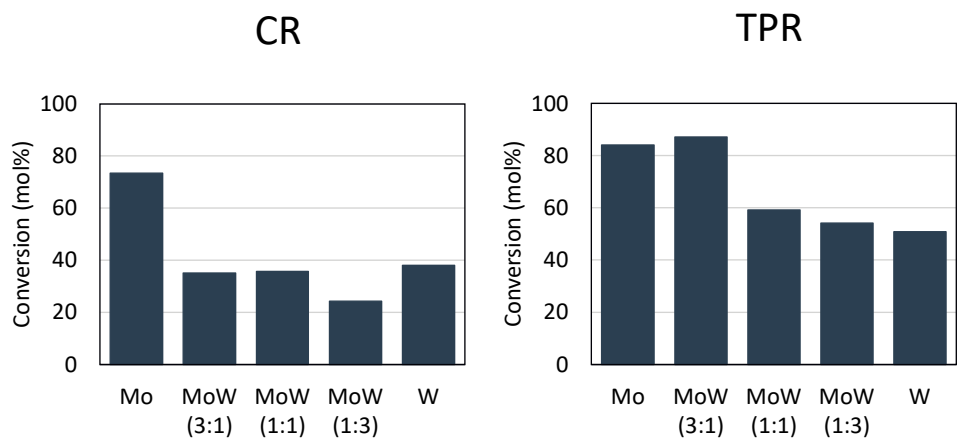

Figure 2.11 Stearic acid conversion over TPR-carburized (right) and CR-carburized (left) Mo, W and three mixed MoW carbide catalysts supported on CNF after 1 h (250 mg catalyst with metal loading of 0.9 mmol/g $_{catalyst}$, 2 g stearic acid, 350 °C, 50 ml solvent, 30 bar H_2).

In general, the TPR-synthesized carbide catalysts with the mainly cubic crystal structure and with smaller nanoparticles (3-4 nm) provided faster hydrodeoxygenation (on a weight basis) than the CR-synthesized carbide catalysts with the hexagonal structure and larger nanoparticle size (4-5 nm). The CR-prepared samples converted ~20-40 mol% of the stearic acid, while the TPR-prepared catalysts converted 50-85 mol%. It has previously been claimed for monometallic carbides that the cubic carbide phase is more active than the hexagonal phase.[8,50,58,59] This is in line with our results for the bimetallic catalysts and could explain the difference in activity between samples synthesized via TPR and CR as well.

Since the particle sizes of the TPR samples are slightly smaller (3-5 nm) compared to those of the CR prepared samples (4-6 nm) part of the increase in activity of the TPR samples can also be explained by the higher carbide surface area in the TPR samples. However, the activity increase is more than the surface area increases therefore we conclude that the difference in crystal structure also plays a role. Please note that these particle are too large for intrinsic particle size effects.[39,60]

The catalysts stability was tested respectively on the 1:1 Mo:W metal carbide catalysts. Subsequent experiments with one batch of carbide catalysts were conducted. After the reaction the catalyst was retrieved by rinsing the reaction solution and directly reused (run 2). The results displayed in Figure S2.18 show that the CR prepared catalysts are more stable than the TPR prepared catalysts.

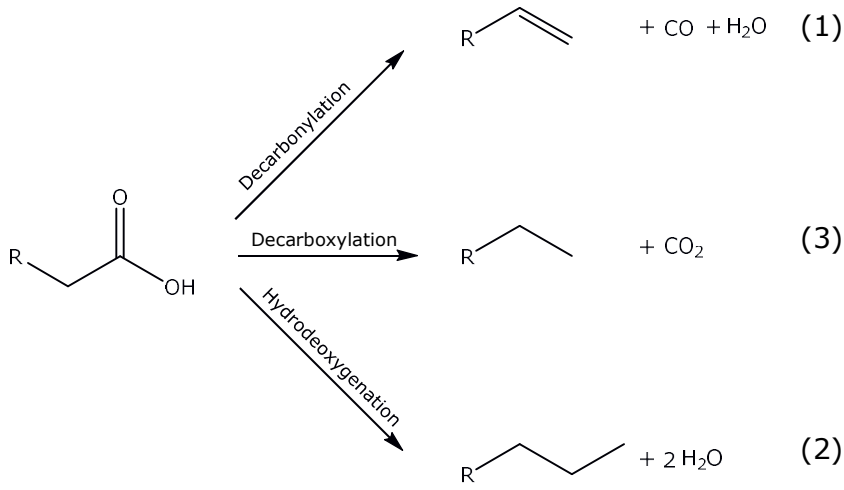

Scheme 2.1 Possible pathways for the deoxygenation of fatty acids

Depending on the reaction conditions and the catalysts, the deoxygenation of fatty acid can occur by different pathways (Scheme 2.1). The fatty acid can be decarbonylated and/or decarboxylated (DCO pathway (1) and (2)) yielding hydrocarbon chains with one carbon atom less as compared to the reactant. Another possibility is the hydrodeoxygenation (HDO) of the fatty acid, resulting in a hydrocarbon with the same chain lengths as the reactant. The conversion of stearic acid over Pd, Pt[61] and Mo and W oxide[43] catalysts goes primarily via de decarboxylation pathway and yields heptadecane. In contrast, the Mo and W carbide, have previously been reported, to convert stearic acid via the HDO route.[39,43,62,63] Figure 2.12 shows that the monometallic carbides and the mixed carbides mainly produce octadecane (C-18) suggesting that the majority of deoxygenation proceeds via the hydrodeoxygenation for all catalysts. Some C-17 products were also observed produced via a direct decarboxylation or decarbonylation (DCO) of the stearic acid indicating that some oxygen containing species were present as catalyst.[39] A direct comparison in selectivity between CR and TPR is not viable since the conversion levels for those catalysts were different. Nevertheless the selectivity of the mixed carbides is similar to that of the monometallic carbides which indicated that similar active sites were formed in the bimetallic catalysts as in the monometallic carbides.

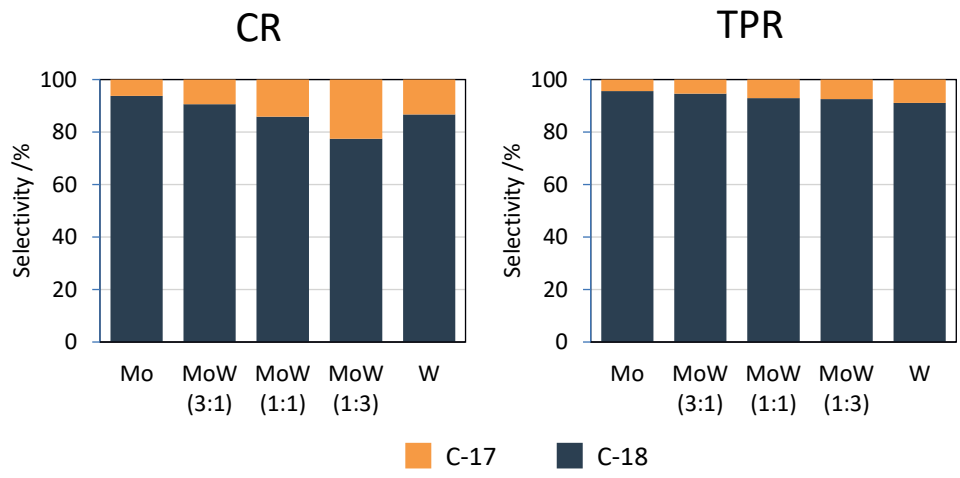

Figure 2.12 HDO and DCO selectivity of TPR-carburized (right) and CR-carburized (left) Mo, W and three mixed MoW carbide catalysts supported on CNF after 1 h (250 mg catalyst with metal loading of 0.9 mmol/g $_{catalyst}$, 2 g stearic acid, 350 °C, 50 ml solvent, 30 bar H_2).

Conclusions

In this study, we demonstrated that a CNF-supported mixed-MoW carbide phase can be synthesized via the CR method and via the TPR method. TGA and TPD-MS were successfully used to show the formation of a mixed MoW phase in CR-prepared samples. For the TPR-prepared samples that comparison could not be made due to the too complex carburization processes. STEM-EDX analysis, however, showed the formation of mixed MoW nanoparticles for catalysts prepared via either method. XANES and EXAFS data confirm these.

The carbides were found to be well distributed over the support with an overall composition close to the intended ones. However, the Mo:W ratio of the nanoparticles varied, which indicates that the synthesized mixed-metal carbides were not completely homogenous with respect to composition at the particle level.

Irrespective of the sample composition and synthesis method the carbides prefer the hydrodeoxygenation pathway with a minor contribution (10%) of the decarbonylation/decarboxylation pathway. The catalytic activity of the mixed-metal carbides falls between that of the two monometallic catalysts while the TPR-prepared samples were more active for the hydrodeoxygenation of fatty acids relative to CR-prepared samples. The higher activity of the TPR-prepared samples was related to the presence of the cubic carbide phase and partially to the smaller nanoparticles sizes (higher surface area).

Acknowledgement

Acknowledgement is made to the Dutch Research Council (NWO, 729.004.022) for financial support. The authors gratefully thank Susan Witte for assistance with the GC-FID measurements. The authors also thank Koen Draijer and Merijn Maas for executing preliminary research during their BSc in Biotechnology at Wageningen University that led to this study.

References

(1) Shim, K.; Lee, W.-C.; Heo, Y.-U.; Shahabuddin, M.; Park, M.-S.; Hossain, M. S. A.; Kim, J. H. Rationally designed bimetallic Au@ Pt nanoparticles for glucose oxidation. *Scientific reports* **2019,** *9* (1), 1.

(2) Tao, F. F.; Zhang, S.; Nguyen, L.; Zhang, X. Action of bimetallic nanocatalysts under reaction conditions and during catalysis: evolution of chemistry from high vacuum conditions to reaction conditions. *Chemical Society Reviews* **2012,** *41* (24), 7980.

(3) Alonso, D. M.; Wettstein, S. G.; Dumesic, J. A. Bimetallic catalysts for upgrading of biomass to fuels and chemicals. *Chemical Society Reviews* **2012,** *41* (24), 8075.

(4) Robinson, A.; Ferguson, G. A.; Gallagher, J. R.; Cheah, S.; Beckham, G. T.; Schaidle, J. A.; Hensley, J. E.; Medlin, J. W. Enhanced Hydrodeoxygenation of m-Cresol over Bimetallic Pt–Mo Catalysts through an Oxophilic Metal-Induced Tautomerization Pathway. *ACS Catalysis* **2016,** *6* (7), 4356.

(5) Diehl, F.; Khodakov, A. Y. Promotion of cobalt Fischer-Tropsch catalysts with noble metals: a review. *Oil & Gas Science and Technology-Revue de l'IFP* **2009,** *64* (1), 11.

(6) Lee, J.; Kim, Y. T.; Huber, G. W. Aqueous-phase hydrogenation and hydrodeoxygenation of biomass-derived oxygenates with bimetallic catalysts. *Green Chemistry* **2014,** *16* (2), 708.

(7) Huber, G. W.; Shabaker, J. W.; Evans, S. T.; Dumesic, J. A. Aqueous-phase reforming of ethylene glycol over supported Pt and Pd bimetallic catalysts. *Applied Catalysis B: Environmental* **2006,** *62* (3-4), 226.

(8) Macedo, L. S.; Oliveira, R. R.; van Haasterecht, T.; Teixeira da Silva, V.; Bitter, H. Influence of synthesis method on molybdenum carbide crystal structure and catalytic performance in stearic acid hydrodeoxygenation. *Applied Catalysis B: Environmental* **2019,** *241*, 81.

(9) Führer, M.; van Haasterecht, T.; Bitter, J. Molybdenum and tungsten carbides can shine too. *Catalysis Science & Technology* **2020**.

(10) Levy, R. B.; Boudart, M. Platinum-Like Behavior of Tungsten Carbide in Surface Catalysis. *Science* **1973,** *181* (4099), 547.

(11) Oyama, S. Preparation and catalytic properties of transition metal carbides and nitrides. *Catal Today* **1992,** *15* (2), 179.

(12) Zhao, Z.; Zhu, Z.; Wang, F.; Li, S.; Bao, X.; Zhang, L.; Lin, S.; Yang, Y. Bimetallic carbides embedded in heteroatom-doped carbon nanotubes for efficient electrocatalytic hydrogen evolution reaction and high-performance lithium storage. *Chemical Engineering Journal* **2021,** *415*, 128885.

(13) Tran, C.-C.; Mohan, O.; Banerjee, A.; Mushrif, S. H.; Kaliaguine, S. A Combined Experimental and DFT Investigation of Selective Hydrodeoxygenation of Guaiacol over Bimetallic Carbides. *Energy & Fuels* **2020,** *34* (12), 16265.

(14) Tran, C.-C.; Akmach, D.; Kaliaguine, S. Hydrodeoxygenation of vegetable oils over biochar supported bimetallic carbides for producing renewable diesel under mild conditions. *Green Chemistry* **2020**.

(15) Li, H.; Hu, M. H.; Zhang, L. Y.; Huo, L. L.; Jing, P.; Liu, B. C.; Gao, R.; Zhang, J.; Liu, B. Hybridization of Bimetallic Molybdenum-Tungsten Carbide with Nitrogen-Doped Carbon: A Rational Design of Super Active Porous Composite Nanowires with Tailored Electronic Structure for Boosting Hydrogen Evolution Catalysis. *Advanced Functional Materials* **2020,** *30* (40).

(16) Gavrilova, N.; Myachina, M.; Dyakonov, V.; Nazarov, V.; Skudin, V. Synthesis of Microporous Mo2C-W2C Binary Carbides by Thermal Decomposition of Molybdenum-Tungsten Blues. *Nanomaterials* **2020,** *10* (12).

(17) Fu, Q.; Peng, B. X.; Masa, J.; Chen, Y. T.; Xia, W.; Schuhmann, W.; Muhler, M. Synergistic Effect of Molybdenum and Tungsten in Highly Mixed Carbide Nanoparticles as Effective Catalysts in the Hydrogen Evolution Reaction under Alkaline and Acidic Conditions. *Chemelectrochem* **2020,** *7* (4), 983.

(18) Tran, C. C.; Hang, Y. L.; Garcia-Perez, M.; Kaliaguine, S. Synergistic effect of Mo-W carbides on selective hydrodeoxygenation of guaiacol to oxygen-free aromatic hydrocarbons. *Catalysis Science & Technology* **2019,** *9* (6), 1387.

(19) Mehdad, A.; Jentoft, R. E.; Jentoft, F. C. Single-phase mixed molybdenum-tungsten carbides: Synthesis, characterization and catalytic activity for toluene conversion. *Catal Today* **2019,** *323*, 112.

(20) Lin, L. F.; Chen, M.; Wu, L. M. Synthesis of Molybdenum-Tungsten Bimetallic Carbide Hollow Spheres as pH-Universal Electrocatalysts for Efficient Hydrogen Evolution Reaction. *Advanced Materials Interfaces* **2018,** *5* (23).

(21) Mehdad, A.; Jentoft, R. E.; Jentoft, F. C. Passivation agents and conditions for Mo2C and W2C: Effect on catalytic activity for toluene hydrogenation. *Journal of Catalysis* **2017,** *347*, 89.

(22) Kislov, V. R.; Skudin, V. V.; Adamu, A. New bimetallic Mo2C-WC/Al2O3 membrane catalysts in the dry reforming of methane. *Kinet Catal+* **2017,** *58* (1), 73.

(23) Xiao, P.; Ge, X.; Wang, H.; Liu, Z.; Fisher, A.; Wang, X. Novel Molybdenum Carbide-Tungsten Carbide Composite Nanowires and Their Electrochemical Activation for Efficient and Stable Hydrogen Evolution. *Advanced Functional Materials* **2015,** *25* (10), 1520.

(24) Nguyen, T. H.; Nguyen, T. V.; Lee, Y. J.; Safinski, T.; Adesina, A. A. Structural evolution of alumina supported Mo-W carbide nanoparticles synthesized by precipitation from homogeneous solution. *Materials Research Bulletin* **2005,** *40* (1), 149.

(25) Li, X.; Ma, D.; Chen, L.; Bao, X. Fabrication of molybdenum carbide catalysts over multi-walled carbon nanotubes by carbothermal hydrogen reduction. *Catalysis Letters* **2007,** *116* (1-2), 63.

(26) Wu, K.; Yang, C.; Zhu, Y.; Wang, J.; Wang, X.; Liu, C.; Liu, Y.; Lu, H.; Liang, B.; Li, Y. Synthesis-controlled α-and β-molybdenum carbide for base-promoted transfer hydrogenation of lignin to aromatic monomers in ethanol. *Ind Eng Chem Res* **2019,** *58* (44), 20270.

(27) Alaba, P. A.; Abbas, A.; Huang, J.; Daud, W. M. A. W. Molybdenum carbide nanoparticle: Understanding the surface properties and reaction mechanism for energy production towards a sustainable future. *Renewable and Sustainable Energy Reviews* **2018,** *91*, 287.

(28) Frank, B.; Friedel Ortega, K.; Girgsdies, F.; Huang, X.; Schlögl, R.; Trunschke, A. CNT supported MoxC catalysts: Impact of loading and carburization parameters. *ChemCatChem* **2013,** *5* (8), 2296.

(29) Lemaître, J.; Vidick, B.; Delmon, B. Control of the catalytic activity of tungsten carbides: I. Preparation of highly dispersed tungsten carbides. *Journal of Catalysis* **1986,** *99* (2), 415.

(30) Oshikawa, K.; Nagai, M.; Omi, S. Characterization of molybdenum carbides for methane reforming by TPR, XRD, and XPS. *J Phys Chem B* **2001,** *105* (38), 9124.

(31) Löfberg, A.; Seyfried, L.; Blehen, P.; Decker, S.; Bastin, J. M.; Frennet, A. Pore structure of bulk tungsten carbide powder catalysts. *Catalysis letters* **1995,** *33* (1), 165.

(32) Nguyen, T. H.; Adesina, A. A.; Yue, E. M. T.; Lee, Y. J.; Khodakov, A.; Brungs, M. P. Synthesis of Mo-W carbide via propane carburization of the precursor sulfide: Kinetic analysis. *J Chem Technol Biot* **2004,** *79* (3), 286.

(33) Decker, S.; Lofberg, A.; Bastin, J. M.; Frennet, A. Study of the preparation of bulk tungsten carbide catalysts with C2H6/H-2 and C2H4/H-2 carburizing mixtures. *Catalysis Letters* **1997,** *44* (3-4), 229.

(34) Wu, Y.; Dang, J.; Lv, Z.; Zhang, S.; Lv, X.; Bai, C. In *Minerals, Metals and Materials Series*, 2018; Vol. Part F12.

(35) Chen, X. Z.; Chen, X.; Qi, J.; Liang, C. H. Self-assembly synthesis of lamellar molybdenum carbides with controllable phases for hydrodeoxygenation of diphenyl ether. *MOLECULAR CATALYSIS* **2020,** *492*.

(36) Ochoa, E.; Torres, D.; Pinilla, J. L.; Suelves, I. Influence of carburization time on the activity of Mo2C/CNF catalysts for the HDO of guaiacol. *Catal Today* **2019**.

(37) Leclercq, L.; Provost, M.; Pastor, H.; Leclercq, G. Catalytic Properties of Transition-Metal Carbides .2. Activity of Bulk Mixed Carbides of Molybdenum and Tungsten in Hydrocarbon Conversion. *Journal of Catalysis* **1989,** *117* (2), 384.

(38) Leclercq, L.; Provost, M.; Pastor, H.; Grimblot, J.; Hardy, A. M.; Gengembre, L.; Leclercq, G. Catalytic properties of transition metal carbides: I. Preparation and physical characterization of bulk mixed carbides of molybdenum and tungsten. *Journal of Catalysis* **1989,** *117* (2), 371.

(39) Stellwagen, D. R.; Bitter, J. H. Structure–performance relations of molybdenum-and tungsten carbide catalysts for deoxygenation. *Green Chemistry* **2015,** *17* (1), 582.

(40) Puello-Polo, E.; Brito, J. L. Effect of the type of precursor and the synthesis method on thiophene hydrodesulfurization activity of activated carbon supported Fe-Mo, Co-Mo and Ni-Mo carbides. *Journal of Molecular Catalysis A: Chemical* **2008,** *281* (1-2), 85.

(41) Han, J.; Duan, J.; Chen, P.; Lou, H.; Zheng, X.; Hong, H. Nanostructured molybdenum carbides supported on carbon nanotubes as efficient catalysts for one-step hydrodeoxygenation and isomerization of vegetable oils. *Green Chemistry* **2011,** *13* (9), 2561.

(42) De la Puente, G.; Centeno, A.; Gil, A.; Grange, P. Interactions between molybdenum and activated carbons on the preparation of activated carbon-supported molybdenum catalysts. *Journal of colloid and interface science* **1998,** *202* (1), 155.

(43) Gosselink, R. W.; Stellwagen, D. R.; Bitter, J. H. Tungsten-Based Catalysts for Selective Deoxygenation. *Carbohydrate research* **2013,** *52* (19), 5089.

(44) Blanco, E.; Aguirre-Abarca, D. A.; de León, J. N. D.; Escalona, N. Relevant aspects of the conversion of guaiacol as a model compound for bio-oil over supported molybdenum oxycarbide catalysts. *New Journal of Chemistry* **2020,** *44* (28), 12027.

(45) Matus, E.; Khitsova, L.; Efimova, O.; Yashnik, S.; Shikina, N.; Ismagilov, Z. Preparation of carbon nanotubes with supported metal oxide nanoparticles: effect of metal precursor on thermal decomposition behavior of the materials. *Eurasian Chemico-Technological Journal* **2019,** *21* (4), 303.

(46) Kugler, E. L.; Clark, C. H.; Wright, J. H.; Dadyburjor, D. B.; Hanson, J. C.; Song, Z.; Cai, T.; Hrbek, J. Preparation, interconversion and characterization of nanometer-sized molybdenum carbide catalysts. *Topics in catalysis* **2006,** *39* (3-4), 257.

(47) Jongerius, A. L.; Gosselink, R. W.; Dijkstra, J.; Bitter, J. H.; Bruijnincx, P. C. A.; Weckhuysen, B. M. Carbon Nanofiber Supported Transition-Metal Carbide Catalysts for the Hydrodeoxygenation of Guaiacol. *ChemCatChem* **2013,** *5* (10), 2964.

(48) Lewandowski, M.; Szymańska-Kolasa, A.; Sayag, C.; Djéga-Mariadassou, G. Activity of Molybdenum and Tungsten oxycarbides in hydrodenitrogenation of carbazole leading to isomerization secondary reaction of bicyclohexyl. Results using bicyclohexyl as feedstock. *Applied Catalysis B: Environmental* **2019**, 118239.

(49) Hugosson, H. W.; Jansson, U.; Johansson, B.; Eriksson, O. Phase stability diagrams of transition metal carbides, a theoretical study. *Chemical Physics Letters* **2001,** *333* (6), 444.

(50) Yang, Q.; Sun, K.; Xu, Y.; Ding, Z.; Hou, R. Tuning crystal phase of molybdenum carbide catalyst to induce the different selective hydrogenation performance. *Applied Catalysis A: General* **2022,** *630*, 118455.

(51) Li, Z. C.; Chen, C. H.; Zhan, E. S.; Ta, N.; Li, Y.; Shen, W. J. Crystal-phase control of molybdenum carbide nanobelts for dehydrogenation of benzyl alcohol. *Chem Commun* **2014,** *50* (34), 4469.

(52) Bouchy, C.; Schmidt, I.; Anderson, J. R.; Jacobsen, C. J. H.; Derouane, E. G.; Derouane-Abd Hamid, S. B. Metastable fcc α-MoC(1-x) supported on HZSM5: Preparation and catalytic performance for the non-oxidative conversion of methane to aromatic compounds. *Journal of Molecular Catalysis A: Chemical* **2000,** *163* (1-2), 283.

(53) dos Santos Politi, J. R.; Vines, F.; Rodriguez, J. A.; Illas, F. Atomic and electronic structure of molybdenum carbide phases: bulk and low Miller-index surfaces. *Physical Chemistry Chemical Physics* **2013,** *15* (30), 12617.

(54) Siepen, K.; Bönnemann, H.; Brijoux, W.; Rothe, J.; Hormes, J. EXAFS/XANES, chemisorption and IR investigations of colloidal Pt/Rh bimetallic catalysts. *Applied organometallic chemistry* **2000,** *14* (10), 549.

(55) Lee, J. S.; Yie, J. E. An XANES study of carbides of molybdenum and tungsten. *Korean Journal of Chemical Engineering* **1991,** *8* (3), 164.

(56) Rocha, A. S.; Da Silva, V. T.; Eon, J. G.; De Menezes, S. M. C.; Faro Jr, A. C.; Rocha, A. B. Characterization by27Al NMR, X-ray absorption spectroscopy, and density functional theory techniques of the species responsible for benzene hydrogenation in Y zeolite-supported carburized molybdenum catalysts. *J Phys Chem B* **2006,** *110* (32), 15803.

(57) Gosselink, R. W.; Hollak, S. A. W.; Chang, S. W.; Van Haveren, J.; De Jong, K. P.; Bitter, J. H.; Van Es, D. S. Reaction pathways for the deoxygenation of vegetable oils and related model compounds. *ChemSusChem* **2013,** *6* (9), 1576.

(58) Choi, J.-S.; Bugli, G.; Djéga-Mariadassou, G. Influence of the Degree of Carburization on the Density of Sites and Hydrogenating Activity of Molybdenum Carbides. *Journal of Catalysis* **2000,** *193* (2), 238.

(59) McCrea, K. R.; Logan, J. W.; Tarbuck, T. L.; Heiser, J. L.; Bussell, M. E. Thiophene hydrodesulfurization over alumina-supported molybdenum carbide and nitride catalysts: Effect of Mo loading and phase. *Journal of Catalysis* **1997,** *171* (1), 255.

(60) Coulter, K.; Xu, X.; Goodman, D. W. Structural and catalytic properties of model supported nickel catalysts. *The Journal of Physical Chemistry* **1994,** *98* (4), 1245.

(61) Snåre, M.; Kubic˘kova, I.; Mäki-Arvela, P.; Eränen, K.; Murzin, D. Y. Heterogeneous catalytic deoxygenation of stearic acid for production of biodiesel. *Ind Eng Chem Res* **2006,** *45* (16), 5708.

(62) Hollak, S. A. W.; Gosselink, R. W.; van Es, D. S.; Bitter, J. H. Comparison of Tungsten and Molybdenum Carbide Catalysts for the Hydrodeoxygenation of Oleic Acid. *Acs Catalysis* **2013,** *3* (12), 2837.

(63) Qin, Y.; Chen, P.; Duan, J. Z.; Han, J. X.; Lou, H.; Zheng, X. M.; Hong, H. P. Carbon nanofibers supported molybdenum carbide catalysts for hydrodeoxygenation of vegetable oils. *Rsc Advances* **2013,** *3* (38), 17485.

Supporting Information

Carbide catalyst synthesis

In this study, the main two methods to prepare carbon nanofiber-supported Mo carbides, W carbides and mixed MoW carbides were investigated, namely carbothermal reduction (CR) and temperature programmed reaction (TPR).

In the CR synthesis, the carbon support containing the metal precursor is heated in an inert atmosphere and the carbon from the support is utilized as reduction and carburization agent. The synthesis pathway of Mo carbides with the use of a carbon-supported ammonium heptamolybdate (AHM) precursor has been studied before and takes place via several steps including precursor decomposition, oxide formation/reduction, and carburization.[S1-5] By contrast, the synthesis of W carbides from ammonium metatungstate (AMT) has been studied less[S1,6], while no reports are available for the supported synthesis of mixed MoW carbides.

During the TPR synthesis, the precursor (AHM or AMT) supported on CNF is heated in an atmosphere with a carbon-containing gas (in our case, methane) and hydrogen. The TPR synthesis of both W carbides and Mo carbides has been previously studied. [S2,7-21] Also in TPR, the formation of the carbides from the precursors takes place via several steps including precursor decomposition, oxide formation/reduction, and carburization.[S2,9,12,13,15,16] However, these earlier studies were done on bulk samples (not on the nanoscale) or with different support materials.

In order to identify and compare the carburization temperature of the monometallic and bimetallic samples, we analyzed the synthesis pathway of the carbides in situ with both TPD-MS and TGA and ex situ with XRD. During precursor decomposition, oxide formation/reduction and carbide formation, different gases evolve and changes in mass and crystal structure occur. TPD-MS gives information on the evolved gases and especially the temperature at which CO evolves gives information on the carburization temperature.[S4,5] TGA is a technique used to investigate the mass losses during the different synthesis steps (and analyze whether these losses correspond to the theoretical weight losses in the assumed reactions). With XRD, we can follow the change in crystal structure during the formation of the oxides and carbides.

Carbothermal reduction synthesis (CR)

As we stated in the main paper, we used TPD-MS, TGA and XRD to follow the CR synthesis of monometallic and bimetallic Mo and W carbides. For comparison, we also prepared and analyzed

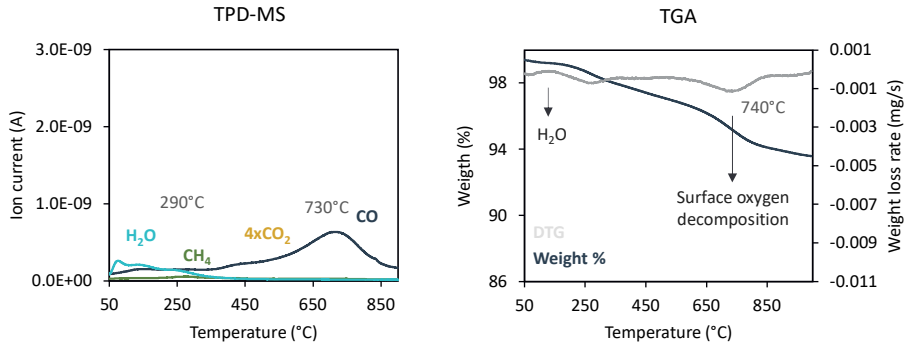

Figure S2.1 TPD-MS (left) and TGA (right) on CNF heated to 900 ˚C under inert gas.

a physical mixture of the monometallic carbides and obtained TGA and TPD-MS data for the bare CNF.

Figure S2.1 shows the TPD-MS and TGA results for the CNF support without any precursors during the CR treatment. The quantity of all measured gases (H_2O, CO_2 and CO) was lower than for the samples with metal precursors (vide infra); see Figure S2.2 and S2.3. The main CO_2 peak is located at 290 ˚C and the amount of evolved CO_2 decreases with increasing temperature. The main CO peak occurs at 730 ˚C. This release of CO_2 and CO is due to the loss of different types of surface oxygen groups from the CNF.[S22] A similar trend is visible in the TGA results. The CNF lost 6 wt% in total, which is significantly less than the weight loss for the samples with metal precursors (~12 wt%, vide infra). The main weight loss occurred at 740 ˚C and is due to the decomposition of surface oxygen groups of the CNF.[S23]

TPD-MS analysis was conducted by heating the impregnated samples under inert gas (N_2). Figure S2.2 shows the evolution of CO (m/z=28), H_2O (m/z=18), NH_3 (m/z=16) and CO_2 (m/z=44, x4) as a function of temperature. All samples show a H_2O peak at 100 ˚C and coinciding H_2O and NH_3 peaks at 250 ˚C. For monometallic Mo, a clear CO_2 peak is visible at 450 ˚C and again at 680 ˚C. These same peaks can also be identified in the image for the physical mixture, but not for the monometallic W sample. The graphs for the bimetallic catalysts show an increasing release of CO_2 with increasing temperature, but without the discrete peak as seen for the Mo sample. At temperatures above 650 ˚C, a large amount of CO is evolved for all catalysts. For monometallic Mo, this CO evolvement occurred at 680 ˚C; it took place at 770 ˚C for monometallic W. The CO peak of the Mo sample is sharper than that of the W sample, indicating a faster transformation. The CO evolution of the bimetallic catalyst occurs at a temperature that lies between the temperatures for each of the monometallic carbides (namely at 690 ˚C, 700 ˚C and 750 ˚C for a

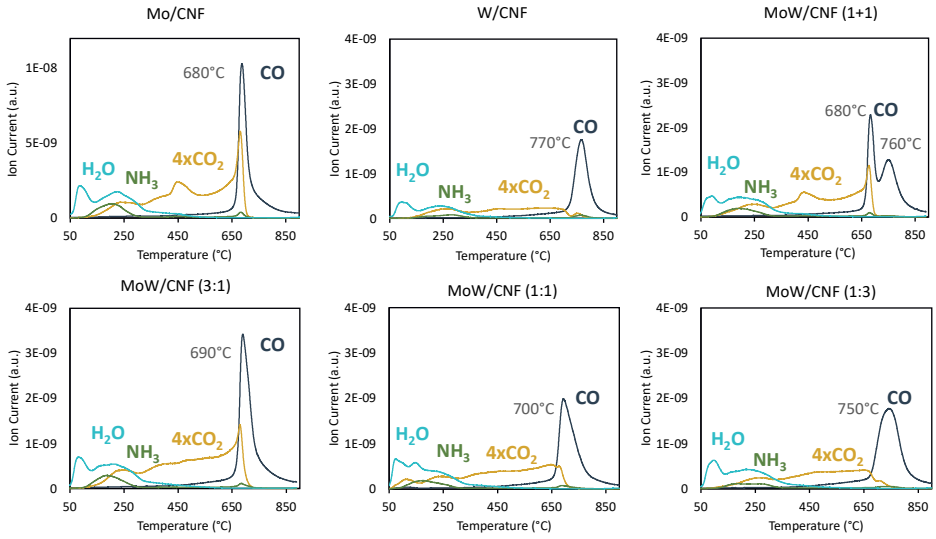

Figure S2.2 TPD-MS spectra of the carbothermal reduction of AHM (Mo), AMT (W) and a mixture of AHM/AMT (MoW) supported on carbon nanofibers exposed to 900 ℃, 5 ℃/min under N_2.

Mo:W ratio of 3:1, 1:1 and 1:3, respectively). This contrasts with what can be seen for the physical mixture (Figure S2.2, upper right), namely two distinctly separate CO peaks at 680 ˚C and 760 ˚C, corresponding to the single peaks observed for the monometallic Mo and W samples, respectively. In addition to the CO, the simultaneous evolution of some CO_2 is observed for all samples except for the monometallic W sample.

In addition, TGA was used to study the CR process. Figure S2.3 shows the weight loss and the weight loss rate (DTG) that occurred during heating to 1000 ˚C under N_2. All of the catalysts show a similar weight loss profile; an initial weight loss of 0.7 wt% at 100 ˚C, which is followed by a weight loss of ~2 wt% at 250 ˚C. At 400 to 550 ˚C, a weight loss of 1.4 wt% and 1.0 wt% is observed for the monometallic Mo sample and the physical mixture, respectively. The other catalysts show a slow decrease in weight over this temperature range (~0.7 wt%). The weight loss occuring at 710 ˚C for the Mo carbide and 810 ˚C for the W carbide was ~5.5 wt%. The DTG peaks for the bimetallic carbides lie between those of the two monometallic carbides, except for the physical mixture which shows two peaks, at 730 ˚C and 810 ˚C. The reaction was assumed to be completed at 1000 ˚C, with an overall weight loss of ~10 wt%.

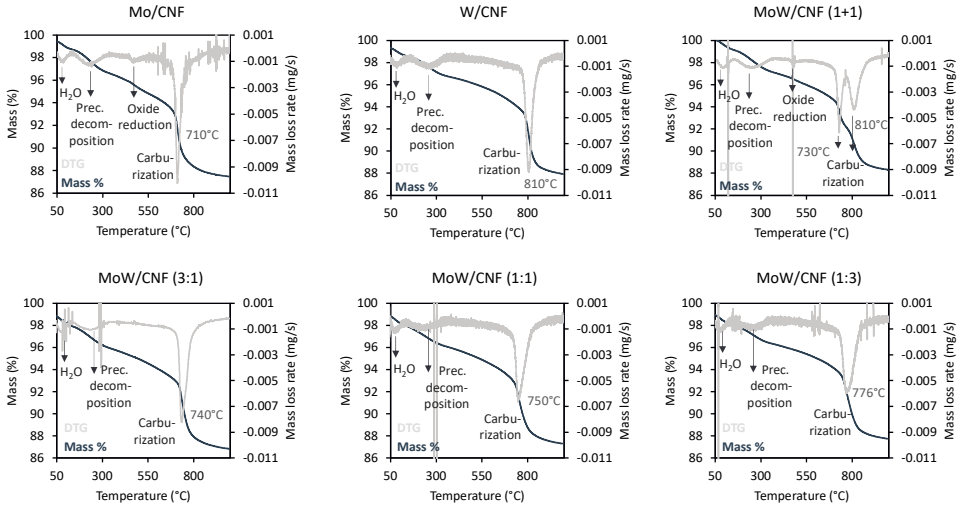

Figure S2.3 Thermogravimetric analysis of the carbothermal reduction *of the oxide precursors of Mo_2C, W_2C and the MoW carbide under inert gas, heated up to 1000 °C.*

Figure S2.4 displays the X-ray diffraction patterns of the two monometallic (Mo and W) carbides and the bimetallic carbide (ratio of 1:1). These CNF-supported catalysts were treated under N_2 up to 660 ˚C, 740 ˚C, 820 ˚C, 860 ˚C and 900 ˚C and examined ex situ. The signals at a 2θ of 28˚ and 43˚ represent the (002) and (101) reflections of the graphitic CNF[S24] and are present in all patterns. At 660 ˚C, the Mo carbide sample shows diffraction lines at 2θ values of 36.8˚, 49.4˚, 53.3˚, 60.2˚, 66.2˚ and 78.6˚, characteristic for the tetragonal MoO_2 phase, while the W carbide shows reflections at a 2θ of 23.6˚ and 33.3˚, corresponding to the cubic WO_3 phase. The pattern

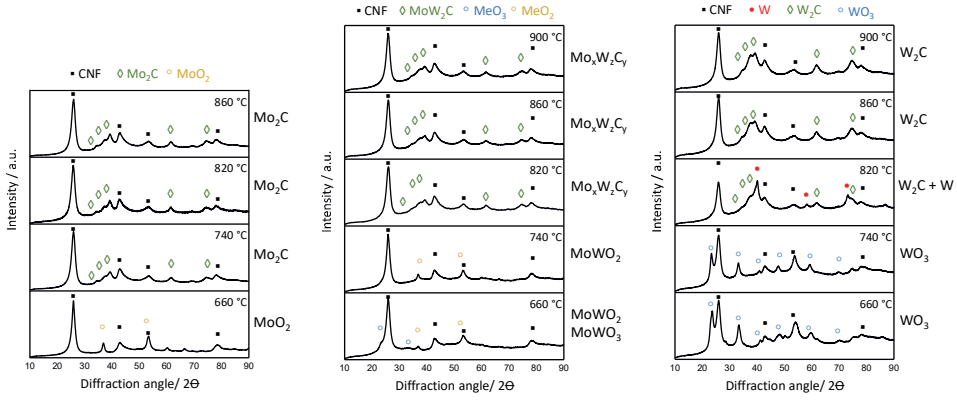

Figure S2.4 XRD results for Mo_2C/CNF (left), MoWC/CNF (center) and W_2C/CNF (right) during synthesis via CR in N_2.

of the bimetallic sample treated at 660 °C shows reflections that fit that of the monometallic dioxide and the trioxide phase (2θ of 23.6˚, 33.2˚, 36.9˚ and 53.32θ). Note that both the dioxide and trioxide patterns of monometallic Mo and W have near identical diffraction patterns. At 740 ˚C, the reflections of the cubic trioxide disappear and only the reflections of tetragonal dioxide are observed. (See also "Evaluation of the XRD carbide reflections".) At higher temperatures, diffractions at 34˚, 37.5˚, 39˚, 61.5˚, and 74.5˚ (2θ), characteristic for the hexagonal MeC_2 phase, appear for all the catalysts. The transformation of the MoO_2 to the Mo_2C occurs at 660 to 740 ˚C, while for the W and mixed samples, this transformation occurs between 740 and 820 ˚C. In addition to these reflections, we also saw reflections at a 2θ of 40.1˚, which can be assigned to cubic W carbide; these reflections were no longer observed after heating the sample to 860 ˚C.

Scheme S2.1 summarizes the synthesis pathway for CR of the monometallic systems.

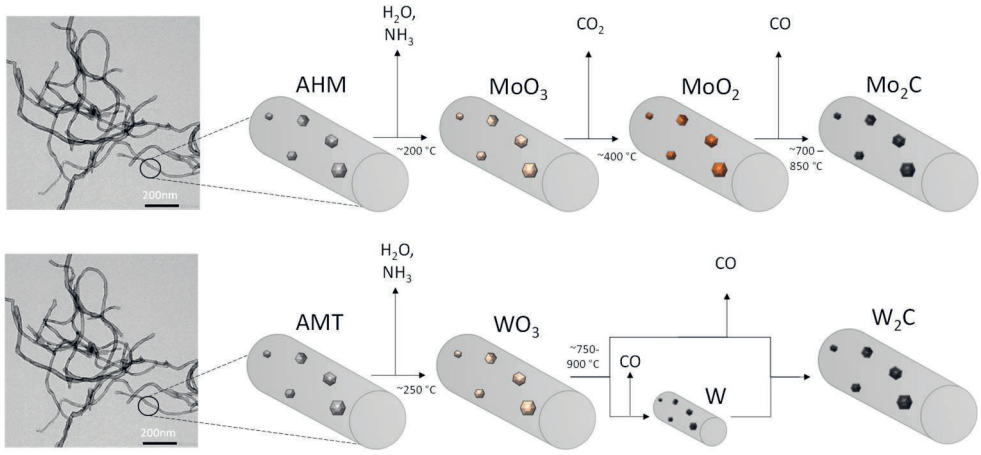

Scheme S2.1 General steps for carbothermal reduction (CR) of impregnated ammonium heptamolybdate (AHM) and ammonium metatungstate (ATM).[S1-5] TEM image on the left show pure CNF.

The first step during the CR is the release of absorbed water at 100 ˚C, which is observed with TGA (weight change of 0.7 wt%) and TPD-MS (H_2O evolution). Next, the breakdown of the ammonium heptamolybdate (AHM) or/and the ammonium metatungstate (AMT) complex at 250 ˚C is correlated to the evolution of NH_3 and H_2O and the measured weight loss of ~2 wt%. Here, the salt is transformed into its trioxide form (MeO_3). These two steps were observed for the monometallic materials as well for the bimetallic systems at similar temperatures.

Table S2.1 compares the measured weight losses with the theoretical (calculated) weight losses during each step (e.g. water evaporation, precursor decomposition, oxide, and carbide

reduction). For the Mo sample, we calculated that there would be a weight loss of 2.7 wt% during the transformation (Mo Precursor → MoO_3), which is lower than the measured value of 1.97 wt%. For the W sample, a weight loss of 1.6 wt% was measured and 1.13 wt% was calculated for the transformation. The slightly higher measured mass changes in comparison with the calculated values is due to mass loss related to the decomposition of oxygen groups on the support's surface (see Figure S2.1). This decomposition does not necessarily occur in proportion to the changes in the precursor, since these groups function as anchoring sites for the metal oxides/carbides.

Table S2.1 Expected and measured weight losses during the CR carburization of the monometallic Mo and W materials.

	Calculated (wt%)	**Measured (wt%)**	**Temp. range (˚C)**
Precursor decomposition:			
$(NH_4)_6Mo_7O_{24}$ *$4H_2O$→ $7MoO_3$ + $7H_2O$ (+ $6NH_3$)	2.67	1.97	150-320
$(NH_4)_6H_2W_{12}O_{40}$ *$4H_2O$→ $12WO_3$ + $8H_2O$ (+ $6NH_3$)	1.58	1.60	140-320
Oxide reduction:			
$2MoO_3$+C_{CNF} → $2MoO_2$ + CO_2	2.29	2.13	350-600
Carburization:			
$2MoO_2$+ 5C → Mo_2C + 4CO	4.10	5.50	650-800
$2WO_3$+7C → W_2C + 6CO (OR: WO_3 → W → WC_2)	5.08	5.62	750-900

From previous studies, it is known that after the formation of the MoO_3, the oxide is further reduced to its MoO_2 form before carburization.[S1,3-5,25-27] We observed a CO_2 peak and a significant weight change (of 1.4 wt%) for the Mo carbide (and for the physical mixture) at ~450 ˚C, which we attribute to the reduction of MoO_3 to MoO_2. These weight changes are in reasonable agreement with the calculated values of 1.87 wt% for Mo. In contrast with what we found for Mo, we detected neither a significant CO_2 peak nor a weight change for the W sample in this temperature range. These observations are also in line with the XRD data, which confirmed the presence of MoO_2 (at 660 °C) but contained no reflections attributable to WO_2. Thus, it appears that MoO_3 is reduced to MoO_2 whereas the WO_3 is not reduced to WO_2. The bimetallic carbide samples behave like the Mo carbide sample. Although no notable peak in the weight change rate was observed by TGA in the expected temperature range, the TPD-MS and XRD results suggest that the bimetallic system consisted of a mixed MeO_2 phase. In comparison with the W sample, the CO_2 evolution at 450 ˚C (indicating the reduction to MeO_2) is much greater for the bimetallic carbides. The XRD pattern confirms this. At 660 ˚C, both MoO_3 and MoO_2 reflections were

detected for the bimetallic system (1:1); at 740 ˚C, the transformation to the MeO_2 phases has been completed. Since the formation of WO_2 did not occur in the monometallic carbide sample, the formation of a mixed oxide ($MoWO_2$) seems likely. This formation of a MeO_2 phase appears to be too slow to observe with TGA.

The final step of the carbide synthesis is the reduction of the MoO_2 or WO_3 to Mo_2C and W_2C, respectively. The carbide formation (carburization) occurs in a temperature range of 650 to 800 ˚C and results in the release of CO (and to a lesser degree, CO_2) detected by TPD-MS and by the significant mass loss measured with TGA, originating from the reaction of carbon from the support with the metal oxide (see Table S2.1). Since the CO release and the weight loss from the bare CNF are significantly lower (see Figure S2.1, right) than the CO release and weight loss seen for the metallic materials (Figure S2.3), we can attribute the bulk of the measured changes in weight and the observed CO release to the carburization process. The small quantity of CO released at 730 ˚C and the weight loss at 749 ˚C detected during the treatment of the bare CNF is attributed to the decomposition of the surface oxygen groups.

The carburization of monometallic Mo occurs at 680 ˚C (TPD-MS) with a measured weight loss of 5.50 wt%; the carburization of W takes place at 770 ˚C (TPD-MS) with a weight loss of 5.62 wt%. The carburization temperatures as deduced from the TPD-MS and TGA data are in accordance with our XRD data. The transformation of MoO_2 to Mo_2C occurs between 660 and 740 ˚C, while the transformation of WO_3 to W_2C occurs at 740 to 820 ˚C. The WO_3 phase is transformed to both metallic W and W_2C at 740 to 820 ˚C. Full carburization of the W carbide takes place between 860 and 900 ˚C. It has been suggested that the reduction of the WO_3 proceeds in two simultaneous steps (see Scheme 1), one in which the WO_3 is directly transformed into the W_2C and another one in which the carbide is formed via the metallic carbide. [S1,6] This could also explain why the CO peak for the carburization of W is broader than for Mo.

The carburization of the physical mixture clearly shows two separate steps for the CO evolution and mass loss due to the formation of the Mo carbide and the W carbide. The co-impregnated bimetallic samples on the other hand carburize in a single step, indicating that in this case a mixed carbide is formed. The bimetallic systems carburize between the temperatures for the individual monometallic carbides. Furthermore, the carburization temperature increases with increasing W content. In the XRD results, we can identify the formation of a hexagonal carbide at 820 ˚C which may correspond to a mixed $Mo_xW_yC_z$ phase.

Temperature programmed reduction synthesis (TPR)

In addition to monometallic and bimetallic carbides, the TPR of which we followed by TPD-MS, TGA, and XRD, we also prepared and analyzed a physical mixture of both carbides for the sake of comparison.

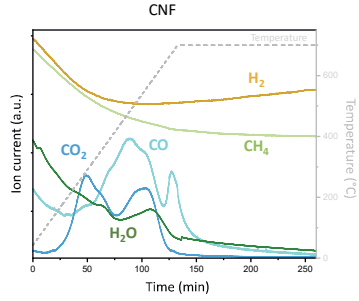

Figure S2.5 TPR-MS on CNF heated to 700 °C under 20% CH_4/H_2.

Figure S2.5 shows the TPD-MS of the CNF support without any precursor during the TPR method. This data was obtained to serve as a comparison with the precursor impregnated materials being carburized shown in Figure S2.6. Gas evolution of CO (m/z=28), H_2O (m/z=18), CH_4 (m/z=16), and CO_2 (m/z=44) was followed. The main CO_2 peak is located at 290 ˚C and second is located at 500 ˚C, simultaneously with a water release. The main CO peak occurred at t 450 ˚C; there was further CO release at 690 ˚C.

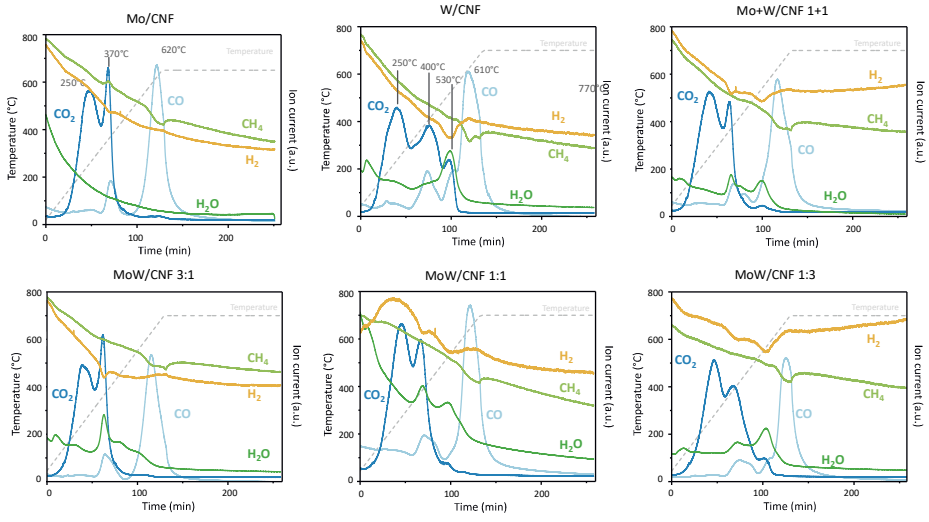

Figure S2.6 TPR of AHM/AMT of the monometallic and bimetallic samples supported on carbon nanofibers. The samples were exposed to 700 °C (AHM) or 650 °C (AMT), 5 °C/min under 20% CH_4/H_2.

The samples were heated up to a temperature ramp of 700 °C at 5 °C /min and an isotherm of 2 h under 20% CH_4/H_2 (total flow of 50 ml/min). The gas evolution of CO (m/z=28), H_2O (m/z=18), CH_4 (m/z=16), and CO_2 (m/z=44) was detected with MS and is displayed in Figure S2.6. At 100 ˚C and at 250 ˚C a H_2O peak is visible. CO_2 evolution occurred at 250 ˚C and 370 ˚C for Mo and at 210 ˚C, 400 ˚C and 510 ˚C for W. The monometallic W and bimetallic systems with a higher content show three distinct CO_2 peaks, while the systems with the higher Mo content show two CO_2 peaks. Simultaneously with the second CO_2 peak (at 350 ˚C) for Mo and the second and third CO_2 peak (at 400 ˚C and 510 ˚C) for W, CO and H_2O were released and H_2 was consumed. At around 650 ˚C, all samples showed a major release of CO. For Mo, CH_4 is consumed and H_2 is released at almost the same temperature as this CO release; the data for W show two separate CH_4 consumption peaks. The first CH_4 consumption occurred simultaneously with the release of CO; the second one occurred at a slightly higher temperature. During the remainder of the isothermal dwell period at 650 ˚C, no more gases were released or consumed.

It should be mentioned that the concentration after carbide formation decreases, which suggest that carbon deposition may occurs, which would poison the surface. However, since the catalysts are active for HDO this can be excluded.

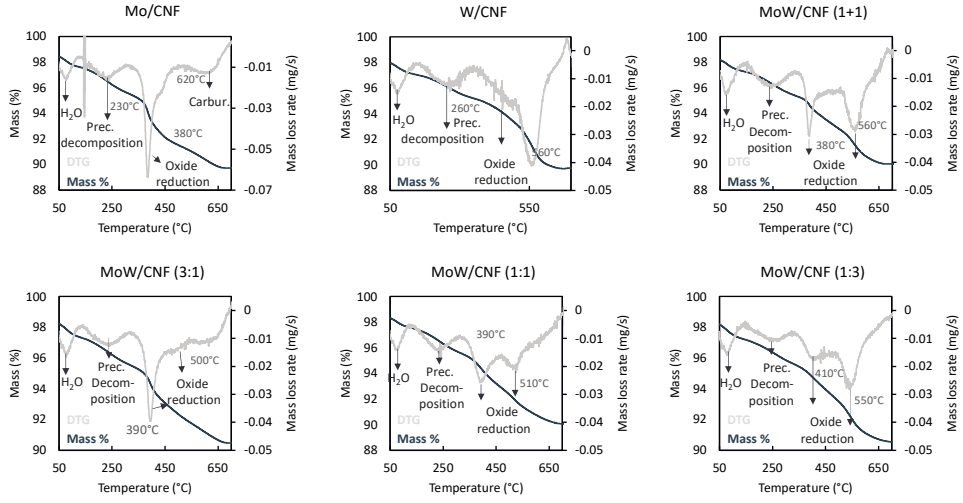

Figure S2.7 Thermogravimetric analysis of the TPR of the oxide precursors of Mo_2C, W_2C and the bimetallic MoW carbide under 20% CH_4/H_2 gas to 700 °C.

The TGA was conducted during the TPR synthesis (20% CH_4/H_2, 700 °C). Figure S2.7 shows the weight loss and the weight loss rate (DTG) for all catalysts. The first significant weight change (0.9 wt%) was observed at ~100 ˚C. At 150 to 300 ˚C, a broad peak in the weight loss rate of about

1.8 wt% is found. The third significant weight loss was found at 380 ˚C for the Mo sample and at 560 of about 1.8 wt %C for the W sample. Both metals lost around 3.3 wt% in this step. For the physical mixture, these two weight rate changes were observed at the same temperatures as were found for the monometallic carbides (380 ˚C and 560 ˚C). Corresponding peaks were also observed for the bimetallic systems at slightly shifted position, namely at 390 ˚C and 500 ˚C for the 1:3 Mo:W ratio, at 390 ˚C and 510 ˚C for the 1:1 ratio and at 410 ˚C and 550 ˚C for the 1:3. For Mo, an additional weight loss peak can be detected at 620 ˚C, whereas the graph for W displays some mass gain at 690 ˚C. For the physical mixture and the bimetallic systems, no clear peak in the weight loss rate was observed in that temperature range.

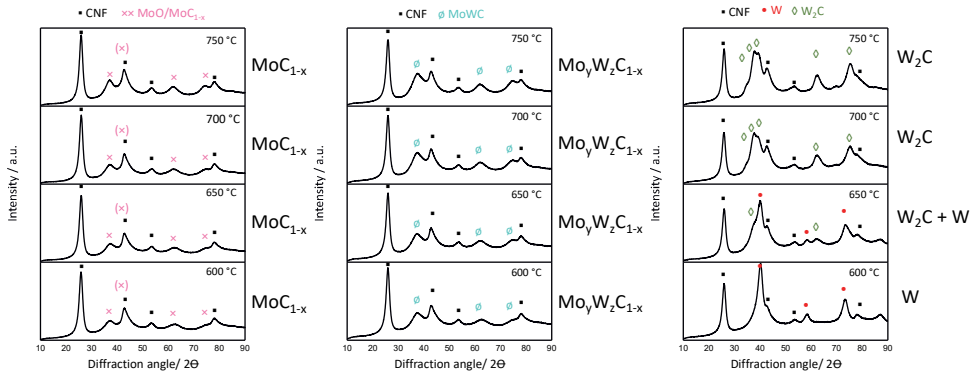

Figure S2.8 XRD of Mo_2C/CNF (right), MoWC/CNF (center) and W_2C/CNF during TPR synthesis.

Figure S2.8 displays the XRD patterns of the carbon-supported carbide catalyst during its transformation during the TPR method. The samples were carburized at 600 ˚C, 650 ˚C, 700 ˚C and 750 ˚C and measured ex situ directly afterwards with XRD. The signals at a 2θ of 28˚ and 43˚ represent the (002) and (101) reflections of the graphitic CNF [S24] and are present in all patterns. At 600 to 750 ˚C, the carbon-supported Mo shows reflections at 37˚ and 67.5˚ 2θ, which can be attributed to the cubic α-M˚C_{1-x} phase. As in the CR carburization process, reflections belonging to the metallic cubic tungsten (40.1˚) were also observed during the TPR method. At 700 ˚C, metallic W was transformed to the hexagonal W_2C phase with its reflections at 34˚, 37.5˚, 39˚, 61.5˚, and 74.5˚ (2θ). For the bimetallic system with the 1:1 Mo:W ratio, reflections representing a cubic α-MeC_{1-x} phase were observed.

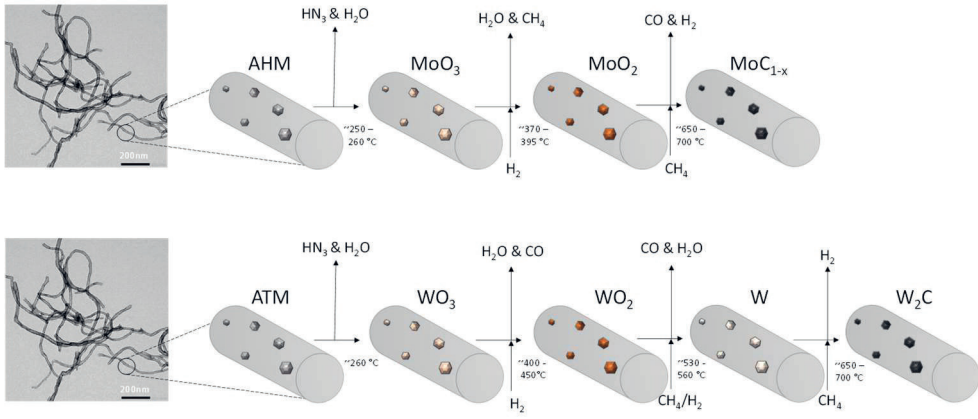

Scheme S2.2 Temperature programmed reduction (TPR) of CNF-support impregnated ammonium heptamolybdate (AHM) and ammonium metatungstate (ATM). TEM image on the left show pure CNF.

We attribute the initial weight loss at 100 ˚C to the evaporation of water absorbed on the CNF. This is supported by the evolution of H_2O as seen in the TPD-MS data. The CO_2 and CO at 210 to 250 ˚C and 400 ˚C result from the support (see Figure S2.5). At 200 to 250 ˚C, the breakdown of the AHM and AMT complex is correlated to the evolution of both H_2O and ammonia (not shown) with a weight loss of 2.58 wt% and 1.85 wt%, respectively. This is when the salt is transformed into its oxide form (MeO_3), with a theoretical weight loss of AHM (2.64 wt%) and AMT (2.00 wt%), respectively. We observed these two steps in the TPR synthesis for all catalysts.

The second CO_2 peak evolves simultaneously with CO and H_2O and the consumption of H_2. For the Mo sample, this peak was detected at 370 ˚C, coinciding with a change in weight of 3.35 wt% (see Table S2.2) (380 ˚C for the corresponding weight change seen in TGA). We attribute this to the reduction of the MoO_3 to MoO_2. This reduction can use either H_2 or carbons from the CNF and H_2; both reactions occur, as evidenced by the mass loss, together with the measured formation of CO/CO_2 and the minor consumption of H_2 with the formation of H_2O. These reduction reactions have a theoretical weight loss of 3.24 wt% and 1.30 wt% (see Table S2.2). Since the contribution of each reaction is unknown, the exact theoretical mass loss cannot be calculated for this step. However, based on the magnitude of the weight loss, we conclude that the reduction takes place mainly with the carbon from the support.

For the W sample, we observed a CO_2 peak simultaneously with CO and H_2O release at 530 ˚C. This suggests that reduction steps occur in which WO_3 is reduced to WO_2 (see Table S2.2). Also for this reduction, carbon originating from the support as well as H_2 are utilized. The weight loss rate indeed shows a shoulder peak (1.94 wt% measured) at 480 ˚C which could be due to the

reduction of WO_3 to WO_2 or to a suboxide. The measured weight loss of 1.94% suggests that the reduction via the carbon from the support contributes less than the reduction using H_2. This is in agreement with the more pronounced H_2 consumption peak observed in TPD-MS.

For all samples, a CO evolution peak is visible in the range of 600 to 700 ˚C in the TPR-MS results. For Mo, this CO evolution corresponds to the actual carburization process. There is a weight loss peak (2.27 wt%) for monometallic Mo in the same temperature range (620 ˚C), which can be attributed to the carburization with methane and the simultaneous evolution of CO (causing a calculated weight loss of 2.11 wt%).

By contrast, for the monometallic W sample, the weight loss is greater (3.28 wt%) than expected (1.97 wt%) for the reduction of the WO_2 to its carbide. This leads to the suggestion that first the reduction of the WO_2 to the metallic form occurred. The theoretical weight loss of this reduction, using H_2, is around 2.42 wt% and the weight loss of reduction that uses the CNF is 3.78 wt%. This indicates that both reduction pathways are utilized to form metallic W. The larger CO peak at 610 ˚C thus corresponds to the reduction of WO_2 to metallic W (and not to the formation of the carbide). This is also supported by XRD which (only) detected a metallic phase at 600 ˚C. The actual carburization of the metallic W to the carbide can be followed by the CH_4 consumption. The W spectra contain two CH_4 peaks; the first one is at 610 ˚C and thus corresponds to the reduction of WO_2 to metallic W (with the aforementioned simultaneous release of CO) and the second methane consumption peak at 690 ˚C indicates the carburization. At the same temperature, a small mass gain (-0.45 wt%, calculated) was found in the TGA (how much, measured?). This is expected since the formation of W_2C from metallic W with the use of CH_4 leads to an increase in weight.

The physical mixture shows the same CO/CO_2 evolution and weight changes, at the same temperatures, as found for the individual monometallic carbides. By contrast, the bimetallic carbides show features that lie between the observations for the individual monometallic carbides. Two weight change and H_2 consumption peaks close to the temperatures of the presumed oxide reduction steps of the monometallic Mo and W are visible. Their shifted positions (towards the other metal) could indicate that mixed oxide particles are present. In that case, for instance for the bimetallic system 1:1, the two peaks at 390 °C and 510 °C can be attributed to the oxide reduction steps. Thus, mixed MeO_3 would first be reduced to mixed MeO_2 (or a suboxide) at 390 ˚C and subsequently, at 510 ˚C, be further reduced to its metallic species (Mo_xW_y). The coinciding CO_2 and H_2O peaks overlap with the large weight loss at 510 °C observed in the TGA, suggesting that also a metallic phase is formed during the synthesis of the bimetallic carbides. Since the DTG peak is not as sharp and high as for the formation of the metallic W, we assume

only a partial reduction towards the mixed metal phase. XRD was not able to detect the metallic phase at 600 ˚C, in contrast with what we saw for monometallic W; only the cubic α-$Mo_xW_yC_{1-z}$ phase was visible. Whether the CO release and the changes in weight are due to the carburization of the oxide or of the metallic phase cannot be deduced based on this data.

To summarize, the CO evolution during the TPR method cannot be used as an indicator for the carburization, since the released CO during the synthesis of the W carbide correlates to the reduction of WO_2 to the metallic W prior to the carburization. Therefore, the actual carburization temperature of the bimetallic systems can best be observed by following the CH_4 methane consumption.

Table S2.2 Measured and calculated weight loss during the TPR carburization of the monometallic Mo and W materials

	Calculated (wt%)	**Measured (wt%)**	**Temp. range (˚C)**
Pre decomposition:			
$(NH_4)_6Mo_7O_{24}$ *$4H_2O$→ $7MoO_3 + 7H_2O + 6NH_3$	2.64	2.58	130-350
$(NH_4)_6H_2W_{12}O_{40}$ *$4H_2O$→ $12WO_3 + 8H_2O + 6NH_3$	2.00	1.85	170-370
Oxide reduction:			
$2MoO_3 + 2C_{CNF} + 2H_2 \rightarrow 2MoO_2 + CO_2 + CH_4$	1.30		
$3MoO_3 + C_{CNF} + H_2 \rightarrow 3MoO_2 + CO_2 + H_20$	3.24		
Overall		3.35	350-480
$2WO_3 + C_{CNF} \rightarrow 2WO_2(/WO_x) + CO_2$	3.03		
$3WO_3 + 3H_2 \rightarrow 3WO_2 + 3H_2O$	1.31		
Overall		1.94	370-500
$WO_2 + 2CH_4 \rightarrow W + 2CO + 4H_2$	2.42		
$WO_2 + C_{CNF} \rightarrow 2W + CO_2$	3.78		
Overall		3.28	500-620
Carburization:			
$2MoO_2 + 5CH_4 \rightarrow Mo_2C + 4CO + 10H_2$	2.11	2.27	600-700
$2W + CH_4 \rightarrow W_2C + 2H_2$	-0.45	n.a.	620-700

Thermogravimetric analysis (TGA)

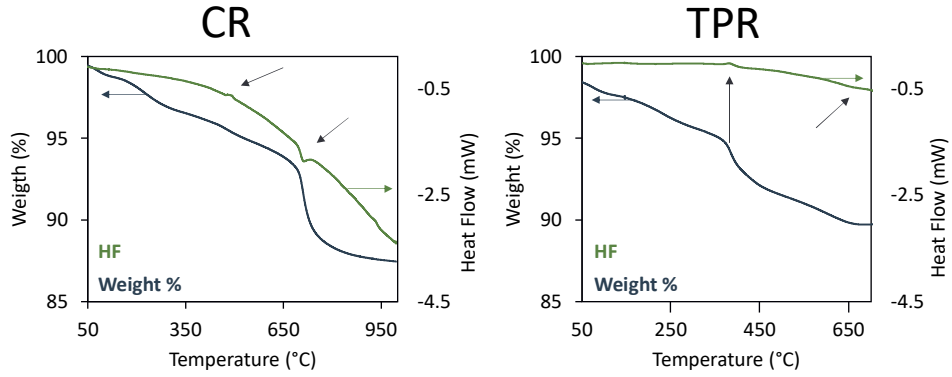

Figure S2.9 TGA-plots of Mo-carbide weight percent and heat flow of both carburization methods CR (left) and TPR (right).

To explore whether thermal effects could yield additional information on the carburization temperature, we also performed differential thermal analysis (DTA) simultaneously with TGA. Figure S2.9 shows the weight loss of the heat flow versus the temperature of the Mo carbide sample during the carburization process. On the left, the CR method is displayed and on the right, TPR. The positive heat flow indicates that the process was exothermic. As shown, the reduction of MoO_3 to MoO_2 occurred at 480 ˚C for CR and at 385 ˚C for TPR. At that point, there is also a large positive spike in the heat flow, showing that the oxide reduction is an exothermic process.[S28] Thus, similar information on the carburization temperature can be obtained from DTA as well as from TGA. For the CR synthesis profile, the heat flow and the weight loss changed at 710 ˚C, indicating the formation of the carbide. The negative spike in the heat flow is indicative of an endothermic process.[S15] The graph for TPR shows no clear changes in the heat flow at the carburization temperature.

Element mapping (STEM-EDX)

Figure S2.10 (CR) and Figure S2.11 (TPR) show HAADF-STEM and EDX images of the bimetallic carbide system with a Mo:W ratio of 1:3 and 3:1. (The main text includes images of the 1:1 system.) For the monometallic carbides, we obtained TEM images but did not apply any element mapping.

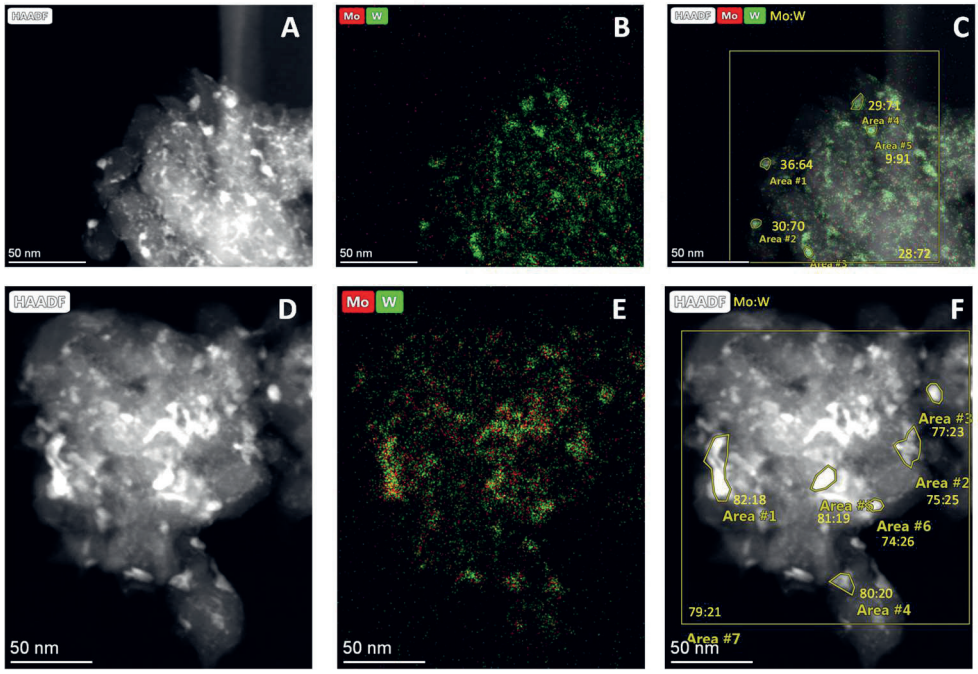

Figure S2.10 STEM characterizations of the CR-prepared MoWC/CNF samples with a Mo:W ratio of 1:3 (A-C) and 3:1 (D-F)

The 1:3 MoW carbide sample synthesized via the CR method (BET surface area = 133 m^2/g, total pore volume = 0.3 *10^{-6} ml/g) showed only nanoparticles that contained both Mo and W. Some particles contained a large proportion of W, e.g. area 5 in Figure S2.10 C, but we observed no particles that contained only Mo or W. The atomic Mo:W ratio (yellow box) of the whole imaged sample was 28:72, which is close to the expected bulk ratio of 1:3. We found similar results for the 3:1 sample synthesized via the CR method (BET surface area = 144 m^2/g, total pore volume = 0.3 *10^{-6} ml/g). We detected no particles that contained only Mo or W; all particles were mixed with an atomic Mo:W ratio of approximately 80:20.

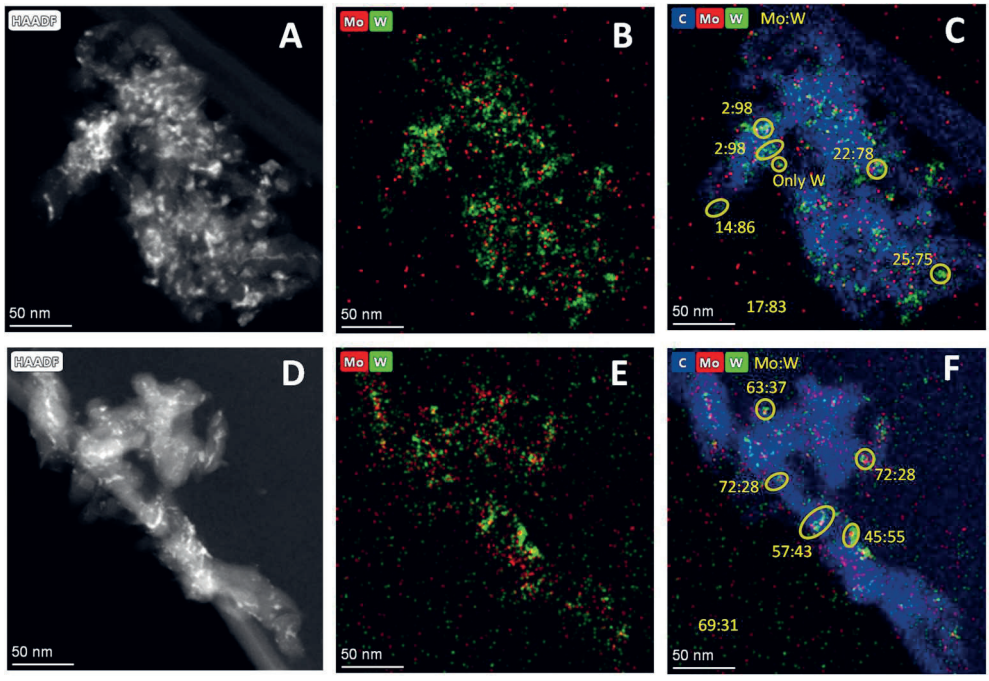

Figure S2.11 STEM characterizations of the TPR-prepared MoWC/CNF sample with a Mo:W ratio of 1:3 (A-C) and 3:1(D-F).

We made similar observations for samples prepared with the TPR method. For the MoW carbide with a Mo:W ratio of 1:3 (BET surface area = 149 m^2/g, total pore volume = 0.3 $*10^{-6}$ m_3/g), almost all nanoparticles were bimetallic. However, we found a few small particles that only contained W. The Mo:W ratio over the whole image was 17:83, which again is in agreement with the expected bulk ratio. Also, the 3:1 bimetallic carbide (BET surface area = 141 m^2/g, total pore volume = 0.3 $*10^{-6}$ ml/g) showed only nanoparticles containing both metals; the bulk ratio of the whole image was 60:31.

In summary, the bimetallic nanoparticles synthesized via both the CR and the TPR method consisted of a mixed metallic phase. These nanoparticles did not have a homogenous distribution, but most had an atomic ratio close to the expected bulk ratio.

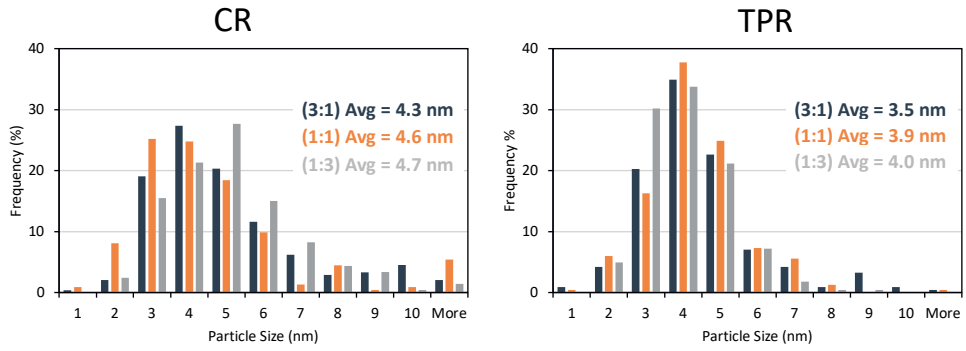

Figure S2. 12 Particle size distribution of CR (left) and TPR (right) carburized bimetallic carbide samples.

Figure S2.12 presents the histograms of the particle size distribution of the bimetallic carbide samples carburized via the CR and the TPR prepared. We found that the average particle size for the TPR synthesized particles is between 3-4 nm, while the CR prepared samples have average particle size in tween 4 and 5 nm.

Pore volume

Table S2.3 Comparison micropore and mesopore area

		Micropore area (m^2/g)	Mesopore area (m^2/g)
CR	**MoWC/CNF (1:1)**	12	0.26
	MoWC/CNF (1:3)	18	0.30
	MoWC/CNF (3:1)	24	0.31
TPR	**MoWC/CNF (1:1)**	20	0.31
	MoWC/CNF (1:3)	31	0.33
	MoWC/CNF (3:1)	29	0.32

The different synthesis temperatures (900 °C for CR and 700 °C for TPR) can have a significant effect on the textural properties of the CNF support, which in turn could results in different mass transfer of the reactant to the catalysts. Both synthesis methods lead to a comparable micropore and mesopore areas, as can be seen from Table S2.3. Thus, no significant difference in textural properties were observed and therefore we can exclude mass transfer limitations during the reaction due to pore size differences.

Evaluation of the XRD carbide reflections

Figure S2.13 and Figure S2.14 show the XRD patterns of the carbide catalysts. The peak position of the carbide are given in the Table S2.4 and Table S2.5. The peaks were corrected for sample height displacement by aligning all the (002) CNF peaks to 25.99°. The experimentally obtained XRD data was compared with reference patterns to determine the (main) carbide phase. The references which had the best match in terms of position and intensity are listed below:

- CR-carburized Mo_2C pattern (PDF 79-0744) 34.359°, 37.975° and 39.413°
- CR-carburized W_2C pattern (PDF 89-2371) 34.459°, 38.034° and 39.519°
- TPR-carburized MoC_{x-1} pattern (PDF 65-0280) 36.388°
- TPR-carburized W_2C pattern (PDF 79-0743) 34.536°, 38.067° and 39.592°

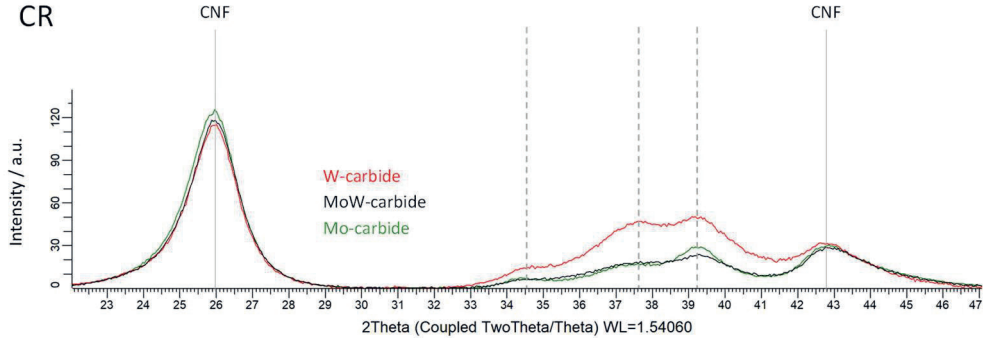

Figure S2.13 XRD patterns of CR-carburized carbides in the 2θ range of 22 to 47°.

Table S2.4 XRD peak position of CR-carburized carbides in the 2θ range of 22 to 47°.

	CNF position	Carbide	Carbide	Carbide
Mo_2C/CNF	25.991	34.434	37.747	39.219
$(Mo,W)_xC$/CNF (3:1)	25.990	34.624	37.791	39.381
$(Mo,W)_xC$/CNF (1:1)	25.992	34.550	37.590	39.322
$(Mo,W)_xC$/CNF (1:3)	25.995	34.653	37.747	39.276
W_2C/CNF	25.992	34.585	37.808	39.179

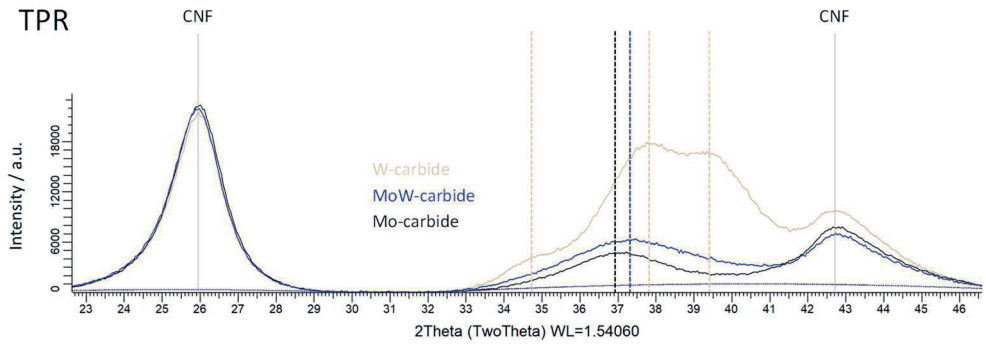

Figure S2.14 XRD patterns of TPR-carburized carbides in the 2θ range of 22 to 47°.

Table S2.5 XRD peak position of TPR-carburized carbides in the 2θ range of 22 to 47°.

	CNF position	Carbide	Carbide	Carbide
MoC_{1-x}/CNF	25.999			37.018
$(Mo,W)_xC_y$/CNF (3:1)	25.995			37.136
$(Mo,W)_xC_y$/CNF (1:1)	25.995			37.491
$(Mo,W)_xC$/CNF (1:3)	25.994			37.647
W_2C/CNF	25.996	35.024	37.888	39.281

It has been suggested that Vegard's law can be used to prove the formation of a mixed-metal carbide phase.[S29] Figure S2.13 reveals that the positions of the carbide peaks are indeed between those of the monometallic carbides. However, the expected systematic shift in peak position with increasing Mo is absent and there is no clear relationship between the peak position and the Mo:W ratio. This could be because the difference between β-Mo_2C and β-W_2C is intrinsically small (0.1 2θ) and since the mixed-metal nanoparticles yield very broad diffraction peaks, this probably results in a relatively large uncertainty for the exact peak position.

Also for the TPR method, we are hesitant to claim proof of a mixed carbide phase based on the XRD data; see Figure S2.14. The W carbide forms a hexagonal crystal structure and the Mo carbide a cubic structure. The bimetallic carbides show reflections best corresponding to the cubic structure. With increasing W content, a shift towards a greater diffraction angle is observed for these samples, which could be due to the formation of a mixed phase. However, we cannot exclude that the sample contains an increasing fraction of the hexagonal structure the reflection of which could be part of the broad reflection peak at 37°. If so, it would also cause this broad reflection to appear to shift to a greater angle.

EXAFS fits of monometallic Mo carbides

The Fourier Transforms of the data and fit is plotted in Figure S2.15. All data are of high quality and multiple shells can be fitted with high accuracy.

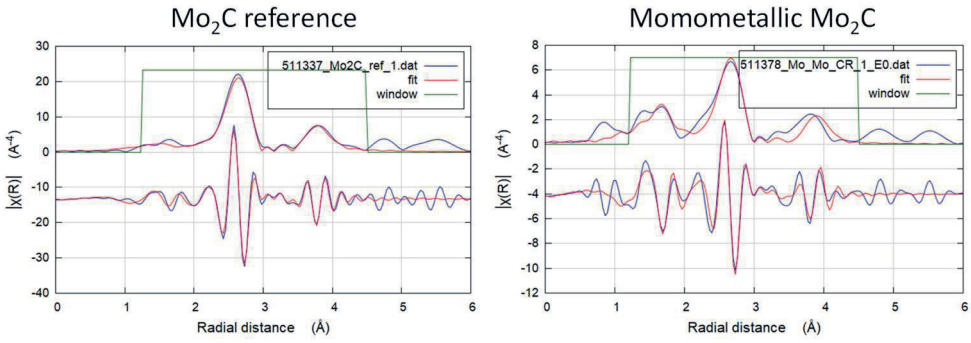

Figure S2.15 k2 weighted Fourier Transform of the Mo K Edge EXAFS data of the Mo_2C reference (left) and the monometallic Mo_2C (left).

Hydrogen mass transfer limitations

Since the reactions were conducted in a batch stirred reactor, possible mass transfer limitations should be considered. Figure S2.16 shows the HDO reaction of Mo carbide catalysts at 300 ˚C (left) and 350 ˚C (right) at different stirring rates. As can be seen from the 300 ˚C experiment, the stearic acid conversion is lower for lower stirring rates (400 rpm), indicating that mass transfer rate of hydrogen is rate limiting. Upon increasing the stirring rate to 800 and 1200 rpm the stearic acid conversion does increase. However, when the stirring is further increased to 1600 rpm, the conversion seems to decrease. A similar trend was observed for the HDO at 350 ˚C. Thus it was concluded that 800 rpm suffices for the reaction.

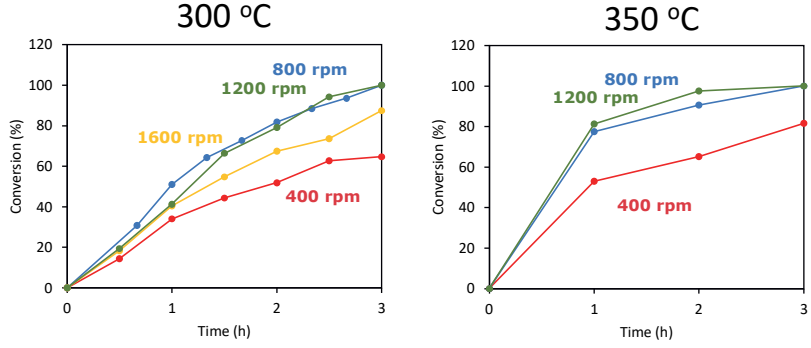

Figure S2.16 Effect of stirring rate on the stearic acid conversion at 300 ˚C and 350 ˚C. (250 mg catalyst with metal loading of 0.9 mol/$g_{catalyst}$, 2 g stearic acid, 50 ml solvent, 30 bar H_2).

Reproducibility

Two separate reaction runs were performed using newly synthesized monometallic and the MoW (1:1) carbide catalyst batches in order to test the experimental reproducibility. In Figure S2.17 the average stearic acid conversion with the standard deviation of the two runs is shown. Based on these results we conclude that the synthesis and experiments were reproducible.

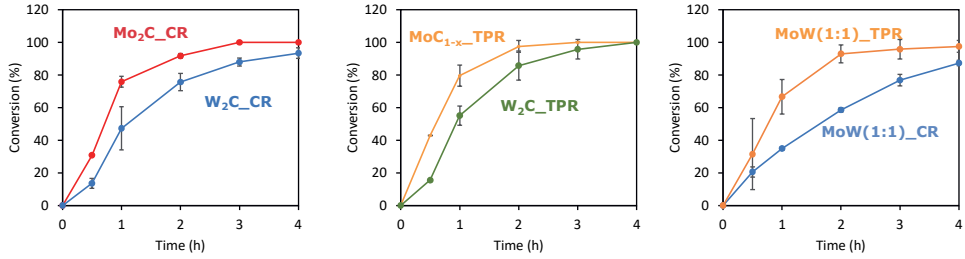

Figure S2.17 Average activity of two separate HDO runs (250 mg catalyst with metal loading of 0.9 mmol/g $_{catalyst}$, 2 g stearic acid, 350 °C, 50 ml solvent, 30 bar H_2).

Evaluation of catalyst stability

To investigate the deactivation of the catalyst, subsequent experiments with one batch of MoW (1:1) carbide catalyst were conducted. Between the runs, the remaining reaction medium was decanted, then the catalysts were washed/decanted one time with 100 ml dodecane before adding the fresh reaction medium. The conversion results are shown in Figure S2.18. Interestingly, the CR prepared catalysts are stable for 3 runs. In contrast the activity of the TPR prepared catalyst slowly drops after the second and third run. Thus the CR prepared catalysts are more stable than the TPR prepared catalysts.

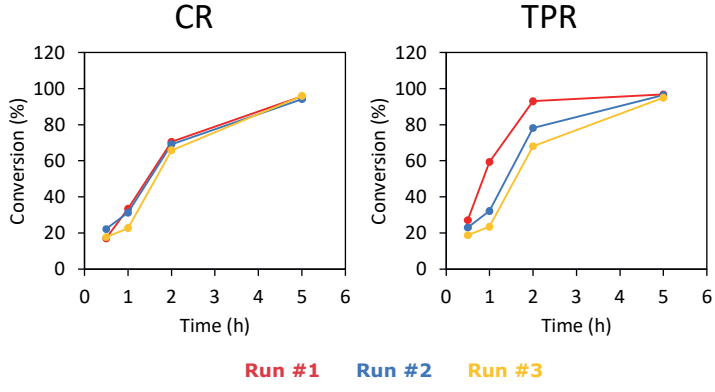

Figure S2.18 Multiple runs of stearic acid conversion (250 mg catalyst with metal loading of 0.9 mol/g $_{catalyst}$, 2 g stearic acid, 350 °C, 50 ml solvent, 30 bar H_2).

References

(S1) Stellwagen, D. R.; Bitter, J. H. Structure–performance relations of molybdenum-and tungsten carbide catalysts for deoxygenation. *Green Chemistry* **2015,** *17* (1), 582.

(S2) Macedo, L. S.; Oliveira, R. R.; van Haasterecht, T.; Teixeira da Silva, V.; Bitter, H. Influence of synthesis method on molybdenum carbide crystal structure and catalytic performance in stearic acid hydrodeoxygenation. *Applied Catalysis B: Environmental* **2019,** *241*, 81.

(S3) Blanco, E.; Aguirre-Abarca, D. A.; de León, J. N. D.; Escalona, N. Relevant aspects of the conversion of guaiacol as a model compound for bio-oil over supported molybdenum oxycarbide catalysts. *New Journal of Chemistry* **2020,** *44* (28), 12027.

(S4) Matus, E.; Khitsova, L.; Efimova, O.; Yashnik, S.; Shikina, N.; Ismagilov, Z. Preparation of carbon nanotubes with supported metal oxide nanoparticles: effect of metal precursor on thermal decomposition behavior of the materials. *Eurasian Chemico-Technological Journal* **2019,** *21* (4), 303.

(S5) Kugler, E. L.; Clark, C. H.; Wright, J. H.; Dadyburjor, D. B.; Hanson, J. C.; Song, Z.; Cai, T.; Hrbek, J. Preparation, interconversion and characterization of nanometer-sized molybdenum carbide catalysts. *Topics in catalysis* **2006,** *39* (3-4), 257.

(S6) Venables, D. S.; Brown, M. E. Reduction of tungsten oxides with carbon. Part 1: Thermal analyses. *Thermochimica acta* **1996,** *282*, 251.

(S7) Carrales-Alvarado, D.; Dongil, A.; Fernández-Morales, J.; Fernández-García, M.; Guerrero-Ruiz, A.; Rodríguez-Ramos, I. Selective hydrogen production from formic acid decomposition over Mo carbides supported on carbon materials. *Catalysis Science & Technology* **2020,** *10* (20), 6790.

(S8) Mehdad, A.; Jentoft, R. E.; Jentoft, F. C. Single-phase mixed molybdenum-tungsten carbides: Synthesis, characterization and catalytic activity for toluene conversion. *Catal Today* **2019,** *323*, 112.

(S9) Sebakhy, K. O.; Vitale, G.; Hassan, A.; Pereira-Almao, P. New Insights into the Kinetics of Structural Transformation and Hydrogenation Activity of Nano-crystalline Molybdenum Carbide. *Catalysis Letters* **2018,** *148* (3), 904.

(S10) Bkour, Q.; Cuba-Torres, C. M.; Marin-Flores, O. G.; Tripathi, S.; Ravishankar, N.; Norton, M. G.; Ha, S. Mechanistic study of the reduction of MoO2 Mo2C under methane pulse conditions. *Journal of Materials Science* **2018,** *53* (18), 12816.

(S11) Cotter, T.; Frank, B.; Zhang, W.; Schlögl, R.; Trunschke, A. The Impact of V Doping on the Carbothermal Synthesis of Mesoporous Mo Carbides. *Chemistry of Materials* **2013,** *25* (15), 3124.

(S12) Bastos, L. C. A.; Monteiro, W. R.; Zacharia, M. A.; da Cruz, G. M.; Rodrigues, J. A. J. Preparation and characterization of Mo/W bimetallic carbides by using different synthesis methods. *Catalysis Letters* **2008,** *120* (1-2), 48.

(S13) Xiao, T.; Hanif, A.; York, A. P.; Sloan, J.; Green, M. L. Study on preparation of high surface area tungsten carbides and phase transition during the carburisation. *Physical Chemistry Chemical Physics* **2002,** *4* (14), 3522.

(S14) Liang, C.; Ying, P.; Li, C. Nanostructured β-Mo2C prepared by carbothermal hydrogen reduction on ultrahigh surface area carbon material. *Chemistry of materials* **2002,** *14* (7), 3148.

(S15) Hanif, A.; Xiao, T. C.; York, A. P. E.; Sloan, J.; Green, M. L. H. Study on the structure and formation mechanism of molybdenum carbides. *Chemistry of Materials* **2002,** *14* (3), 1009.

(S16) Choi, J.-S.; Bugli, G.; Djéga-Mariadassou, G. Influence of the Degree of Carburization on the Density of Sites and Hydrogenating Activity of Molybdenum Carbides. *Journal of Catalysis* **2000,** *193* (2), 238.

(S17) Decker, S.; Lofberg, A.; Bastin, J. M.; Frennet, A. Study of the preparation of bulk tungsten carbide catalysts with C2H6/H-2 and C2H4/H-2 carburizing mixtures. *Catalysis Letters* **1997,** *44* (3-4), 229.

(S18) Deeva, E. B.; Kurlov, A.; Abdala, P. M.; Lebedev, D.; Kim, S. M.; Gordon, C. P.; Tsoukalou, A.; Fedorov, A.; Müller, C. R. In Situ XANES/XRD Study of the Structural Stability of Two-Dimensional Molybdenum Carbide Mo2CT x: Implications for the Catalytic Activity in the Water–Gas Shift Reaction. *Chemistry of Materials* **2019,** *31* (12), 4505.

(S19) Rodella, C. B.; Barrett, D. H.; Moya, S. F.; Figueroa, S. J.; Pimenta, M. T.; Curvelo, A. A. S.; da Silva, V. T. Physical and chemical studies of tungsten carbide catalysts: effects of Ni promotion and sulphonated carbon. *RSC Advances* **2015,** *5* (30), 23874.

(S20) Bouchy, C.; Schmidt, I.; Anderson, J. R.; Jacobsen, C. J. H.; Derouane, E. G.; Derouane-Abd Hamid, S. B. Metastable fcc α-MoC(1-x) supported on HZSM5: Preparation and catalytic performance for the non-oxidative conversion of methane to aromatic compounds. *Journal of Molecular Catalysis A: Chemical* **2000,** *163* (1-2), 283.

(S21) Bouchy, C.; Derouane-Abd Hamid, S. B.; Derouane, E. G. A new route to the metastable FCC molybdenum carbide α-MoC(1-x). *Chem Commun* **2000**, DOI:10.1039/a907534h 10.1039/a907534h(2), 125.

(S22) Rodrigues, E. G.; Pereira, M. F. R.; Chen, X. W.; Delgado, J. J.; Orfao, J. J. M. Influence of activated carbon surface chemistry on the activity of Au/AC catalysts in glycerol oxidation. *Journal of Catalysis* **2011,** *281* (1), 119.

(S23) Toebes, M. L.; van Heeswijk, E. M. P.; Bitter, J. H.; van Dillen, A. J.; de Jong, K. P. The influence of oxidation on the texture and the number of oxygen-containing surface groups of carbon nanofibers. *Carbon* **2004,** *42* (2), 307.

(S24) Jongerius, A. L.; Gosselink, R. W.; Dijkstra, J.; Bitter, J. H.; Bruijnincx, P. C. A.; Weckhuysen, B. M. Carbon Nanofiber Supported Transition-Metal Carbide Catalysts for the Hydrodeoxygenation of Guaiacol. *ChemCatChem* **2013,** *5* (10), 2964.

(S25) Macedo, L. S.; Stellwagen, D. R.; da Silva, V. T.; Bitter, J. H. Stability of Transition-metal Carbides in Liquid Phase Reactions Relevant for Biomass-Based Conversion. *Chemcatchem* **2015,** *7* (18), 2816.

(S26) Li, X.; Ma, D.; Chen, L.; Bao, X. Fabrication of molybdenum carbide catalysts over multi-walled carbon nanotubes by carbothermal hydrogen reduction. *Catalysis Letters* **2007,** *116* (1-2), 63.

(S27) Pielaszek, J.; Mierzwa, B.; Medjahdi, G.; Marêché, J. F.; Puricelli, S.; Celzard, A.; Furdin, G. Molybdenum carbide catalyst formation from precursors deposited on active carbons: XRD studies. *Applied Catalysis A: General* **2005,** *296* (2), 232.

(S28) Brush, A.; Evans, E. J.; Mullen, G. M.; Jarvis, K.; Mullins, C. B. Tunable Syn-gas ratio via bireforming over coke-resistant Ni/Mo<inf>2</inf>C catalyst. *Fuel Processing Technology* **2016,** *153*, 111.

(S29) Fu, Q.; Peng, B. X.; Masa, J.; Chen, Y. T.; Xia, W.; Schuhmann, W.; Muhler, M. Synergistic Effect of Molybdenum and Tungsten in Highly Mixed Carbide Nanoparticles as Effective Catalysts in the Hydrogen Evolution Reaction under Alkaline and Acidic Conditions. *Chemelectrochem* **2020,** *7* (4), 983.


3

Chapter 3

Catalytic performance of carbonsupported mixed MoW carbides for the deoxygenation of stearic acid

This Chapter is based on: M. Führer, T. van Haasterecht, and H. Bitter. “Catalytic performance of carbon-supported mixed MoW carbides for the deoxygenation of stearic acid.” Catalysis Today

Abstract

Supported bimetallic molybdenum and tungsten carbides are viable replacements for noble metal catalysts and are suitable for the decarboxylation/decarbonylation and (hydro-)deoxygenation of renewable triglyceride-based feedstocks. Here, we show that the Mo:W ratio in bimetallic carbide can steer the product yield towards either aldehydes, alcohols, alkenes or alkanes. The mixed carbides with a higher Mo/W ratio (3:1) reached higher yields of aldehydes and alcohols, while the carbides with a lower Mo/W (1:3) ratio yielded high concentrations of alkenes. Interestingly, a physical mixture of two monometallic (1+1) carbides had a similar catalytic performance to the 1:1 mixed carbides. The intrinsic activity (turnover frequency (TOF)) of the catalysts was assessed based on both H_2 and CO chemisorption. The TOF_{H2} related linearly with the Mo/W ratio, while the TOF_{CO} did not show a relevant relationship. Therefore H_2 chemisorption is suggested as the preferred way to assess the intrinsic activities of these catalysts.

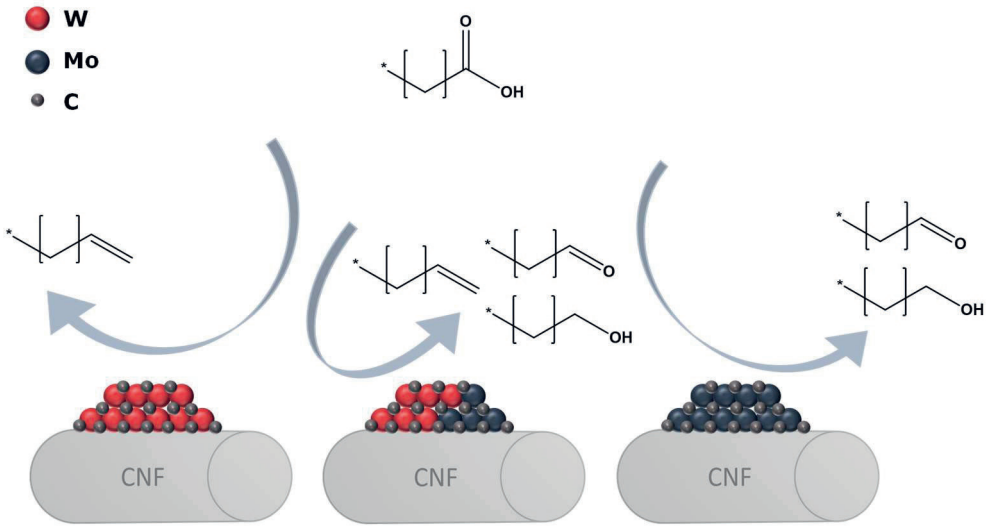

Introduction

Transition metal carbides like tungsten and molybdenum carbide display similar or better catalytic activities than noble metals while being less expensive and potentially having a higher tolerance against poisons.[1-4] Since the seminal article of Levy and Boudart in 1973[5], it became clear that Mo and W carbides are efficient catalysts for reactions that involve hydrogen activation such as hydrogenation[6], hydrodeoxygenation[7] or hydrogenolysis[8]. Lately, also bimetallic carbide catalysts e.g. CoMo-carbide[9], MoNi-carbide[10-13] and CoW-carbide[14] have attracted attention.

For instance, Smirnov et al.[15] used SiO_2 supported NiMo-carbide catalysts with different ratios of Mo_2C and Ni for the hydrodeoxygenation of anisole and the decarboxylation of ethyl caprate. A positive relation was found between the content of a Ni-Mo alloy and activity for the hydrogenation of anisole. A similar relation was found for the decarboxylation activity of ethyl caprate. Shao et al.[16] and Iyer et al.[17,18] found that unsupported Co_6W_6C catalysts form an active Co-WC phase for the dry reforming of methane to produce syngas. It was stated that these bimetallic carbides had improved activity and stability in comparison to other catalysts that are used for dry reforming (e.g. Ni and Mo_2C).

Also bimetallic Mo and W carbides have recently been used to study a potential synergetic effect between Mo and W carbides. Tran et al.[19] already showed that in a bulk MoW-carbide system a metallic W phase is present which increases the oxophilicity of the catalysts and increases the number of hydrogen activating sites. The number of sites in the mixed system is higher as expected from mixing the two monocarbides. This in turn lead to enhanced hydrodeoxygenation (HDO) activity and resulted in a shift in selectivity. The monometallic Mo_2C is active for both direct deoxygenation (producing benzene) and hydrogenation–dehydration (producing phenol), while the bimetallic MoW carbide strongly favours the deoxygenation pathway (producing benzene). Fu et al.[20] observed a synergistic effect when combining Mo_2C and W_2C supported on carbon nanotubes for the hydrogen evolution reaction (HER). The mixed carbide with a ratio of 3:1 Mo:W achieved the best electrocatalytic performance in the HER (lowest current density at 0.1V and Tafel slope of 34 mV/dec) in comparison to the monometallic and the bimetallic mixture of 1:1 and 1:3 Mo:W (Tafel slope of 45-112 mV/dec). This was attributed to a weaker Mo-H_{Abs} bond after the addition of W into the Mo-carbide system.

Motivated by these studies, we investigated bimetallic MoW-carbide catalysts for the hydrodeoxygenation of stearic acid. Monometallic Mo and W carbide catalysts are active for the

conversion of stearic (and oleic acid) into alkenes, oxygenates and alkanes following the HDO pathway (Scheme 1).[21-23]. This is in contrast to the noble metals like Pt, which follow under the same reaction conditions the decarboxylation (DCO, dashed blue box in Scheme 3.1) pathway.[22,24] The HDO pathway involves first the hydrogenation of stearic acid into aldehydes and alcohols i.e., oxygenates and subsequently, the oxygenates can further react via hydrogenation/dehydration yielding alkenes, which in turn can be hydrogenated to the alkanes (blue box in Scheme 3.1). Interestingly, when comparing carbon-supported Mo-carbides to W-carbides catalysts, the former ones were more selective towards oxygenates at low conversion levels, while the W-carbides were more selective towards alkenes even at high conversions.[21] The differences in intermediate product selectivity between the two carbides can be explained by the more oxophilic nature of W-carbide surface compared to Mo-carbide.[19,21]

In this paper, we want to establish to which extent we can combine the properties of both W-carbide and Mo-carbide by using carbon nanofiber supported mixed MoW-carbides. We will examine how the catalytic performance of mixed MoW carbides depends on the Mo:W ratio. The supported bimetallic carbide catalysts will be prepared by the carbothermal reduction and the hydrodeoxygenation of stearic acid (350 °C, 30 bar of H_2) will be used as test reaction.

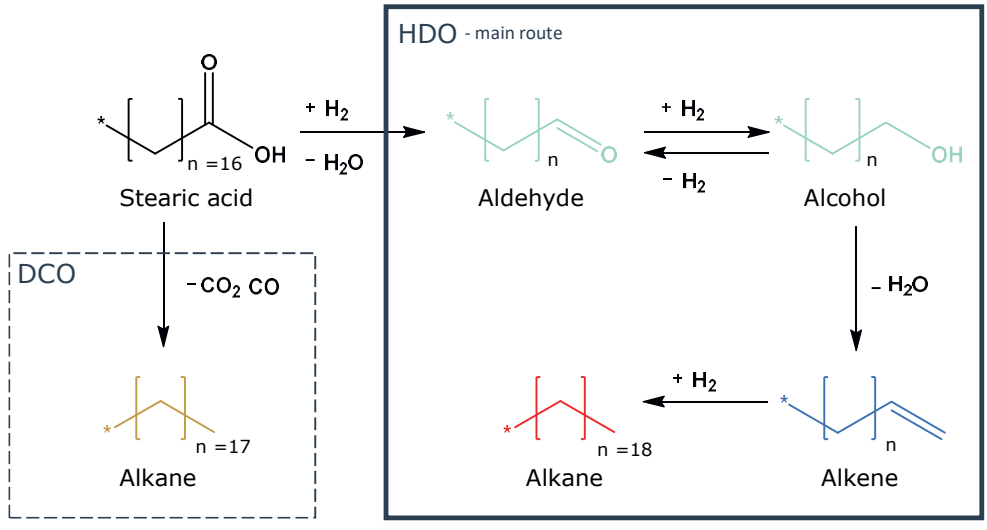

Scheme 3.1 Reaction pathway of the decarbonylation and decarboxylation (DCO) and hydrodeoxygenation (HDO) of stearic acid.

Materials & Methods

Catalyst synthesis

Carbon nanofibers (CNF) were grown from a mixture of hydrogen (102 ml/min), nitrogen (450 ml/min) and carbon monoxide (260 ml/min) at 550 °C and 3 barg for 24 h over a reduced 5 wt.% Ni/SiO_2 catalyst (3 g), as reported previously.[1] After synthesis the carbon fibers were treated three times (with intermediate washing with water) with a boiling 1 M KOH solution for 1 h to dissolve the SiO_2. Subsequently, the CNF were treated by refluxing 65% concentrated nitric acid for 1.5 h, to remove the nickel and introduce oxygen-containing functional groups on the CNF surface. Finally, the CNF were washed with demineralized water to neutral pH and ground to a 90-120 μm fraction.

CNF supported catalyst precursors were synthesized by incipient wetness impregnation. Ammonium heptamolybdate (AHM; Sigma-Aldrich, 99.98% trace metals basis), ammonium metatungstate (AMT; Sigma-Aldrich, 99.98% trace metals basis) or a mixture of both salts (molar ratio of Mo:W = 1:3, 1:1 and 3:1) was dissolved in demineralized water. Molar loadings of all catalysts were kept constant at 0.9 mmol metal $g^{-1}_{catalyst}$. After impregnation, the catalysts were dried overnight at 110 °C.

Catalysts were carburized via the carbothermal reduction, where a heat treatment was applied for 2h at 900 °C (β = 5 °C/min) under an N_2 flow (50 ml/min). Thus, the carburization was achieved by carbon originating from the support. To avoid contact with air, the carburized catalysts were directly transferred to the glove box workstation, which operated under constant N_2 flow.

In comparison to the bimetallic carbides, a physical mixture of the monometallic carbides was used. The catalyst precursors of monometallic Mo and W were mixed before the carburization.

Characterization

TEM images were acquired using a JEOL JEM-1400 Plus microscope operated at 100 kV. For the sample preparation, ~10 mg of the sample powder was diluted in 1 ml ethanol and deposited on a commercial carbon-coated copper grid. Particle size distributions were obtained by counting 300-400 particles using ImageJ software.

Nitrogen physisorption was used to assess the textural properties of the samples. Nitrogen adsorption/desorption isotherms were recorded at liquid nitrogen temperature using a Micromeritics, Tristar II Plus. Before measurement 100 mg of the sample was degassed at

200 °C for 2 h using a Micromeritics VacPrep 061. For assessing pore volumes, pore sizes and surface area the Brunauer-Emmet-Teller (BET)[25] approach was used.

CO and H_2 chemisorptions were performed on an AutoChem II (Micromeritics). Before the measurement, 200 mg of the catalyst precursor was first flushed for 30 min under He (20 ml/min), then *in situ* carburized at 900 °C (β = 5 °C /min) under He (50 ml/min) and cooled to room temperature under He (50 ml/min). For the CO chemisorption, the samples were maintained at 35 °C under He (50 ml/min). Pulses of 0.5 ml 10 % CO/He were injected into the He flow. The CO uptake was assessed by TCD and mass spectrometry. The procedure was similar for the H_2 chemisorption, except that 10 % H_2/Argon was injected into Argon which was used as carrier gas. After the chemisorption measurements the samples were analyzed by XRD to assess whether the same crystalline carbide phase was formed during the in situ carburization as during the ex-situ carburization used for the catalytic experiments. During the transfer from the chemisorption to the XRD workstation the carbide catalysts have been in contact with air.

XRD patterns were recorded on a Bruker D8 Advance using an Lynxeye-XE-T PSD detector and using Cu-K$\alpha_{1,2}$ radiation (λ = 1.542 Å). The measurements were taken from 2θ = 20° to 2θ = 50° with a collection time of 1 sec.

Temperature Programmed Desorption of ammonia (NH_3-TPD) was performed on a Micromeritics AutoChem 2920 apparatus. About 100 mg of the catalyst precursor was first flushed for 15 min under He (50 ml/min) and then *in situ* carburized at 900 °C (β = 5 °C /min) under He (50 ml/min). Subsequently, the sample was cooled to 100 °C and then 20 pules of NH_3 with 10 % NH_3/He were applied while flowing He (25 ml/min). Afterwards, the sample was heated to 600 °C with a ramp of 5 °C/min and held for 30 min to desorb the NH_3 in a pure He flow.

Catalytic testing

The catalytic reactions were performed in a 100 mL stainless steel Parr autoclave, 4598 Micro batch reactor system. During a standard procedure, the reactor was filled with 250 mg catalyst and 50 ml (Sigma-Aldrich, ReagentPlus ®, ≥99%) (transferred under N2 as described above), 2 g stearic acid (octadecanoic acid, Sigma-Aldrich, ≥95%, FCC, FG), 1 g of tetradecane as internal standard (Sigma-Aldrich, ≥99%). The mixture was twice purged with 30 bar Ar and afterwards flushed with H_2. Subsequently, the reactor was pressurized to 30 bar of H_2, heat up to 350 °C (14 °C/min) and stirred at 800 rpm. The first sample (t=0 min) was taken when the reactor reached a temperature of 70 °C (the melting point of stearic acid). The catalytic reaction was

run for 4 h. A Parr 4878 Automated Liquid Sampler allows collection of filtered liquid samples from the reactor taken at regular time intervals to investigate the product distribution. After taking a sample the pressure was readjusted (when needed) to the setpoint it was found before taking the sample. Prior to GC-FID analysis, 100 μL of the sample was diluted with 900 μL of CH_2Cl_2:MeOH (2:1 v/v%) to dissolve the stearic acid and oxygenate products. Product (normalized) yields were calculated according to (1). The molar carbon balance of the liquid samples of all catalysts is between 80-95%.

$$Yield_{productX} = \frac{[Product_x]}{\sum[Product]+[Stearic\ Acid]} * 100 \qquad (3.1)$$

With [$Product_x$] concentration of a specific product x, [Product] concentration of all products, [stearic acid] concentration of stearic acid at a given time.

The total metal based reaction rate (TMR) is calculated based on the converted moles of stearic acid per mol of metal (W + Mo). The turnover frequency (TOF) values were based on CO or H_2 chemisorption site density and the stearic acid conversion after 1 hour. The following equation was used:

$$TOF = \frac{Mol\ stearic\ acid\ converted}{Reaction\ time\ (s)*Mol\ of\ active\ sit} \qquad (3.2)$$

Results & Discussion

Characterization of bimetallic carbides

In a separate paper, we focused on the synthesis and characterization of CNF supported mixed carbides.[26] Here a brief summary (Figure 3.1) of these results is given to understand the most important characteristics of the samples. In addition to that new characterization results relevant for the use of these materials as catalysts for stearic acid deoxygenation will be presented (N_2 physisorption, TEM, H_2/CO/NH_3 chemisorption and XRD).

In the carbothermal reduction synthesis, the carbon support containing the metal precursor is heated in an inert atmosphere and the carbon from the support is utilized as reduction and carburization agent. During the reduction of the (Mo/W) oxide to the carbide CO is released measured by TPD-MS and a mass loss was detected by TGA.[26] For the synthesis of mixed metal carbides, the *in-situ* TPD-MS and TGA analyses of the carburization process were used to assess whether the carburization of the mixed carbides proceeds in one step or several. In fact, it does proceed in one step as shown in Figure 3.1 A with a carburization temperature (CO release) inbetween those of the monometallic carbides. A physical mixture of the carbide precursors

shows again two carburization peaks at the positions of the respective monometallic carbides. This indicates that the mixed carbides consist of a single mixed phase. A similar trend can be observed in Figure 3.1 B where the thermogravimetric analysis is plotted as DTG (derivate of the mass loss) versus temperature i.e. a single peak representing carburization for the mixed materials. Further investigation of the synthesized carbides with STEM-EDX (Figure 3.1 C) revealed that they indeed have mixed Mo:W nanoparticles with average compositions matching the W and Mo content of the samples.

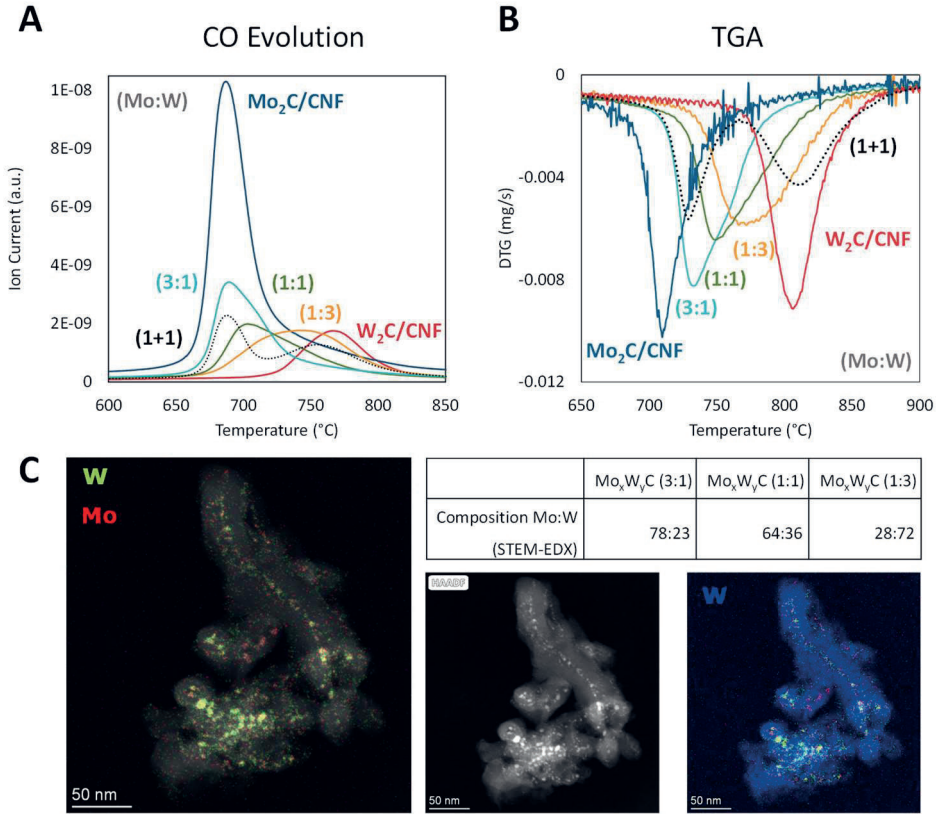

Figure 3.1 A: TCD signal representing CO evolution during CR synthesis of monometallic and mixed-metal carbides. B: Comparison of weight change rates during CR synthesis of monometallic and mixed-metal carbides. C: HAADF-STEM image with EDX map overlays of the CR-prepared monometallic and mixed-metal carbides.

The textual properties of the support and synthesized catalyst were studied with nitrogen physisorption. The surface area (BET), total pore volume and micropore volume are listed in Table 3.1. The surface area of parent CNF support is 199 m^2/g, which is in agreement with earlier studies for CNF made via the same synthesis protocol.[27-29] Among the carbide catalysts

no large differences in the textural properties were observed, showing that the Mo or W content does not affect the textual properties of the catalyst. However, the BET surface areas of the catalysts were reduced by ca. 40% when compared to the CNF support. This is partly due to the loading of the support with metal carbides (assuming the carbides are non porous). In addition, in the parent CNF some amorphous carbon can be present (causing the higher micropore volume observed in Table 3.1) which can be lost during the carburization process. Moreover, pore blocking by the metal-carbide can occur which all can explain the decrease in BET surface area.[30-32]

Table 3.1 Textural properties of CNF, Mo_2C/CNF, W_2C/CNF and mixed MoW-carbides, as determined by N_2-physisorption.

	BET surface area (m^2/g)	Pore volume (cm^3/g)	Micropore volume (cm^3/g)
CNF	199	0.4	$2.0*10^{-2}$
Mo_2C/CNF	131	0.3	$1.8*10^{-3}$
W_2C/CNF	102	0.3	$3.4*10^{-3}$
Mo_xW_yC/CNF (1:1)	114	0.3	$5.3*10^{-3}$
Mo_xW_yC/CNF (1:3)	133	0.3	$9.7*10^{-3}$
Mo_xW_yC/CNF (3:1)	144	0.3	$1.1*10^{-3}$

The structure and particle size of CNF supported carbide catalysts are further examined by transmission electron microscope (TEM) as depicted in Figure 3.2. The carbide particles appear as spherical shaped particles supported on the fibers. The carbide nanoparticles size of the synthesized carbides is typically 4-6 nm with averages between 4.3 and 5.7 nm as indicated in Figure 3.2. All mixed carbides thus have similar particle sizes in line with those reported earlier.[21,27]

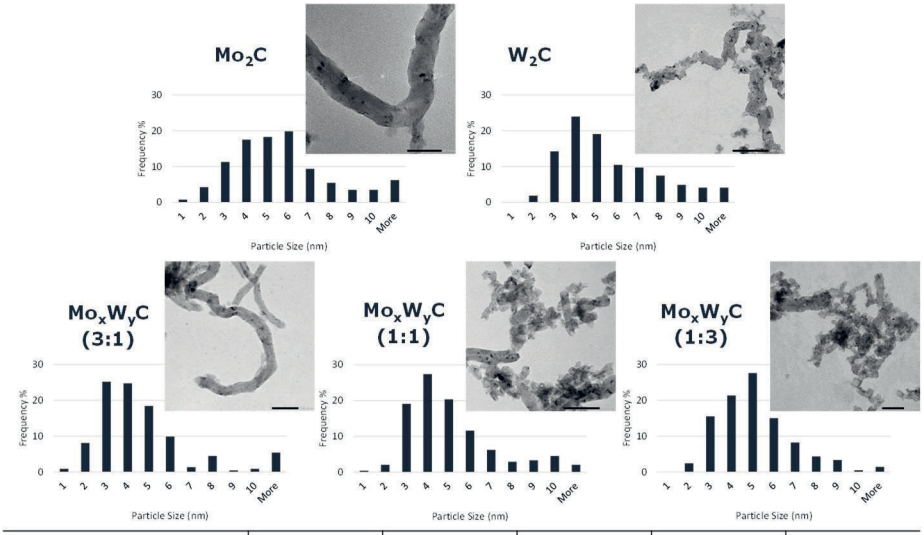

	Mo_2C	MoW (3:1)	MoW (1:1)	MoW (1:3)	W_2C
Mean diameter (nm)	5.7	4.7	4.6	4.3	5.2
Std. Dev. (nm)	3.7	1.9	2.2	3.1	2.5

Figure 3.2 TEM images and particle size distribution of monometallic Mo and W and bimetallic MoW-carbide catalysts

In order to get more insight into the number and nature of the (re)active sites CO/H_2-chemisorption (for metallic sites) and NH_3-TPD experiments (for acids sites) were performed. H_2-chemisorption[33,34] and especially CO chemisorption[33-38] are commonly used to probe the carbidic sites. Please note that it is essential to perform chemisorption without exposure of the samples to air since that might (surface) oxidize the carbide. Therefore we carburized our samples *in situ*. Table 3.2 shows the measured CO and H site densities. The CO uptake for all carbide catalysts is in the range of 44-52 µmol/g. The pure Mo-carbide has the lowest (44.4 µmol/g) and the pure W-carbide has the highest CO uptake (51.7 µmol/g). The mixed carbide catalysis show values intermediate to those of the pure carbides. For the H_2-chemisorption the W-carbide (30.2 µmol/g) had the highest uptake followed by the Mo carbide (22.8 µmol/g) but here the mixed carbides showed the lowest site densities (15-21 µmol/g). In addition to H_2-chemisorption, the measured site densities were lower compared to the CO site density. Clearly, both probe gases do not measure the same sites. In addition also the ratio between these sites is varying among samples since the ratio of the CO to H site densities varied between 1.7 and 3.1 (Table 3.2).

Table 3.2 CO and H site densities (µmol/g) of Mo_2C/CNF, W_2C/CNF and three mixed MoW-carbides with different Mo:W ratios.

	Mo_2C	Mo_xW_yC (3:1)	Mo_xW_yC (1:1)	Mo_xW_yC (1:3)	W_2C
CO site density (µmol/g)	44.4 ±2.7	47.8 ±4.8	46.7 ±5.2	48.6 ±3.9	51.7 ±5.2
H site density (µmol/g)	22.8 ±10.4	15.2 ±3.0	19.2 ±6.6	21.2 ±1.3	30.2 ±1.0
Ratio CO/H	1.9	3.1	2.4	2.3	1.7

*Uncertainties based on the duplicate measurements of the chemisorption.

In addition, we also probed the acidic sites of the fresh monometallic Mo and W carbide catalysts by NH_3-TPD. No desorption could be detected showing that the amount of acid sites on these materials is insignificant (Figure S3.1).

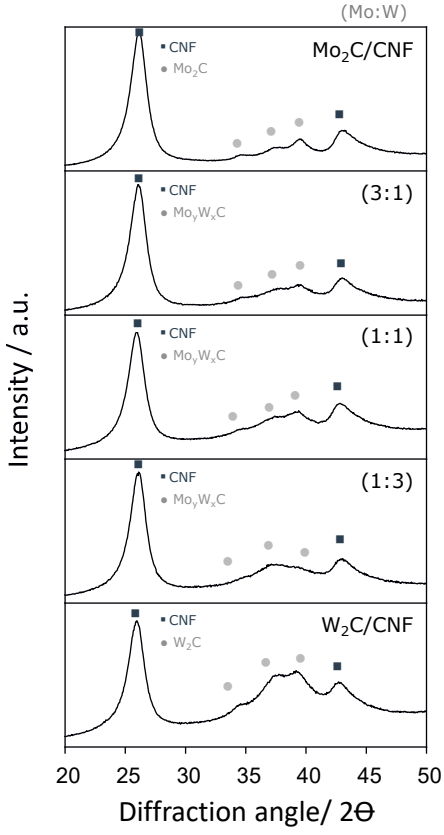

Figure 3.3 XRD pattern of monometallic carbide catalyst samples and bimetallic carbide catalyst samples post chemisorption analysis.

In order to assess the nature of the carbide phases formed during the *in-situ* carburization in the chemisorption equipment, the catalysts were investigated with XRD directly after the (CO and H_2) chemisorption measurements (Figure 3.3). The signals at 2θ=28° and 2θ=43° represent the (002) and (101) reflections of the CNF.[29] Further, the XRD pattern displays the characteristic peaks of the hexagonal semi carbide phases (W_2C, Mo_2C) indicating that all catalysts are carburized and have the same crystal structure regardless of their composition. For the Mo_2C these peaks are at 2θ= 34.4°, 37.8° and 39.4° (PDF 79-0744) and for W_2C at 2θ= 34.5°, 38.0° and 39.5° (PDF 89-2371). It is expected that $I_{carbide}/I_{CNF}$ increases with increasing W-loading since the molar loading is constant, and tungsten is a much heavier scatterer than molybdenum. The
sample fall within the expected
r the (1: 3) sample does not
ich we can not explain at this

moment.

Nevertheless, these XRD results are identical to the post synthesis XRD measurements showing that small differences in carburization (smaller scale) set-up do not affect the carburization process.

Catalytic performance

The catalytic performance (selectivity and activity) of the prepared catalysts was evaluated for the stearic acid hydrodeoxygenation in a batch reactor (350 °C and 30 bar H_2).

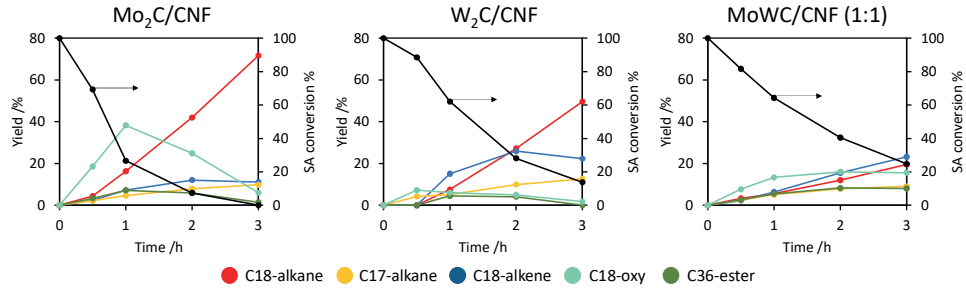

Figure 3.4 Stearic acid conversion and product distribution over time of Mo_2C/CNF, W_2C/CNF, bimetallic Mo:W carbides with ratio of 1:1. (250 mg catalysts, 2 g stearic acid, 350 °C, 50 ml solvent, 30 bar H_2)

Figure 3.4 presents product yields over time for the monometallic carbides, the three bimetallic carbides with different ratios and a physical mixture of the two monometallic carbides (W-carbide and Mo-carbide). The two main possible pathways (Scheme 3.1) of stearic acid towards hydrocarbons are (1) the direct decarboxylation (DCO) involving C-C cleavage yielding C17 alkanes and (2) the hydrodeoxygenation (HDO) yielding C18 products. The formation of DCO products (C17) is observed for all carbide catalysts but with low selectivity (~10%). All the carbide catalysts do show high selectivity towards products of the HDO pathway (oxygenates, saturated and unsaturated C18). However, there are substantial differences in the product distribution profiles. The Mo carbide reaches high yields towards oxygenates (max 38 mol% after 1h), while the W-carbide more selectively produces alkenes (max 26 mol% in 2h) as the main intermediate product. The bimetallic systems with a 1:1 metal ratio simultaneously produce significant amounts of both, alkenes and oxygenates as intermediate products. Formation of higher C36-esters via condensation of oxygenates was observed to be a minor reaction pathway over all of the tested carbide catalysts.

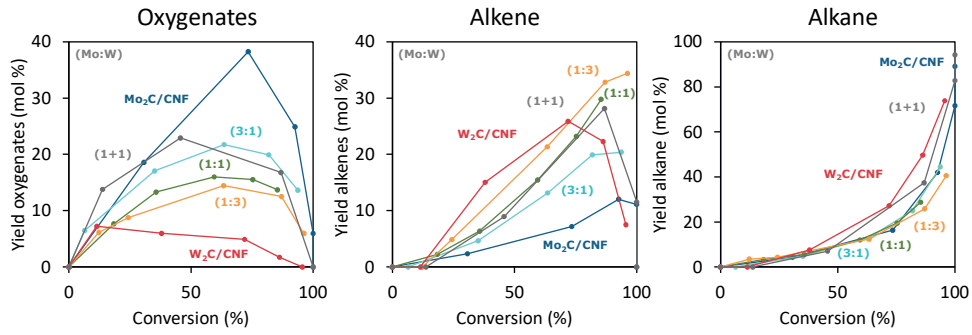

Figure 3.5 Oxygenates, alkene and alkane yield vs conversion of monometallic and bimetallic carbide systems during stearic acid hydrodeoxygenation (250 mg catalysts, 2 g stearic acid, 350 °C, 50 ml solvent, 30 bar H_2)

To make a clearer comparison of the catalytic behaviour between the different carbide catalysts, the yield as a function of the conversion for oxygenates, alkenes and alkanes over the mono and bimetallic carbides was plotted in Figure 3.5. The monometallic Mo carbide catalyst yielded maximum oxygenates of 40% (C18-oxy) at conversion levels of 80 mol% and the monometallic W carbide yielded maximum alkene of 28% (C18-alkene) production at 70 mol% conversions. The bimetallic carbides reach oxygenates and alkene yields in between that of the monometallic carbide, where the bimetallic system with higher Mo wt.% also reaches higher oxygenates yields while the system with higher W wt. % higher yields of alkenes. Interestingly, the bimetallic catalysts retain highly selective towards the alkene at higher stearic acid conversions (20-40 mol% alkenes at > 80 % conversion), while the monometallic W-carbide showed lower alkene yield at higher conversions (10 mol% alkenes at 90% conversion). Another interesting observation was made for the physical mixture which behaves in terms of selectivity similar to the 1:1 bimetallic carbide system.

Table 3.3 Activity of the carbide catalysts based on weight (TMR), CO chemisorption (TOF_{CO}) and H_2 chemisorption (TOF_{H2})

Catalyst	**Mo_2C**	**Mo_xW_yC (3:1)**	**Mo_xW_yC (1:1)**	**Mo_xW_yC (1:3)**	**W_2C**
TMR *10^2 (min^{-1})[a]	9.6	4.6	4.7	3.2	4.9
TOF_{CO} (min^{-1})[b]	9.7	4.3	4.5	2.9	4.3
TOF_{H2} (min^{-1})[c]	18.9	13.5	10.9	6.7	7.4

a. Converted moles of stearic acid per mol W and/or Mo after 1h
b. Turnover frequency based on CO chemisorption after 1h
c. Turnover frequency based on H_2 chemisorption after 1h

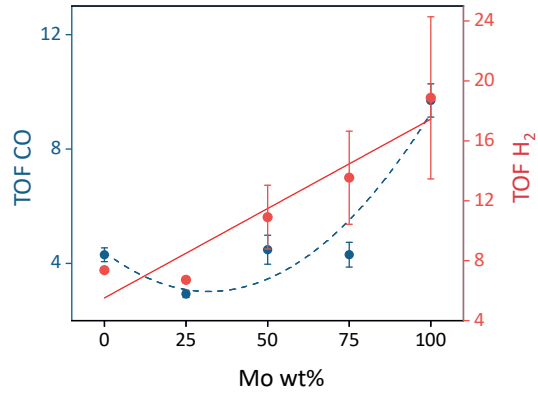

Figure 3.6 CO and H_2 density sites based TOF versus Mo wt%

The initial activity (in the 1st hour) for all catalysts is reported in Table 3.3. The activity is expressed as both total metal based rate (TMR, converted moles of stearic acid per mol W and/or Mo) and turn-over-frequency (TOF, converted moles of stearic acid per mol surface sites) using the site density from CO (TOF_{CO}) and H_2-chemisorption (TOF_{H2}), see Table 3.2. The TMR shows that the monometallic Mo-carbide is the most active, being almost two times more active than the monometallic W-carbide. The bimetallic carbides are comparable in activity to the W-carbide. When only comparing the TOF value of the two monometallic carbides either the TOF_{CO} or TOF_{H2} could be used since the ratio active site form H_2 and CO are similar. For the bimetallic carbides, this ratio changes and thus a different picture of the activity is obtained for the TOF_{CO} or TOF_{H2}. This trend is highlighted by plotting both TOF versus the Mo content of the catalysts in Figure 3.6. For the bimetallic mixtures, the TOF_{CO} does not so show a clear relation with the Mo content and appears similar to that of the monometallic W. In contrast, the TOF_{H2} increases linearly with the increasing Mo wt%.

Overall Discussion

Characterization

Depending on the carburization conditions different textual and structural properties e.g. complex crystal structures and different phase compositions (carbide versus oxycarbides) may emerge.[39] For that reason it is important to establish these properties among a set of different carbide catalysts and to enable the comparison of the different catalysts, since e.g. crystal structures,[27,40] phase compositions[23] and particle sizes[39] can affect the catalytic activity and selectivity. First of all the BET surface area and pore volume measured by N_2 physisorption did not show significant differences among the carbide catalysts. The XRD measurements revealed that the synthesis via the carbothermal reduction for both the monometallic carbides and

bimetallic carbide samples results in a metal carbide phase with a hexagonal crystal structure. Since no other oxides or oxycarbide phase was detected we conclude that a fully carburized phase (Me_2C, Me=Mo or W) with the same structure was obtained for all catalysts. TEM images of the bimetallic and monometallic carbide catalysts were taken to examine the particle size. The average nanoparticle size for all catalysts (Figure 3.2) was found to be in a similar range of 4-6 nm which is in agreement with similarly prepared carbide catalysts.[21,23,27] For the bimetallic catalyst the interaction between Mo and W had been demonstrated by the changes in carburization temperature.[26] The formation of mixed metal carbides was proven by HAADF-STEM analysis which revealed that the carburization process results in individual nanoparticles containing both Mo and W in a composition that is on average close to those of their respective bulk ratio.[26] Thus we conclude that the bimetallic catalysts consist of nanoparticles containing both Mo and W but without discernible difference in terms of surface area, crystal phase and nanoparticle size compared to the monometallic samples. However, by performing H_2 and CO chemisorption (Table 3.2) to probe the carbidic sites of the prepared carbide catalysts[33,41], differences between the mono and bimetallic carbide could be established. The CO site density of supported Mo_2C was slightly lower (44 μmol/g) in comparison to the W_2C (52 μmol/g). The bimetallic carbides have CO site densities in-between that of the pure metal carbides (47-48 μmol/g). In contrast, the results of the H_2-chemisorption show that the bimetallic carbides have lower site densities (15-22 μmol/g) than the monometallic carbides (23 and 30 μmol/g for the Mo-carbide and W-carbide respectively). As a result, the CO/H_2 ratios are similar for the monometallic carbide catalysts (1.7-1.9) but increase for the bimetallic carbides (2.3-3.1). The fact that this ratio increases for the bimetallic carbides, while the CO site density for bimetallic catalyst is as would be expected based on the results of Mo-carbide and W-carbide, shows that the decrease in H_2 site density for the bimetallic catalysts is not simply due to a difference in particle size, which is also in agreement with the TEM analysis. The decrease in H_2 sites for the bimetallic catalyst thus appears to be a direct consequence of the formation of the mixed metal carbides. We therefore suggest that the molecular adsorption of CO on the metal centers of the carbide surface[42,43] is not significantly affected by the alloying while the ensembles of sites required for the dissociative adsorption of H_2[44] are diminished due to the alloying.

Catalytic performance

The catalytic selectivity and activity of the different carbide catalysts were evaluated for the hydrodeoxygenation of stearic acid in a batch reactor (350°C and 30 bar H_2). As mentioned earlier, the deoxygenation of stearic acid can occur either via the decarboxylation (and decarbonylation) pathway (DCO) yielding hydrocarbon chains with one carbon atom less than the reactant or via the hydrodeoxygenation (HDO) resulting in hydrocarbons with same chain

lengths. Direct decarboxylation and/or decarbonylation of stearic acid into C17 hydrocarbons has previously been reported to occur over WO_x and MoO_x species.[22,23] We observed only small amounts (~10 %) of DCO products in the reaction mixture, suggesting that no or low amounts of oxide species were present in the catalyst. This is in agreement with β-Mo_2C as the dominant crystal phase and the absence of metal oxide species (MoO_3 and WO_3/WO_2 crystalline phases) revealed by the XRD analysis. Additionally, the absence of acid sites revealed by NH_3-TPD further demonstrates the absence of significant amount of oxy-carbide surface sites on the in-situ prepared catalyst.

For the HDO reaction pathway over Mo and W carbide catalysts, it has been reported that bi-functional properties are present in the form of a metallic hydrogenation and acidic dehydration functionality.[45] These acid sites are the result of some form of oxygen introduction to the carbide surface which can either be introduced after the carburization by exposure to air (passivation)[46] or originates from *in-situ* generation of O*-Me_2C species[45] when the catalyst is exposed to oxygen from the reactant or to the formed water.[47,48] Since on our Mo and W carbide catalysts no NH_3 desorption and thus no acid sites could be detected, our results agree with the latter explanation. For the bimetallic MoW carbide catalysts these bi-functional properties also remain, since all the catalysts preferred HDO route yielding C18 products. However, a marked difference in product composition over time was observed between the W-carbide, bimetallic-carbides and Mo-carbide catalysts. A clear difference in the main intermediate was observed with high yields of oxygenates (aldehyde and alcohol, ~40 mol%) observed up to high conversion with Mo-carbide while high yields of unsaturated C18 (~25 mol%) were found for W-carbide at high conversion level. This can be explained by a difference in the relative rates of acid hydrogenation and alcohol dehydration between Mo-carbide and W-carbide. For the Mo-carbide the hydrogenation of the acid proceeds relatively fast compared to the dehydration rate to the alkene, this results in increased levels of oxygenates as the main intermediate. In comparison, for the W-carbide the hydrogenation of the acid to oxygenates occurs slower than the dehydration toward the alkene, which results in elevated levels of alkenes as the main intermediate. The higher dehydration activity of W-carbide is then likely related to higher acidity. The difference between the Mo and the W carbide has earlier been explained by their differences in oxyphilic properties (and hydrogenation power).[21,33,35,49,50] The more oxophilic W-carbide is more likely to generate acids sites upon exposure to oxygen or in reactions with oxygenated compounds. The observation that with the W-carbide no alkenes are present at the initial stage of the reaction (Figure 3.4 and 5) suggests that it takes some time until sufficient amounts of acidic sites are formed.

The mixed Mo:W carbides reached oxygenate and alkene yields in between that of the monometallic caribes. The bimetallic systems with a higher Mo wt% have higher selectivity towards oxygenates, while the bimetallic systems with higher W content are more selective for alkenes. Interestingly, we observed that the bimetallic catalysts with a ratio of 1:3 Mo to W retain high selectivity towards the alkene at higher stearic acid conversions (35 mol% alkenes at > 80 % conversion), while the monometallic W-carbide showed lower alkene yield at higher conversions (10 mol% alkenes at 90 % conversion). Hence, the addition of molybdenum to W carbide catalysts delays full hydrogenation of the alkenes. This may appear counterintuitive since we have established that Mo is the better hydrogenation catalyst. However, Figure 3.5 also shows that higher alkane yields are obtained over monometallic W-carbide at each measured conversion level. This is the result of the much higher intermediate alkene concentration with the monometallic W-carbide. Reducing the dehydration activity by the addition of Mo can thus result in a shift of maximum alkene production to higher conversion levels.

Interestingly, the physical mixture (1+1) and the bimetallic system (1:1) do behave similarly (see Figure 3.5). The oxygenates, alkenes and alkane yields of the physical mixture and the bimetallic system are nearly identical at each conversion level. Thus irrespective whether the carbide catalysts do contain mixed ($Mo_xW_yC_z$) nanoparticles or monometallic carbides (Mo_2C + W_2C), the catalytic selectivity of both catalysts is similar. These results suggest that mixed Mo-W carbide active centers either have catalytic properties in between those of Mo and W or that the nanoparticles consist of ensembles still mainly Mo-carbide or W-carbide in nature.

Besides the differences in product distribution also the catalytic activity of the monometallic and bimetallic catalysts were compared. It should be mentioned that comparing the activities is not straightforward considering the bifunctional nature of the catalyst and the mentioned possibility of the *in-situ* formation of new active sites. Hence, we limit ourselves to a comparison of the initial activity in which mainly the activity of the catalyst with respect to the acid hydrogenation is evaluated (Table 3.3). On a total metal basis the Mo-carbide was found to be the most active catalyst (9.6 min^{-1}) followed by the W-carbide catalyst (4.9 min^{-1}) and the mixed metal carbides are found to be the least active (3.2-4.7 min^{-1}). To get more insight into the reason for the decreased activity of the bimetallic catalysts we also compared the site based activities (Table 3.3 and Figure 3.6) using the site density from both CO and H_2 chemisorption (Table 3.2). For the monometallic catalyst, the TOF based on either CO or H_2 shows that the Mo-carbide has a higher site based initial activity than W-carbide. These trends are consistent with previous reports.[21,23] Since the ratio between CO and H_2 uptake is nearly the same for the monometallic carbides (1.7-1.9), either can be used for a comparative evaluation of the site

based activity. We demonstrate that this is not the case for bimetallic catalysts for which the CO/H_2 ratio differs from the monometallic carbides (2.3-3.1). We already concluded that changes in CO/H_2 ratio is due to a decrease in H_2 site density when forming the mixed metal carbide phase. Thus the decreased activity on a total metal basis correlates to a decrease in the H_2 site density. Figure 3.6 reveals that for the TOF_{H2} a linear relation is obtained with the Mo content of the catalyst. In other words, the sites probed by H_2 in the bimetallic catalyst act as a linear combination of those present in pure Mo-carbide and W-carbide sites. On the other hand, using the TOF_{CO} values would lead to the conclusion that the surface of bimetallic particles behaves more like the monometallic W-carbide, which we know is not the case since we have established that the bimetallic catalysts have a behavior which is in-between the pure metal carbides with respect to their product formation. Given these results and the fact that the initial reaction step is in fact a hydrogenation reaction, i.e. requiring hydrogen activation, we suggest that H_2 based activity is the best descriptor for the TOF.

Conclusion

The catalytic performance of MoW mixed metal carbide catalysts in the stearic acid deoxygenation has been studied. Both monometallic carbides (W-carbide and Mo-carbide) and the bimetallic carbides (MoW-carbide with different ratios) preferred the HDO pathway over the DCO pathway, which is consistent with the presents of a pure metal carbide phase without strong acid sites according to XRD and ammonia TPD. The Mo:W ratio was found to influence the product yield towards either oxygenates or alkenes in the HDO pathway. The more Mo-rich samples have a higher yield towards oxygenates, while the more W-rich samples have higher yields towards the alkene intermediate. The behaviour of the 1:1 MoW-carbide was found to be similar to a physical mixture of monometallic Mo and W-carbides. Based on the characterization with TEM and both CO and H_2 chemisorption it was shown that the formation of a bimetallic phase results in a decrease in H_2 site density. The linear relation of the H_2 site based activity together with the evolution of the product distribution as function of the Mo content of the catalyst, suggests that the H_2 site density is a better descriptor for site base activity than the CO site density. Therefore, we conclude that although the formation of a bimetallic carbide results in loss of hydrogenation sites, the properties of the monometallic catalyst (having higher hydrogenation activity for Mo-carbide and higher dehydration activity for the W-carbide) are proportionally transferable to the bimetallic systems.

Acknowledgement

Acknowledgement is made to the Dutch Research Council (NWO) for financial support (grant number NOW 729.004.002). The authors gratefully thank Susan Witte for assistance with GC-FID measurements. We also would like to thank Sebastian Haben for performing the NH_3-TPD analysis and Raghavendra Meena for the discussion regarding the CO and H_2 dissociation on the carbide surface.

References

(1) Führer, M.; van Haasterecht, T.; Bitter, J. Molybdenum and tungsten carbides can shine too. *Catalysis Science & Technology* **2020**.

(2) Mehdad, A.; Jentoft, R. E.; Jentoft, F. C. Single-phase mixed molybdenum-niobium carbides: Synthesis, characterization and multifunctional catalytic behavior in toluene conversion. *Journal of catalysis* **2017,** *351*, 161.

(3) Szymanska-Kolasa, A.; Lewandowski, M.; Sayag, C.; Brodzki, D.; Djega-Mariadassou, G. Comparison between tungsten carbide and molybdenum carbide for the hydrodenitrogenation of carbazole. *Catal Today* **2007,** *119* (1-4), 35.

(4) Da Costa, P.; Lemberton, J.-L.; Potvin, C.; Manoli, J.-M.; Perot, G.; Breysse, M.; Djega-Mariadassou, G. Tetralin hydrogenation catalyzed by Mo2C/Al2O3 and WC/Al2O3 in the presence of H2S. *Catal Today* **2001,** *65* (2–4), 195.

(5) Levy, R. B.; Boudart, M. Platinum-Like Behavior of Tungsten Carbide in Surface Catalysis. *Science* **1973,** *181* (4099), 547.

(6) Kojima, I.; Miyazaki, E.; Inoue, Y.; Yasumori, I. Catalytic activities of TiC, WC, and TaC for hydrogenation of ethylene. *J. Catal.;(United States)* **1979,** *59* (3).

(7) Kumar, A.; Phadke, S.; Bhan, A. Acetic acid hydrodeoxygenation on molybdenum carbide catalysts. *Catalysis Science and Technology* **2018,** *8* (11), 2938.

(8) Lee, J. S.; Locatelli, S.; Oyama, S. T.; Boudart, M. Molybdenum carbide catalysts 3. Turnover rates for the hydrogenolysis of n-butane. *Journal of Catalysis* **1990,** *125* (1), 157.

(9) Al-Megren, H. A.; Xiao, T.; Gonzalez-Cortes, S. L.; Al-Khowaiter, S. H.; Green, M. L. Comparison of bulk CoMo bimetallic carbide, oxide, nitride and sulfide catalysts for pyridine hydrodenitrogenation. *Journal of Molecular Catalysis A: Chemical* **2005,** *225* (2), 143.

(10) Masoumi, S.; Dalai, A. K. NiMo carbide supported on algal derived activated carbon for hydrodeoxygenation of algal biocrude oil. *Energy Conversion and Management* **2021,** *231*, 113834.

(11) Chen, H.; Wang, Q.; Zhang, X.; Wang, L. Effect of support on the NiMo phase and its catalytic hydrodeoxygenation of triglycerides. *Fuel* **2015,** *159*, 430.

(12) Zhao, L.; Fang, K.; Jiang, D.; Li, D.; Sun, Y. Sol-gel derived Ni-Mo bimetallic carbide catalysts and their performance for CO hydrogenation. *Catal Today* **2010,** *158* (3-4), 490.

(13) Zhang, S.; Shi, C.; Chen, B.; Zhang, Y.; Zhu, Y.; Qiu, J.; Au, C. Catalytic role of β-Mo2C in DRM catalysts that contain Ni and Mo. *Catal Today* **2015,** *258*, 676.

(14) Izhar, S.; Yoshida, M.; Nagai, M. Characterization and performances of cobalt-tungsten and molybdenum-tungsten carbides as anode catalyst for PEFC. *Electrochimica Acta* **2009,** *54* (4), 1255.

(15) Smirnov, A. A.; Geng, Z.; Khromova, S. A.; Zavarukhin, S. G.; Bulavchenko, O. A.; Saraev, A. A.; Kaichev, V. V.; Ermakov, D. Y.; Yakovlev, V. A. Nickel molybdenum carbides: Synthesis, characterization, and catalytic activity in hydrodeoxygenation of anisole and ethyl caprate. *Journal of Catalysis* **2017,** *354*, 61.

(16) Shao, H.; Kugler, E. L.; Ma, W.; Dadyburjor, D. B. Effect of temperature on structure and performance of in-house cobalt– tungsten carbide catalyst for dry reforming of methane. *Ind Eng Chem Res* **2005,** *44* (14), 4914.

(17) Iyer, M. V.; Norcio, L. P.; Kugler, E. L.; Dadyburjor, D. B. Kinetic Modeling for Methane Reforming with Carbon Dioxide over a Mixed-Metal Carbide Catalyst. *Ind Eng Chem Res* **2003,** *42* (12), 2712.

(18) Iyer, M. V.; Norcio, L. P.; Punnoose, A.; Kugler, E. L.; Seehra, M. S.; Dadyburjor, D. B. Catalysis for Synthesis Gas Formation from Reforming of Methane. *Topics in Catalysis* **2004,** *29* (3), 197.

(19) Tran, C. C.; Hang, Y. L.; Garcia-Perez, M.; Kaliaguine, S. Synergistic effect of Mo-W carbides on selective hydrodeoxygenation of guaiacol to oxygen-free aromatic hydrocarbons. *Catalysis Science & Technology* **2019,** *9* (6), 1387.

(20) Fu, Q.; Peng, B. X.; Masa, J.; Chen, Y. T.; Xia, W.; Schuhmann, W.; Muhler, M. Synergistic Effect of Molybdenum and Tungsten in Highly Mixed Carbide Nanoparticles as Effective Catalysts in the Hydrogen Evolution Reaction under Alkaline and Acidic Conditions. *Chemelectrochem* **2020,** *7* (4), 983.

(21) Stellwagen, D. R.; Bitter, J. H. Structure–performance relations of molybdenum-and tungsten carbide catalysts for deoxygenation. *Green Chemistry* **2015,** *17* (1), 582.

(22) Hollak, S. A. W.; Gosselink, R. W.; van Es, D. S.; Bitter, J. H. Comparison of Tungsten and Molybdenum Carbide Catalysts for the Hydrodeoxygenation of Oleic Acid. *Acs Catalysis* **2013,** *3* (12), 2837.

(23) Gosselink, R. W.; Stellwagen, D. R.; Bitter, J. H. Tungsten-Based Catalysts for Selective Deoxygenation. *Carbohydrate research* **2013,** *52* (19), 5089.
(24) Snåre, M.; Kubic˘kova, I.; Mäki-Arvela, P.; Eränen, K.; Murzin, D. Y. Heterogeneous catalytic deoxygenation of stearic acid for production of biodiesel. *Ind Eng Chem Res* **2006,** *45* (16), 5708.
(25) Sinha, P.; Datar, A.; Jeong, C.; Deng, X.; Chung, Y. G.; Lin, L.-C. Surface area determination of porous materials using the Brunauer–Emmett–Teller (BET) method: limitations and improvements. *The Journal of Physical Chemistry C* **2019,** *123* (33), 20195.
(26) Führer, M.; van Haasterecht, T.; Bitter, J. H. Synthesis and Characterization of Supported Mixed MoW Carbide Catalysts. *Submitted* **2022**.
(27) Macedo, L. S.; Oliveira, R. R.; van Haasterecht, T.; Teixeira da Silva, V.; Bitter, H. Influence of synthesis method on molybdenum carbide crystal structure and catalytic performance in stearic acid hydrodeoxygenation. *Applied Catalysis B: Environmental* **2019,** *241*, 81.
(28) Toebes, M. L.; van Heeswijk, E. M. P.; Bitter, J. H.; van Dillen, A. J.; de Jong, K. P. The influence of oxidation on the texture and the number of oxygen-containing surface groups of carbon nanofibers. *Carbon* **2004,** *42* (2), 307.
(29) Jongerius, A. L.; Gosselink, R. W.; Dijkstra, J.; Bitter, J. H.; Bruijnincx, P. C. A.; Weckhuysen, B. M. Carbon Nanofiber Supported Transition-Metal Carbide Catalysts for the Hydrodeoxygenation of Guaiacol. *ChemCatChem* **2013,** *5* (10), 2964.
(30) Souza Macedo, L.; Teixeira da Silva, V.; Bitter, J. H. Activated Carbon, Carbon Nanofibers and Carbon-Covered Alumina as Support for W2C in Stearic Acid Hydrodeoxygenation. *ChemEngineering* **2019,** *3* (1), 24.
(31) Rocha, A. S.; da Silva, V. T.; Faro Jr, A. C. Carbided Y zeolite-supported molybdenum: On the genesis of the active species, activity and stability in benzene hydrogenation. *Applied Catalysis A: General* **2006,** *314* (2), 137.
(32) Ghampson, I. T.; Sepúlveda, C.; Garcia, R.; Fierro, J. G.; Escalona, N.; DeSisto, W. J. Comparison of alumina-and SBA-15-supported molybdenum nitride catalysts for hydrodeoxygenation of guaiacol. *Applied Catalysis A: General* **2012,** *435*, 51.
(33) Tran, C.-C.; Akmach, D.; Kaliaguine, S. Hydrodeoxygenation of vegetable oils over biochar supported bimetallic carbides for producing renewable diesel under mild conditions. *Green Chemistry* **2020**.
(34) Lee, J. S.; Lee, K. H.; Lee, J. Y. Selective chemisorption of carbon monoxide and hydrogen over supported molybdenum carbide catalysts. *The Journal of Physical Chemistry* **1992,** *96* (1), 362.
(35) Mehdad, A.; Jentoft, R. E.; Jentoft, F. C. Single-phase mixed molybdenum-tungsten carbides: Synthesis, characterization and catalytic activity for toluene conversion. *Catal Today* **2019,** *323*, 112.
(36) Lee, W. S.; Wang, Z.; Zheng, W.; Vlachos, D. G.; Bhan, A. Vapor phase hydrodeoxygenation of furfural to 2-methylfuran on molybdenum carbide catalysts. *Catalysis Science and Technology* **2014,** *4* (8), 2340.
(37) Da Costa, P.; Lemberton, J. L.; Potvin, C.; Manoli, J. M.; Perot, G.; Breysse, M.; Djega-Mariadassou, G. Tetralin hydrogenation catalyzed by Mo2C/Al2O3 and WC/Al2O3in the presence of H2S. *Catal Today* **2001,** *65* (2-4), 195.
(38) Choi, J.-S.; Bugli, G.; Djéga-Mariadassou, G. Influence of the Degree of Carburization on the Density of Sites and Hydrogenating Activity of Molybdenum Carbides. *Journal of Catalysis* **2000,** *193* (2), 238.
(39) Shrestha, A.; Gao, X. T.; Hicks, J. C.; Paolucci, C. Nanoparticle Size Effects on Phase Stability for Molybdenum and Tungsten Carbides. *Chemistry of Materials* **2021,** *33* (12), 4606.
(40) Yang, Q.; Sun, K.; Xu, Y.; Ding, Z.; Hou, R. Tuning crystal phase of molybdenum carbide catalyst to induce the different selective hydrogenation performance. *Applied Catalysis A: General* **2022,** *630*, 118455.
(41) Zhu, J.; Uslamin, E. A.; Kosinov, N.; Hensen, E. J. Tuning the reactivity of molybdenum (oxy) carbide catalysts by the carburization degree: CO 2 reduction and anisole hydrodeoxygenation. *Catalysis Science & Technology* **2020,** *10* (11), 3635.
(42) Wang, T.; Li, Y. W.; Wang, J.; Jiao, H.; Wang, S. Adsorption equilibria of CO coverage on Mo2C surfaces. *Journal of Physical Chemistry C* **2012,** *116* (10), 6340.
(43) Wu, W.; Wu, Z.; Liang, C.; Chen, X.; Ying, P.; Li, C. In situ FT-IR spectroscopic studies of CO adsorption on fresh Mo2C/Al2O3 catalyst. *J Phys Chem B* **2003,** *107* (29), 7088.
(44) Posada-Pérez, S.; Viñes, F.; Valero, R.; Rodriguez, J. A.; Illas, F. Adsorption and dissociation of molecular hydrogen on orthorhombic β-Mo2C and cubic δ-MoC (001) surfaces. *Surf Sci* **2017,** *656*, 24.
(45) Sullivan, M. M.; Bhan, A. Acetone Hydrodeoxygenation over Bifunctional Metallic–Acidic Molybdenum Carbide Catalysts. *ACS Catalysis* **2016,** *6* (2), 1145.
(46) Führer, M.; van Haasterecht, T.; Bitter, J. H. Cinnamaldehyde hydrogenation over carbon supported molybdenum and tungsten carbide catalysts. *Chem Commun* **2022**, DOI:10.1039/D2CC05322E 10.1039/D2CC05322E.
(47) Sullivan, M. M.; Bhan, A. Acid site densities and reactivity of oxygen-modified transition metal carbide catalysts. *Journal of Catalysis* **2016,** *344*, 53.
(48) Mortensen, P. M.; de Carvalho, H. W. P.; Grunwaldt, J.-D.; Jensen, P. A.; Jensen, A. D. Activity and stability of Mo2C/ZrO2 as catalyst for hydrodeoxygenation of mixtures of phenol and 1-octanol. *Journal of Catalysis* **2015,** *328*, 208.
(49) Tran, C.-C.; Mohan, O.; Banerjee, A.; Mushrif, S. H.; Kaliaguine, S. A Combined Experimental and DFT Investigation of Selective Hydrodeoxygenation of Guaiacol over Bimetallic Carbides. *Energy & Fuels* **2020,** *34* (12), 16265.
(50) Mehdad, A.; Jentoft, R. E.; Jentoft, F. C. Passivation agents and conditions for Mo2C and W2C: Effect on catalytic activity for toluene hydrogenation. *Journal of Catalysis* **2017,** *347*, 89.

Supporting Information

NH_3 TPD

Figure S3.1 shows the NH_3-TPD results of the adsorption and desorption. The NH_3-TPD gives an indication of the amount of acidic sites on the catalysts. No NH_3 pulses were adsorbed. Only low amounts of NH_3 were adsorbed during the pulse chemisorption for both catalysts. This is also in agreement with the desorption profile; the TCD signal of the monometallic carbide Mo and W does not show NH_3 desorption with increasing temperature. No significant difference was observed between the monometallic carbide catalyst. The NH_3 TPR indicate that both monometallic catalysts do not contain acid sites directly after the carburization.

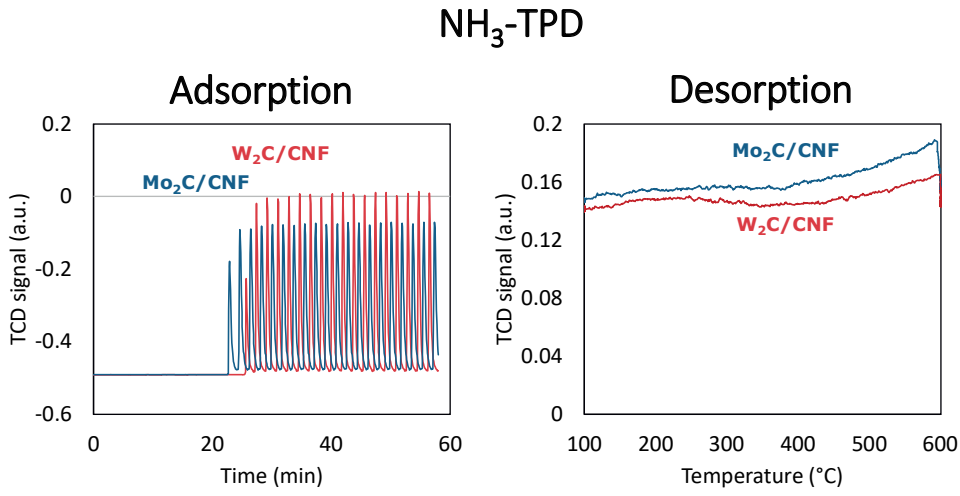

Figure S3.1 NH_3-TPD of fresh (red) tungsten and (blue) molybdenum carbide.

4

Chapter 4

Cinnamaldehyde hydrogenation over carbon supported molybdenum and tungsten carbide catalysts

This Chapter is based on: M. Führer, T, van Haasterecht, and H. Bitter. "Cinnamaldehyde hydrogenation over carbon supported molybdenum and tungsten carbide catalysts." Chemical Communications 58.98 (2022): 13608-13611.

Abstract

The potential of carbon supported Mo and W carbides to replace Pt is shown for the hydrogenation of cinnamaldehyde. Although the carbide catalysts are 4-6 times less active, both the carbides and Pt are selective towards C=C hydrogenation. Unlike Pt, the carbides additionally form β-methylstyrene.

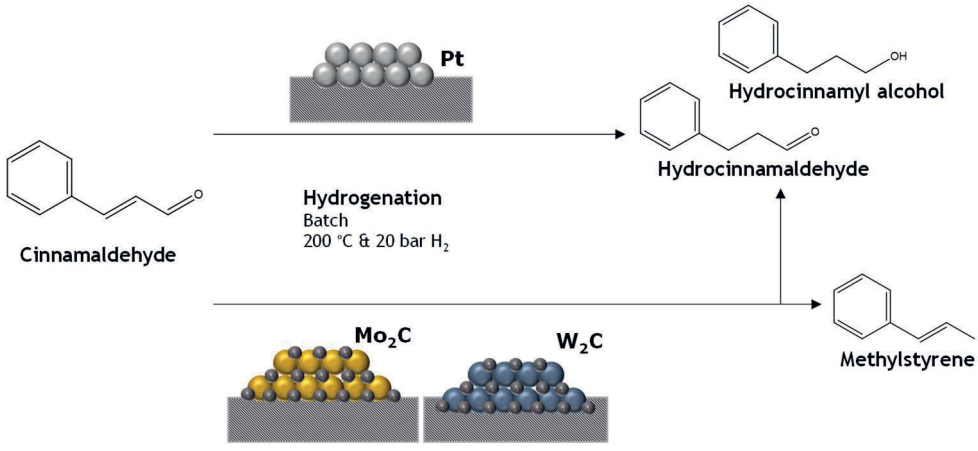

Introduction

Since the 70-ies of the last century, it is clear that tungsten and molybdenum carbide based catalysts are potential alternatives to the scarce and expensive noble metal based catalysts (like Pt) for reactions that involve hydrogen activation.[1] Since then these metal carbides were investigated for use in many reactions like isomerisation, hydrodenitrogenation, syngas conversion and as electrocatalysts in fuel cells.[2,3] Later, the potential of molybdenum and tungsten carbide for biomass related conversions such as (hydro-)deoxygenation and dehydration to remove the oxygen of the biomass for the production of chemicals and biofuels (see [4,5] for some reviews) has been shown. Recently, transition metal carbides have been applied for catalytic hydrogen transfer reactions.[6,7] In addition, some studies[8,9] show that tungsten carbide exhibits regioselectivity in hydrogenolysis. For instance, Fang et al.[9] showed high selectivity towards phenol when starting with guaiacol.

Though the above mentioned examples show the potential of molybdenum and tungsten carbides for hydrogenation as replacement for scarce noble metals like Pt, their potential for chemoselective hydrogenations has not been studied. These selective hydrogenations are often exemplified by cinnamaldehyde or crotonaldehyde hydrogenation towards either unsaturated alcohols or saturated aldehydes.[10-12]

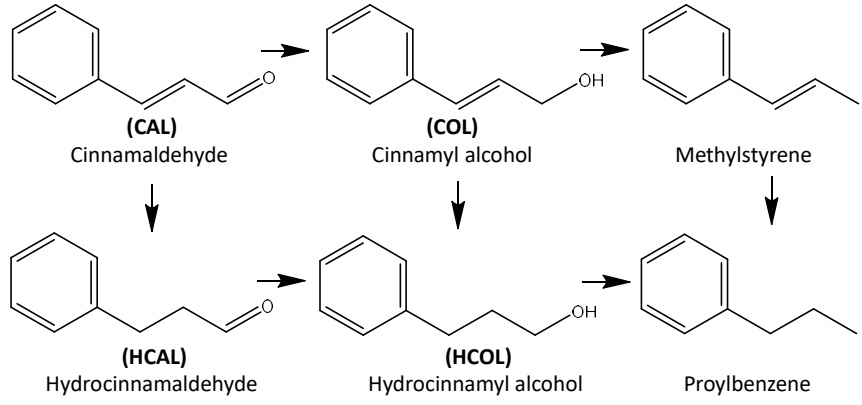

Scheme 4.1 Reaction scheme of the cinnamaldehyde hydrogenation.[13,14]

The hydrogenation of α,β-unsaturated aldehydes like cinnamaldehyde is an important step toward valuable chemicals for the pharmaceutical, perfumery and flavour industries.[15,16] In addition, the hydrogenation of cinnamaldehyde has been widely used for a fundamental understanding in the investigation of chemo-selectivity in heterogeneous catalysis. Cinnamaldehyde can undergo C=C hydrogenation to yield hydrocinnamaldehyde (HCAL) and/or

C=O hydrogenation to yield cinnamyl alcohol (COL) as illustrated in Scheme 4.1. Thermodynamically the hydrogenation of C=C is more favourable due to the lower bond energy of C=C.[10,17] Both HCAL and COL can be further hydrogenated to the saturated hydrocinnamyl alcohol (HCOL). Another possible pathway is the hydrogenolysis of COL into β-methylstyrene which can be further hydrogenated into propylbenzene. Propylbenzene can also be produced by the direct hydrogenolysis of HCOL.[13]

Noble metals with large d-bandwidth such as Pt or Ru have been widely used for the selective hydrogenation of CAL. They are highly active and their selectivity can be steered towards the C=O hydrogenation, as has been reviewed by Wang et al.[10]. Different strategies for steering the selective have been reported like modifying the support[18-20], adjusting the particle size/dispersion[21-24], the addition of a second metal[25] or changing the reaction conditions (e.g. reaction medium[26,27]). Here we investigated the potential of carbon nanofiber (CNF) supported Mo and W carbide as an alternative catalysts for the hydrogenation of cinnamaldehyde.

Materials & Methods

Catalyst preparation

Carbon nanofibers (CNF) were grown from a mixture of hydrogen (102 ml/min), nitrogen (450 ml/min) and carbon monoxide (260 ml/min) at 550 °C and 3 barg for 24 hrs over a reduced 5 wt.% Ni/SiO_2 catalyst (3 g), as reported previously.[28] To remove SiO_2 after growth, the mixture (CNF+Ni+SiO_2) was three times refluxed in 1 M KOH for 1 h with intermediate decanting and washing with 1 M KOH. Next, the CNF was treated by refluxing in 65% concentrated nitric acid for 1.5 h, to remove the remaining nickel and to introduce surface oxygen groups on the CNF. Finally, the CNF were washed with demi water to neutral pH and ground to a 90-120 μm fraction.

All CNF supported catalysts were synthesized by Incipient Wetness Impregnation. Aqueous solutions of ammonium heptamolybdate (AHM; Sigma-Aldrich, 99.98% trace metals basis), ammonium metatungstate (AMT; Sigma-Aldrich, 99.98% trace metals basis) or Tetraammineplatinum(II) nitrate (Sigmar-Aldrich, 99.995% trace metals basis) were used as precursor. After impregnation, the catalysts were dried overnight at 110 °C and stored for further use. The metal loadings of Pt, Mo and W were 5 wt%, 8.5 wt% and 15 wt%, respectively.

The carburization was performed at 650 °C (ramp of 5 °C/min) for the Mo-carbide and at 750 °C (ramp of 5 °C/min) for the W-carbide, for 2 h in flowing 20% CH_4/H_2 with 10 mL/min vertical furnace. This method is known as temperature-programmed reduction (TPR) method.

The reduction of 200 mg Pt/CNF was conducted in the same vertical furnace as mentioned above. The reduction temperature was ramped at 5 °C /min to 300 °C and held for 2 h in a flow of 30 ml/min H_2 and 60 ml/min N_2.

Catalyst characterization

XRD patterns were recorded on a Bruker D8 Advance equipped with a Lynxeye-XE-T PSD detector and a Cu-K$\alpha_{1,2}$ tube generating X-rays with λ = 1.542 Å. The measurements were taken from 2θ = 20° to 2θ = 80° with a step size of 0.05°.

TEM images were taken with a JEOL JEM-1400 Plus microscope operated at 100 kV. For the sample preparation, 10 mg of the catalyst sample was added to 1 mL absolute ethanol and homogenized in an ultrasonic bath for 10 sec. Then 2 µL was dropped on a carbon-supported Cu grid (400 mesh) and dried at room temperature. The data were analysed with ImageJ and MS Excel to obtain the mean particle size and distribution of around 300 particles.

CO pulse chemisorption was performed on a Mircromeritics AutoChem II 2920. Prior to the measurement, 200 mg of reduced Pt catalysts were activated at 300°C for 2 h before being evacuated for 2h at 300°C under Argon to remove any adsorbed H_2. Subsequently, the system was cooled down to 35°C and outgassed for 0.5h before the measurements. For the carbide samples, a similar CO method was developed, however instead of the reduction, the dried carbide precursors were carburised at 600 °C for 1 h under a mixture of 20 % CH_4 in H_2.

The catalysts were analysed by X-Ray Photoelectron Spectroscopy (XPS) using a JPS-9200 photoelectron spectrometer (JEOL). Spectra were obtained using monochromatic Al Kα X-Ray radiation at 12 kV and 20 mA, with an analyser energy pass of 10 eV for narrow scans and 50 eV for wide scans. The obtained spectra were processed using CASAXPS 2.3.22PR 1.0 peak fit program.

Metal leaching was assessed by Inductively Coupled Plasma (ICP-OES, Perkin Elmer AVIO 500) of the reaction mixture after filtering. 0.1 ml of the filtrate was added to 1 ml of 30% aqueous hydrogen peroxide and 9 ml of 65% nitric acid. The mixture was then digested with microwaves at 210 °C and 190 W for 40 mins.

Catalyst testing

The hydrogenation reaction was performed in a 100 mL stainless steel Parr autoclave, 4598 Micro batch reactor system. Typically, the reactor was filled with 250 mg or 100 mg catalyst, 50 ml toluene containing 1.36 g/l xylene and 13.6 g/l of cinnamaldehyde. Next, the loaded reactor

was twice purged with 30 bar Ar and afterwards flushed with H_2. Subsequently, the reactor was pressurized to 20, 10 and 40 bar of H_2, heated up to either 140, 170 or 200 °C while stirring at 800 rpm. The reaction was performed for 3-7 h (depending on the catalyst). Liquid samples from the reactor were taken at regular time intervals to investigate the product distribution. The samples were analysed using a GC-FID.

The following formulas were used to evaluate catalyst performance:

Conversion:

$$x_{CAL} = \frac{100}{[CAL]_{t,0}} * [CAL]_t \tag{4.1}$$

Normalized selectivity:

$$S_{N,Product\ x} = \frac{[Product\ X]_t}{\Sigma[Products]_t} * 100\% \tag{4.2}$$

With $[CAL]_{t,0}$ the concentration of cinnamaldehyde at start of reaction, $[CAL]_t$ concentration of cinnamaldehyde at time t, $[Product\ X]_t$ concentration of product X at time t and $\Sigma[Product]_t$ concentration of all products at time t.

The blank run (with no catalysts) for CAL hydrogenation was performed in the batch reactor at 200 °C and 20 bar, and only HCAL was produced as product. The conversion of CAL was less than 20 % after 5h and reached 50% after 24h under the reaction conditions used in this investigation; this value is much smaller in comparison to the reactivity of the catalysts.

Results & Discussion

Figure 4.1A displays representative TEM images and particle size distributions of the carbide and Pt catalysts. The average particle size for the carbide samples is between 3-4 nm and for the Pt samples around 2-3 nm. These images suggest that the carbide particles, as well as the metallic Pt, are well dispersed on the carbon support.

Figure 4.1B shows the XRD patterns of the two carbide catalysts and the Pt catalyst. The signals at 2θ=28 and 2θ=43° represent the (002) and (101) reflections of the CNF.[29] The reflections marked with the green diamond indicate the presence of the hexagonal β-W_2C phase (PDF 79-0743).[30] The Mo carbide sample shows reflections representing the cubic α-MoC_{1-x} phase (PDF 65-0280), marked with yellow dots.[31] The blue triangles indicated the characteristic metallic Pt

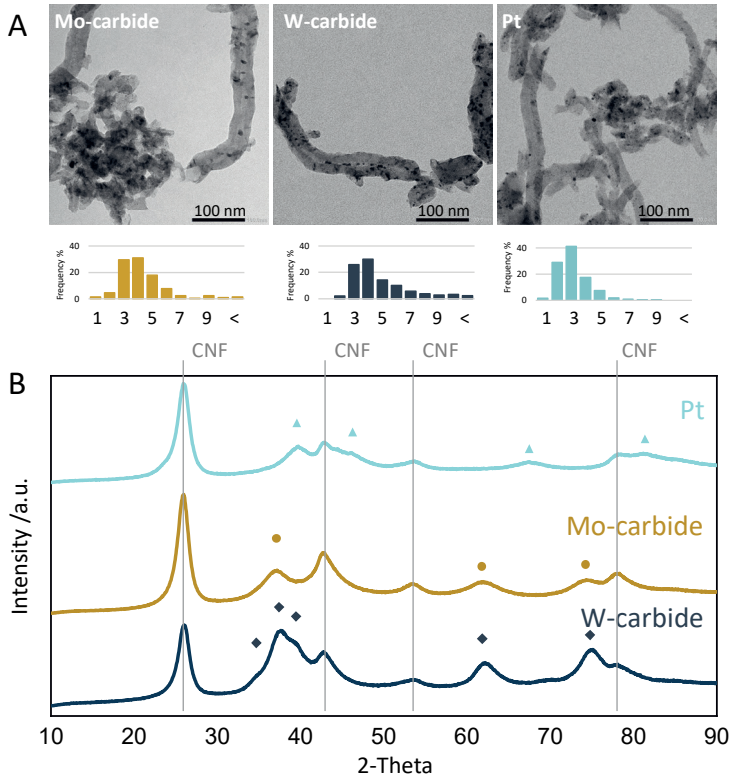

Figure 4.1 A) TEM images and B) XRD pattern of the CNF supported Pt, Mo-carbide and W-carbide catalysts. ▲ metallic Pt, ● cubic α-MoC_{1-x} and ♦ hexagonal β-W_2C

crystal structure (PDF 88-2343).[32,33] TEM and XRD prove the successful synthesis of Pt and carbide nanoparticles with a particle sizes in a similar range.

CO chemisorption was used to establish the number of active sites as it is commonly used for Pt and carbide catalysts.[34,35] The carbide catalysts were carburized *in situ,* directly before the CO chemisorption to avoid any exposure to air. The Pt catalyst is activated in hydrogen prior to the CO chemisorption. Table 4.1 lists the CO chemisorption capacities of the freshly activated catalysts. It can be seen that the CO uptake for the Mo-carbide was around 67.5 µmol/g and that for the W-carbide was 20.4 µmol/g. For the Pt, a CO uptake of 58.1 µmol/g was measured. Thus, the CO uptakes for Pt and Mo-carbide are in a comparable range, while the W-carbide has a significantly lower CO uptake which indicates a higher concentration of potential active sites for Mo-carbide and Pt catalysts compared to the W-carbide catalyst.

Table 4.1 Hydrogenation of cinnamaldehyde (50 ml toluene, 13.6 g/l CAL, T= 200 °C, 20 bar H_2, 800 rpm), CO uptake and catalytic activity (TOF)

	Catalyst amount (mg)	Metal loading (wt%)	CO uptake (µmol/g)*1	TOF (min^{-1})*2
Pt/CNF	100	5.0	58.1 ± 0.6	86
Mo/CNF	250	8.5	67.5 ± 1.3	14
W/CNF	250	15.0	20.4 ± 3.9	22

**1 Average of duplicate measurements. *2 TOF calculated at ~40 % conversion*

The CAL hydrogen performance of the three catalysts was investigated in a gas-liquid batch reactor at 200 °C and 20 bar H_2. The reaction progress was assessed by periodically taking samples which were analysed by GC-FID. A detailed description of the experimental procedure can be found in the ESIs (Catalytic hydrogenation). Figure 4.2A shows the conversion of CAL over the three different catalysts as function of time. Clearly, the Pt catalyst shows the highest weight-based activity for the CAL hydrogenation among the different catalysts (full conversion within 1 h). For the Mo-carbide, full conversion was obtained within 5 hours while the W_2C catalyst only reached a maximum conversion of 95% after 7 h. In order to better compare the activity of the different catalysts also the turnover frequencies (TOF), based on the site density obtained from CO chemisorption, are given in Table 4.1. The Pt catalyst also has the highest TOF (86 min^{-1}) revealing about 4-6 times higher activity than the carbides, which show a very similar activity.

In order to understand the reaction pathway over the different catalysts, the normalized product distribution at selected conversion levels of X=40% and X=90% are given in Figure 4.2B. The

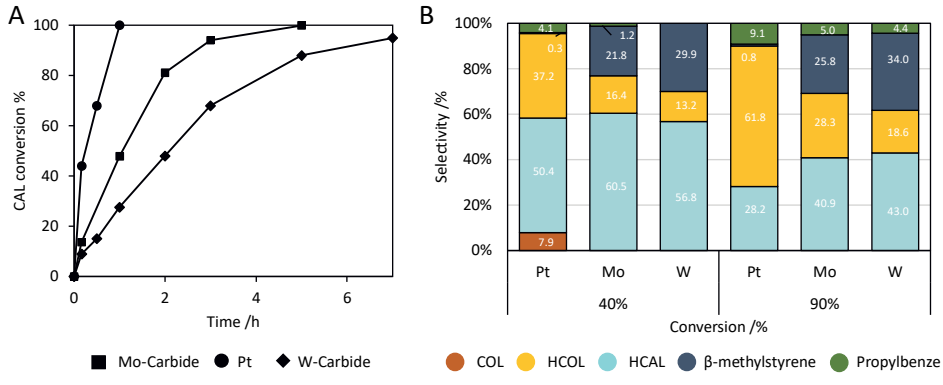

Figure 4.2 A) CAL conversion and B) normalized product distribution at 40% and 90% conversion of CNF supported MoC_{1-x}, W_2C and Pt catalysts (50 ml toluene, 13.6 g/l CAL, T= 200 °C, 20 bar H_2, 800 rpm).

selectivity at 40% conversion shows that both Pt and the carbides favour the hydrogenation via the C=C bond, initially producing HCAL as main product. Subsequently, for all catalysts at higher conversion (X=90%) the selectivity towards HCAL is decreased as it is further hydrogenated via C=O reduction resulting in increasing levels of HCOL. A closer inspection of HCAL selectivity at 90 % conversion shows that Mo and W carbide catalysts still provide significantly higher selectivity of semi-hydrogenation product, HCAL (S=40.9% and S=43.0% respectively), than the Pt catalysts (S=28.2%). Instead higher yields for the twice hydrogenated product, HCOL (S=61.8 %), were observed for the Pt catalysts. Thus, the further hydrogenation of the HCAL to HCOL is relatively slower for the carbide catalysts than for the Pt catalysts. Besides C=C hydrogenation also C=O hydrogenation occurs over Pt as is evidenced by the presence of a minor amount of COL (S=7.9%). Another striking difference is the observation that the carbide catalyst also produces β-methylstyrene, which is nearly absent with the Pt catalyst. The production of β-methylstyrene gives evidence that the carbide catalysts also follow the hydrogenation pathway via the COL. However, only trace amounts of COL were observed with the carbide catalysts, which leads to the suggestion that the C-O hydrogenolysis occurs fast (relative to C=O reduction) over the carbides. Unlike Pt, which shows only minor amounts of β-methylstyrene, the carbide catalysts thus also favour C-OH hydrogenolysis over C=C reduction. Finally, all catalysts also show some formation of the fully hydrogenated product propyl benzene, which in the case of Pt likely proceeds via hydrogenolysis of HCOL and in the case of the carbides could also proceed via β-methylstyrene.

The remarkable change in chemoselectivity between Pt based catalysts and carbide catalysts can be explained by the formation of acid sites on the carbide surface.[3,36] The brief exposure to ambient air during the transfer from the carburisation reactor to the hydrogenation vessel causes surface oxidation on the carbide surface, which was also observed by the XPS analysis (Figure S4.1).

A range of unidentified products could be detected during the hydrogenation with GC-FID especially for the W carbide catalyst (at long retention times, see chromatograms in Figure S4.2 of ESI). Further analysis with GC-MS revealed the formation of C18 coupling products. Additionally for W-carbide a substantial decrease in the carbon balance was noted (70% remaining) after 5 hrs of reaction, which reveals that for the W carbide some of the reactants are converted via side reactions, resulting in additional products that were not visible with GC-FID. For Pt and Mo-carbide the carbon balance remained in an acceptable range (90-95%, see Table S4.1). These differences might be attributed to the acidic properties of the tungsten carbide surfaces, as is shown has previously been shown.[36]

The results above show that the carbide catalysts are 4-6 times less active than the Pt catalysts. However, considering the fact that transition metals are more abundant[37] and therefore less expensive than noble metals, the Mo-carbide are a viable non-noble alternative to Pt. Therefore, in the next step, we further investigated the effect of pressure and temperature on the activity and selectivity of the Mo-carbide catalyst.

The effect of pressure on the carbide catalyst activity was determined between 10-40 bar and is shown in Figure S4.3. Going from 10 to 20 bar H_2 the reaction rate increases while going from 20 to 40 bar the H_2 pressure did not have an influence on the reaction rate. No clear effect of the pressure on the selectivity was observed.

Figure 4.3 shows the influence of the temperature on the catalytic performance (selectivity and conversion) of Mo-carbide/CNF between 140-200 °C. By increasing the temperature from 140 °C to 170 °C the conversion increased from 19 to 30% after 5 hrs of reaction. Further increasing the temperature to 200 °C results in full conversion within 5 hrs. Figure 4.3 also shows how the selectivity is affected by the temperature. It can be observed that at all temperatures HCAL is the dominant product at low conversion. This shows that the C=C hydrogenation is the main pathway at all temperatures. However, at lower reaction temperatures an increase in the selectivity towards COL can be observed. This can be attributed to a relatively larger decrease in the rate of C=C hydrogenation compared to the C=O hydrogenation as is evident from the increase in COL/HCAL ratio at low conversion with decreasing temperature (Figure S4.4). This indicates that the hydrogenation selectivity of Mo-carbide can be steered by changing the reaction temperature.

Finally, the stability of the Mo-carbide catalyst was assessed. Upon the first reuse, the catalyst activity decreased by about a factor 2 while this activity remained at this level for the third reused (see Figure S4.5). Metal leaching was determined by ICP analysis of the recovered reaction

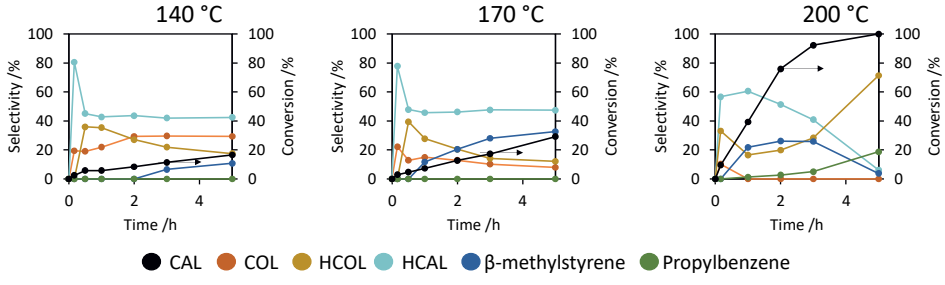

Figure 4.3 CAL Conversion and product yield of the Mo-carbide catalyst at 140, 170 and 200 °C (50 ml toluene, 13.6 g/l CAL, 20 bar H_2, 800 rpm).

solution and found to be ~0.1% Mo (of the 8.5 wt%) after the first reaction. XRD characterisation (Figure S4.6) of the spent catalyst give no evidence for bulk oxidation, nor particle growth and therefore these are less likely deactivation mechanisms.

Conclusion

In conclusion, these findings demonstrate the potential of especially Mo-carbide catalysts for the hydrogenation of α,β-unsaturated aldehydes as alternative catalysts. The carbide catalysts and Pt, both favour the hydrogenation of the C=C bond to produce HCAL, although the carbides were less active. The main difference between Pt and the carbide was the high selectivity towards β-methylstyrene with the carbide catalysts. Investigation of the effect of temperature for the Mo-carbide revealed a shift in selectivity towards the C=O hydrogenation product (COL) with decreasing temperature. These results highlight that the selectivity of the carbide catalysts can be steered by lowering the temperature. Investigation into how the properties of the catalysts (variation in support, particle size and crystal structure) influence the selectivity, as has already been shown for noble metal catalysts, is still needed for the carbide catalysts.

Acknowledgement

The research was financed by Dutch Research Council (NWO). The authors thank Kai-Ching Fan (MSc student at Wageningen University) for the preliminary work which led to this article. We also thank Susan Witte for helping with the GC measurements, Barend van Lagen for the XPS measurements and Dmitry Pirgach for the ICP.

References

(1) Levy, R. B.; Boudart, M. Platinum-Like Behavior of Tungsten Carbide in Surface Catalysis. *Science* **1973,** *181* (4099), 547.

(2) Furimsky, E. Metal carbides and nitrides as potential catalysts for hydroprocessing. *Applied Catalysis A: General* **2003,** *240* (1–2), 1.

(3) Sullivan, M. M.; Chen, C. J.; Bhan, A. Catalytic deoxygenation on transition metal carbide catalysts. *Catalysis Science and Technology* **2016,** *6* (3), 602.

(4) Smith, K. J. Metal carbides, phosphides, and nitrides for biomass conversion. *Current Opinion in Green and Sustainable Chemistry* **2020,** *22*, 47.

(5) Pang, J.; Sun, J.; Zheng, M.; Li, H.; Wang, Y.; Zhang, T. Transition metal carbide catalysts for biomass conversion: A review. *Applied Catalysis B: Environmental* **2019,** *254*, 510.

(6) Liu, Z.; Wang, X.; Zou, X.; Lu, X. Molybdenum Carbide Catalysts for Chemoselective Transfer Hydrogenation of Nitroarenes. *ChemistrySelect* **2018,** *3* (18), 5165.

(7) Wu, K.; Yang, C.; Zhu, Y.; Wang, J.; Wang, X.; Liu, C.; Liu, Y.; Lu, H.; Liang, B.; Li, Y. Synthesis-controlled α-and β-molybdenum carbide for base-promoted transfer hydrogenation of lignin to aromatic monomers in ethanol. *Ind Eng Chem Res* **2019,** *58* (44), 20270.

(8) Fang, H.; Roldan, A.; Tian, C.; Zheng, Y.; Duan, X.; Chen, K.; Ye, L.; Leoni, S.; Yuan, Y. Structural tuning and catalysis of tungsten carbides for the regioselective cleavage of CO bonds. *Journal of Catalysis* **2019,** *369*, 283.

(9) Fang, H. H.; Du, J. M.; Tian, C. C.; Zheng, J. W.; Duan, X. P.; Ye, L. M.; Yuan, Y. Z. Regioselective hydrogenolysis of aryl ether C-O bonds by tungsten carbides with controlled phase compositions. *Chem Commun* **2017,** *53* (74), 10295.

(10) Wang, X.; Liang, X.; Geng, P.; Li, Q. Recent Advances in Selective Hydrogenation of Cinnamaldehyde over Supported Metal-Based Catalysts. *ACS Catalysis* **2020,** *10* (4), 2395.

(11) Dandekar, A.; Vannice, M. A. Crotonaldehyde Hydrogenation on Pt/TiO2and Ni/TiO2SMSI Catalysts. *Journal of Catalysis* **1999,** *183* (2), 344.

(12) Zanella, R.; Louis, C.; Giorgio, S.; Touroude, R. Crotonaldehyde hydrogenation by gold supported on TiO2: structure sensitivity and mechanism. *Journal of Catalysis* **2004,** *223* (2), 328.

(13) Yepez, A.; Hidalgo, J. M.; Pineda, A.; Černý, R.; Jíša, P.; Garcia, A.; Romero, A. A.; Luque, R. Mechanistic insights into the hydroconversion of cinnamaldehyde using mechanochemically-synthesized Pd/Al-SBA-15 catalysts. *Green Chemistry* **2015,** *17* (1), 565.

(14) Hájek, J.; Kumar, N.; Mäki-Arvela, P.; Salmi, T.; Murzin, D. Y.; Paseka, I.; Heikkilä, T.; Laine, E.; Laukkanen, P.; Väyrynen, J. Ruthenium-modified MCM-41 mesoporous molecular sieve and Y zeolite catalysts for selective hydrogenation of cinnamaldehyde. *Applied Catalysis A: General* **2003,** *251* (2), 385.

(15) Mohire, S. S.; Yadav, G. D. Selective Synthesis of Hydrocinnamaldehyde over Bimetallic Ni–Cu Nanocatalyst Supported on Graphene Oxide. *Ind Eng Chem Res* **2018,** *57* (28), 9083.

(16) Manikandan, D.; Divakar, D.; Sivakumar, T. Utilization of clay minerals for developing Pt nanoparticles and their catalytic activity in the selective hydrogenation of cinnamaldehyde. *Catalysis Communications* **2007,** *8* (11), 1781.

(17) Gallezot, P.; Richard, D. Selective hydrogenation of α, β-unsaturated aldehydes. *Catalysis Reviews* **1998,** *40* (1-2), 81.

(18) Zhang, X.; Guo, Y. C.; Zhang, Z. C.; Gao, J. S.; Xu, C. M. High performance of carbon nanotubes confining gold nanoparticles for selective hydrogenation of 1, 3-butadiene and cinnamaldehyde. *Journal of catalysis* **2012,** *292*, 213.

(19) Toebes, M. L.; Zhang, Y.; Hájek, J.; Nijhuis, T. A.; Bitter, J. H.; Van Dillen, A. J.; Murzin, D. Y.; Koningsberger, D. C.; de Jong, K. P. Support effects in the hydrogenation of cinnamaldehyde over carbon nanofiber-supported platinum catalysts: characterization and catalysis. *Journal of catalysis* **2004,** *226* (1), 215.

(20) Ma, H.; Wang, L.; Chen, L.; Dong, C.; Yu, W.; Huang, T.; Qian, Y. Pt nanoparticles deposited over carbon nanotubes for selective hydrogenation of cinnamaldehyde. *Catalysis Communications* **2007,** *8* (3), 452.

(21) Jiang, F.; Cai, J.; Liu, B.; Xu, Y.; Liu, X. Particle size effects in the selective hydrogenation of cinnamaldehyde over supported palladium catalysts. *RSC advances* **2016,** *6* (79), 75541.

(22) Wei, H.; Gomez, C.; Liu, J.; Guo, N.; Wu, T.; Lobo-Lapidus, R.; Marshall, C. L.; Miller, J. T.; Meyer, R. J. Selective hydrogenation of acrolein on supported silver catalysts: A kinetics study of particle size effects. *Journal of catalysis* **2013,** *298*, 18.

(23) Plomp, A. J.; Vuori, H.; Krause, A. O. I.; de Jong, K. P.; Bitter, J. H. Particle size effects for carbon nanofiber supported platinum and ruthenium catalysts for the selective hydrogenation of cinnamaldehyde. *Applied Catalysis A: General* **2008,** *351* (1), 9.

(24) Bus, E.; Prins, R.; van Bokhoven, J. A. Origin of the cluster-size effect in the hydrogenation of cinnamaldehyde over supported Au catalysts. *Catalysis Communications* **2007,** *8* (9), 1397.

(25) Zhang, W.; Xin, H.; Zhang, Y.; Jin, X.; Wu, P.; Xie, W.; Li, X. Bimetallic Pt-Fe catalysts supported on mesoporous TS-1 microspheres for the liquid-phase selective hydrogenation of cinnamaldehyde. *Journal of Catalysis* **2021,** *395*, 375.

(26) Chatterjee, M.; Zhao, F.; Ikushima, Y. Effect of synthesis variables on the hydrogenation of cinnamaldehyde over Pt-MCM-48 in supercritical CO2 medium. *Applied Catalysis A: General* **2004,** *262* (1), 93.

(27) Wang, H.; Liu, B.; Liu, F.; Wang, Y.; Lan, X.; Wang, S.; Ali, B.; Wang, T. Transfer hydrogenation of cinnamaldehyde catalyzed by Al2O3 using ethanol as a solvent and hydrogen donor. *ACS Sustainable Chemistry & Engineering* **2020,** *8* (22), 8195.

(28) Toebes, M. L.; van Heeswijk, E. M. P.; Bitter, J. H.; van Dillen, A. J.; de Jong, K. P. The influence of oxidation on the texture and the number of oxygen-containing surface groups of carbon nanofibers. *Carbon* **2004,** *42* (2), 307.

(29) Jongerius, A. L.; Gosselink, R. W.; Dijkstra, J.; Bitter, J. H.; Bruijnincx, P. C. A.; Weckhuysen, B. M. Carbon Nanofiber Supported Transition-Metal Carbide Catalysts for the Hydrodeoxygenation of Guaiacol. *ChemCatChem* **2013,** *5* (10), 2964.

(30) Mitran, R. A.; Radulescu, M. C.; Buhalteanu, L.; Tanase, L. C.; Dumitrescu, D. G.; Matei, C. Formation of pure-phase W2C nanoparticles through carbothermal reduction in the presence of Pd(0) nanoparticles. *Journal of Alloys and Compounds* **2016,** *682*, 679.

(31) Macedo, L. S.; Stellwagen, D. R.; da Silva, V. T.; Bitter, J. H. Stability of Transition-metal Carbides in Liquid Phase Reactions Relevant for Biomass-Based Conversion. *Chemcatchem* **2015,** *7* (18), 2816.

(32) Hyde, T. Crystallite size analysis of supported platinum catalysts by XRD. *Platinum Metals Review* **2008,** *52* (2), 129.

(33) Führer, M.; van Haasterecht, T.; Masoud, N.; Barrett, D. H.; Verhoeven, T.; Hensen, E.; Tromp, M.; Rodella, C. B.; Bitter, H. The Synergetic Effect of Support-oxygen Groups and Pt Particle Size in the Oxidation of α-D-glucose: A Proximity Effect in Adsorption. *ChemCatChem* **2022**.

(34) Aegerter, P. A.; Quigley, W. W. C.; Simpson, G. J.; Ziegler, D. D.; Logan, J. W.; McCrea, K. R.; Glazier, S.; Bussell, M. E. Thiophene hydrodesulfurization over alumina-supported molybdenum carbide and nitride catalysts: Adsorption sites, catalytic activities, and nature of the active surface. *Journal of Catalysis* **1996,** *164* (1), 109.

(35) Oyama, S. Preparation and catalytic properties of transition metal carbides and nitrides. *Catal Today* **1992,** *15* (2), 179.

(36) Stellwagen, D. R.; Bitter, J. H. Structure–performance relations of molybdenum-and tungsten carbide catalysts for deoxygenation. *Green Chemistry* **2015,** *17* (1), 582.

(37) Bullock, R. M.; Chen, J. G.; Gagliardi, L.; Chirik, P. J.; Farha, O. K.; Hendon, C. H.; Jones, C. W.; Keith, J. A.; Klosin, J.; Minteer, S. D. Using nature's blueprint to expand catalysis with Earth-abundant metals. *Science* **2020,** *369* (6505), eabc3183.

Supporting Information

Acidic properties of the catalyst

XPS measurements were done to further investigate the extent of oxidation of the carbide surface. The narrow scan of the Mo carbide and the W carbides samples was taken and shown in Figure S4.1. The W-4f region shows signals at 31.4 eV and 33.6 eV corresponding to tungsten carbide which is in agreement with literature data.[S1,2] The signals observed at 35.0 eV and 37.1 eV are related to tungsten oxide (W6+).

The Mo-3d region shows two signals (231.5 eV and the 228.3 eV) originating from the carbide. The signal at 234.7 eV has been assigned to Mo(VI) oxide species.[S1,3]

Since oxygen is visible on these samples it can be concluded that the carbidic surface gets partly oxidized during the brief exposure to air when transferring the catalyst from the carburization oven into the XPS analyser (or the reaction vessel). The oxidation was less pronounced for the Mo-carbide than for the W-carbide, which is in accordance with the literature. [S1] Since the oxides are expected to have acidic properties [S4], it can be concluded that some acidity will be introduced during the exposure of the sample to air. This, in turn, might change the selectivity of the catalysts since it has been shown before[S5] that oxides are active for decarboxylation/decarbonylation while carbides are active for hydrodeoxygenation.

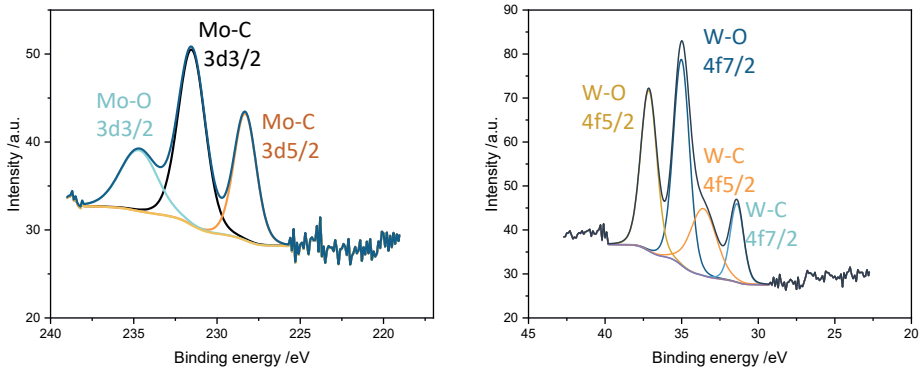

Figure S4.1 XPS spectra of W-carbide/CNF, W-4f (right) and Mo-carbide/CNF, Mo-3d (left).

Carbon Balance over W-carbide

As can be seen from Table S4.1, the carbon balance of W_2C during the hydrogenation of CAL decreases significantly. Figure S4.2 shows the GC-FID spectra of the three catalysts at a high

conversion level (90-100 %). Next to the known products (propylbenzene, methylsterene, HCAL and HCOL), we observed peaks at the retention time of 29-35 min. From GC-MS analysis these peaks were identified to represent C18 compounds (such as 1,5-Diphenyl-3-pentanone, 2,5-Diphenyl-1,5-hexadiene, 1,5-Diphenyl-1,5-hexadiene and Benzene, 1,1'-(1,6-hexanediyl)bis-). Remarkable is that W-carbide has more of these C18 compounds (33 % at 5h) in comparison to Mo-carbide (12 % at 5h) and the Pt (4 % at 1h).

Table S4.1 Carbon balance of W_2C over time

Catalyst	Reaction time (h)	Carbon Balance (%)	Unidentified products (%)	Final Carbon Balance (%)
W	5	36	33	69
Mo	5	85	12	97
Pt	1	95	4	99

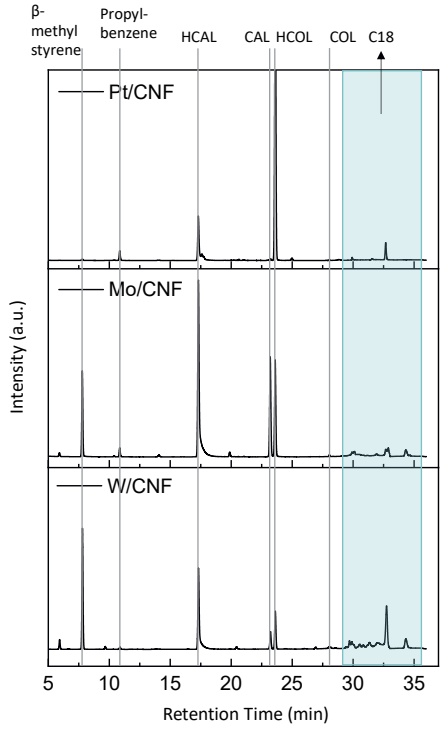

Figure S4.2 GC-FID chromatograms of CAL hydrogenation over Pt, Mo carbide and W carbide catalysts

Catalysts' selectivity at different pressures

The hydrogenation was conducted at 200 °C with varying H_2 pressures (10, 20 and 40 bar). The conversion and the selectivity of Mo-carbide catalyst at these different pressures are shown in Figure S4.3. When comparing the activities measured for 20 and 40 bar, it can be concluded that the CAL conversion is almost independent of the H_2 pressure. With both pressures, the CAL conversion reaches full conversion after 5 h. However, at 10 bar the conversion significantly decreases to 40 % after 5 h. The selectivity of the Mo-carbide was not significantly influenced by the pressure and predominantly HCAL and β-methylstyrene were formed.

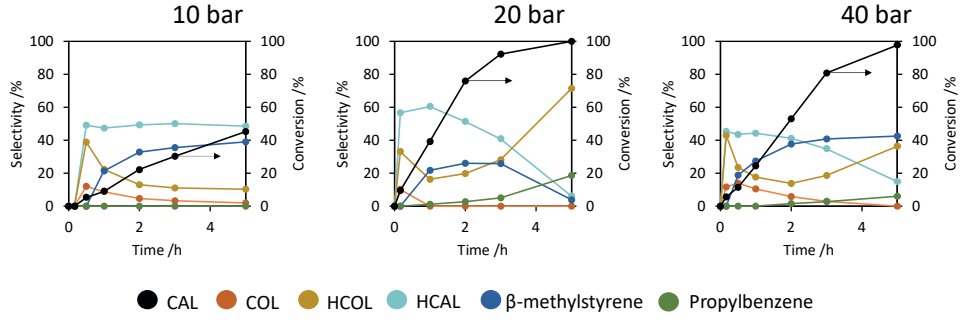

Figure S4.3 CAL conversion and product yield of the Mo-carbide catalyst at 10 and 40 bar (50 ml toluene, 13.6 g/l CAL, T = 200 °C, 800 rpm)

COL/HCAL ratio as function of temperature

Figure S4.4 shows the ratio between COL to HCAL at low conversion (5-40 %). For the hydrogenation at 140 °C, the COL/HCAL ratio stays ~0.7 whereas at 170 °C and 200 °C the ratio decreases with increasing conversion rates from 0.3 to 0.2 and 0.1 to 0.0, respectively. This data shows that at lower temperatures the selectivity towards COL hydrogenation increases.

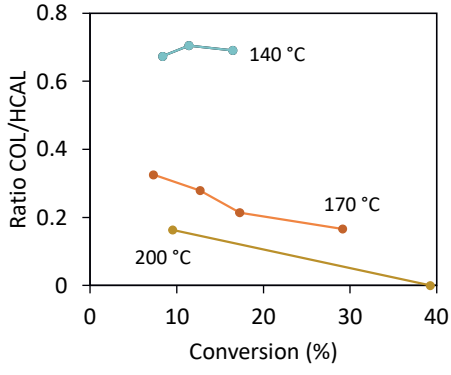

Figure S4.4 COL to HCAL ratio at CAL conversions from 5 to 40 %

Evaluation of catalyst stability

To investigate the deactivation of the catalyst, subsequent experiments with one batch of Mo-carbide catalyst were conducted. Between the runs, the remaining reaction medium was decanted, then the catalysts were washed/decanted repeatedly with toluene before adding the fresh reaction medium. As can be seen from Figure S4.5, the catalyst loses activity after the first run but is rather stable after the 2nd run.

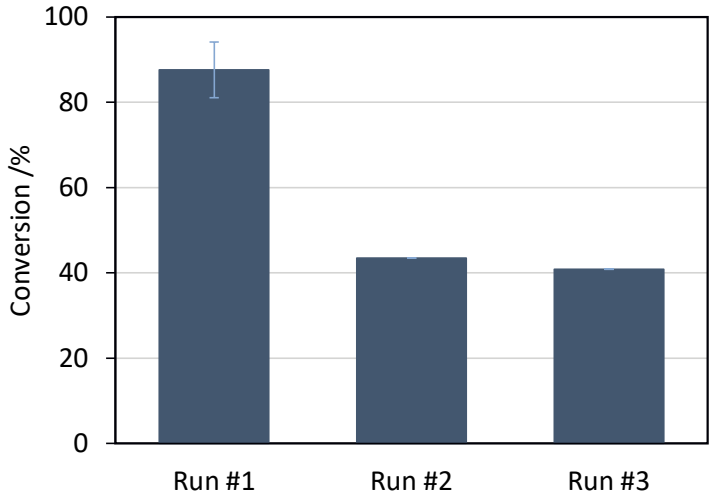

Figure S4.5 Multiple runs of CAL conversion (50 ml toluene, 13.6 g/l CAL, T = 200 °C, 20 bar H_2, 800 rpm) upon recycling Mo-carbide catalyst

In order to elucidate the cause of the catalyst deactivation, the spent Mo-carbide catalyst was characterised by XRD shown in Figure S4.6. The signals at 2θ=28 and 2θ=43° represent the (002) and (101) reflections of the CNF.[S6] The reflections marked with the green diamond indicate the presence of the hexagonal β-W_2C phase (PDF 79-0743). [S7] The Mo carbide sample shows reflections representing the cubic α-MoC_{1-x} phase (PDF 65-0280), marked with yellow dots.[S8] The characteristic carbide reflections are observed for both fresh and spent catalysts. This result shows that no bulk oxidation of the carbide catalyst occurs during the reaction. When comparing the peak intensity of fresh with the spent catalysts a decrease in intensity can be observed. This indicates metal leaching during the reaction might have occurred. This argument is further supported by the amounts metal found in the liquid phase. ICP analysis shows that ~0.1 % Mo of the 8.5 wt.% was found in the reactant medium after the first run (with a duration of 4 h). It need to be mentioned that the obtained metal concentration was measured close to the detection limit of the analyser. No other metals were found.

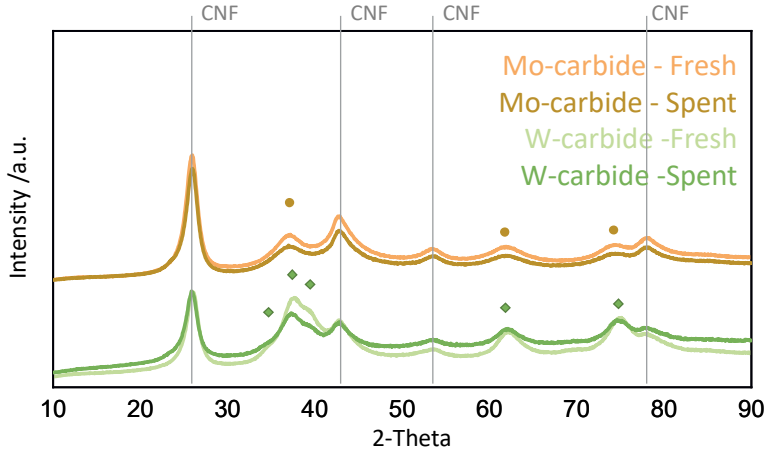

Figure S4.6 XRD of the spent and fresh Mo and W carbide

References

(S1) Stellwagen, D. R.; Bitter, J. H. Structure–performance relations of molybdenum-and tungsten carbide catalysts for deoxygenation. *Green Chemistry* **2015,** *17* (1), 582.

(S2) Guo, H.; Qi, Z.; Liu, Y.; Xia, H.; Li, L.; Huang, Q.; Wang, A.; Li, C. Tungsten-based catalysts for lignin depolymerization: the role of tungsten species in C–O bond cleavage. *Catalysis Science & Technology* **2019,** *9* (9), 2144.

(S3) Abou Hamdan, M.; Lilic, A.; Vecino-Mantilla, M.; Nikitine, C.; Vilcocq, L.; Jahjah, M.; Pinel, C.; Perret, N. Influence of reduction carburization parameters on the performance of supported molybdenum carbide catalysts in succinic acid hydrogenation. *Ind Eng Chem Res* **2020**.

(S4) Hollak, S. A. W.; Gosselink, R. W.; van Es, D. S.; Bitter, J. H. Comparison of Tungsten and Molybdenum Carbide Catalysts for the Hydrodeoxygenation of Oleic Acid. *Acs Catalysis* **2013,** *3* (12), 2837.

(S5) Gosselink, R. W.; Stellwagen, D. R.; Bitter, J. H. Tungsten-Based Catalysts for Selective Deoxygenation. *Carbohydrate research* **2013,** *52* (19), 5089.

(S6) Jongerius, A. L.; Gosselink, R. W.; Dijkstra, J.; Bitter, J. H.; Bruijnincx, P. C. A.; Weckhuysen, B. M. Carbon Nanofiber Supported Transition-Metal Carbide Catalysts for the Hydrodeoxygenation of Guaiacol. *ChemCatChem* **2013,** *5* (10), 2964.

(S7) Mitran, R. A.; Radulescu, M. C.; Buhalteanu, L.; Tanase, L. C.; Dumitrescu, D. G.; Matei, C. Formation of pure-phase W2C nanoparticles through carbothermal reduction in the presence of Pd(0) nanoparticles. *Journal of Alloys and Compounds* **2016,** *682*, 679.

(S8) Macedo, L. S.; Stellwagen, D. R.; da Silva, V. T.; Bitter, J. H. Stability of Transition-metal Carbides in Liquid Phase Reactions Relevant for Biomass-Based Conversion. *Chemcatchem* **2015,** *7* (18), 2816.

5

Chapter 5

Particle size effect on the stability of carbon nanofiber supported Mo carbide catalysts in the hydrogenation of cinnamaldehyde

The manuscript of this chapter is in preparation.

Abstract

Carbon supported Mo (and W) carbides were shown earlier to be viable replacements for supported Pt for the hydrogenation of cinnamaldehyde with respect to activity and selectivity. However, the stability of these materials was not studied in great detail. Here we will demonstrate that the carbide nanoparticle size is a critical factor for the stability in the cinnamaldehyde hydrogenation performed in a fixed bed continuous flow reactor. The Mo carbide with larger nanoparticles (4-5 nm) showed enhanced stability since it lost only 0.4% of activity within 40 hrs. The Mo catalyst with smaller nanoparticles (3-4 nm) lost 63.2% of activity within 40 hrs. The deactivation of the catalysts was ascribed to particle growth and site blocking by carbonaceous species. The latter could be partially recovered by re-carburisation.

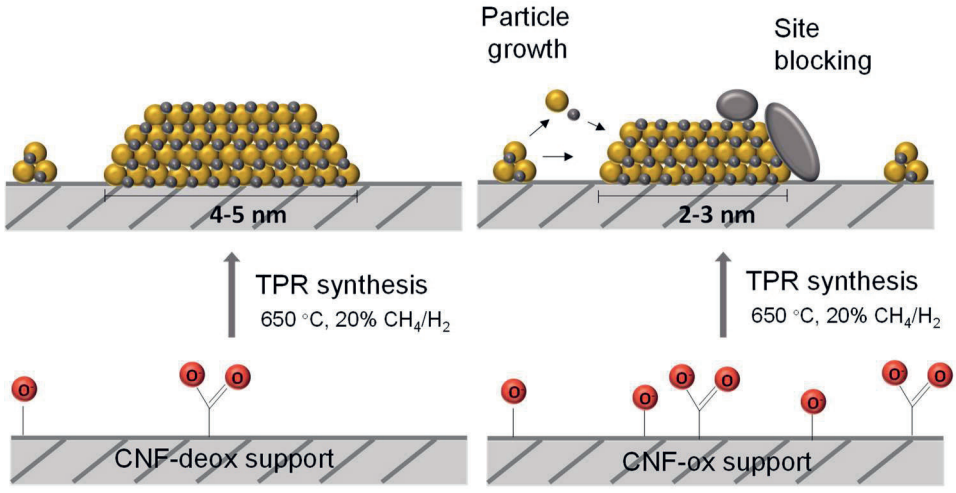

Introduction

The hydrogenation of cinnamaldehyde (CAL) is an important reaction in the preparation of various fine chemicals for the pharmaceutical, fragrance and flavour industries and is also widely used as a model reaction for a fundamental understanding of the chemo-selectivity in (heterogenous) catalysis.[1] Cinnamaldehyde can undergo C=C hydrogenation to yield hydrocinnamaldehyde (HCAL) and/or C=O hydrogenation to yield cinnamyl alcohol (COL) as illustrated in Scheme 5.1.

Recently we have shown that carbon supported Mo and W carbides are promising catalysts for the hydrogenation of CAL.[2] As such they are suitable replacements for scarce and expensive noble metals such as Pt.[3] We showed that the Mo and W carbide catalysts are active for the CAL hydrogenation and favour C=C hydrogenation, like Pt. The stability of these carbides is however still an issue especially in liquid-phase reactions.[4] We found that the Mo carbide catalysts lost 50% of its activity after the first run in a batch reactor.[2] Although we could exclude bulk oxidation and metal leaching as possible deactivation mechanisms, the exact deactivation mechanism was not determined.

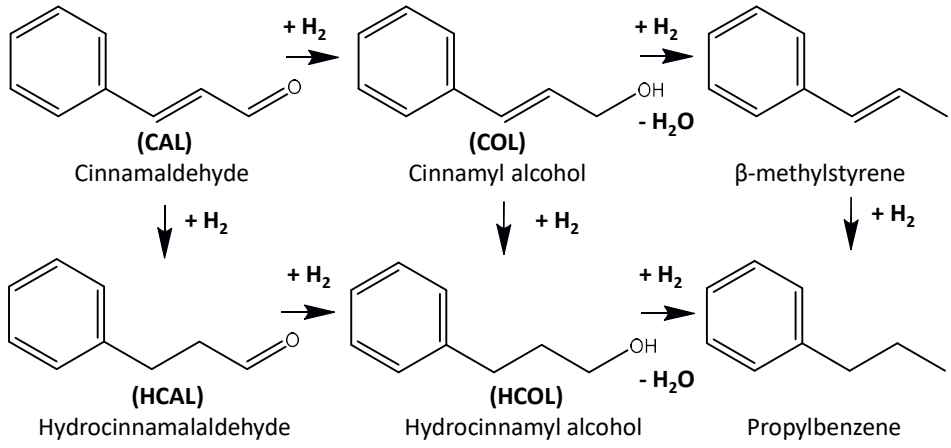

Scheme 5.1 Cinnamaldehyde hydrogenation reaction.[5]

Next to oxidation and leaching also blocking of the active site (e.g. coke deposition) and crystallite growth are often described deactivation mechanisms for (carbide-based) catalysts.[4] Blocking of active sites can occur due to strong chemisorption of species on the catalytic sites themselves or due to the physical blocking of the access, via pore blocking, to the active site.[6] These species can

be adsorbed reactants/products or polymeric species formed by condensation of the reactants/products. Often these adsorbed can be largely removed, i.e. the adsorption is reversible, by adequately cleaning the catalyst surface with a heat treatment and/or by streaming/flushing.[7] In cases where the species cannot be removed the adsorption is called irreversible.

During particle growth, the active surface area of the catalyst is lost due to an increase in the crystallite size or particle size.[4] Please note that particles consist of crystallites. Particles are in general visualized by electron microscopy (TEM) while crystallites are visualized by X-Ray diffraction. Though particles and crystallites are not the same often their distinction is not always clearly indicated. There exist two major routes of crystallite growth; coalescence and Ostwald ripening.[8] During coalescence two smaller crystallites merge into a bigger one. This process is often also called sintering. Ostwald ripening means that smaller species, atomic species or aggregates, dissolve into the solution or evaporate to the gas phase and precipitate onto a larger crystallite.[4] General strategies to overcome crystallite/particle growth are careful control over catalyst properties such as metal–support interaction[9] and crystallite/particle size[10].

For CAL hydrogenation often reported deactivation mechanisms for noble metals are leaching [5,11,12] and particle growth[5,13]. For instance, Cattaneo et al.[5] found that the conversion over TiO_2 supported AuPd decreased from 73% to 50% after the first run in a batch reactor, which was attributed to metal leaching and particle growth. To enhance the stability of the catalysts, the authors improved the metal-support interactions by using higher calcination/reduction temperatures (200-400 °C). Although the activity of the AuPd catalysts did decrease for CAL hydrogenation, the stability was increased for 4 consecutive reactions. The final reaction solution revealed the absence of leached metals, confirming that higher temperatures increased the metal-support integration. This study shows that the catalysts preparation and thus the careful control over the catalyst properties affects the stability.

Catalytic hydrogenation reactions are traditionally conducted in batch reactors. However, to investigate the stability of a catalyst a fixed bed continuous flow reactor is preferable.[14] Due to the nature of the batch reactor, catalyst deactivation cannot be observed directly within one run. Hence, experimentally, to investigate catalytic stability the catalyst needs to be recycled, and multiple subsequent experiments need to be run. For the experimental approach after each reaction, the reactor needs to be emptied and the catalyst needs to be separated from the reaction mixture. For the carbide based catalyst, this is cumbersome since the catalyst needs to be protected e.g. by the solvent to prevent its oxidation. Moreover, reactant and products remaining in the pores are known to deteriorate via unwanted side reactions and can also deactivate the

catalyst. An additional regeneration step after each run would thus be required. Hence, to study the deactivation of (carbide) catalysts, a continuous flow fixed bed reactor is preferred.[15,16] However, studies of hydrogenation of CAL in a continuous flow fixed bed reactor are lacking[1] and only a few studies do exist (exclusively using noble metal catalysts).[17-22] One of these few studies that used a continuous rector for the liquid phase selective hydrogenation of cinnamaldehyde is published by Durndell et al.[21]. In that study, it was shown that the hydrogenation of Pt/SiO_2 was significantly enhanced in activity and selectivity towards C=O activation when using a continuous flow fixed bed reactor in comparison to a batch reactor. In addition, negligible catalyst deactivation occurs under extended flow operation due to the continuous removal of poisons from the reaction zone.

Our earlier study revealed that particle growth or/and site blocking might be the major deactivation mechanisms of the carbide catalysts during the CAL hydrogenation reaction. Here we want to investigate the role of carbide particle size on the stability of the catalyst when used in a continuous flow fixed bed reactor. Stellwagen et al.[23] indicated that larger particles were more stable for the deoxygenation of fatty acid performed in batch reactors. The author and also we here in this study varied the carbide particle size by using carbon nanofibers (CNFs) with different amount of oxygen groups, which are expected to be anchoring/nucleation sites, on their surface, which were subsequently impregnated with a solution of ammonium heptamolybdate. Surface oxygen groups were introduced to the CNFs by treatment with nitric acid as opposed to CNF which experienced a hydrochloride treatment and did not bear oxygen groups. The impregnation of the CNFs with more surface oxygen groups is expected to result in higher metal dispersion, e.g. smaller particles. The carbides are then synthesized via the temperature programmed reduction method and the textural and chemical properties were examined by N_2-physisorption, XRD, TEM and CO chemisorption. In contrast to our earlier work, the catalytic testing was performed in a continuous flow fixed bed reactor.

Materials & Methods

Catalyst synthesis

Carbon nanofibers (CNFs) were grown from a mixture of hydrogen (102 ml/min), nitrogen (450 ml/min) and carbon monoxide (260 ml/min) at 550 °C and 3 barg for 24 h over a reduced 5 wt% Ni/SiO_2 catalyst (3 g), as reported previously.[24] To remove the SiO_2 from the product, the product was treated three times with a boiling 1 M KOH solution. Finally the product was decanted followed by washing with water.

Next, the CNF sample was refluxed with hot concentrated acid to remove the nickel. One part of the CNF was refluxed in concentrated HCl and remained fully hydrophobic (i.e. negligible amount of surface oxygen groups, denoted as CNF-HCl). The other part of the CNF was refluxed in concentrated nitric acid to introduce surface oxygen groups on the CNF surface (denoted as CNF-ox). Finally, both CNFs were ground and sieved to obtain 90-120 μm particles.

The supports (CNF-HCl and CNF-ox) were then impregnated using dissolved ammonium heptamolybdate (AHM; Sigma-Aldrich, 99.98% trace metals basis) to obtain 8.5 wt% MoC. After impregnation, the catalyst was dried overnight at 110 °C.

For the carburization, the temperature-programmed reduction (TPR) method was used. This reaction was performed in a vertical fixed bed flow reactor placed in a furnace (Carbolite Gero 30-3000 °C), using 20% CH_4/H_2 (total flow of 10 min^{-1}). The temperature was increased to 650 °C (β = 5 °C/min) for 2 h, as previously reported.[25] The catalyst supported on CNF-HCl was denoted as a-MoC/CNF and the one supported on CNFox as b-MoC/CNF.

Characterization

XRD patterns were recorded on a Bruker D8 Advance with a Lynxeye-XE-T PSD detector equipped with a Cu-Kα1,2 tube generating X-rays with λ = 1.542 Å. The measurements were taken from 2θ = 20° to 2θ = 80° with a step size of 0.05° at 1 sec^{-1}.

TEM images were taken with a JEOL JEM-1400 Plus microscope operated at 100 kV. For the sample preparation, 10 mg of the catalyst sample was added to 1 mL absolute ethanol and homogenized in an ultrasonic bath for 10 sec. Then 2 µL was dropped on a carbon covered Cu grid (400 mesh) and dried at room temperature. The data were analysed with ImageJ and MS Excel to obtain the mean particle size (d_s) and distribution of around 200 particles. The average number was calculated by the following equation, in which d_i the diameter of a Mo particle is:

$$d_s = \sum d_i^3 / \sum d_i^2 \quad (5.1)$$

CO pulse chemisorption was performed on a Mircromeritics AutoChem II 2920. Prior to the measurement, the samples were in situ carburized at 600 °C for 1 h in a mixture of 20 % CH_4 in H_2 (total flow of 50 min^{-1}). Subsequently, the system was cooled to 35°C and flushed with He for 30 mins to remove the adsorbed gas. After the removal of adsorbed gas, pulses of 10% CO/He were injected over the catalyst. Mass spectroscopy was used to assess the CO uptake.

Temperature-programmed desorption combined with mass spectrometry (TPD-MS) analyses were performed with a Micromeritics AutoChem II 2920 coupled to a Pfeiffer Vacuum

ThermoStar™ mass spectrometer. To determine the amount and type of surface oxygen group, 100 mg of the CNF-HCl and CNF-ox were heated to 900 °C at 10 °C/min under helium (total flow of 20 min^{-1}). Prior to the heat treatment, the samples were in situ treated according to TPR conditions (600 °C for 1 h under a mixture of 20 % CH_4 in 50 min^{-1} of H_2). The desorbed gas was assessed by the MS. Similar experiments were also performed using a TCD detector (TPD-TCD), in that case, no information on the nature of the evolved gases could be obtained.

Thermogravimetry analysis (TGA) was performed in Mettler-Toledo MultiSTAR TGA/DSC. To analyse the amount of surface oxygen groups 40 mg of the sample was placed in alumina crucibles and heated to 900 °C (with a 5 °C /min ramp) in a 100 mL/min N_2 flow. The determine the metal content after the hydrogenation reaction, the metal weight of the catalysts was measured by TGA after treatment to 1000 °C (with 5 °C /min ramp) under 100 mL/min air flow.

N_2 physisorption was conducted on a Micromeritics Tristar II Plus at -196 °C. 100 mg of sample was degassed at 300 °C for 2 h in Micromeritics VacPrep 061.

Hydrogenation

Catalyst testing was conducted using a continuous flow fixed bed reactor with a downstream back pressure regulator. The stainless steel reactor (ID=0.5 cm, 5 cm length) was placed in a vertical furnace (Carbolite Gero 30-3000 °C) having a 3 cm isothermal zone. The catalyst (250 mg) was kept inside the reactor between two quartz wool plugs. The reactant mixture consisting of 13.6 g/l cinnamaldehyde and 1.36 g/l xylene (as internal standard) was added via an HPLC pump (0.1 mL/min), H_2 was added by combining the liquid stream (1 mL/min) and the gas stream in a T-joint. Prior to the hydrogenation, a carburization was performed as described in the section on catalyst preparation. The hydrogenation was performed at 110, 140 and 170 °C at 20 bar(g) H_2. The exit stream passed through a back pressure regulator, and the samples were collected periodically (every 1 h) by an autosampler. The composition of the liquid phase was determined by gas chromatography with an FID detector. The samples were filtered (0.2 μm filter) before injection.

A scheme of the set-up can be found in the Supplementary (Figure S5.1).

The following equations were used to calculate the conversion, product selectivity and the Turn-over frequency (TOF). With [Product X] concentration of a specific product x, Σ [Product] concentration of all products, $[CAL]_t$ concentration of CAL at a given time.

Conversion:

$$x_{CAL} = \frac{[CAL]_t}{[CAL]_{t,0}} * 100\% \quad (5.2)$$

Normalized selectivity:

$$S_{N,Product\ x} = \frac{[Product\ X]_t}{\Sigma\,[Products]_t} * 100\% \quad (5.3)$$

The turnover frequency (TOF) values were based on the number of sites determined by CO chemisorption. The following equation was used:

$$TOF = \frac{mmol_{CAL}converted * min^{-1}}{mmol\ of\ CO\ sites} \quad (5.4)$$

Metal leaching was assessed by Inductively Coupled Plasma analysis (ICP-OES, Perkin Elmer AVIO 500) of the reaction mixture after filtering. 0.1 ml of the filtrate was added to 1 ml of 30% aqueous hydrogen peroxide and 9 ml of 65% nitric acid. The mixture was then digested with microwaves at 210 °C and 190 W for 40 mins.

Regeneration

In order to regenerate the catalysts after the first run of hydrogenation (with a duration of 24 h), the following procedure was applied. First, the reactant and the remaining products are removed by flushing with toluene (1 ml/min) and Argon (10 ml/min) at 140 °C and 20 bar(g) for 1h. Afterwards, the catalyst was dried by only flushing with argon (10 ml/min) at 140 °C and 0 bar(g) for 15 min. During the cooling of the catalysts to room temperature, the catalyst was kept under the same argon flow. To regenerate the catalysts, it was re-carburized under the same conditions as described in the section on catalyst preparation.

Results and Discussion

Support and Catalysts characterization

Support oxygen groups

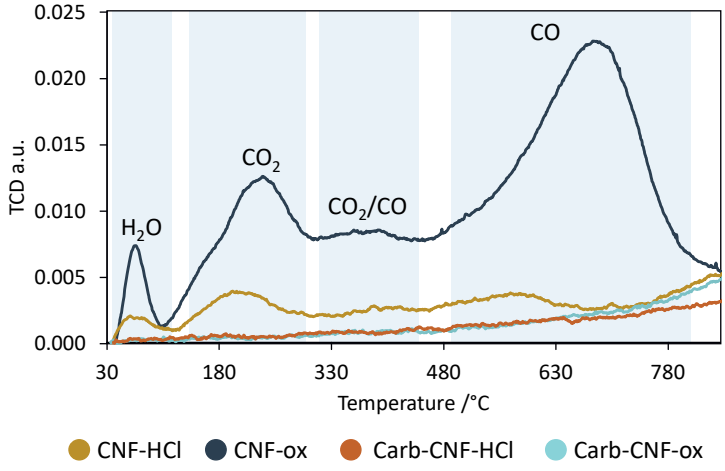

Figure 5.1 TPD-TCD of different CNF supports; 'Carb' represents to samples treated by TPR treatment in 20% CH_4/H_2 at 650 °C

The nature of the oxygen containing surface groups on the CNFs (CNF-ox and CNF-HCl) and their counterparts which were exposed to carburization conditions (TPR conditions: 650 °C in 20% H_2/CH_4 resulting in Carb-CNF-ox and Carb-CNF-HCl) was accessed by TPD-TCD. The TCD profiles of the four CNFs as function of temperature are displayed in Figure 5.1. From the TCD profile of the CNF-ox four different peaks at 100 °C, 220 °C, 400 °C and 700 °C can be identified. From the MS data shown in the Supporting Information (SI) Figure S5.2, these peaks can be attributed to the release of water at ~100 °C, CO_2 at 220 °C, a mixture of CO_2/CO at 400 °C and CO at 700 °C. The release of CO and CO_2 indicates the decomposition of surface oxygen groups, such as carboxylic acids, anhydrides, lactones and phenols, which are initially introduced during the nitric acid treatment.[26-29]

When comparing the TPD profiles of CNF-ox and CNF-HCl, it becomes clear that substantial amounts of oxygen surface groups are released from the CNF-ox, while only low amounts of oxygen groups were released from the CNF-HCl during the thermal treatment. A similar trend was observed for the TGA data, in which the weight loss up to 1000 °C corresponds to the total amount of surface oxygen groups present on the CNF. The weight loss of fresh CNF-HCl is relatively small, about 1.4 wt.%, as can be seen in Figure S5.3, while the weight loss of fresh CNF-ox was 5.8 wt.%. The TPD-TCD and the TGA data confirm, that the nitric acid oxidation

treatment increased the number of oxygen groups while the hydrochloride treatment leads to an oxygen free surface.[23,30]

From the TPD-TCD profiles of both carburized (Carb-) CNFs no peaks (H_2O, CO or CO_2) were observed indicating that the oxygen surface groups were removed during the carburization process. Hence, the oxygen surface groups are still present during the impregnation and can affect the properties of the catalyst e.g. by forming anchoring sites for the Mo metal salt. However, after the carburization, the oxygen surface groups are removed and therefore cannot affect the catalytic performance.

In summary, the TPD and TGA characterization showed that there are significant amounts of surface oxygen group (5.8 wt.%) present after the nitric acid treatment on CNF-ox whereas CNF-HCl had a negligible amount of surface oxygen group functionalities. After TPR synthesis the surface oxygen group on CNF-HCl and CNF-ox were decomposed at the carburization temperatures (650 °C). Hence, the oxygen surface groups are removed during the carburisation process and most likely do not play a role in the hydrogenation reaction.

Influence of the surface oxygen groups on the characteristics of the catalyst

Table 5.1. Overview of textural properties of the CNF-HCl, CNFox, a-MoC/CNF and b-MoC/CNF. (Average of a duplicate measurement)

	BET (m^2/g)	**Total pore volume (cm^3/g)**	**Micropore Area (m^2/g)**
CNF_{HCl}	189 ± 2	0.41 ± 0.00	42 ± 1
CNF_{ox}	197 ± 4	0.38 ± 0.01	41 ± 1
a-MoC/$CNF_{(HCl)}$	108 ± 2	0.31 ± 0.00	12 ± 1
b-MoC/$CNF_{(ox)}$	101 ± 4	0.29± 0.01	10 ± 1

Nitrogen physisorption experiments were performed to obtain information on the effect of the pre-treatment (nitric acid/ hydrochloride) and the carburization on the structure of the CNF and Mo carbide catalysts. The adsorption isotherms of the CNF and catalysts are given in Figure S5.4. The derived values of BET area, total pore volumes and micropore volumes of all samples are summarized in Table 5.1. These textural properties of the supports show that the specific surface area (189 m^2/g versus 197 m^2/g), the total pore volume (0.41 cm^3/g versus 0.38 cm^3/g) and the micropore volume (42 m^2/g versus 41 m^2/g) of the both CNFs are similar. For the catalysts in compassion, these textual properties were 40-50% lower. This decrease in surface area of the carbide containing samples compared to the parent CNF can be ascribed to a combined effect of

to the loss of amorphous carbon during the carburization process to the presence of the metal-carbide (assuming it is non porous) and pore blocking by the metal.[31-33]

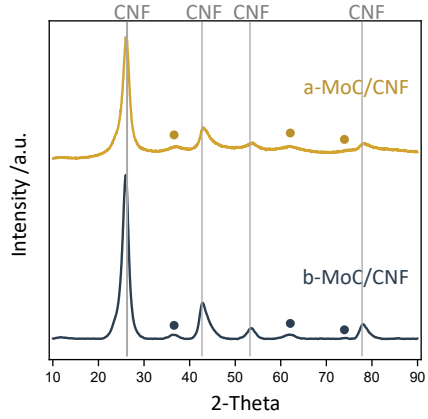

Figure 5.2 XRD patterns of the a-MoC/CNF and b-MoC/CNF.

The nature of the carbide phases formed during the carburization was accessed by XRD and is displayed in Figure 5.2. The signals at 2θ=28°, 45°, 53° and 79° represent the (002) and (101) reflections of the CNF.[34] Both Mo carbide catalysts show additional peaks with a similar pattern with signals at 32°, 60° and 75°. Based on database PDF-2-2004, these signals represent the α-cubic phase of MoC_{1-x}, which has been reported before for MoC_{1-x} synthesized with the TPR method.[2,25,35]

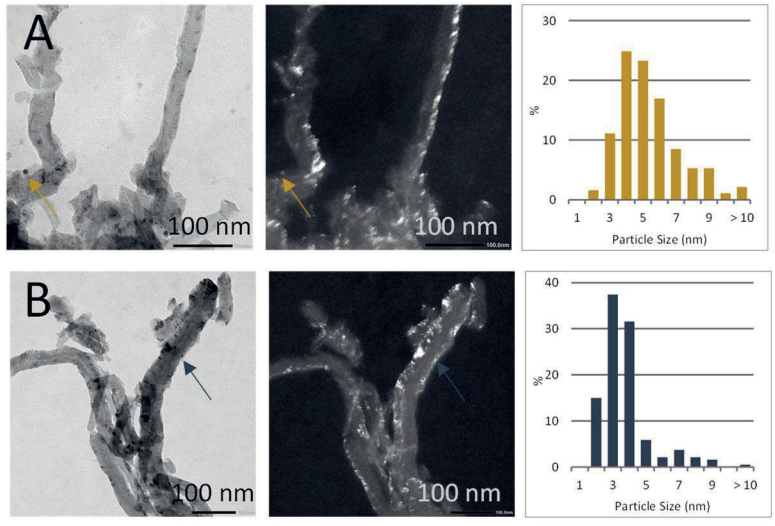

Figure 5.3 Representative TEM images, HAAFD images and particle size distribution of CNF-supported Mo-carbide catalysts (A) a-MoC/CNF and (B) b-MoC/CNF.

Table 5.2 Particle size and CO uptake of a-MoC/CNF and b-MoC/CNF.

	Average particle size[a] (nm)	Surface average size [a] (nm)	CO uptake [b] (µmol/g)
a-MoC/CNF$_{(HCl)}$	4.9 ± 1.9	6.5	55.5 ± 0.9
b-MoC/CNF$_{(ox)}$	3.2 ± 1.5	4.9	67.2 ± 0.9

a. Around 200 particles counted
b. Average of a duplicate measurement

Transmission electron microscopy (TEM) images were taken to examine the structure and particle size of the CNF supported Mo carbides. A representative bright field image, high-angle annular dark field image and the particle size distribution of a-MoC/CNF and b-MoC/CNF are shown in Figure 5.3 A and B, respectively. The carbide particles appear as spherical shaped particles on the carbon nanofibers (examples of carbide particles are indicated by the arrows). The mean particle size as estimated from the images is for a-MoC/CNF 4.9 ± 1.9 nm and for b-MoC/CNF 3.3 ± 1.6 nm (see Table 5.2). The standard deviation is rather large indicating that the particle size distribution is broad particle size distribution. For this reason, the surface average was calculated which is 6.5 nm for the a-MoC/CNF and 4.9 nm for the b-MoC/CNF.

The smaller particle sizes for a-Mo/CNF which has the higher number of surface oxygen groups (prior to the carburisation, Figure 5.1) show that the oxygen surface groups are beneficial for obtaining small particles as expected. This has also been observed by Stellwagen et al.[23] who showed that CNF-ox supported Mo and W particles were significantly smaller (1-2 nm) in comparison to CNF-HCl supported particles (~10 nm) albeit the authors prepared the samples by CR. This might explain the difference in particle size in comparison to what we found (the here prepared samples are TPR synthesized).

To get more insight into the number and nature of the (re)active sites CO chemisorption was performed. Table 5.2 shows the measured CO site densities. The CO uptake for the a-MoC/CNF catalyst is in the range of 55.5 µmol/g and for the b-MoC/CNF catalyst is in the range of 67.2 µmol/g. The chemisorption data is qualitatively in line with the TEM images; the a-MoC/CNF has a lower CO uptake and thus smaller particles than the b-MoC/CNF.

Cinnamaldehyde (CAL) hydrogenation

The catalytic performance of a-MoC/CNF and b-MoC/CNF were tested for the hydrogenation of CAL in a continuous flow fixed bed reactor. The reactions were performed at 20 bar, gas/liquid ratio = 10, 0.1 mL/min liquid flow rate at varying temperatures (90-140 °C for a-MoC/CNF and 110-170 °C for b-MoC/CNF). Among these temperatures, we chose to compare the catalysts at

140 °C (as both show an appreciable activity at this temperature). The conversion and selectivity plots of different temperatures are shown and discussed in the SI, Figure S5.5.

Activity and stability

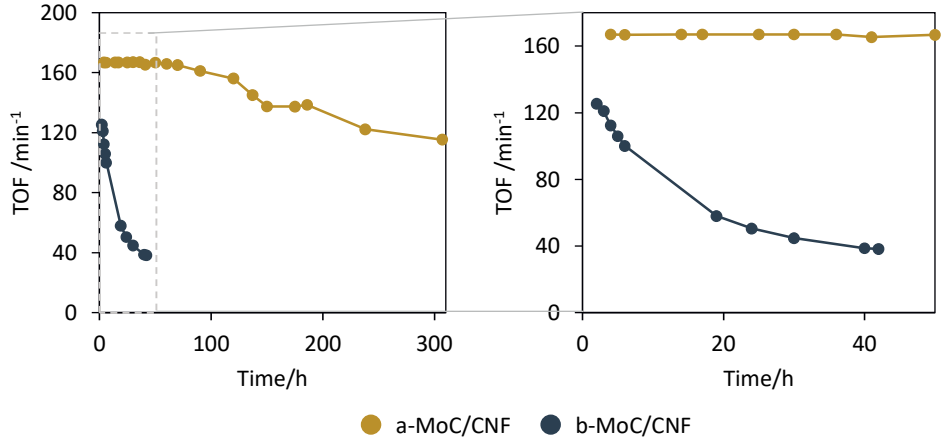

Figure 5.4 TOF of CAL over a-MoC$_{1-x}$/CNF and b-MoC$_{1-x}$/CNF. Reaction condition: 250 mg, 0.1 mL/min liquid flow, 1 mL/min H_2 flow, 0.1 M CAL concentration, 140 °C and 20 bar.

Figure 5.4 shows the. It should be noticed that the activity of the a-MoC/CNF catalysts is shown here for t = 310 hrs, while TOF based on the CO density sites over the two different catalysts as function of time the b-MoC/CNF is plotted for only t = 40 hrs. The Figure reveals striking differences in catalysts stability. The TOF of a-MoC/CNF remained ~170 min^{-1} for the first 100 hrs and after 300 h the activity decreased to 115 min^{-1}. In contrast, the TOF of b-MoC/CNF decreased from 125 min^{-1} to 38 min^{-1} within the first 40 hrs. Expressing this in deactivation rates (Table 5.3), the a-MoC/CNF decreases only by 0.4% in the first 40 hrs, while b-MoC/CNF decreases 63.2% within the first 40 hrs. This shows that the a-MoC/CNF catalyst is more stable over time in compassion to the b-MoC/CNF. We found that these results were reproducible over newly synthesised catalysts (see SI, Figure S5.6 and Figure S5.7).

Selectivity

In order to understand the reaction pathway over the two catalysts, the product yields over time are given in Figure 5.5. The a-MoC/CNF catalyst initially forms HCOL as main product, indicating the full hydrogenation of CAL. With a longer reaction time, the selectivity to HCOL decreased whereas the selectivity to the C=O hydrogenation product, HCAL increased and became the dominant product after 70 hrs. After this, the product distribution remains stable. This leads to the suggestion that the hydrogenation of HCAL to HCOL is inhibited with time but the first

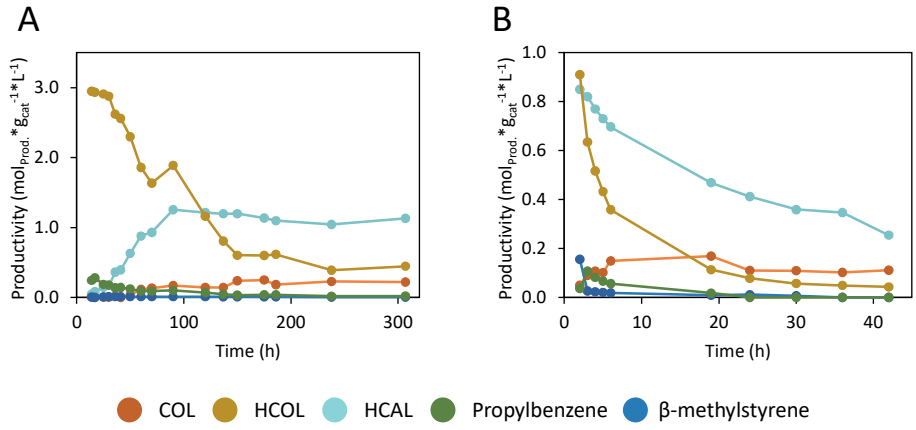

Figure 5.5 Product selectivity and conversion of CAL over a-MoC/CNF (5-6nm) and b-MoC/CNF (4-5 nm). Reaction condition: 250 mg, 0.1 mL/min liquid flow, 1 mL/min H_2 flow, 0.1 M CAL concentration, 140 °C and 20 bar.

hydrogenation to HCAL remains possible. A possible explanation could be that the carbide catalysts have two different active sites; one that hydrogenates (C=C) CAL to HCAL and is not inhibited and the other that hydrogenates (C=O) HCAL to HCOL.

The product yields of b-Mo/CNF also change within the running period of 43 hrs. Initially, similar yields of HCAL and HCOL were found. Both product yields are decreasing drastically within the first 20 hrs. Although the b-MoC/CNF favour the C=C hydrogenation resulting in higher yields of HCAL over the whole running period, the formation of COL gives evidence for the C=O hydrogenation, although in low yields. These results show that the product selectivity is depending on the conversion level. At high conversion levels, hydrogenation over C=O bond is preferred, while at lower conversion levels the hydrogenation over the C=C bond increases.

Moreover, the selectivity towards propylbenzene and β-methylsterene remained low (>5% selectivity) for both catalysts. In our earlier work[2], we observed that the carbide catalyst also produces β-methylstyrene and we attributed that at that time to the formation of oxides (acid sites) during the transfer of the catalysts from the carburisation reactor to the hydrogenation reactor. In this study, the carbide catalysts were in situ carburised and thus not exposed to air. Therefore the low amount of propylbenzene and β-methylsterene were expected, as only low amounts of acid sites can be present in the carbides catalysts since they were not exposed to air.

In addition, the activity, selectivity and the deactivation rate of the two catalysts are compared at different temperatures and reported in Table 5.3. The a-MoC/CNF catalyst shows the highest

weight-based conversion rates. This becomes more clear when comparing the conversion at lower reaction temperatures (110 °C). The conversion at 2h of the a-MoC/CNF is here 73.5% whereas the b-MoC/CNF has a conversion of 29.7% at 2h. A similar trend was found for the TOF. The TOF of a-MoC/CNF at 110 and 140 °C was found to be 166.5 and 122.7 min^{-1}, respectively. Whereas the TOF of the b-MoC/CNF significantly decreases to 125.4 min^{-1} (110 °C) and 41.0 min^{-1} (140 °C).

Table 5.3 Conversion, TOF and (COL, HCAL, & HCOL) selectivity of a-MoC/CNF and b-MoC/CNF at 2 and 40 h of the reaction.

	T. (°C)	Conversion (%)		TOF (min^{-1})[a]		COL (%)		HCAL (%)		HCOL (%)		Deac. (%)
		2 h	40 h	2 h	40 h	2 h	40 h	2 h	40 h	2 h	40 h	
a-MoC/ CNF	140	99.4	99.0	166.5	165.3	0.1	0.0	0.7	12.7	80.4	82.3	0.4
	110	73.5	29.5	122.7	49.3	24.4	33.2	38.0	46.1	22.1	12.7	44.0
b-MoC/ CNF	140	90.7	27.7	125.4	38.7	3.2	27.2	40.2	62.0	35.5	10.7	63.2
	110	29.7	0.9	41.0	1.2	45.6	48.1	47.1	51.9	7.4	0.0	28.8

[a]TOF based on CO uptake

The carbon balance was found to be ~90 for the a-MoC/CNF (see Table S5.1). However, the carbon balance of the b-MoC/CNF was initially lower (~62%) and stabilise ~80-90% after 15 hrs of reaction (see Table S5.2). A range of unidentified products (especially at longer retention times) could be detected during the hydrogenation. As also earlier shown,[2] the formation of C18 coupling products is possible over this type of catalyst.

To sum up, the catalyst with (an initial) larger Mo carbide nanoparticle (a-MoC/CNF) is more active and stable in comparison to the catalysts with smaller nanoparticles (b-MoC/CNF). Both catalysts favour the C=C hydrogenation as evidenced by higher product selectivity towards the HCAL.

Evaluating the catalyst deactivation mechanism

Clearly, the b-MoC/CNF with smaller particles size do deactivate rapidly. Often, four pathways are defined for carbide catalyst deactivation e.g. (a) blocking of the active site (e.g. coke deposition), (b) crystallite growth, (c) leaching and (d) oxidation.[4] In order to elucidate which mechanism causes the deactivation, the recovered catalysts were analysed by TEM and XRD. In addition, ICP experiments of the reaction mixture were analysed to investigate metal leaching.

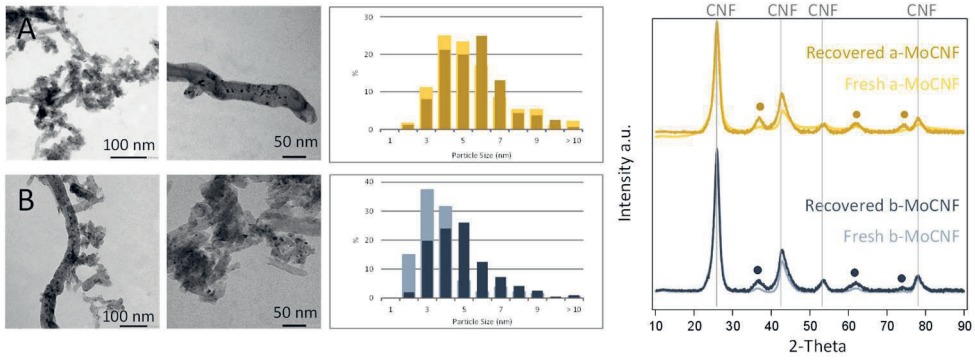

Figure 5.6 Main characteristics measured by TEM and XRD of recovered a-MoC/CNF (A) and b-MoC/CNF (B).

In Figure 5.6 (right), the TEM analysis of the recovered a-MoC/CNF and b-MoC/CNF are given, respectively. The particle diameter of catalysts with an initial larger particle size (a-MoC/CNF) increases slightly (+3%), as can be seen in Table 5.4. The surface average particle size of the a-MoC/CNF decreases slightly about -6%. In contrast, the particle diameter and surface average of the catalysts with smaller initial particles (b-MoC/CNF) significantly increase by about +35% and +14%, respectively. These results are in accordance with the XRD data (Figure 5.6, left) in which sharper peaks for recovered catalysts were observed, indicating larger particles. Thus, these data indicate that smaller nanoparticles are prone to grow during the hydrogenation reaction and are thus less stable.

Table 5.4 Particle size of recovered a-MoC/CNF and b-MoC/CNF in comparison to the fresh catalysts. Values for fresh catalysts between brackets.

	Number average particle size (nm)	**Surface average particle size (nm)**
a-MoC/CNF	5.1 ± 1.7 (4.9 ± 1.9)	6.2 (6.4)
b-MoC/CNF	4.4 ± 1.7 (3.2 ± 1.5)	5.7 (4.9)

Deactivation due to particle growth is irreversible and detrimental in the long term. Two major routes lead to particle growth: (a) coalescence (or particle diffusion) and (b) Ostwald ripening.[8,36] To determine the type of growth mechanism (Ostwald ripening or coalescence) is of interest since this knowledge can aid in the development of strategies to avoid particle growth. Based on the result presented here a definitive conclusion with respect to the growth mechanism cannot be drawn. However, ~0.2% of dissolved Mo (from the 8.5 wt.% of Mo_2C) was detected in the liquid phase after 10 hrs of reaction by ICP, which can indicate that Ostwald ripping is certainly contributing to the particle growth. In addition, these low metal concentration found in the reaction mixture indicates that the extent of Mo leaching from the catalysts is low and thus

leaching does not significantly contribute to the deactivation of b-MoC/CNF. It should be mentioned that the obtained metal concentration was measured close to the detection limit of the analyser. No other metals were found.

Oxidation as potential deactivation mechanism is unlikely since our catalysts were not exposed to air after the in situ carburization. This is also confirmed by XRD which indicated (Figure 5.6) that no bulk oxidation of the carbide catalysts occurs during the reaction. However, water is formed during the reaction which can result in surface oxidation.[37-39] These oxidized surface sites can explain the formation of β-methylsterene from COL or propylbenzene from HCOL. For the formation of these products, we have found that acid sites are required which can be generated by oxygen adsorption forming O*-Me_2C species.[2] However, the GC analysis shows only trace amounts of these products (>5%). Knowing this, surface oxidation of the carbide surface is unlikely and catalysts deactivation by oxidation is therefore excluded as a potential deactivation mechanism.

Another potential source of deactivation is the blocking of the active sites by adsorption of a carbonaceous species. This species that blocked the site can either be adsorbed reactant and/or reaction products or side products that form via polymerisation and condensation of the reactant/products (C18 compounds).[11,40] We observed higher deactivation rates for both catalysts at lower temperatures, which is indicating that adsorbed reaction products and reactants block the active sites.[41] We also know that hydrocarbon transformation into complex structures via polymerisation and condensation (C18 coupling products) does occur during the reaction. These C18 coupling products were earlier identified by GC-MS.[2] Considering these, site blocking by either the adsorbed reaction reactant/products (C18-products) and C18 couplings products as possible deactivation mechanism is highly likely and has been found earlier for noble metal catalysts.[21]

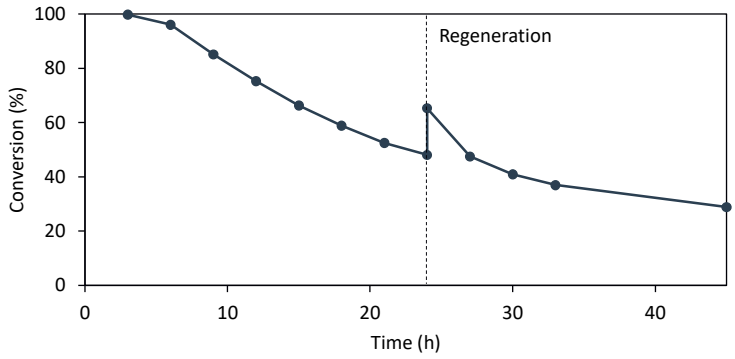

Figure 5.7 Conversion of fresh and upon regenerated b-MoC/CNF catalyst. Reaction condition: 250 mg, 0.1 mL/min liquid flow, 1 mL/min H_2 flow, 0.1 M CAL concentration, 140 °C and 20 bar.

To test whether the observed site blocking is reversible, the catalyst was regenerated to remove these adsorbed species by heat treatment (recarburization). Firstly, the used catalyst was washed using toluene and argon at 140 °C and then dried under argon at 140 °C. After cooling the catalysts under argon flow, the catalyst was re-carburized by the TPR methods. As can be seen from Figure 5.7 (and also from the run shown in Figure 5.5), the fresh catalyst deactivates from 100% to ~45% within the first 20 hrs. After regeneration, the Mo carbide catalyst achieved an initial conversion of ~65% conversion, demonstrating that ~20% of the conversion activity can be recovered. Moreover, the selectivity towards both C=C and C=O hydrogenation remained upon regeneration (Figure S5.8). These results indicate that the regeneration method partially removed the deposited species and partly recovered the deactivated CNF supported Mo carbide. In addition, it can be stated this 20% of observed deactivation was caused by active site blocking.

To identify the adsorbed species we tried to extract the desorbed species by solvent extraction. Trace amount of CAL and proplybenzene were observed (see Table S5.3). However, it was not

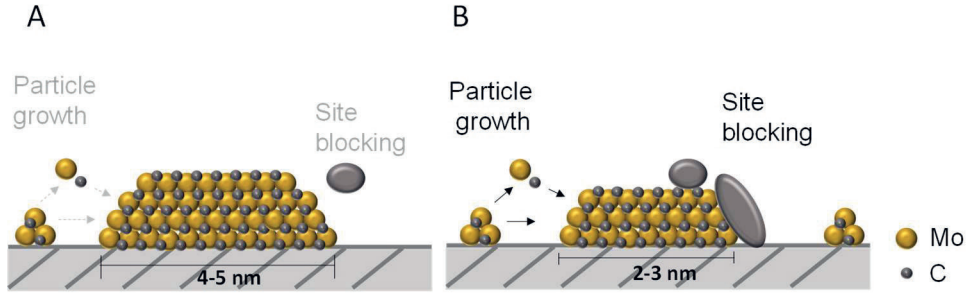

Figure 5.8 Possible deactivation mechanisms on a-MoC/CNF (A) and b-MoC/CNF (B). Black text indicates likely to occur, grey text indicates less likely to occur.

possible to identify the amount of the deposit species on catalysts and to estimate the difference in adsorbed species between the two recovered catalysts (a-MoC/CNF and b-MoC/CNF).

Considering the results above (see Table 5.5 for a summary), the rapid deactivation observed for the catalyst with smaller particles (b-MoC/CNF) can be attributed to particle growth and site blocking due to desorbed species (Figure 5.8). In total 63.2% of the activity was lost during 40 hrs of hydrogenation reaction. We observed a particle growth of 35% for the b-MoC/CNF catalysts suggesting that ~40% of the deactivation can be addressed to particle growth. The precise growth mechanism (e.g. Ostwald ripening or coalescence) of the Mo carbide remains to be elucidated. As particle growth is irreversible, the regenerated activity of 20% activity after re-carburisation was attributed to the removal of desorbed species. The adsorption of these species appears to be stronger for smaller particles and the larger particles effectively repel the product from the active site.

Table 5.5 Overview of the results.

	a-MoC/CNF	**b-MoC/CNF**
CNF	CNF- HCl	CNF-ox
Particle size Fresh (nm)	4.9 ± 1.9	3.2 ± 1.5
Particle size Spent (nm)	5.1 ± 1.7	4.4 ± 1.7
Conversion, 140°C (%)	99	88
Conversion, 110°C (%)	74	30
TOF, 140C (h^{-1})	2.8	2.0
Deactivation rate within 40 h (%)	**-0.4**	**-63.2**
Selectivity, high conversion rates	C=C Hydrogenation	C=C Hydrogenation

Conclusion

Carbon nanofiber supported molybdenum carbides with different particle sizes 3.2 vs 4.9 nm have been prepared. It has been shown that the carbide particle size is an important factor in the stability of the catalysts in the cinnamaldehyde hydrogenation. When the particle size increases, the stability of the Mo carbides improved since it the 4.9 nm particles only lost 0.4% of activity within 40 hrs. Whereas as the catalysts with a smaller particle size (3.2 nm) lost 63.2% of its activity within 40 hrs. The increased stability for larger particles is related to an improved resistance against site blocking by carbonaceous species and particle growth. The catalytic activity could be partially regained by re-carburisation, during which the carbonaceous species

are removed. The selectivity of Mo carbides supported on CNF has not been affected by the particle size, both catalysts prefer the C=C hydrogenation yielding hydrocinnamaldehyde.

Acknowledgements

Acknowledgement is made to the Dutch Research Council (NWO) for financial support (grant number NWO 729.004.002). The authors want to thank Susan Witte for helping with the GC analysis and Dmitry Pirgach for the ICP analysis.

References

(1) Wang, X.; Liang, X.; Geng, P.; Li, Q. Recent Advances in Selective Hydrogenation of Cinnamaldehyde over Supported Metal-Based Catalysts. *ACS Catalysis* **2020,** *10* (4), 2395.

(2) Führer, M.; van Haasterecht, T.; Bitter, J. H. Cinnamaldehyde hydrogenation over carbon supported molybdenum and tungsten carbide catalysts. *Chem Commun* **2022**, DOI:10.1039/D2CC05322E 10.1039/D2CC05322E.

(3) Führer, M.; van Haasterecht, T.; Bitter, J. Molybdenum and tungsten carbides can shine too. *Catalysis Science & Technology* **2020**.

(4) Macedo, L. S.; Stellwagen, D. R.; da Silva, V. T.; Bitter, J. H. Stability of Transition-metal Carbides in Liquid Phase Reactions Relevant for Biomass-Based Conversion. *Chemcatchem* **2015,** *7* (18), 2816.

(5) Cattaneo, S.; Freakley, S. J.; Morgan, D. J.; Sankar, M.; Dimitratos, N.; Hutchings, G. J. Cinnamaldehyde hydrogenation using Au–Pd catalysts prepared by sol immobilisation. *Catalysis Science & Technology* **2018,** *8* (6), 1677.

(6) Bartholomew, C. H. Mechanisms of catalyst deactivation. *Applied Catalysis A: General* **2001,** *212* (1-2), 17.

(7) Argyle, M.; Bartholomew, C. Heterogeneous catalyst deactivation and regeneration: a review. *Catalysts* **2015,** *5* (1), 145.

(8) van Haasterecht, T.; Swart, M.; de Jong, K. P.; Bitter, J. H. Effect of initial nickel particle size on stability of nickel catalysts for aqueous phase reforming. *Journal of Energy Chemistry* **2016,** *25* (2), 289.

(9) Farmer, J. A.; Campbell, C. T. Ceria maintains smaller metal catalyst particles by strong metal-support bonding. *Science* **2010,** *329* (5994), 933.

(10) Campbell, C. T.; Parker, S. C.; Starr, D. E. The effect of size-dependent nanoparticle energetics on catalyst sintering. *Science* **2002,** *298* (5594), 811.

(11) Hájek, J.; Kumar, N.; Nieminen, V.; Mäki-Arvela, P.; Salmi, T.; Murzin, D. Y.; Červený, L. Deactivation in liquid-phase hydrogenation of cinnamaldehyde over alumosilicate-supported ruthenium and platinum catalysts. *Chemical Engineering Journal* **2004,** *103* (1), 35.

(12) Su, J.; Shi, W.; Liu, X.; Zhang, L.; Cheng, S.; Zhang, Y.; Botton, G. A.; Zhang, B. Probing the performance of structurally controlled platinum-cobalt bimetallic catalysts for selective hydrogenation of cinnamaldehyde. *Journal of Catalysis* **2020,** *388*, 164.

(13) Bus, E.; Prins, R.; van Bokhoven, J. A. Origin of the cluster-size effect in the hydrogenation of cinnamaldehyde over supported Au catalysts. *Catalysis Communications* **2007,** *8* (9), 1397.

(14) Westerterp, K.; Molga, E.; Van Gelder, K. Catalytic hydrogenation reactors for the fine chemicals industries. Their design and operation. *Chemical engineering and processing: process intensification* **1997,** *36* (1), 17.

(15) De Vylder, A.; Lauwaert, J.; Van Auwenis, S.; De Clercq, J.; Thybaut, J. W. Catalyst stability assessment in a lab-scale liquid-solid (LS) ^{2} plug-flow reactor. *Catalysts* **2019,** *9* (9), 755.

(16) Van Der Klis, F.; Gootjes, L.; Van Haveren, J.; Van Es, D.; Bitter, J. From batch to continuous: Au-catalysed oxidation of d-galacturonic acid in a packed bed plug flow reactor under alkaline conditions. *Reaction Chemistry & Engineering* **2018,** *3* (4), 540.

(17) Niesz, K.; Hornyak, I.; Borcsek, B.; Darvas, F. Nanoparticle synthesis completed with in situ catalyst preparation performed on a high-pressure high-temperature continuous flow reactor. *Microfluidics and Nanofluidics* **2008,** *5* (3), 411.

(18) Avril, A.; Hornung, C.; Urban, A.; Fraser, D.; Horne, M.; Veder, J.-P.; Tsanaktsidis, J.; Rodopoulos, T.; Henry, C.; Gunasegaram, D. Continuous flow hydrogenations using novel catalytic static mixers inside a tubular reactor. *Reaction Chemistry & Engineering* **2017,** *2* (2), 180.

(19) Bai, Y.; Cherkasov, N.; Huband, S.; Walker, D.; Walton, R. I.; Rebrov, E. Highly selective continuous flow hydrogenation of cinnamaldehyde to cinnamyl alcohol in a Pt/SiO2 coated tube reactor. *Catalysts* **2018,** *8* (2), 58.

(20) Durndell, L. J.; Cucuzzella, C.; Parlett, C. M.; Isaacs, M. A.; Wilson, K.; Lee, A. F. Platinum catalysed aerobic selective oxidation of cinnamaldehyde to cinnamic acid. *Catal Today* **2019,** *333*, 161.

(21) Durndell, L. J.; Wilson, K.; Lee, A. F. Platinum-catalysed cinnamaldehyde hydrogenation in continuous flow. *RSC Advances* **2015,** *5* (97), 80022.

(22) Müller, A.; Ludwig, M.; Arlit, M.; Lange, R. Evaluation of reactor concepts for the continuous production of fine chemicals using the selective hydrogenation of cinnamaldehyde over palladium catalysts. *Catal Today* **2015,** *241*, 214.

(23) Stellwagen, D. R.; Bitter, J. H. Structure–performance relations of molybdenum-and tungsten carbide catalysts for deoxygenation. *Green Chemistry* **2015,** *17* (1), 582.

(24) van der Lee, M. K.; van Dillen, J.; Bitter, J. H.; de Jong, K. P. Deposition precipitation for the preparation of carbon nanofiber supported nickel catalysts. *J Am Chem Soc* **2005,** *127* (39), 13573.
(25) Macedo, L. S.; Oliveira, R. R.; van Haasterecht, T.; Teixeira da Silva, V.; Bitter, H. Influence of synthesis method on molybdenum carbide crystal structure and catalytic performance in stearic acid hydrodeoxygenation. *Applied Catalysis B: Environmental* **2019,** *241*, 81.
(26) Führer, M.; van Haasterecht, T.; Masoud, N.; Barrett, D. H.; Verhoeven, T.; Hensen, E.; Tromp, M.; Rodella, C. B.; Bitter, H. The Synergetic Effect of Support-oxygen Groups and Pt Particle Size in the Oxidation of α-D-glucose: A Proximity Effect in Adsorption. *ChemCatChem* **2022,** *14* (19), e202200493.
(27) Figueiredo, J. L. Functionalization of porous carbons for catalytic applications. *J Mater Chem A* **2013,** *1* (33), 9351.
(28) Figueiredo, J. L.; Pereira, M. F. R. The role of surface chemistry in catalysis with carbons. *Catal Today* **2010,** *150* (1-2), 2.
(29) Figueiredo, J. L.; Pereira, M. F. R.; Freitas, M. M. A.; Orfao, J. J. M. Modification of the surface chemistry of activated carbons. *Carbon* **1999,** *37* (9), 1379.
(30) Ros, T. G.; Van Dillen, A. J.; Geus, J. W.; Koningsberger, D. C. Surface oxidation of carbon nanofibres. *Chemistry–A European Journal* **2002,** *8* (5), 1151.
(31) Souza Macedo, L.; Teixeira da Silva, V.; Bitter, J. H. Activated Carbon, Carbon Nanofibers and Carbon-Covered Alumina as Support for W2C in Stearic Acid Hydrodeoxygenation. *ChemEngineering* **2019,** *3* (1), 24.
(32) Rocha, A. S.; da Silva, V. T.; Faro Jr, A. C. Carbided Y zeolite-supported molybdenum: On the genesis of the active species, activity and stability in benzene hydrogenation. *Applied Catalysis A: General* **2006,** *314* (2), 137.
(33) Ghampson, I. T.; Sepúlveda, C.; Garcia, R.; Fierro, J. G.; Escalona, N.; DeSisto, W. J. Comparison of alumina-and SBA-15-supported molybdenum nitride catalysts for hydrodeoxygenation of guaiacol. *Applied Catalysis A: General* **2012,** *435*, 51.
(34) Jongerius, A. L.; Gosselink, R. W.; Dijkstra, J.; Bitter, J. H.; Bruijnincx, P. C. A.; Weckhuysen, B. M. Carbon Nanofiber Supported Transition-Metal Carbide Catalysts for the Hydrodeoxygenation of Guaiacol. *ChemCatChem* **2013,** *5* (10), 2964.
(35) Bouchy, C.; Derouane-Abd Hamid, S. B.; Derouane, E. G. A new route to the metastable FCC molybdenum carbide α-MoC(1-x). *Chem Commun* **2000**, DOI:10.1039/a907534h 10.1039/a907534h(2), 125.
(36) Van Haasterecht, T.; Ludding, C.; De Jong, K.; Bitter, J. Toward stable nickel catalysts for aqueous phase reforming of biomass-derived feedstock under reducing and alkaline conditions. *Journal of Catalysis* **2014,** *319*, 27.
(37) Mortensen, P. M.; de Carvalho, H. W. P.; Grunwaldt, J.-D.; Jensen, P. A.; Jensen, A. D. Activity and stability of Mo2C/ZrO2 as catalyst for hydrodeoxygenation of mixtures of phenol and 1-octanol. *Journal of Catalysis* **2015,** *328*, 208.
(38) Namiki, T.; Yamashita, S.; Tominaga, H.; Nagai, M. Dissociation of CO and H2O during water–gas shift reaction on carburized Mo/Al2O3 catalyst. *Applied Catalysis A: General* **2011,** *398* (1), 155.
(39) Medford, A. J.; Vojvodic, A.; Studt, F.; Abild-Pedersen, F.; Norskov, J. K. Elementary steps of syngas reactions on Mo2C(0 0 1): Adsorption thermochemistry and bond dissociation. *Journal of Catalysis* **2012,** *290*, 108.
(40) Ertl, G.; Knözinger, H.; Weitkamp, J. Handbook of heterogeneous catalysis. *Weinheim: VCH* **1997,** *2*, 427.
(41) Leppelt, R.; Schumacher, B.; Plzak, V.; Kinne, M.; Behm, R. Kinetics and mechanism of the low-temperature water–gas shift reaction on Au/CeO2 catalysts in an idealized reaction atmosphere. *Journal of Catalysis* **2006,** *244* (2), 137.

Supporting Information

Reactor set up

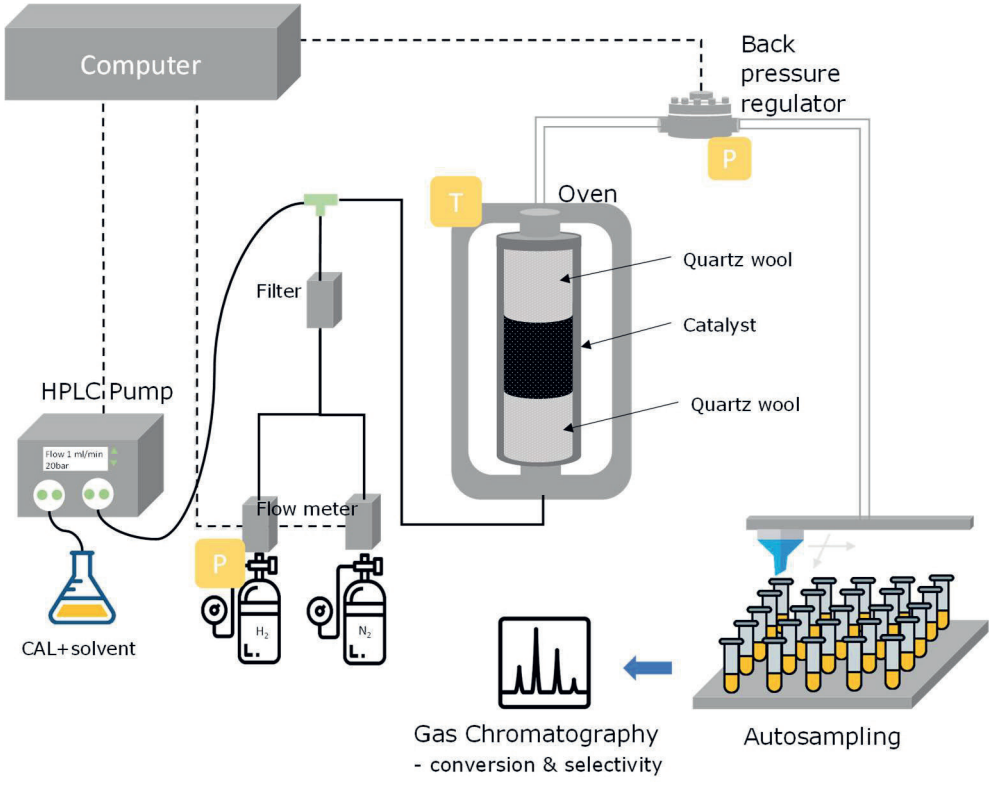

Figure S5.1 Continuous flow system including in-situ carburization and catalytic CAL hydrogenation reaction

In Figure S5.1 a schematic overview of the flow set-up is presented.

Surface oxygen groups

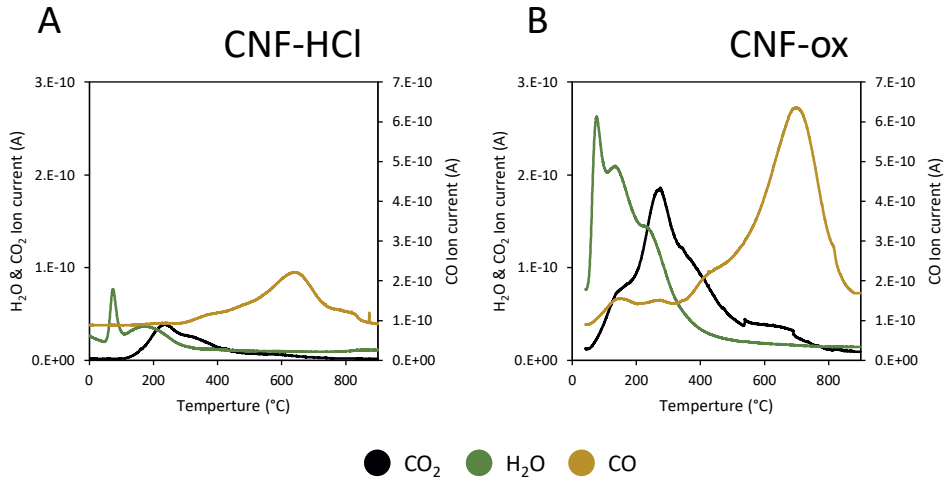

Figure S5.2 H_2O, CO_2 and CO spectra of (A) CNF-HCl and (B) CNF-ox.

TPD-MS has been performed to investigate the nature of the oxygen-containing groups introduced into CNF. The MS signals for CO and CO_2 as function of temperature give information on the amount and nature of the oxygen groups. Figure S5.2 show the MS profile of CNF-ox and CNF-HCl. According to Figueiredo et al.,[1-3] carboxylic acids decompose to CO_2 at 100-450 °C, anhydrides decompose into CO + CO_2 at 350-600 °C, lactones release CO_2 at higher temperatures like 550–800 °C, phenols release CO at 500-750 °C and carbonyl and quinones decompose by releasing CO at 650-900 °C. Thus, CO_2 is released at low temperatures, while the decomposition of CO peaks can be found in a higher temperature range.

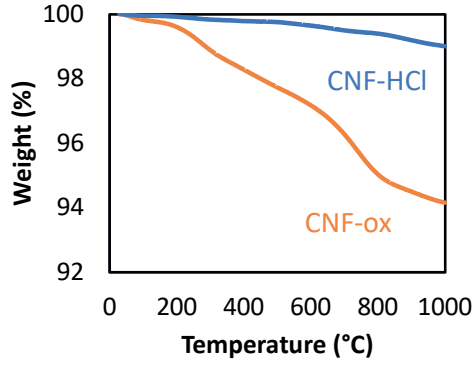

Figure S5.3 TGA profile of fresh CNF-HCl and CNF-ox.

The TGA profile of fresh CNF-ox and CNF-HCl are shown in Figure S5.3. The weight loss of CNF-ox was 5.8% and for CNF-HCl was 1.4%, showing that there were more oxygen groups on CNF-ox.

N_2-Physisorption Data

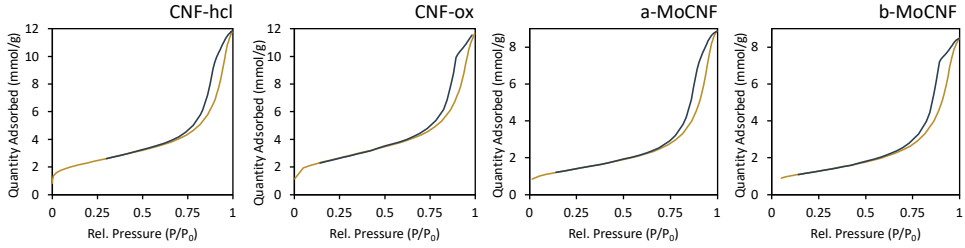

Figure S5.4 Adsorption–desorption isotherm of N_2 of the CNF-ox, CNF-HCl and the two Mo/CNF catalysts

The adsorption isotherms shown in Figure S5.4 are characteristic of multilayer adsorption/desorption accompanied by capillary condensation in relatively large mesopores, causing a hysteresis loop. The shape of the hysteresis loops indicates a distribution of cylindrical pores open on both sides.[4]

Hydrogenation of cinnamaldehyde at different temperatures

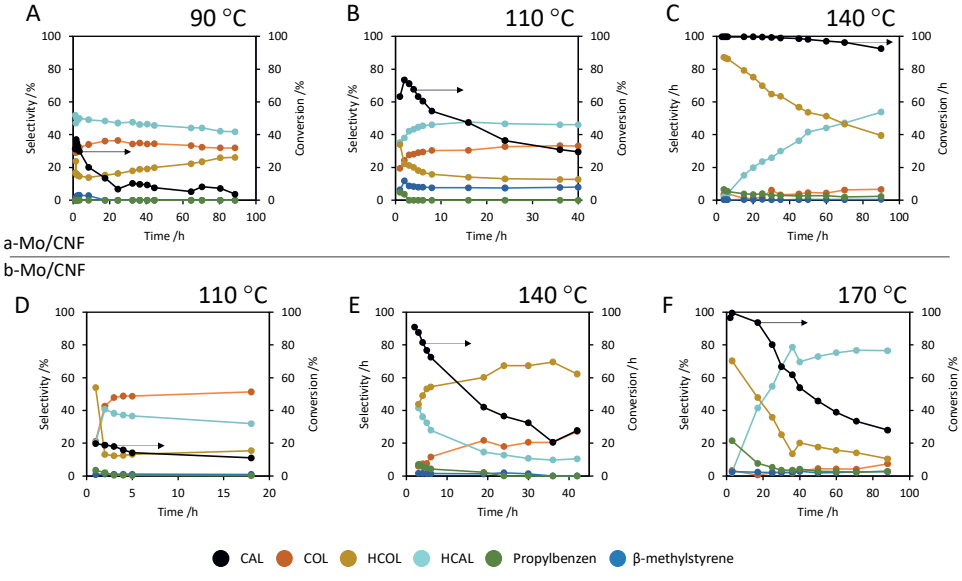

Figure S5.5 Hydrogenation over a-MoCNF (A-C) and b-MoCNF (D-F) at different temperatures. Reaction condition: 250 mg, 0.1 mL/min liquid flow, 1 mL/min H_2 flow, 0.1 M CAL concentration, 90-170 °C and 20 bar.

Figure S5.5 presents the conversion (in black) and the product selectivity over time for the two catalysts at different temperatures. The catalytic performance of the a-MoCNF was accessed at 90, 110 and 140 °C (Figure S5.4 A-C), whereas that of the b-MoCNF was evaluated at 110, 140 and 170 °C. The conversion of both catalysts increases with increasing temperature. The (initial) conversion of the a-MoCNF is higher than that of the b-MoCNF at the same temperature (e.g. 110 °C and 140°C). The product selectivity changes depending on the conversion. At lower conversion both catalysts hydrogenate C=O bond, producing more COL. The selectivity at higher conversion shows that both carbides favour the hydrogenation via the C=C bond, initially producing HCAL as main product. Subsequently, for all catalysts at higher conversion, the selectivity towards COL and HCAL is decreased as it is further hydrogenated resulting in increasing levels of HCOL.

Hydrogenation reproducibility

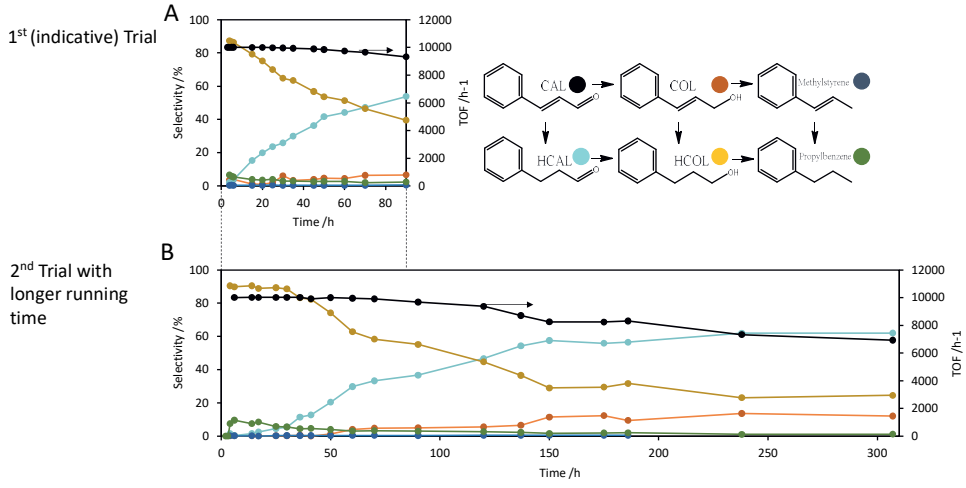

Figure S5.6 Selectivity and activity of two separate hydrogenation reactions over a-Mo/CNF catalysts. (A) first run with 90h of running time. (B) second run with a running time of 308h. Reaction condition: 250 mg, 0.1 mL/min liquid flow, 1 mL/min H_2 flow, 0.1 M CAL concentration, 140 °C and 20 bar.

Two separate hydrogenation reactions were performed using newly synthesized catalyst in order to test the experimental reproducibility. Figure S5.6 A shows the hydrogenation over CAL with a reaction run of 90 hrs. Within this 90 hrs, the conversion decreases to 92%. A similar deactivation rate was found for the Duplo experiment shown in Figure S5.6 B. The second reaction ran for 307 hrs and the conversion decreased to 70%.

Also for the b-MoCNF catalysts the reproducibility was proven. Figure S5.7 shows two separate hydrogenation reactions using newly synthesized b-MoCNF catalyst. The TOF and the selectivity

show a similar trend over the first 24 hrs of the reaction. The TOF decreases from ~8000 h^{-1} to ~4000 h^{-1}. The standard deviation of the activity was calculated to be ± 5-10%, which is in an acceptable range considering that it is a freshly carburised catalyst and the fast deactivation rate.

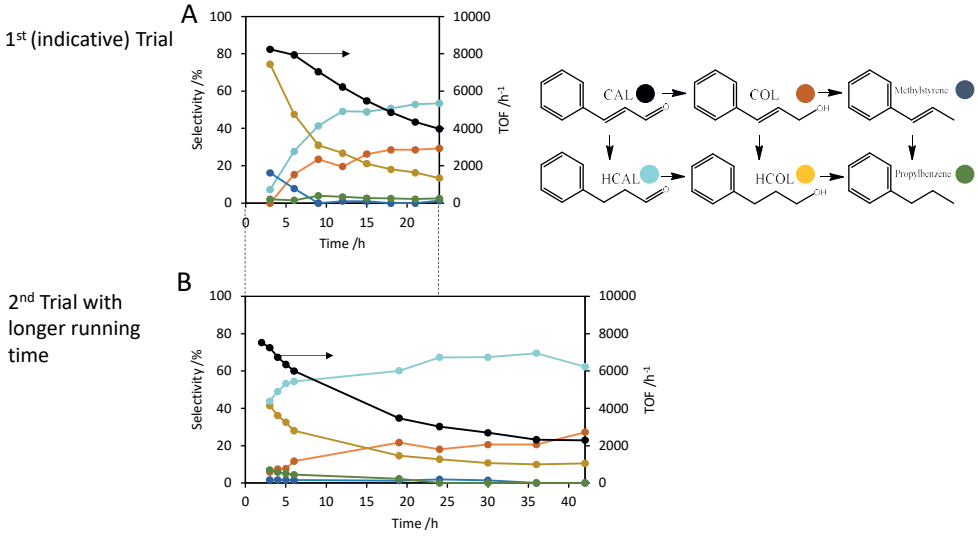

Figure S5.7 Selectivity and activity of two separate hydrogenation reactions over b-Mo/CNF catalysts. (A) first run with 90h of running time. (B) second run with a running time of 308h. Reaction condition: 250 mg, 0.1 mL/min liquid flow, 1 mL/min H_2 flow, 0.1 M CAL concentration, 140 °C and 20 bar.

Regeneration of Mo carbide catalysts

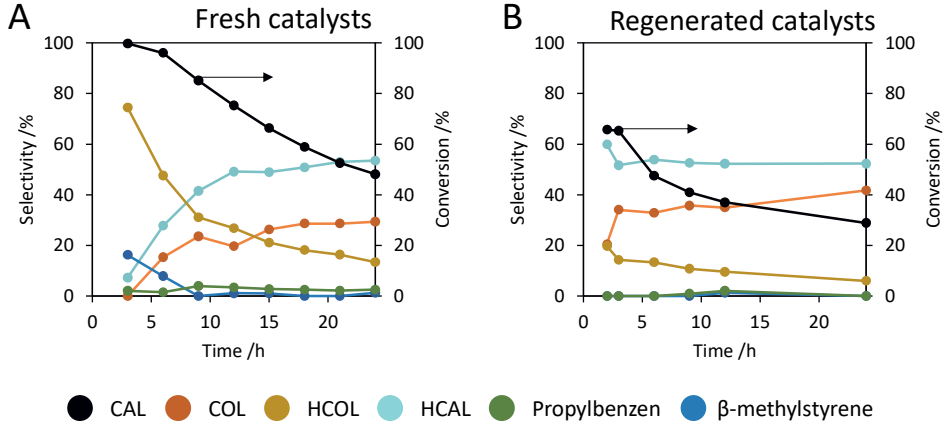

Figure S5.8 Product distribution and conversion of the CAL hydrogenation over fresh (A) and regenerated (B) b-MoCNF. Reaction condition: 250 mg, 0.1 mL/min liquid flow, 1 mL/min H_2 flow, 0.1 M CAL concentration, 140 °C and 20 bar.

Figure S5.8 shows the product selectivity and conversion of A the fresh catalysts and B the regenerated b-MoC/CNF catalysts. The fresh catalysts show similar behaviour as described in the main text (see Figures 5.4 and 5.5). For the regeneration, the used catalyst was washed using toluene and argon at 140 °C and then dried under argon at 140 °C. After cooling the catalysts under argon flow, the catalyst was re-carburized by the TPR method After the regeneration, the Mo carbide catalyst achieved an initial conversion of ~65% conversion, demonstrating that ~20% of the conversion activity can be recovered. Moreover, the selectivity towards both C=C and C=O hydrogenation remained upon regeneration (Figure S5.8).

Carbon balance

The carbon balance of a-MoCNF and b-MoCNF are shown in Tables S5.1 and S5.2. For the carbon balance of a-MoCNF tend to be stable over the time with a carbon balance of 90%. In contrast to the for b-MoCNF the initial carbon balance is much lower at 60-70%. The carbon balance increases over time to 86% occurred. The difference in the carbon balances between the a-MoCNF and b-MoCNF can be related to the unknown products detected in GC. The quantity of the unknown products was found to be more in b-MoCNF (10%) than a-MoCNF (~5%) based on the area. This product does slowly decrease with longer reaction times. It is suggested that this compound (with a retention time of 8.5 min) is similar to propylbenzene (3.4 min) or β -methylstyrene (6.4 min), as these retention times are close. Unfortunately, the GC-MS measurements give no evidence for this product.

In addition, we observed peaks at later retention times than all the known products, which have been detected also in our previous study.[5] From GC-MS analysis these peaks were identified to represent C18 compounds (such as 1,5-Diphenyl-3-pentanone, 2,5-Diphenyl-1,5-hexadiene, 1,5-Diphenyl-1,5-hexadiene and Benzene, 1,1'-(1,6-hexanediyl)bis-).

Table S5.1 Carbon balance of CAL hydrogenation over a-MoCNF

Time (h)	3	4	5	6	15	17	25	30
Carbon balance (%)	89	90	90	89	83	91	90	90

Table S5.2 Carbon balance of CAL hydrogenation over b-MoCNF

Time (h)	3	6	9	12	15	18	21	25
Carbon balance (%)	62	71	74	74	81	83	83	86

Extraction experiment

In order to further confirm and identify the deposit species, an experiment to extract these carbonaceous species was performed. The results of both recovered catalysts are shown in Table S5.3. For a-MoCNF used for 90 hrs, trace amounts of CAL and propylbenzene were extracted. Similar results were also observed for the extraction performed on b-MoCNF used for 40 hrs. It shows that for both catalysts, the same reactants and products were adsorbed on the surface in trace amounts. Overall, based on this extraction experiment, it can be concluded that there were some carbonaceous species deposited on the recovered catalysts. However, no conclusive difference in the adsorbed species between the two catalysts was observed.

Table S5.3 Type and amount of carbonaceous deposits extracted from the recovered a-MoCNF (Hydrogenation at 140 °C and used for 90 hrs) and b-MoCNF (Hydrogenation at 140 °C and used for 40 hrs).

	Toluene	**Methanol**	**DCM**
a-MoCNF$_{(HCl)}$	Trace amounts of CAL & propylbenzene	Trace amounts of CAL	Trace amounts of CAL
b-MoCNF$_{(ox)}$	Trace amounts of CAL & propylbenzene	-	-

References

(S1) Figueiredo, J. L. Functionalization of porous carbons for catalytic applications. *J Mater Chem A* **2013,** *1* (33), 9351.

(S2) Figueiredo, J. L.; Pereira, M. F. R. The role of surface chemistry in catalysis with carbons. *Catal Today* **2010,** *150* (1-2), 2.

(S3) Figueiredo, J. L.; Pereira, M. F. R.; Freitas, M. M. A.; Orfao, J. J. M. Modification of the surface chemistry of activated carbons. *Carbon* **1999,** *37* (9), 1379.

(S4) Toebes, M. L.; van Heeswijk, E. M. P.; Bitter, J. H.; van Dillen, A. J.; de Jong, K. P. The influence of oxidation on the texture and the number of oxygen-containing surface groups of carbon nanofibers. *Carbon* **2004,** *42* (2), 307.

(S5) Führer, M.; van Haasterecht, T.; Bitter, J. H. Cinnamaldehyde hydrogenation over carbon supported molybdenum and tungsten carbide catalysts. *Chem Commun* **2022**, DOI:10.1039/D2CC05322E 10.1039/D2CC05322E.

6

Chapter 6

Molybdenum and tungsten carbides can shine too

This Chapter is based on: M. Führer, T. van Haasterecht, and H. Bitter. "Molybdenum and tungsten carbides can shine too." Catalysis Science & Technology 10.18 (2020): 6089-6097.

Abstract

In this perspective, we argue that carbides of transition metals such as molybdenum and tungsten hold great potential for the catalytic conversions of future feedstocks due to their ability to remain active in the presence of impurities in the feedstock. The presence of N and S impurities, found in increasing amounts in fossil-based feedstocks and also in new renewable feedstocks (such as biomass) may cause the carbides to convert to their respective nitrides or sulphides. These phases are catalytically active for similar reactions as the carbides and so these impurities would not lead to complete catalyst deactivation as they do for noble metal catalysts. Establishing the full potential of transition metal carbides as catalysts requires studies that use real feedstocks to look into the role of heteroatoms during the processing of fossil and novel feedstocks.

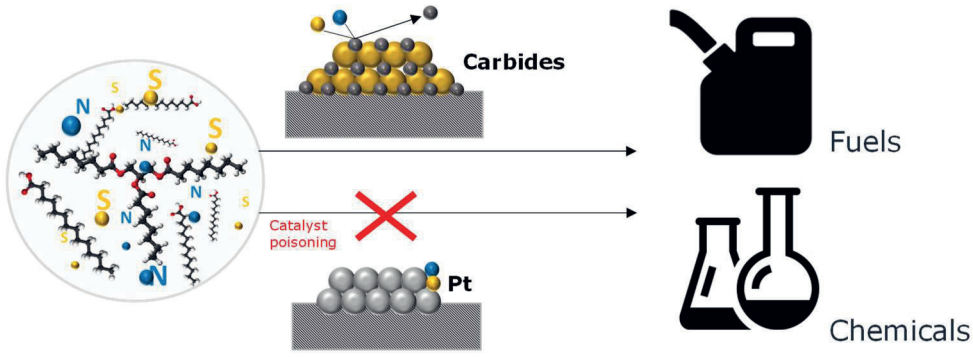

Introduction

Catalyzing chemical conversions to produce chemicals and fuels is becoming more demanding since the used feedstocks are changing. Fossil-based feedstocks are becoming heavier and now contain more impurities with N, S and P compounds[1,2] and new renewable feedstocks such as biomass are emerging. An important class of catalysts used to convert the current feedstocks is based on metals (e.g. Pt, Ni, Co, Fe). Particularly noble metal catalysts are highly active and have been widely studied, but their limited availability is leading to an increasing demand for alternative catalysts and it also makes them expensive. In addition, noble metal catalysts have difficulty dealing with the impurities present in the newer feedstocks; these impurities interact strongly with the metal and cause catalyst deactivation.

Transition metal carbides, such as those of molybdenum and tungsten, are considered viable alternatives to noble metal catalysts.[3,4] This is based on the ground breaking work by Levy and Boudart in 1973 who showed that W carbide and Pt have similarities in electronic structure and catalytic behaviour in the formation of water from H_2 and O_2 at room temperature.[5] Subsequently, these carbides have been shown applicable for a wide variety of catalytic reactions, such as hydrogenation (HYD), hydrodeoxygenation (HDO), hydrodesulphurisation (HDS), hydrodenitrogenation (HDN) and isomerisation.[1,6,7]

In this perspective, we discuss the potential of tungsten and molybdenum carbides as an alternative for noble metal catalysts for use in the conversion of traditional fossil feedstocks, heavier fossil feedstocks and renewable biomass feedstocks. We point out the tolerance of transition metal carbides with respect to N and S impurities and the ability to (partially) convert the carbides to their respective nitrides or sulphides. The availability and catalytic activity of these carbide catalysts have both been mentioned before, but their relative stability in the presence of such impurities barely has. Although carbides can (partially) convert to nitrides and sulphides under the relevant reaction conditions, that does not necessarily lead to a complete loss of catalyst performance, as is the case for noble metals.[4] Thus, taking the compositions of some fossil as well as most new feedstocks into account, Mo and W carbides may become the preferred choice over noble metals.

Need for non-noble metal catalysts

Noble metals (Group 8 in the periodic table) are often used as catalytically active metals because of their good performance (activity/selectivity) and excellent stability.[8] These metals are less

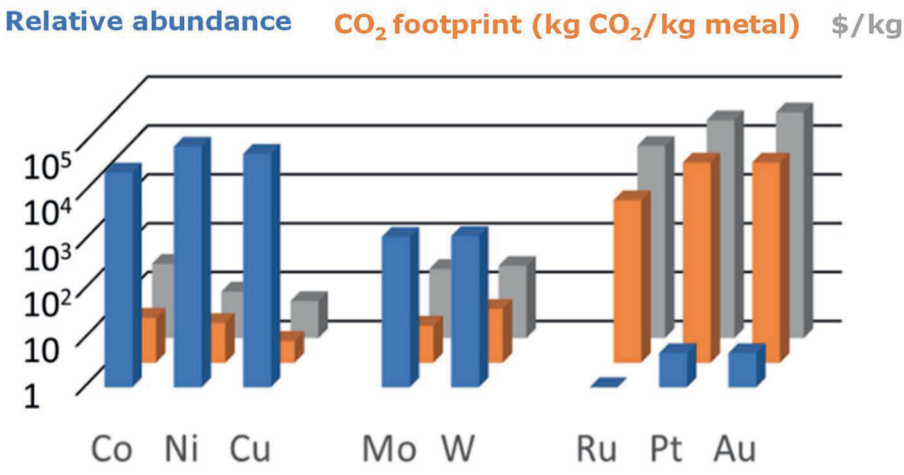

Figure 6.1 Abundance, CO_2 footprint and price of some metals relevant for catalysis.

prone to oxidation and therefore also less prone to leaching (dissolution) than non-noble metals, which is especially relevant for liquid-phase reactions. However, a major drawback of noble metals is their limited availability. Even though spent catalysts can and should be recycled, the expected growth of applications such as in electrolysers and fuel cells will require a vast amount of catalyst material and thus of noble metals.[9-11]

Figure 6.1 shows the abundance in the earth's crust of some relevant metals used in catalysis.[12,13] As expected, each metal's abundance is inversely proportional to its price and its CO_2 footprint, which makes non-noble metals an obvious choice as replacements for noble metals.[14,15] Well known is the use of nickel for reactions for which Pt used to be the preferred catalyst.[16-18] For example, Ni-based catalysts have been applied in the production of renewable hydrogen via aqueous-phase reforming.[18-20] However, the stability of Ni for its use in the aqueous phase is still an issue.[18] Cobalt and copper have also been considered as a replacement for noble metal catalysts. For example, cobalt and copper are highly active in the (steam) reforming of methane, methanol and ethanol.[21]

Based on the abundance of the non-noble metals, iron (not shown in Figure 6.1) is always the preferred choice as it is the most abundant of all metals (5% by weight). However, not all catalytic conversions can be performed with that single element. Therefore, a plethora of catalysts based on different metals is both needed and currently available. Next to an element's abundance on earth, the efforts associated with recovery, processing as well as accessibility are points of

attention. For example, the European Union has published a list of critical raw materials.[22] Their supply is not necessarily limited in terms of (future) abundance, but can also be restricted by their (currently) limited accessibility due to, for example, geopolitical circumstances. Therefore, adopting a general strategy of diversification, i.e. having alternatives for a given metal, is highly recommended. We argue that Mo and W, each having an elemental abundance that lies between that of the non-noble and the noble metals and a price comparable to that of non-noble metals, should be further explored as alternatives for noble metals.

State of the art of tungsten and molybdenum carbides

Mo and W carbides versus noble metal catalysts

Since the 1970s, tungsten and molybdenum carbides have emerged as alternatives for noble metal catalysts.[23,24] From a characterisation point of view[25-27] and from a performance[5,28] point of view, these carbides resemble noble metals (especially Pt). For instance, in 1992, Oyama made a comparison between transition metal carbides and nitrides and noble metals.[3] The crystallographic structure of these nitrides and carbides is determined by geometric and electronic factors. The geometric factor as identified by Hägg[29] determines that simple structures (i.e. fcc, hcp and hex) are formed if the ratio between the atomic radii of the non-metal and the metal is less than 0.59; this is the case for carbides and nitrides of transition metals. The electronic factor finds its basis in the Engel-Brewer theory[30], which states that nitrogen and carbon atoms combine their valence s-p electrons with those of the interstitial sites of the host metal (s-d-p bands of Mo and W). This explains why the catalytic activity of carbides and nitrides resembles that of noble metals.[3,4,31] Mo and W nitrides and carbides have excellent catalytic activities in reactions such as HYN, HDO, isomerisation and methanation. Particularly in HDO reactions, transition metal carbides reach yields close to those of noble metal catalysts. However, the selectivity of these newer catalysts differs from those of the noble metal catalysts.[3] Some carbide catalysts enable unique reaction pathways that result in valuable products (e.g. enhanced HDO and isomerisation selectivity); this leads to the suggestion that carbides and nitrides catalysts can even be more desirable than noble metals.[4] For instance, for the n-hexane reaction (614-630 K, excess H_2), WC was twice as active as W_2C and 0.5 wt% Pt/Al_2O_3 and showed enhanced selectivity for isomerisation products.[3] Further, Stellwagen and Bitter[32] studied the activity and selectivity of W and Mo carbide supported on carbon nanofibers in stearic acid HYD (batch reactor, 350 °C, 30 bar of H_2 pressure). Interestingly, supported W carbides catalysts were selective (>50%) towards highly valued alkenes at the intermediate conversion level, while supported Mo carbides were selective for oxygenates (octadecanol and octadecanal). Both

intermediate products (the alkenes and the oxygenates) are platform chemicals for synthesising a wide range of value-added products[32] and are not normally observed with noble metal catalysts. For example, the conversion of stearic acid over Pd and Pt catalysts yields primarily heptadecane via the decarboxylation pathway.[33]

Challenges and opportunities for Mo and W carbides

Mo and W carbides are versatile and diverse catalysts, yet even after fifty years of research, captured in many reviews on the use of metal carbides in catalysis[4,6,7,34-42], it is still often unclear what the exact nature of the active site in these catalysts is. For example, Sullivan et al.[7] reviewed the role of different synthesis techniques (temperature-programmed reduction and ultra-high vacuum) in the performance and characteristics of metal carbide catalysts, especially supported and unsupported W and Mo carbides. They emphasised that metal carbides undergo changes in their morphology and surface composition during synthesis and/or when used for a reaction under oxidative conditions. The authors stressed the need for in-situ studies[7] to enable preventing the influence of O_2 on the material.

Recently, a number of review papers have described the use of metal carbide-based catalysts to upgrade biobased feedstocks.[6,7,41-43] For example, Chan-Thaw and Villa[6] reviewed both the influence of the synthesis techniques (temperature-programmes reduction, ball milling and carbothermal hydrogen reduction) for unsupported and supported metal carbides and their use in the transformation of biomass to biofuels and fine chemicals. Examples of HYD and HDO of first-generation (vegetable oils) and second-generation (cellulose, hemicellulose and lignin) biomass with molybdenum and tungsten carbide catalysts were given. The carbides exhibit similar catalytic performances as Pt-group metals for HDO, HYD and isomerisation of biomass feedstocks. Although carbides are more resistant towards sulphur and nitride poisoning (see Section 3), the carbide catalysts become deactivated due to coke deposition, leaching and over-reduction. The use of a support, e.g. a porous support (carbon nanotubes or mesoporous carbon), increases the stability of the carbides and leads to better control of the particle size.[6,36]

Pang et al.[40] also reviewed the use of metal carbides (supported and unsupported W & Mo) for biomass conversion and indicated their great potential in HDO of cellulose, lignin and other platform chemical conversions. They emphasised that the use of carbides in biomass conversions needs to be explored more thoroughly and suggested to explore traditional carbides (Re, Ti, V or Zr carbides) further to gain a fundamental understanding regarding structure-performance relationships of Mo and W carbides for biomass conversions.[40] In addition, Pang at al. looked at

issues encountered during carbide synthesis.[40] Obtaining highly dispersed and phase-pure (WC vs W_2C) metal carbides is still challenging. Carbon decomposition during the reaction and the existence of mixed carbide phases (WC or W_2C) hamper the comprehension of the structure-performance correlation of these materials, which again stresses the need for in-situ investigations.[40,44]

To gain more insight into the property-performance relationships of carbides, also quantum mechanical calculations have been applied. For example, Alaba et al.[38] reviewed different Density Functional Theory (DFT) studies on Mo carbide nanoparticles (as a catalyst for hydrogenation and hydrogen production) to identify and categorise the different existing Mo carbide phases. Depending on the preparation method and the carburisation agent, five different crystal structures were characterised: α-MoC_{1-x}, α-Mo_2C, β-Mo_2C, γ-MoC and η-MoC. These structure differences do not only affect the stability of the catalyst but also influence the electrochemical activity. Among the different Mo carbide phases, α-MoC_{1-x} and β-Mo_2C are the most stable and they display remarkable catalytic behaviours in electrochemical catalysis due to their large ionic contribution.[38]

The aforementioned studies and reviews have demonstrated the applicability of transition metal carbides in a wide range of reactions and their potential as a replacement for noble metal catalysts for fossil and biomass feedstocks. However, almost all of these studies also highlighted the need for further (in-situ) investigations to obtain information on structure-performance relationships.

Carbides, nitrides and sulphides in reactions involving H_2 activation/transfer

Carbides are efficient catalysts for reactions involving H_2 activation/transfer, i.e., carbides are able to split hydrogen and transfer the hydrogen atoms to different reactant molecules in a reversible manner. That makes them suitable catalysts for reactions that involve hydrogen activation, such as ammonia synthesis and decomposition, hydrogenation, hydrogenolysis, hydro-isomerisation, methanation and hydroprocessing.[45] The Supplementary Information contains a summary of those thermocatalytic reactions.

It is noteworthy that aside from the transition metal carbides, also nitrides and sulphides have emerged as catalysts with activity for H_2 activation and transfer reactions.[31,46] For example, Monnier et al. tested γ-Al_2O_3-supported molybdenum, tungsten and vanadium nitrides for the HDO of oleic acid and canola oil.[47] The molybdenum nitride showed a superior oleic acid HDO

performance in comparison with the other nitrides; after 20 h of steady state conditions, the Mo nitride yielded a three times higher selectivity for n-alkane than was obtained by V and W nitride. Furthermore, the Mo nitride was operated for 450 h in the continuous operation of canola oil hydrotreatment with only minimal deactivation. Grilc et al.[48] studied the hydrodeoxygenation of liquefied lignocellulosic biomass over unsupported MoS_2, MoO_2, Mo_2C and WS_2. MoS_2 showed the highest hydrogenolysis selectivity as nearly 85% hydroxyl group conversion was reached within 30 min at 300 °C (~30% for MoO_2, ~40% for Mo_2C, ~60% for WS).[48] This shows that Mo and W nitrides and sulphides can be active for the same type of reactions as their respective carbides.

Potential of Mo and W carbide catalysts for use with S- and N-containing feedstock

Clearly, Mo and W carbides (as well as nitrides and sulphides) are versatile catalysts and potential replacements for noble metal catalysts even though the exact working mechanism and the nature of the active site of the carbide catalyst are not always known. However, with respect to stability, more research efforts are required.

Often, four pathways are defined for catalyst deactivation i.e., 1) blocking of the active site (e.g. coke deposition), 2) crystallite growth, 3) leaching and 4) oxidation. These pathways have also been reviewed for metal carbides in liquid phase reactions by our group.[36] For Mo and W carbides, minor changes in the atmosphere of the catalyst can already result in different catalytic behaviours. A prime example is the exposure to air which can change the surface of the carbide through the formation of oxy-carbides and oxides.[39,49,50].

S and N impurities in novel feedstocks

Sulphur and nitrogen compounds are present in fossil feedstocks such as crude oil and coal. The exact amounts of sulphur and nitrogen in crude oil and coal depend on origin and type. For example, Furimsky et al.[51] stated that conventional crude oil contains 1.8 wt% sulphur and 0.1 wt% nitrogen, whereas the sulphur content of coal samples lies between 0.1 and 10 wt% depending on the source of the coal, while the nitrogen content ranging from 0.5 to 1.5 wt% (see Table S6.1 Supplemental Information).[52-54] Traditional catalysts based on noble metals cannot cope well with these heteroatoms. Catalysts based on metals like Fe, Pt, Ru, Ni and Co as used in (de)hydrogenation, (steam) reforming and ammonia and Fischer-Tropsch (FT) synthesis are poisoned by H_2S and NH_3.[55] The removal of such harmful impurities from the feedstock is therefore essential to maintain catalyst activity and selectivity. In current refineries, (reduced)

metal catalysts are protected by upstream hydrotreating steps, i.e. hydrodesulphurisation (HDS) and hydrodenitrogenation (HDN).[56-58]

Significant amounts of sulphur/sulphide (S) and ammonia (N) can also be present in biomass-derived feedstocks before and after processing (gasification, pyrolysis, digestion). According to Robinson et al., the sulphur content ranges from ~14 to 2200 ppm depending on the biomass source and the season.[59,60] Even pure vegetable oils still contain ~10 ppmw of sulphur.[61]

Converting biomass or a fossil resource to syngas (H_2/CO) followed by conversion of the syngas to the desired products (alcohols, alkenes, alkanes) via FT synthesis is gaining interest. When using syngas obtained from biomass, additional gas cleaning steps should be implemented to protect the FT catalyst (based on Fe or Co) against poisoning with S. This issue is exemplified by the increased interest in the fermentation of syngas[62] as an alternative to metal-based conversions.

Mo and W carbide catalysts could be employed as alternatives for reduced metal catalysts in the upgrading of many of the biomass-derived sources (either syngas or other more complex molecules). The use of Mo_2C in gas-to-liquid (GTL) processes has already been established for the synthesis of MeOH,[63] higher alcohols[64] and FT of fuel/diesel/hydrocarbons[65,66] from pure syngas sources. The use of Mo and W carbides in the decarboxylation and hydrodeoxygenation of vegetable oils is another example.[67] Both the hydrogenation of pyrolysis oil[68] and reforming of methane[69-73] with Mo_2C and W_2C have been demonstrated. To evaluate the true potential of Mo and W carbides, the effect of the S and N content in these feed sources needs to be taken into account.

Stability and activity of carbides, nitrides and sulphides

For reduced metal catalysts, the formation of a strong metal-S bond inevitably results in surface sulphidation and consequently in deactivation.[74] Especially noble metals, such as platinum and palladium, suffer from deactivation in the presence of sulphur compounds.[75] During simultaneous HDS, HDO and HYD (450 °C, 200 ppm O_2, 5 wt% cumene, 95% tetradecane), a Pt catalyst supported on alumina deactivated immediately upon addition of sulphur.[56]

Also the effect of nitrogen compounds on noble metal catalysts has been studied. Augusto et al. showed that Pt or Pd supported on zeolite Y catalysts used for tetralin HYD was deactivated by quinoline (499 ppm) as well as by dibenzothiophene (100 ppm).[76] Similarly, the catalytic activity of Rh-based catalysts is strongly inhibited by sulphur compounds during methane oxidation or

steam reforming.[77] Already after addition of 1 ppmv of SO_2 or H_2S, the catalytic activity of Rh/γ-Al_2O_3 during the methane/steam reforming can become significantly decreased; after adding 10 ppmw, the catalytic activity decreases to zero.[77] Transition metals such as Co and Ni are also prone to deactivation by sulphur poisoning. As an example, a drop in methanation activity of more than 3 orders of magnitude can occur for Co, Ni and Ru in the presence of only 15 ppb of H_2S.[78]

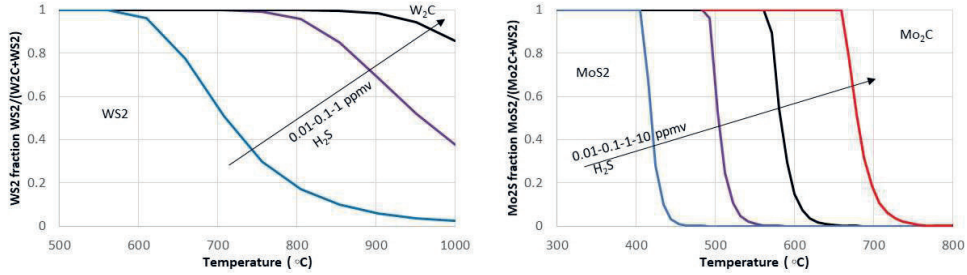

Figure 6.2 The stability regions for Mo and W sulphides and carbides as the fraction of sulphide versus temperature for WS_2-W_2C (left) and MoS_2-Mo_2C (right) in the presence of 0.01-10 ppm of H_2S in H_2 calculated with the HSC Chemistry software (metallic species omitted).

For Mo and W carbides, their response to S and N impurities also needs to be considered. The presence of S or N in the feedstock can result in the transformation of carbide to a nitride and sulphide under relevant reaction conditions. Figure 6.2 shows that the transition of MoS_2 to Mo_2C occurs in a temperature range of 400 to 700 °C in the presence of 0.01 to 10 ppm H_2S, while the stability of WS_2 already is affected at 600 °C at only 0.01 ppm. In general, equilibrium calculations using the HSC Chemistry package show that, thermodynamically, W_2C is unstable in the presence of both S (as H_2S) as well as N (as NH_3) and strongly favours the formation of W sulphides and nitrides. Mo_2C is only resistant to sulphur at very high temperatures and low sulphur concentrations (e.g. above 650 °C at 1 ppm H_2S). Thus, the conversion of carbides to sulphides or nitrides is thermodynamically possible at conditions relevant for crude oil processing and biomass upgrading (with the exception of high-temperature steam reforming). It should be noted that the thermodynamic calculations are valid for the bulk phase and that the results will be different for more reactive (supported) nanoparticles. The rate at which a favourable transformation occurs also depends on other factors besides bulk versus supported catalyst, e.g., support type and particle size. Furthermore, partial transformations might occur, e.g., surface sulphidation might result in a passivation layer, serving as a diffusion barrier that prevents or slows down the sulphidation of the whole particle.[79]

Transformation from carbide to sulphide or nitride might, therefore, occur during processing of heavy oil-based feedstocks (which contain more sulphur)[80-82] or biomass (which contains N and S in the feed). Interestingly, the (partial) conversion of Mo or W carbides to sulphides or nitrides should not necessarily result in deactivation because also the nitrides and sulphides are active for reactions involving hydrogen transfer (hydrogenation/dehydrogenation), as we already mentioned.[56,83-86]

This is further illustrated by the fact that prime examples of Mo catalysts are hydrotreating catalysts (CoMo- and NiMo-based), which are active in the sulphide state. That the relevant reactions are hydrogenation reactions shows that Mo sulphides could also play a role in the catalysis of other (de)hydrogenation reactions. For instance, the Mo sulphides traditionally used for hydrotreating reactions ($NiMoS_2$, $CoMoS_2$) are also active for HDO reactions of fatty acids and bio oils.[87] In addition, there are examples of the use of W_2C[58] and especially Mo_2C[88-92] in HDS (see Table S6.2 in the Supplemental Information). In addition, Mo and W nitrides are active for HDO, HDN and HDS reactions and in some cases (CoMo and NiMo) are even superior to the sulphide catalysts.[93] Although Mo_2C carbides display greater activity in HDS reactions than MoS_x, the difference in activity can either be explained by the change in the number of active sites on the catalyst surface or is due to the difference in intrinsic chemical activity.[79] However, this clearly shows that for Mo- and W-based catalysts, sulphur is not a poison, although it is for noble metal catalysts. For both the Mo carbide and the Mo nitride catalysts, their activity is retained when the surface becomes sulphated during HDS of thiophene at 400 °C.[94]

Considering the above, one might expect that Mo and W carbide and/or sulphide catalysts are a good choice for other hydrogen transfer reactions in which S or N impurities are expected. However, this potential advantage appears to have been overlooked so far since not many studies have focused on the effect of impurities. Therefore, for reactions other than HDS, only limited experimental information is available on the actual performance of Mo and W carbides in the presence of real feedstocks containing S and N. Already in 2002, Furimsky et al. mentioned that experimental information on hydrogen adsorption in the presence of H_2S or by partially sulphided carbides and nitrites was lacking.[1]

Table 6.1 Overview of use of Mo_2C and WC in the presence of S

Reaction	T/p	S-source	Performance/remarks	Ref
Steam reforming, oxidative-stream reforming of tri-methyl pentane	1000 °C 1 bar	≤ 1000 ppm thiophene	- Activity remains up to 100 ppm - Higher concentrations of S result in surface oxidation and coke formation	[95]
CO_2/CH_4 reforming	1050 °C 1 bar	250-500 ppm dimethyl sulphide	- Mo_2C deactivates at 800 °C due to reversible CS_2 chemisorption - Rh is S-tolerant under these conditions	[73]
Steam reforming of methanol	185-240 °C 1 bar	5 ppm H_2S	- S decreases the activity but the catalyst does not become fully deactivate - Deactivation is reversible	[63]
Hydrogenation of cumene	250 °C 51 bar	30-100 ppm S (thiophene, (di-)benzo-thiophene)	- With 30-60 ppm S, Mo_2C is superior to noble metals - At 100 ppm, Mo_2C deactivates - S present as surface sulphide	[56]
Aqueous phase hydrogenation of furfural	120-150 °C 120 bar	380 ppm thiophene	- Similar activity in presence and absence of S	[80]
Steam reforming of hexadecane	965 °C, 1 bar	125-500 ppm benzo-thiophene	- Deactivation dependent on sulphur concentration - Deactivation minimal at S concentration below 100 ppm	[96]
Water gas shift reaction	200- 240 °C, 1bar	without and with 5 ppm H_2S	- MoS_2 sites active in the presence of sulphur - Mo_2C catalyst quickly poisoned by sulphur, but partly regenerated	[60]
Partial oxidation of methane to syngas	750 °C, 8 bar	0.1% of H_2S	- High S concentration leads to carbon deposition and sulphidation of the catalyst (catalyst deactivation) - At lower S concentration (<0.1 %), no change in catalyst phase, but carbon acceleration on the reactor wall	[97]
Tetralin hydrogenation	300 °C, 40 bar	200 ppm H_2S (dimethyl-sulphide)	- Decease in tetralin conversion upon adding H_2S - Minimal deactivation of supported Mo_2C and WC - Near-complete deactivation of Pt/Al_2O_3	[98]

A few studies have been conducted with bulk Mo_2C and the addition of S compounds to the feed; Table 6.1 summarises them. Two of these studies (steam reforming at 1000 °C[71] and dry methane reforming at 1050 °C[73,95]) used conditions in which, according to Figure 6.2, sulphide formation

is not expected. Indeed, the authors reported no MoS_2 formation for increased temperatures and the activity of the catalyst remained intact at high sulphur concentrations. On the other hand, the introduction of sulphur during steam reforming of MeOH resulted in an immediate but limited decrease in activity (of about 30%) and the formation of surface sulphur was detected with XPS.[63] Also in the liquid phase HYD of furfural, trace amounts of S were found with XPS while the catalytic activity remained. In the hydrogenation of cumene, the formation of a surface carbosulphide phase was identified with XPS, while XRD showed that the bulk Mo_2C was unaffected[56], revealing that only surface modification had occurred.

Thompson et al. investigated the effect of sulphur on Mo_2C and Pt/Mo_2C during the water-gas-shift reaction.[60] Both catalysts became deactivated by exposing them to H_2S but the Mo_2C became only partially deactivated due to the formation of a still active MoS_2 phase, while the Pt/Mo_2C catalyst showed irreversible deactivation of the platinum. We found only one study that included Mo and W carbides as supported catalysts.[98] In this work, da Costa et al. compared the effect of H_2S on Mo_2C and WC supported on Al_2O_3. The carbide activity was tested and compared in the presence and absence of 200 ppm H_2S during tetralin HYD (300 °C, 4 MPa). In the absence of sulphur, the supported Mo_2C and WC reached a yield of 6.5 mol% and 8 mol%, respectively. In the presence of sulphur, the conversion was slightly lower (4.5 mol% for Mo_2C/Al_2O_3; 6 mol% for WC/Al_2O_3), but there was no complete deactivation of the carbide catalysts.[98]

While these studies concern very different reactions and conditions, they show that the carbides are able to tolerate sulphur in the feedstock. For the further development of stable carbide-based catalysts, it is essential to explore the mode of interaction of the N/S compound with the catalyst first. The partial transformation of a carbide to a sulphide or nitride might have a limited influence on catalytic performance as argued before; however, blocking of the active sites by a nitrogen/sulphur compound may still lead to deactivation. Therefore, a fundamental understanding of the interaction between the carbides surfaces and the sulphur/nitrogen-containing molecules is needed to understand the catalytic performance of these materials.[4,99]

A few articles have been published regarding the behaviour of Mo carbide towards sulphide adsorption/desorption.[79] For instance, Rodriguez et al. used photoemission and XANES to establish the chemistry of SO_2, H_2S, and CH_3SH on Mo carbide (and metallic Mo). The adsorption of SO_2 on Mo_2C at around - 123 to 26 °C first led to the formation of SO_3 and SO_4 and, with increasing temperatures, to the formation of sulphided and oxidised carbides. The interaction between H_2S and the Mo carbides was strong and led to substantial sulphidation, even at low

temperatures. For the CH_2S, the methyl group dissociated with increasing temperature while CH_yS species coexisted on the carbide surface. However, the carbide was not modified by the sulphide. This shows that molybdenum carbides are either tolerant towards sulphur-containing molecules or form a still active MoS_x phase, depending on the molecule in question and the temperature. Thus, the adsorption/desorption behaviour of carbide material depends on the sulphur compound and conditions (e.g. temperature).

Limited research has been conducted towards the effect of sulphur on bulk tungsten carbide.[100-102] In 1981, Ko et al. published a study on the effect of oxygen and surface on the bonding and reactivity of carbon monoxide, hydrogen, formaldehyde, and methanol on tungsten and tungsten carbide surfaces. They found that the W(100)-(5x1)C surface rapidly adsorbed H_2S which led to site competition with CO. The surface reactivity for formaldehyde and methanol decreased significantly after the sulphur treatment; however, it was still more active than metallic tungsten.[100] Schulz-Ekloff and co-workers (1975) showed that in the presence of 25 $\mu g/m^2$ H_2S, the ammonia yield was reduced by 50%. After adding 50 $\mu g/m^2$ H_2S, the complete inhibition of the tungsten carbide occurred.[101]

In summary, based on thermodynamic arguments carbide catalysts might change the nature of their active site when used in the presence of S and N impurities during the processing of crude oil or renewable feedstock. However, they can remain catalytically active since the sulfide and nitride phases also possess activity for the same type of reactions. This distinguishes them from noble metal catalysts which quickly deactivate in the presence of sulfur or nitrogen containing compounds. The limited direct evidence available from experiments appears to support this view. Under which conditions the different types of carbides remain (partially) active and how the impurities interact with the carbides needs further investigation to define an operational window of the carbides.

Outlook

Future feedstock for chemicals and fuels, whether fossil or renewable in nature, will put new demands on the robustness of catalysts used in their processing. Tungsten and molybdenum carbides hold great potential for catalytic applications as replacements for noble metals. Both W and Mo have higher abundance and as a result lower cost compared to their noble metal counterparts. However, it has previously been stressed in a number of reviews that more detailed investigations into the nature of the active sites of these materials is still required.[7, 40, 43]

It is our view that W and Mo carbides possess advantages beyond their availability and lower cost which should be the focus of further research to advance the field of W and Mo carbide catalysis and move towards industrial applications. We, therefore, stress that there is the need to study and gain more insight into the role of heteroatoms in the performance of carbide catalysts. We have argued that Mo and W carbide and/or sulphide catalysts can become the preferred choice for a wide range of hydrogen transfer reactions relevant to the upgrading of both novel crude oil and renewable feedstock in which S or N impurities are present. This is because Mo and W carbides are either less susceptible to poisoning by these S containing compound compared to noble metals or can be converted into their still active sulfide/nitride phases. Although not many studies have focused on the effect of impurities, the limited experimental evidence available for mainly bulk molybdenum carbide in the presence of thiols/thioesthers supports this view.

Therefore, we propose that more studies are needed that focus on realistic feedstocks to show the true potential of these catalysts under real conditions, especially considering the effect that impurities like N and S in real feedstocks may have on the nature of the active site and the stability of these catalysts.

Secondly, more fundamental studies are still needed to understand the interaction of different S and N compounds, e.g. sulphide versus sulphate species, with the various types of Mo and W carbide catalysts. For this also the use of in-situ surface sensitive spectroscopic techniques would be required, understandably involving controlled conditions and the use of model compounds and feedstocks. In addition, theoretical calculations can provide us with a broader insight into adsorption of sulphur and sulfidation of Mo and W carbide catalysts in relation to their structural and electronic properties.

We propose these as the next avenues to explore. In any case, the potential for Mo and W carbides as supported catalysts is evident. It is not only noble metals that shine.

Acknowledgements

The authors would like to thank the Dutch Research Council (NWO) for its financial support.

References

(1) Furimsky, E. Metal carbides and nitrides as potential catalysts for hydroprocessing. *Applied Catalysis A: General* **2003,** *240* (1–2), 1.

(2) Breysse, M.; Djega-Mariadassou, G.; Pessayre, S.; Geantet, C.; Vrinat, M.; Pérot, G.; Lemaire, M. Deep desulfurization: reactions, catalysts and technological challenges. *Catal Today* **2003,** *84* (3), 129.

(3) Oyama, S. Preparation and catalytic properties of transition metal carbides and nitrides. *Catal Today* **1992,** *15* (2), 179.

(4) Chen, J. G. Carbide and nitride overlayers on early transition metal surfaces: preparation, characterization, and reactivities. *Chemical reviews* **1996,** *96* (4), 1477.

(5) Levy, R. B.; Boudart, M. Platinum-Like Behavior of Tungsten Carbide in Surface Catalysis. *Science* **1973,** *181* (4099), 547.

(6) Chan-Thaw, C. E.; Villa, A. Metal carbides for biomass valorization. *Applied Sciences (Switzerland)* **2018,** *8* (2).

(7) Sullivan, M. M.; Chen, C. J.; Bhan, A. Catalytic deoxygenation on transition metal carbide catalysts. *Catalysis Science and Technology* **2016,** *6* (3), 602.

(8) Ertl, G.; Knözinger, H.; Weitkamp, J. Handbook of heterogeneous catalysis. *Weinheim: VCH* **1997,** *2*, 427.

(9) Gasteiger, H. A.; Kocha, S. S.; Sompalli, B.; Wagner, F. T. Activity benchmarks and requirements for Pt, Pt-alloy, and non-Pt oxygen reduction catalysts for PEMFCs. *Applied Catalysis B: Environmental* **2005,** *56* (1-2), 9.

(10) Morales-Guio, C. G.; Stern, L.-A.; Hu, X. Nanostructured hydrotreating catalysts for electrochemical hydrogen evolution. *Chemical Society Reviews* **2014,** *43* (18), 6555.

(11) Guil-Lopez, R.; Martinez-Huerta, M. V.; Guillen-Villafuerte, O.; Pena, M. A.; Fierro, J. L. G.; Pastor, E. Highly dispersed molybdenum carbide as non-noble electrocatalyst for PEM fuel cells: Performance for CO electrooxidation. *Int. J. Hydrog. Energy* **2010,** *35* (15), 7881.

(12) Nuss, P.; Eckelman, M. J. Life cycle assessment of metals: a scientific synthesis. *PLoS One* **2014,** *9* (7), e101298.

(13) Lide, D. R. *CRC handbook of chemistry and physics*; CRC press, 2004.

(14) Harrison, P. G.; Lloyd, N. C.; Azelee, W. Non-noble metal environmental catalysts: Synthesis, characterization and catalytic activity. *Studies in Surface Science and Catalysis* **1995,** *96*, 487.

(15) Shi-Yao, L.; Bei-Lu, L. Study on non-noble metal catalysts for automotive emission control. *Reaction Kinetics and Catalysis Letters* **1996,** *57* (1), 183.

(16) Shabaker, J.; Huber, G.; Dumesic, J. Aqueous-phase reforming of oxygenated hydrocarbons over Sn-modified Ni catalysts. *Journal of Catalysis* **2004,** *222* (1), 180.

(17) van Haasterecht, T.; Swart, M.; de Jong, K. P.; Bitter, J. H. Effect of initial nickel particle size on stability of nickel catalysts for aqueous phase reforming. *Journal of Energy Chemistry* **2016,** *25* (2), 289.

(18) Van Haasterecht, T.; Ludding, C.; De Jong, K.; Bitter, J. Toward stable nickel catalysts for aqueous phase reforming of biomass-derived feedstock under reducing and alkaline conditions. *Journal of Catalysis* **2014,** *319*, 27.

(19) Shabaker, J. W.; Huber, G. W.; Dumesic, J. A. Aqueous-phase reforming of oxygenated hydrocarbons over Sn-modified Ni catalysts. *Journal of Catalysis* **2004,** *222* (1), 180.

(20) Shabaker, J. W.; Simonetti, D. A.; Cortright, R. D.; Dumesic, J. A. Sn-modified Ni catalysts for aqueous-phase reforming: Characterization and deactivation studies. *Journal of Catalysis* **2005,** *231* (1), 67.

(21) van Haasterecht, T.; Ludding, C. C. I.; de Jong, K. P.; Bitter, J. H. Stability and activity of carbon nanofiber-supported catalysts in the aqueous phase reforming of ethylene glycol. *Journal of Energy Chemistry* **2013,** *22* (2), 257.

(22) EU Commission - Deloitte Sustainability, B. G. S., Bureau de Recherches Géologiques et Minières, Netherlands Organisation for Applied Scientific Research. Study on the review of the list of Critical Raw Materials. **2017**.

(23) Leclercq, L.; Imura, K.; Yoshida, S.; Barbee, T.; Boudart, M. Synthesis of new catalytic materials: Metal carbides of the group VI B elements. *Studies in Surface Science and Catalysis* **1979,** *3*, 627.

(24) Volpe, L.; Boudart, M. Compounds of molybdenum and tungsten with high specific surface area: II. Carbides. *Journal of Solid State Chemistry* **1985,** *59* (3), 348.

(25) Bennett, L. H.; Cuthill, J. R.; Mcalister, A. J.; Erickson, N. E.; Watson, R. E. Electronic-Structure and Catalytic Behavior of Tungsten Carbide. *Science* **1974,** *184* (4136), 563.

(26) Wu, W.; Wu, Z.; Liang, C.; Chen, X.; Ying, P.; Li, C. In situ FT-IR spectroscopic studies of CO adsorption on fresh Mo2C/Al2O3 catalyst. *J Phys Chem B* **2003,** *107* (29), 7088.

(27) Ingham, B.; Brady, C. D. A.; Burnstein, G. T.; Ryan, M. P. EXAFS Analysis of Electrocatalytic WC Materials. *J. Phys. Chem.* **2009,** *113* (40), 17407.

(28) Scanlon, M. D.; Bian, X.; Vrubel, H.; Amstutz, V.; Schenk, K.; Hu, X.; Liu, B.; Girault, H. H. Low-cost industrially available molybdenum boride and carbide as "platinum-like" catalysts for the hydrogen evolution reaction in biphasic liquid systems. *Physical Chemistry Chemical Physics* **2013,** *15* (8), 2847.

(29) Hägg, G. Gesetzmässigkeiten im kristallbau bei hydriden, boriden, carbiden und nitriden der übergangselemente. *Z. Phys. Chem. B* **1931,** *12*, 33.

(30) Hume-Rothery, W. The Engel-Brewer theories of metals and alloys. *Progress in Materials Science* **1968,** *13*, 229.

(31) Hargreaves, J. Heterogeneous catalysis with metal nitrides. *Coordination Chemistry Reviews* **2013,** *257* (13-14), 2015.

(32) Stellwagen, D. R.; Bitter, J. H. Structure–performance relations of molybdenum-and tungsten carbide catalysts for deoxygenation. *Green Chemistry* **2015,** *17* (1), 582.

(33) Snåre, M.; Kubic˘kova, I.; Mäki-Arvela, P.; Eränen, K.; Murzin, D. Y. Heterogeneous catalytic deoxygenation of stearic acid for production of biodiesel. *Ind Eng Chem Res* **2006,** *45* (16), 5708.
(34) Stottlemyer, A. L.; Kelly, T. G.; Meng, Q. H.; Chen, J. G. G. Reactions of oxygen-containing molecules on transition metal carbides: Surface science insight into potential applications in catalysis and electrocatalysis. *Surface Science Reports* **2012,** *67* (9-10), 201.
(35) Lam, E.; Luong, J. H. Carbon materials as catalyst supports and catalysts in the transformation of biomass to fuels and chemicals. *ACS catalysis* **2014,** *4* (10), 3393.
(36) Macedo, L. S.; Stellwagen, D. R.; da Silva, V. T.; Bitter, J. H. Stability of Transition-metal Carbides in Liquid Phase Reactions Relevant for Biomass-Based Conversion. *Chemcatchem* **2015,** *7* (18), 2816.
(37) Urzhuntsev, G. A.; Kodenev, E. G.; Echevskii, G. V. Prospects for Using Mo- and W-Containing Catalysts in Hydroisomerization: A Patent Review. II: Catalysts Based on Molybdenum and Tungsten Carbides. *Catalysis in Industry* **2016,** *8* (3), 224.
(38) Alaba, P. A.; Abbas, A.; Huang, J.; Daud, W. M. A. W. Molybdenum carbide nanoparticle: Understanding the surface properties and reaction mechanism for energy production towards a sustainable future. *Renewable and Sustainable Energy Reviews* **2018,** *91*, 287.
(39) Iglesia, E.; Ribeiro, F. H.; Boudart, M.; Baumgartner, J. E. Synthesis, Characterization, and Catalytic Properties of Clean and Oxygen-Modified Tungsten Carbides. *Catal Today* **1992,** *15* (2), 307.
(40) Pang, J.; Sun, J.; Zheng, M.; Li, H.; Wang, Y.; Zhang, T. Transition metal carbide catalysts for biomass conversion: A review. *Applied Catalysis B: Environmental* **2019,** *254*, 510.
(41) Lin, Z.; Wan, W.; Yao, S.; Chen, J. G. Cobalt-modified molybdenum carbide as a selective catalyst for hydrodeoxygenation of furfural. *Applied Catalysis B: Environmental* **2018,** *233*, 160.
(42) Robinson, A. M.; Hensley, J. E.; Medlin, J. W. Bifunctional Catalysts for Upgrading of Biomass-Derived Oxygenates: A Review. *Acs Catalysis* **2016,** *6* (8), 5026.
(43) Smith, K. J. Metal carbides, phosphides, and nitrides for biomass conversion. *Current Opinion in Green and Sustainable Chemistry* **2020,** *22*, 47.
(44) Fang, H.; Roldan, A.; Tian, C.; Zheng, Y.; Duan, X.; Chen, K.; Ye, L.; Leoni, S.; Yuan, Y. Structural tuning and catalysis of tungsten carbides for the regioselective cleavage of CO bonds. *Journal of Catalysis* **2019,** *369*, 283.
(45) Oyama, S. T. Crystal structure and chemical reactivity of transition metal carbides and nitrides. *Journal of solid state chemistry* **1992,** *96* (2), 442.
(46) Dongil, A. B. Recent Progress on Transition Metal Nitrides Nanoparticles as Heterogeneous Catalysts. *Nanomaterials-Basel* **2019,** *9* (8).
(47) Monnier, J.; Sulimma, H.; Dalai, A.; Caravaggio, G. Hydrodeoxygenation of oleic acid and canola oil over alumina-supported metal nitrides. *Appl Catal a-Gen* **2010,** *382* (2), 176.
(48) Grilc, M.; Veryasov, G.; Likozar, B.; Jesih, A.; Levec, J. Hydrodeoxygenation of solvolysed lignocellulosic biomass by unsupported MoS2, MoO2, Mo2C and WS2 catalysts. *Applied Catalysis B: Environmental* **2015,** *163*, 467.
(49) Kumar, A.; Bhan, A. Oxygen content as a variable to control product selectivity in hydrodeoxygenation reactions on molybdenum carbide catalysts. *Chemical Engineering Science* **2019,** *197*, 371.
(50) Sullivan, M. M.; Held, J. T.; Bhan, A. Structure and site evolution of molybdenum carbide catalysts upon exposure to oxygen. *Journal of Catalysis* **2015,** *326*, 82.
(51) Furimsky, E. Catalytic hydrodeoxygenation. *Applied Catalysis A: General* **2000,** *199* (2), 147.
(52) Grzybek, T.; Pietrzak, R.; Wachowska, H. X-ray photoelectron spectroscopy study of oxidized coals with different sulphur content. *Fuel Processing Technology* **2002,** *77*, 1.
(53) Hou, J.; Ma, Y.; Li, S.; Shi, J.; He, L.; Li, J. Transformation of sulfur and nitrogen during Shenmu coal pyrolysis. *Fuel* **2018,** *231*, 134.
(54) Wang, Z.; Li, Q.; Lin, Z.; Whiddon, R.; Qiu, K.; Kuang, M.; Cen, K. Transformation of nitrogen and sulphur impurities during hydrothermal upgrading of low quality coals. *Fuel* **2016,** *164*, 254.
(55) Argyle, M.; Bartholomew, C. Heterogeneous catalyst deactivation and regeneration: a review. *Catalysts* **2015,** *5* (1), 145.
(56) Dhandapani, B.; Clair, T. S.; Oyama, S. Simultaneous hydrodesulfurization, hydrodeoxygenation, and hydrogenation with molybdenum carbide. *Applied Catalysis A: General* **1998,** *168* (2), 219.
(57) Zhang, Y.-J.; Xin, Q.; Rodriguez-Ramos, I.; Guerrero-Ruiz, A. Simultaneous hydrodesulfurization of thiophene and hydrogenation of cyclohexene over dimolybdenum nitride catalysts. *Applied Catalysis A: General* **1999,** *180* (1), 237.
(58) Pawelec, B.; Mariscal, R.; Fierro, J. L. G.; Greenwood, A.; Vasudevan, P. T. Carbon-supported tungsten and nickel catalysts for hydrodesulfurization and hydrogenation reactions. *Appl Catal a-Gen* **2001,** *206* (2), 295.
(59) Robinson, J. M.; Barrett, S. R.; Nhoy, K.; Pandey, R. K.; Phillips, J.; Ramirez, O. M.; Rodriguez, R. I. Energy Dispersive X-ray Fluorescence Analysis of Sulfur in Biomass. *Energy & Fuels* **2009,** *23* (4), 2235.
(60) Schaidle, J. A.; Lausche, A. C.; Thompson, L. T. Effects of sulfur on Mo2C and Pt/Mo2C catalysts: Water gas shift reaction. *Journal of Catalysis* **2010,** *272* (2), 235.
(61) He, B.; Van Gerpen, J.; Thompson, J. Sulfur content in selected oils and fats and their corresponding methyl esters. *Applied engineering in agriculture* **2009,** *25* (2), 223.
(62) Daniell, J.; Köpke, M.; Simpson, S. Commercial biomass syngas fermentation. *Energies* **2012,** *5* (12), 5372.
(63) Lausche, A. C.; Schaidle, J. A.; Thompson, L. T. Understanding the effects of sulfur on Mo2C and Pt/Mo2C catalysts: Methanol steam reforming. *Applied Catalysis A: General* **2011,** *401* (1-2), 29.

(64) Wu, Q.; Christensen, J. M.; Chiarello, G. L.; Duchstein, L. D. L.; Wagner, J. B.; Temel, B.; Grunwaldt, J. D.; Jensen, A. D. Supported molybdenum carbide for higher alcohol synthesis from syngas. *Catal Today* **2013,** *215*, 162.
(65) Vo, D. V. N.; Adesina, A. A. Kinetics of the carbothermal synthesis of Mo carbide catalyst supported on various semiconductor oxides. *Fuel Processing Technology* **2011,** *92* (6), 1249.
(66) Schaidle, J. A.; Thompson, L. T. Fischer-Tropsch synthesis over early transition metal carbides and nitrides: CO activation and chain growth. *Journal of Catalysis* **2015,** *329*, 325.
(67) Gosselink, R. W.; Hollak, S. A. W.; Chang, S. W.; Van Haveren, J.; De Jong, K. P.; Bitter, J. H.; Van Es, D. S. Reaction pathways for the deoxygenation of vegetable oils and related model compounds. *ChemSusChem* **2013,** *6* (9), 1576.
(68) Li, W.; Zhao, Z.; Ren, P.; Wang, G. Effect of molybdenum carbide concentration on the Ni/ZrO<inf>2</inf>catalysts for steam-CO<inf>2</inf>bi-reforming of methane. *RSC Advances* **2015,** *5* (122), 100865.
(69) Brungs, A. J.; York, A. P. E.; Claridge, J. B.; Márquez-Alvarez, C.; Green, M. L. H. Dry reforming of methane to synthesis gas over supported molybdenum carbide catalysts. *Catalysis Letters* **2000,** *70* (3-4), 117.
(70) Huang, J.; Huang, T.; Liu, L.; Huang, W.; Ma, R. Mo2C/SBA-15 Modified by Ni for the Dry Reforming of Methane. *Energy Sources, Part A: Recovery, Utilization and Environmental Effects* **2011,** *33* (24), 2249.
(71) Gao, H.; Yao, Z.; Shi, Y.; Jia, R.; Liang, F.; Sun, Y.; Mao, W.; Wang, H. Simple and large-scale synthesis of β-phase molybdenum carbides as highly stable catalysts for dry reforming of methane. *Inorganic Chemistry Frontiers* **2018,** *5* (1), 90.
(72) York, A. P. E.; Claridge, J. B.; Márquez-Alvarez, C.; Brungs, A. J.; Tsang, S. C.; Green, M. L. H. Synthesis of early transition metal carbides and their application for the reforming of methane to synthesis gas. *Studies in Surface Science and Catalysis* **1997,** *110*, 711.
(73) Pritchard, M. L.; McCauley, R. L.; Gallaher, B. N.; Thomson, W. J. The effects of sulfur and oxygen on the catalytic activity of molybdenum carbide during dry methane reforming. *Applied Catalysis A: General* **2004,** *275* (1-2), 213.
(74) Dunleavy, J. Sulfur as a catalyst poison. *Platinum Metals Review* **2006,** *50* (2), 110.
(75) Satterfield, C. N. *Heterogeneous catalysis in industrial practice. 2nd edition*, 1991.
(76) Augusto, C. C. C.; Zotin, J. L.; da Costa Faro, A. Effect of sulfur or nitrogen poisoning on the activity and selectivity of Y-zeolite-supported Pt–Pd catalysts in the hydrogenation of tetralin. *Catalysis letters* **2001,** *75* (1-2), 37.
(77) Mancino, G.; Cimino, S.; Lisi, L. Sulphur poisoning of alumina supported Rh catalyst during dry reforming of methane. *Catal Today* **2016,** *277*, 126.
(78) RIBEIRO∗, F. H.; SCHACH VON WITTENAU, A. E.; BARTHOLOMEW, C. H.; SOMORJAI, G. A. Reproducibility of turnover rates in heterogeneous metal catalysis: compilation of data and guidelines for data analysis. *Catalysis Reviews* **1997,** *39* (1-2), 49.
(79) Rodriguez, J. A.; Dvorak, J.; Jirsak, T. Chemistry of SO2, H2S, and CH3SH on carbide-modified Mo (110) and Mo2C powders: Photoemission and XANES studies. *The Journal of Physical Chemistry B* **2000,** *104* (48), 11515.
(80) Li, Z.; Choi, J. S.; Wang, H.; Lepore, A. W.; Connatser, R. M.; Lewis, S. A.; Meyer, H. M.; Santosa, D. M.; Zacher, A. H. Sulfur-Tolerant Molybdenum Carbide Catalysts Enabling Low-Temperature Stabilization of Fast Pyrolysis Bio-oil. *Energy and Fuels* **2017,** *31* (9), 9585.
(81) Wang, H.; Wang, Y. Characterization of deactivated bio-oil hydrotreating catalysts. *Topics in Catalysis* **2016,** *59* (1), 65.
(82) Ma, X.; Sun, L.; Song, C. A new approach to deep desulfurization of gasoline, diesel fuel and jet fuel by selective adsorption for ultra-clean fuels and for fuel cell applications. *Catal Today* **2002,** *77* (1-2), 107.
(83) Boullosa-Eiras, S.; Lødeng, R.; Bergem, H.; Stöcker, M.; Hannevold, L.; Blekkan, E. A. Catalytic hydrodeoxygenation (HDO) of phenol over supported molybdenum carbide, nitride, phosphide and oxide catalysts. *Catal Today* **2014,** *223*, 44.
(84) Lee, J. S.; Yeom, M. H.; Park, K. Y.; Nam, I. S.; Chung, J. S.; Kim, Y. G.; Moon, S. H. Preparation and benzene hydrogenation activity of supported molybdenum carbide catalysts. *Journal of Catalysis* **1991,** *128* (1), 126.
(85) Da Costa, P.; Potvin, C.; Manoli, J. M.; Breeysse, M.; Djega-Mariadassou, G. Supported molybdenum carbides lie between metallic and sulfided catalysts for deep HDS. *Catalysis Letters* **2003,** *86* (1-3), 133.
(86) Massoth, F. E.; Kibby, C. L. Studies of Molybdena-Alumina Catalysts .5. Relation between Catalyst Sulfided State and Activity for Thiophene Hydrodesulfurization. *Journal of Catalysis* **1977,** *47* (3), 300.
(87) Christensen, J. M.; Duchstein, L. D. L.; Wagner, J. B.; Jensen, P. A.; Temel, B.; Jensen, A. D. Catalytic Conversion of Syngas into Higher Alcohols over Carbide Catalysts. *Ind Eng Chem Res* **2012,** *51* (11), 4161.
(88) Jin, G.; Zhu, J.; Fan, X.; Sun, G.; Gao, J. Effect of Ni Promoter on Dibenzothiophene Hydrodesulfurization Performance of Molybdenum Carbide Catalyst. *Chinese Journal of Catalysis* **2006,** *27* (10), 899.
(89) Lee, J. S.; Boudart, M. Hydrodesulfurization of thiophene over unsupported molybdenum carbide. *Appl Catal* **1985,** *19* (1), 207.
(90) McCrea, K. R.; Logan, J. W.; Tarbuck, T. L.; Heiser, J. L.; Bussell, M. E. Thiophene hydrodesulfurization over alumina-supported molybdenum carbide and nitride catalysts: Effect of Mo loading and phase. *Journal of Catalysis* **1997,** *171* (1), 255.
(91) Park, H. K.; Kim, D. S.; Kim, K. L. Hydrodesulfurization of dibenzothiophene over supported and unsupported molybdenum carbide catalysts. *Korean Journal of Chemical Engineering* **1998,** *15* (6), 625.
(92) Puello-Polo, E.; Gutierrez-Alejandre, A.; Gonzalez, G.; Brito, J. L. Relationship Between Sulfidation and HDS Catalytic Activity of Activated Carbon Supported Mo, Fe-Mo, Co-Mo and Ni-Mo Carbides. *Catalysis Letters* **2010,** *135* (3-4), 212.

(93) Dolce, G.; Savage, P.; Thompson, L. Hydrotreatment activities of supported molybdenum nitrides and carbides. *Energy & Fuels* **1997,** *11* (3), 668.
(94) Aegerter, P. A.; Quigley, W. W. C.; Simpson, G. J.; Ziegler, D. D.; Logan, J. W.; McCrea, K. R.; Glazier, S.; Bussell, M. E. Thiophene hydrodesulfurization over alumina-supported molybdenum carbide and nitride catalysts: Adsorption sites, catalytic activities, and nature of the active surface. *Journal of Catalysis* **1996,** *164* (1), 109.
(95) Cheekatamarla, P. K.; Thomson, W. J. Poisoning effect of thiophene on the catalytic activity of molybdenum carbide during tri-methyl pentane reforming for hydrogen generation. *Applied Catalysis A: General* **2005,** *287* (2), 176.
(96) Cheekatamarla, P. K.; Thomson, W. J. Catalytic activity of molybdenum carbide for hydrogen generation via diesel reforming. *Journal of Power Sources* **2006,** *158* (1), 477.
(97) Xiao, T. C.; Wang, H. T.; York, A. P. E.; Green, M. L. H. Effect of sulfur on the performance of molybdenum carbide catalysts for the partial oxidation of methane to synthesis gas. *Catalysis Letters* **2002,** *83* (3-4), 241.
(98) Da Costa, P.; Lemberton, J.-L.; Potvin, C.; Manoli, J.-M.; Perot, G.; Breysse, M.; Djega-Mariadassou, G. Tetralin hydrogenation catalyzed by Mo2C/Al2O3 and WC/Al2O3 in the presence of H2S. *Catal Today* **2001,** *65* (2–4), 195.
(99) Liu, P.; Rodriguez, J. A.; Muckerman, J. T. Sulfur adsorption and sulfidation of transition metal carbides as hydrotreating catalysts. *Journal of Molecular Catalysis A: Chemical* **2005,** *239* (1), 116.
(100) Ko, E.; Madix, R. Effects of oxygen and sulfur on the bonding and reactivity of carbon monoxide, hydrogen, formaldehyde, and methanol on tungsten and tungsten carbide surfaces. *The Journal of Physical Chemistry* **1981,** *85* (26), 4019.
(101) Schulz-Ekloff, G. n.; Baresel, D.; Sarholz, W. Crystal face specificity in ammonia synthesis on tungsten carbide. *J. Catal.;(United States)* **1976,** *43*, 353.
(102) Lewandowski, M.; Szymanska-Kolasa, A.; Sayag, C.; Beaunier, P.; Djega-Mariadassou, G. Atomic level characterization and sulfur resistance of unsupported W2C during dibenzothiophene hydrodesulfurization. Classical kinetic simulation of the reaction. *Appl. Catal. B-Environ.* **2014,** *144*, 750.

Supporting Information

N and S content in different feedstocks

Table S6.1 lists the N and S content of coals from the following mines: the Zhundong (ZD) coal from the Xinjiang province, Yimin (YM) lignite from Inner Mongolia, Zhaotong (ZT) lignite produced in the Yunnan province and Shenmu from the Shanxi province, lignites from Mequinenza (Spain) and Labin (Croatia), highly volatile bituminous coals from Czeczot and Siersza and medium volatile bituminous coal from Zofio´wka (Poland).

Table S6.1 N and S content of coals from different origins

Name and origin	N (wt%)	S (wt%)	Ref.
ZD_ Zhundong (Xinjiang province, China)	0.57	0.38	S1
YM_Yimin (Mongolia)	0.81	0.13	S1
ZT_haotong (Yunnan province, China)	1.82	0.57	S1
Shenmu (Shanxi province, China)	1.11	0.34	S2
Mequinenza (Spain)	0.80	10.30	S3
Labin (Croatia)	1.20	10.00	S3
Czeczot (Poland)	1.00	1.40	S3
Siersza (Poland)	1.10	1.10	S3
Zofio´wka (Poland)	1.50	0.60	S3

Carbon driven reactions

A renewed interested in HDO has arisen due the increased use of biomass as a renewable carbon source. In general, biomass-derived feedstocks have a higher oxygen content than fossil fuels and, therefore, need to be deoxygenated. W and Mo carbides have been used in HDO reactions and compared with noble metals. Mostly model compounds such as stearic or oleic acid instead of biomass-derived oils or cresol instead of lignin-derived phenolic compounds were used as substrate. [S4,5] HDS and HDN reactions are usually catalysed by Ni-Mo/Al_2O_3 and take place during the industrial refining process of petroleum feedstocks. Mo and W carbides have been shown to be valuable replacement catalysts for both reaction, HDS and HDN. [S6-8] A classical industrial catalyst for isomerisation reactions is platinum. However, also Mo and W have shown to be valuable catalysts for isomerisation reactions. Another benefit of Mo and W, especially for isomerisation, in HDS and HDN reactions is their tolerance towards sulphur (see Table 6.1). Also

for NH_3 synthesis and decomposition, Mo and W have demonstrated to be active and Mo and W carbide are suitable catalysts.

For all reactions, both supported and bulk carbide catalysts studies have been conducted. Mainly carbon and alumina were used as support. Carbonaceous materials have a large surface area and high porosity, durability and stability and therefore are attractive materials to support metal catalysts. Also, aluminium oxide is a widely used material as a support for carbides because of its mechanical and textural properties (e.g., thermal stability, high surface area, surface chemistry). [S9] The support ensures stability of the metal particles in the catalytically active phase and enhances the downstream process.

Table S6.2 Overview of potential reactions using tungsten carbides or molybdenum carbides as replacement for (noble) metal catalyst. Hydrogenation (HYD), hydrodeoxygenation (HDO), hydrodesulphurisation (HDS), hydrodenitrogenation (HDN), isomerisation (Iso) and NH_3 synthesis/decomposition reactions are shown

Reaction		Catalyst	Replacement	Feedstock
HDO	Bulk	Mo_2C	Pd, Pt, Ru, Rh, Ni, Cu	Acetic acid,[S10] acetone,[S11] Anisole,[S12-15] benzofuran,[S7] ethanol,[S16] funeral,[S12,17-19] m-cresol,[S20] methyl stearate,[S21] phenol,[S14,22] propanal,[S23] stearic acid[S21]
		W_2C	Pd, Pt, Ru, Rh, Ni, Cu	acetaldehyde,[S24] acetic acid,[S24] benzofuran[S25], ethylene glycol[S24]
	Supported	Mo_2C/C	Pt, Pd, Ru, Rh (supported)	Decanal,[S26] guaiacol,[S27] lignin,[S28] methoxyphenol,[S29] oleic acid,[S4,30,31] stearic acid,[S21,26,32] vegetable oil,[S21,30,33,34] Acrylic acid,[S35] benzofuran[S36]
		Mo_2C/Al_2O_3	CoMo and NiMo supported on Al_2O_3	
		Wo_2C/C		Guaiacol,[S27] oleic acid and palmitic acid[S31]
HDS	Bulk	Mo_2C	Pt/Al_2O_3, MoS_2/Al_2O_3	Dibenzothiophene[S7,37]
		W_2C	Ni	Thiophene[S8]
	Sup.	Mo_2C/AC	Ni-Mo/Al_2O_3	Dibenzothiophene,[S6] thiophene[S38]
		Mo_2C/Al_2O_3	Ni	Dibenzothiophene,[S7,36,37,39] hexane,[S40] thiophene[S41-43]
HDN	Bulk	Mo_2C	sulfide Ni-Mo/Al_2O_3	Amines[S44] carbazole,[S45-47] indole,[S48,49] pyridine,[S50] quiniline[S51,52]
		W_2C		Carbazole[S46]
	Sup.	Mo_2C/Al_2O_3	Ni-Mo/Al_2O_3	Coal-derived feeds,[S53,54] pyridine,[S55] quinoline[S36,55]
		Mo_2C/AC		Indole[S6,56]
ISO	B.	Mo_2C	Pt	butane[S57,58] and heptane[S59-61]
		W_2C		Butane,[S57] dimethylpentane,[S62] heptane,[S60,61] neopentane,[S62,63] nethylcyclohexane[S62]

	Sup.	Mo_2C/CNF		Vegetable oils [S26]
		W_2C/Al_2O_3	Pt/SiO_2	Heptane [S64]
HYD	Bulk	Mo_2C	Pt, Pd/Al_2O_3	Benzene, [S65] butane, [S57] CO, [S66-68] CO_2, [S69-71] ethane, [S72] ethanol, [S16] ethylene, [S73] furfural, [S74] levulinic acid, [S75] long-chain alkadienes, [S76] nitroarenes [S77], toluene [S78,79]
		W_2C	Pt	Butane, [S57] CO [S8,68]
	Supported	Mo_2C/CNT Mo_2C/Al_2O_3	Ru	Levulinic acid [S80] Benzene, [S81] CO_2, [S82] CO, [S66,83] ethylene glycol [S84]
		W_2C/C W_2C/Al_2O_3		Ethylene glycol [S84], pentene [S8] Ethylene glycol [S84]
NH_3 synthesis		α & β Mo_2C	Iron, Mo nitride	(N_2+3H_2) [S85]
NH_3 decomp.		W_2C	Ru, Fe NH_3	Ammonia [S86-88]
		Mo_2C	Mo_2N	Ammonia [S89,90]

References

(S1) Wang, Z.; Li, Q.; Lin, Z.; Whiddon, R.; Qiu, K.; Kuang, M.; Cen, K. Transformation of nitrogen and sulphur impurities during hydrothermal upgrading of low quality coals. *Fuel* **2016,** *164*, 254.

(S2) Hou, J.; Ma, Y.; Li, S.; Shi, J.; He, L.; Li, J. Transformation of sulfur and nitrogen during Shenmu coal pyrolysis. *Fuel* **2018,** *231*, 134.

(S3) Grzybek, T.; Pietrzak, R.; Wachowska, H. X-ray photoelectron spectroscopy study of oxidized coals with different sulphur content. *Fuel Processing Technology* **2002,** *77*, 1.

(S4) Hollak, S. A. W.; Gosselink, R. W.; van Es, D. S.; Bitter, J. H. Comparison of Tungsten and Molybdenum Carbide Catalysts for the Hydrodeoxygenation of Oleic Acid. *Acs Catalysis* **2013,** *3* (12), 2837.

(S5) Chen, C. J.; Lee, W. S.; Bhan, A. Mo2/C catalyzed vapor phase hydrodeoxygenation of lignin-derived phenolic compound mixtures to aromatics under ambient pressure. *Applied Catalysis A: General* **2016,** *510*, 42.

(S6) Celzard, A.; Mareche, J. F.; Furdin, G.; Fierro, V.; Sayag, C.; Pielaszek, J. Preparation and catalytic activity of active carbon-supported Mo2C nanoparticles. *Green Chemistry* **2005,** *7* (11), 784.

(S7) Dhandapani, B.; Clair, T. S.; Oyama, S. Simultaneous hydrodesulfurization, hydrodeoxygenation, and hydrogenation with molybdenum carbide. *Applied Catalysis A: General* **1998,** *168* (2), 219.

(S8) Pawelec, B.; Mariscal, R.; Fierro, J. L. G.; Greenwood, A.; Vasudevan, P. T. Carbon-supported tungsten and nickel catalysts for hydrodesulfurization and hydrogenation reactions. *Appl Catal a-Gen* **2001,** *206* (2), 295.

(S9) Hanefeld, U.; Lefferts, L. *Catalysis: An Integrated Textbook for Students*; John Wiley & Sons, 2018.

(S10) Kumar, A.; Phadke, S.; Bhan, A. Acetic acid hydrodeoxygenation on molybdenum carbide catalysts. *Catalysis Science and Technology* **2018,** *8* (11), 2938.

(S11) Sullivan, M. M.; Bhan, A. Acetone Hydrodeoxygenation over Bifunctional Metallic–Acidic Molybdenum Carbide Catalysts. *ACS Catalysis* **2016,** *6* (2), 1145.

(S12) Lee, W.-S.; Wang, Z.; Wu, R. J.; Bhan, A. Selective vapor-phase hydrodeoxygenation of anisole to benzene on molybdenum carbide catalysts. *Journal of Catalysis* **2014,** *319*, 44.

(S13) Lee, W.-S.; Kumar, A.; Wang, Z.; Bhan, A. Chemical Titration and Transient Kinetic Studies of Site Requirements in Mo2C-Catalyzed Vapor Phase Anisole Hydrodeoxygenation. *ACS Catalysis* **2015,** *5* (7), 4104.

(S14) Chen, C. J.; Lee, W. S.; Bhan, A. Hydrodeoxygenation of lignin-derived phenolic compounds on transition metal carbides. *Abstr Pap Am Chem S* **2016,** *251*.

(S15) Kumar, A.; Bhan, A. Oxygen content as a variable to control product selectivity in hydrodeoxygenation reactions on molybdenum carbide catalysts. *Chemical Engineering Science* **2019,** *197*, 371.

(S16) Kelly, T. G.; Chen, J. G. G. Controlling C-O, C-C and C-H bond scission for deoxygenation, reforming, and dehydrogenation of ethanol using metal-modified molybdenum carbide surfaces. *Green Chemistry* **2014,** *16* (2), 777.

(S17) McManus, J. R.; Vohs, J. M. Deoxygenation of glycolaldehyde and furfural on Mo<inf>2</inf>C/Mo(100). *Surf Sci* **2014,** *630*, 16.

(S18) Xiong, K.; Lee, W. S.; Bhan, A.; Chen, J. G. Molybdenum carbide as a highly selective deoxygenation catalyst for converting furfural to 2-methylfuran. *ChemSusChem* **2014,** *7* (8), 2146.

(S19) Shi, Y.; Yang, Y.; Li, Y. W.; Jiao, H. Theoretical study about Mo2C(101)-catalyzed hydrodeoxygenation of butyric acid to butane for biomass conversion. *Catalysis Science and Technology* **2016,** *6* (13), 4923.

(S20) Chen, C. J.; Bhan, A. Mo2C Modification by CO2, H2O, and O-2: Effects of Oxygen Content and Oxygen Source on Rates and Selectivity of m-Cresol Hydrodeoxygenation. *Acs Catalysis* **2017,** *7* (2), 1113.

(S21) Han, J.; Duan, J.; Chen, P.; Lou, H.; Zheng, X. Molybdenum carbide-catalyzed conversion of renewable oils into diesel-like hydrocarbons. *Advanced Synthesis and Catalysis* **2011,** *353* (14-15), 2577.

(S22) Engelhardt, J.; Lyu, P.; Nachtigall, P.; Schüth, F.; García, Á. M. The Influence of Water on the Performance of Molybdenum Carbide Catalysts in Hydrodeoxygenation Reactions: A Combined Theoretical and Experimental Study. *ChemCatChem* **2017,** *9* (11), 1985.

(S23) Ren, H.; Yu, W.; Salciccioli, M.; Chen, Y.; Huang, Y.; Xiong, K.; Vlachos, D. G.; Chen, J. G. Selective hydrodeoxygenation of biomass-derived oxygenates to unsaturated hydrocarbons using molybdenum carbide catalysts. *ChemSusChem* **2013,** *6* (5), 798.

(S24) Yu, W. T.; Mellinger, Z. J.; Barteau, M. A.; Chen, J. G. G. Comparison of Reaction Pathways of Ethylene Glycol, Acetaldehyde, and Acetic Acid on Tungsten Carbide and Ni-Modified Tungsten Carbide Surfaces. *Journal of Physical Chemistry C* **2012,** *116* (9), 5720.

(S25) Liu, R.; Pang, M.; Chen, X.; Li, C.; Xu, C.; Liang, C. W2C nanorods with various amounts of vacancy defects: Determination of catalytic active sites in the hydrodeoxygenation of benzofuran. *Catalysis Science and Technology* **2017,** *7* (6), 1333.

(S26) Han, J.; Duan, J.; Chen, P.; Lou, H.; Zheng, X.; Hong, H. Nanostructured molybdenum carbides supported on carbon nanotubes as efficient catalysts for one-step hydrodeoxygenation and isomerization of vegetable oils. *Green Chemistry* **2011,** *13* (9), 2561.

(S27) Jongerius, A. L.; Gosselink, R. W.; Dijkstra, J.; Bitter, J. H.; Bruijnincx, P. C. A.; Weckhuysen, B. M. Carbon Nanofiber Supported Transition-Metal Carbide Catalysts for the Hydrodeoxygenation of Guaiacol. *ChemCatChem* **2013,** *5* (10), 2964.

(S28) Jongerius, A. L.; Bruijnincx, P. C. A.; Weckhuysen, B. M. Liquid-phase reforming and hydrodeoxygenation as a two-step route to aromatics from lignin. *Green Chemistry* **2013,** *15* (11), 3049.

(S29) Liu, S. D.; Wang, H. Y.; Smith, K. J.; Kim, C. S. Hydrodeoxygenation of 2-Methoxyphenol over Ru, Pd, and Mo2C Catalysts Supported on Carbon. *Energy & Fuels* **2017,** *31* (6), 6378.
(S30) Kim, S. K.; Yoon, D.; Lee, S. C.; Kim, J. Mo2C/graphene nanocomposite as a hydrodeoxygenation catalyst for the production of diesel range hydrocarbons. *ACS Catalysis* **2015,** *5* (6), 3292.
(S31) Wang, F.; Jiang, J. C.; Wang, K.; Zhai, Q. L.; Sun, H.; Liu, P.; Feng, J. F.; Xia, H. H.; Ye, J.; Li, Z. X.et al. Activated carbon supported molybdenum and tungsten carbides for hydrotreatment of fatty acids into green diesel. *Fuel* **2018,** *228*, 103.
(S32) Souza Macedo, L.; Oliveira, R. R.; van Haasterecht, T.; Teixeira da Silva, V.; Bitter, H. Influence of synthesis method on molybdenum carbide crystal structure and catalytic performance in stearic acid hydrodeoxygenation. *Applied Catalysis B: Environmental* **2019,** *241*, 81.
(S33) Qin, Y.; Chen, P.; Duan, J. Z.; Han, J. X.; Lou, H.; Zheng, X. M.; Hong, H. P. Carbon nanofibers supported molybdenum carbide catalysts for hydrodeoxygenation of vegetable oils. *Rsc Advances* **2013,** *3* (38), 17485.
(S34) Qin, Y.; He, L.; Duan, J.; Chen, P.; Lou, H.; Zheng, X.; Hong, H. Carbon-supported molybdenum-based catalysts for the hydrodeoxygenation of maize oil. *ChemCatChem* **2014,** *6* (9), 2698.
(S35) Rocha, A. S.; Souza, L. A.; Oliveira, R. R.; Rocha, A. B.; Teixeira da Silva, V. Hydrodeoxygenation of acrylic acid using Mo2C/Al2O3. *Applied Catalysis A: General* **2017,** *531*, 69.
(S36) Dolce, G.; Savage, P.; Thompson, L. Hydrotreatment activities of supported molybdenum nitrides and carbides. *Energy & Fuels* **1997,** *11* (3), 668.
(S37) Park, H. K.; Kim, D. S.; Kim, K. L. Hydrodesulfurization of dibenzothiophene over supported and unsupported molybdenum carbide catalysts. *Korean Journal of Chemical Engineering* **1998,** *15* (6), 625.
(S38) Puello-Polo, E.; Gutierrez-Alejandre, A.; Gonzalez, G.; Brito, J. L. Relationship Between Sulfidation and HDS Catalytic Activity of Activated Carbon Supported Mo, Fe-Mo, Co-Mo and Ni-Mo Carbides. *Catalysis Letters* **2010,** *135* (3-4), 212.
(S39) Jin, G.; Zhu, J.; Fan, X.; Sun, G.; Gao, J. Effect of Ni Promoter on Dibenzothiophene Hydrodesulfurization Performance of Molybdenum Carbide Catalyst. *Chinese Journal of Catalysis* **2006,** *27* (10), 899.
(S40) Zhu, Q. L.; Zhao, X. T.; Zhao, Z. M.; Ma, H. J.; Deng, Y. Q. Preparation of supported molybdenum carbide catalyst using n-hexane and its hydrodesulfurization activity. *Chinese Journal of Catalysis* **2005,** *26* (12), 1047.
(S41) Lee, J. S.; Boudart, M. Hydrodesulfurization of thiophene over unsupported molybdenum carbide. *Appl Catal* **1985,** *19* (1), 207.
(S42) Aegerter, P. A.; Quigley, W. W. C.; Simpson, G. J.; Ziegler, D. D.; Logan, J. W.; McCrea, K. R.; Glazier, S.; Bussell, M. E. Thiophene hydrodesulfurization over alumina-supported molybdenum carbide and nitride catalysts: Adsorption sites, catalytic activities, and nature of the active surface. *Journal of Catalysis* **1996,** *164* (1), 109.
(S43) McCrea, K. R.; Logan, J. W.; Tarbuck, T. L.; Heiser, J. L.; Bussell, M. E. Thiophene hydrodesulfurization over alumina-supported molybdenum carbide and nitride catalysts: Effect of Mo loading and phase. *Journal of Catalysis* **1997,** *171* (1), 255.
(S44) Schwartz, V.; da Silva, V. T.; Oyama, S. T. Push–pull mechanism of hydrodenitrogenation over carbide and sulfide catalysts. *Journal of Molecular Catalysis A: Chemical* **2000,** *163* (1-2), 251.
(S45) Szymańska, A.; Lewandowski, M.; Sayag, C.; Djéga-Mariadassou, G. Kinetic study of the hydrodenitrogenation of carbazole over bulk molybdenum carbide. *Journal of Catalysis* **2003,** *218* (1), 24.
(S46) Szymanska-Kolasa, A.; Lewandowski, M.; Sayag, C.; Brodzki, D.; Djega-Mariadassou, G. Comparison between tungsten carbide and molybdenum carbide for the hydrodenitrogenation of carbazole. *Catal Today* **2007,** *119* (1-4), 35.
(S47) Lewandowski, M.; Szymańska-Kolasa, A.; Da Costa, P.; Sayag, C. Catalytic performances of platinum doped molybdenum carbide for simultaneous hydrodenitrogenation and hydrodesulfurization. *Catal Today* **2007,** *119* (1-4), 31.
(S48) Li, S. Z.; Lee, J. S. Molybdenum nitride and carbide prepared from heteropolyacid II. Hydrodenitrogenation of indole. *Journal of Catalysis* **1998,** *173* (1), 134.
(S49) Kotarba, A.; Adamski, G.; Piskorz, W.; Sojka, Z.; Sayag, C.; Djega-Mariadassou, G. Modification of electronic properties of Mo2C catalyst by potassium doping: Impact on the reactivity in hydrodenitrogenation reaction of indole. *J Phys Chem B* **2004,** *108* (9), 2885.
(S50) Choi, J. G.; Brenner, J. R.; Thompson, L. T. Pyridine hydrodenitrogenation over molybdenum carbide catalysts. *Journal of Catalysis* **1995,** *154* (1), 33.
(S51) Schlatter, J. C.; Oyama, S. T.; Metcalfe III, J. E.; Lambert Jr, J. M. Catalytic behavior of selected transition metal carbides, nitrides, and borides in the hydrodenitrogenation of quinoline. *Ind Eng Chem Res* **1988,** *27* (9), 1648.
(S52) Ramanathan, S.; Oyama, S. T. New Catalysts for Hydroprocessing - Transition-Metal Carbides and Nitrides. *J Phys Chem-Us* **1995,** *99* (44), 16365.
(S53) Sajkowski, D. J.; Oyama, S. T. Catalytic hydrotreating by molybdenum carbide and nitride: Unsupported Mo2N and Mo2C/Al2O3. *Applied Catalysis A: General* **1996,** *134* (2), 339.
(S54) Sajkowski, D. J.; Oyama, S. T. American Chemical Society, Division of Petroleum Chemistry, Preprints, 1990; p 233.
(S55) Dolce, G. M.; Thompson, L. T. Materials Research Society Symposium - Proceedings, 1997; p 47.
(S56) Sayag, C.; Benkhaled, M.; Suppan, S.; Trawczynski, J.; Djéga-Mariadassou, G. Comparative kinetic study of the hydrodenitrogenation of indole over activated carbon black composites (CBC) supported molybdenum carbides. *Applied Catalysis A: General* **2004,** *275* (1-2), 15.

(S57) Neylon, M. K.; Choi, S.; Kwon, H.; Curry, K. E.; Thompson, L. T. Catalytic properties of early transition metal nitrides and carbides: n-butane Hydrogenolysis, dehydrogenation and isomerization. *Applied Catalysis A: General* **1999,** *183* (2), 253.

(S58) Liebig, S.; Gerlach, T.; Doukkali, K.; Grünert, W. In *Studies in Surface Science and Catalysis*, 2000; Vol. 130 C.

(S59) Blekkan, E. A.; Pham-Huu, C.; Ledoux, M. J.; Guille, J. Isomerization of n-Heptane on an Oxygen-Modified Molybdenum Carbide Catalyst. *Industrial and Engineering Chemistry Research* **1994,** *33* (7), 1657.

(S60) Lamic, A.-F.; Pham, T. L. H.; Potvin, C.; Manoli, J.-M.; Djéga-Mariadassou, G. Kinetics of bifunctional isomerization over carbides (Mo, W). *Journal of Molecular Catalysis A: Chemical* **2005,** *237* (1-2), 109.

(S61) Lamic, A. F.; Shin, C. H.; Djéga-Mariadassou, G.; Potvin, C. Characterization of Mo2C-WO2 composite catalysts for bifunctional isomerization: A new pulse method to quantify acid sites. *Applied Catalysis A: General* **2006,** *302* (1), 5.

(S62) Ribeiro, F. H.; Betta, R. A. D.; Boudart, M.; Baumgartner, J.; Iglesia, E. Reactions of Neopentane, Methylcyclohexane, and 3,3-Dimethylpentane on Tungsten Carbides - the Effect of Surface Oxygen on Reaction Pathways. *Journal of Catalysis* **1991,** *130* (1), 86.

(S63) Iglesia, E.; Ribeiro, F. H.; Boudart, M.; Baumgartner, J. E. Synthesis, Characterization, and Catalytic Properties of Clean and Oxygen-Modified Tungsten Carbides. *Catal Today* **1992,** *15* (2), 307.

(S64) Iglesia, E.; Baumgartner, J. E.; Ribeiro, F. H.; Boudart, M. Bifunctional Reactions of Alkanes on Tungsten Carbides Modified by Chemisorbed Oxygen. *Journal of Catalysis* **1991,** *131* (2), 523.

(S65) Oliveira Jr, R. R.; Rocha, A. S.; Teixeira Da Silva, V.; Rocha, A. B. Investigation of hydrogen occlusion by molybdenum carbide. *Applied Catalysis A: General* **2014,** *469*, 139.

(S66) Kim, H. G.; Lee, K. H.; Lee, J. S. Carbon monoxide hydrogenation over molybdenum carbide catalysts. *Research on Chemical Intermediates* **2000,** *26* (5), 427.

(S67) Qi, K. Z.; Wang, G. C.; Zheng, W. J. A first-principles study of CO hydrogenation into methane on molybdenum carbides catalysts. *Surf Sci* **2013,** *614*, 53.

(S68) Ranhotra, G. S.; Haddix, G. W.; Bell, A. T.; Reimer, J. A. Catalysis over molybdenum carbides and nitrides. I. Catalyst characterization. *Journal of Catalysis* **1987,** *108* (1), 24.

(S69) Tominaga, H.; Nagai, M. Density functional study of carbon dioxide hydrogenation on molybdenum carbide and metal. *Applied Catalysis A: General* **2005,** *282* (1-2), 5.

(S70) Posada-Pérez, S.; Viñes, F.; Ramirez, P. J.; Vidal, A. B.; Rodriguez, J. A.; Illas, F. The bending machine: CO<inf>2</inf>activation and hydrogenation on δ-MoC(001) and β-Mo<inf>2</inf>C(001) surfaces. *Physical Chemistry Chemical Physics* **2014,** *16* (28), 14912.

(S71) Xu, W.; Ramirez, P. J.; Stacchiola, D.; Rodriguez, J. A. Synthesis of α-MoC1 and β-MoCy catalysts for CO2 hydrogenation by thermal carburization of Mo-oxide in hydrocarbon and hydrogen mixtures. *Catalysis Letters* **2014,** *144* (8), 1418.

(S72) Yao, S.; Yan, B.; Jiang, Z.; Liu, Z.; Wu, Q.; Lee, J. H.; Chen, J. G. Combining CO2 Reduction with Ethane Oxidative Dehydrogenation by Oxygen-Modification of Molybdenum Carbide. *ACS Catalysis* **2018,** *8* (6), 5374.

(S73) Gao, F.; Wang, Y.; Tysoe, W. T. Ethylene hydrogenation on Mo(CO)6 derived model catalysts in ultrahigh vacuum: From oxycarbide to carbide to MoAl alloy. *Journal of Molecular Catalysis A: Chemical* **2006,** *249* (1-2), 111.

(S74) Deng, Y. C.; Gao, R.; Lin, L. L.; Liu, T.; Wen, X. D.; Wang, S.; Ma, D. Solvent Tunes the Selectivity of Hydrogenation Reaction over alpha-MoC Catalyst. *J Am Chem Soc* **2018,** *140* (43), 14481.

(S75) Quiroz, J.; Mai, E. F.; Da Silva, V. T. Synthesis of Nanostructured Molybdenum Carbide as Catalyst for the Hydrogenation of Levulinic Acid to γ-Valerolactone. *Topics in Catalysis* **2016,** *59* (2-4), 148.

(S76) Li, Y.; Fan, Y.; Luo, G. Investigation into the Liquid Selective Hydrogenation of Long Chain Alkadienes on Molybdenum Carbide and Metallic Molybdenum and/or Boride Mixture Prepared by a Thermosynthesis Method at Moderate Temperature. *Industrial and Engineering Chemistry Research* **2004,** *43* (6), 1334.

(S77) Liu, Z.; Wang, X.; Zou, X.; Lu, X. Molybdenum Carbide Catalysts for Chemoselective Transfer Hydrogenation of Nitroarenes. *ChemistrySelect* **2018,** *3* (18), 5165.

(S78) Frauwallner, M. L.; López-Linares, F.; Lara-Romero, J.; Scott, C. E.; Ali, V.; Hernández, E.; Pereira-Almao, P. Toluene hydrogenation at low temperature using a molybdenum carbide catalyst. *Applied Catalysis A: General* **2011,** *394* (1-2), 62.

(S79) Mehdad, A.; Jentoft, R. E.; Jentoft, F. C. Passivation agents and conditions for Mo2C and W2C: Effect on catalytic activity for toluene hydrogenation. *Journal of Catalysis* **2017,** *347*, 89.

(S80) Mai, E. F.; Machado, M. A.; Davies, T. E.; Lopez-Sanchez, J. A.; Teixeira Da Silva, V. Molybdenum carbide nanoparticles within carbon nanotubes as superior catalysts for γ-valerolactone production via levulinic acid hydrogenation. *Green Chemistry* **2014,** *16* (9), 4092.

(S81) Lee, J. S.; Yeom, M. H.; Park, K. Y.; Nam, I. S.; Chung, J. S.; Kim, Y. G.; Moon, S. H. Preparation and benzene hydrogenation activity of supported molybdenum carbide catalysts. *Journal of Catalysis* **1991,** *128* (1), 126.

(S82) Nagai, M.; Kurakami, T.; Omi, S. Activity of carbided molybdena-alumina for CO<inf>2</inf>hydrogenation. *Catal Today* **1998,** *45* (1-4), 235.

(S83) Shou, H.; Davis, R. J. Multi-product steady-state isotopic transient kinetic analysis of CO hydrogenation over supported molybdenum carbide. *Journal of Catalysis* **2013,** *306*, 91.

(S84) Ji, N.; Zhang, T.; Zheng, M.; Wang, A.; Wang, H.; Wang, X.; Shu, Y.; Stottlemyer, A. L.; Chen, J. G. Catalytic conversion of cellulose into ethylene glycol over supported carbide catalysts. *Catal Today* **2009,** *147* (2), 77.

(S85) Kojima, R.; Aika, K. I. Molybdenum nitride and carbide catalysts for ammonia synthesis. *Applied Catalysis A: General* **2001,** *219* (1-2), 141.
(S86) Pansare, S. S.; Torres, W.; Goodwin, J. G. Ammonia decomposition on tungsten carbide. *Catalysis Communications* **2007,** *8* (4), 649.
(S87) Pansare, S. S.; Torres, W.; Goodwin Jr, J. G.; Gangwal, S. K. ACS National Meeting Book of Abstracts, 2006.
(88) Pansare, S. S.; Goodwin, J. G. Ammonia decomposition on tungsten-based catalysts in the absence and presence of syngas. *Ind Eng Chem Res* **2008,** *47* (12), 4063.
(S89) Zheng, W.; Cotter, T. P.; Kaghazchi, P.; Jacob, T.; Frank, B.; Schlichte, K.; Zhang, W.; Su, D. S.; Schüth, F.; Schlögl, R. Experimental and theoretical investigation of molybdenum carbide and nitride as catalysts for ammonia decomposition. *J Am Chem Soc* **2013,** *135* (9), 3458.
(S90) Choi, J. G. Ammonia decomposition over vanadium carbide catalysts. *Journal of Catalysis* **1999,** *182* (1), 104.

7

Chapter 7

General Discussion

The increasing interest in molybdenum and tungsten carbide catalysts has ever been increasing during the last 50 years, as inferred from the number of publications on these materials (Figure 7.1). Often it is stated, and this is stated here as well, that these carbides can be considered alternatives to noble metal catalysts. Nevertheless, compared with the number of papers on Pt catalysts (Figure 7.1), studies about carbide catalysts make up only a small group.[1] This can be explained by a number of challenges that need to be overcome for these carbide based catalysts. Especially their stability, their cumbersome preparation, and the lack of understanding of the relationship between the catalysts' properties and their performance need to be addressed.[2] The previous chapters covered new insights regarding these challenges. In this chapter, the most important findings from these chapters will be discussed and integrated into a broader perspective, and recommendations for future research will be given. For this, the chapter is divided into the following four discussion points and additional recommendations and concluding remarks.

1. **Mo and W carbide catalysts can shine too – comparison of carbides and noble metals**
2. **Formation of oxycarbides – What does the active site of carbides look like?**
3. **Influence of mixing W and Mo carbides on catalytic performance and challenges in their synthesis**
4. **Stability of transition metal carbides**

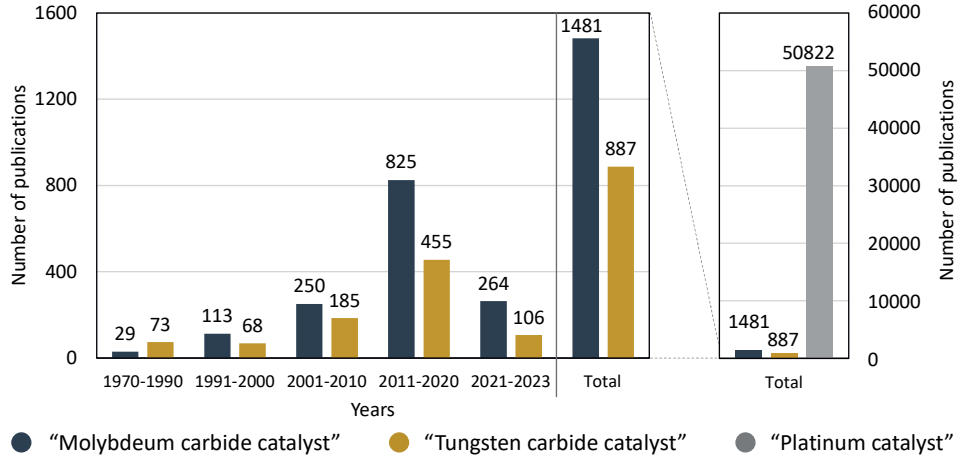

Figure 7.1 Number of publications on "tungsten carbide catalyst/s", "molybdenum carbide catalyst/s" and "platinum catalyst/s" based on the Scopus database (5 December 2022)

1. Mo and W carbide catalysts can shine too – comparison of carbides and noble metals

As outlined in Chapters 1 and 6, Mo and W metal carbides are claimed to have three main advantages over noble metals. The first and often mentioned advantage is the earth abundancy of these non-noble metals, which makes them less expensive than the scarce noble metals.[3] The second advantage is the – overlooked – potential tolerance of Mo and W carbides to N and S impurities contained in both crude oil and renewable feedstocks (Chapter 6).[4] Mo and W carbides have the ability to change the nature of their active site to their respective nitrides or sulphides when used in the presence of N and S impurities. These phases are catalytically active for reactions similar to those of the carbides and do not necessarily lead to complete catalyst deactivation like in the case of noble metal catalysts in the presence of N and S impurities.[5-7] The third advantage of transition metal carbides is their catalytic activity for hydrogen transfer reactions, which is similar or even better than that of noble metals.[8-14] This was shown for the first time in the ground-breaking work of Levy and Boudart in 1973,[15] where the authors demonstrated that the incorporation of carbon into the metallic W increases its reactivity for the formation of water from hydrogen and oxygen and the isomerization of 2,2-dimethlpropane to 2-methylbutane. In addition, it was shown that the carbon enriched tungsten catalyst and the Pt catalysts had similar electronic structures and catalytic behaviours. The noble-metal-like properties of the carbides are attributed to a lattice expansion through the incorporation of carbon into interstitial sites of Mo and W.[15-17]

Since the ground breaking work of Levy and Boudart,[15] the number of publications on "tungsten carbide catalyst/s" and "molybdenum carbide catalyst/s" has drastically increased (see Figure 7.1). Those publications deal with many applications of Mo and W carbides, such as isomerization, hydrodesulfurization and hydrodenitrogenation reactions, fuel cell electrocatalysis and syngas conversion.[8-12] **The primary motive was to investigate the replacement of noble metals with metal carbides** since the catalytic behaviour of carbide catalysts resembles that of noble metals for many of the reactions listed. Although the activity of carbides is often claimed to be similar to that of noble metals, as can be seen in Table 7.1, product selectivity is often different, which is also stated in the reviews of Oyama[18] and Chen.[19] This indicates that carbide catalysts facilitate different catalytic pathways. For instance, in the (hydro-)deoxygenation of free fatty acids, using stearic acid as a model compound, the carbide catalysts and Pt catalyst form alkanes as final products but their reaction pathways differ and thus their resulting hydrocarbon products. As shown in Figure 7.2, Pt catalysts primarily yield heptadecane (C17) via the decarboxylation pathway (DCO, carbon-carbon scission), while the carbides prefer the hydrodeoxygenation pathway (HDO, no carbon-carbon scission), which results in the

formation of a variety of C-18 products, like fatty alcohols, aldehydes (oxygenates, C18-oxy) and alkenes (C18-alkene). This offers the potential to make different value-added products that can be used for many applications, but their selective preparation needs to be addressed. Fatty alcohols and aldehydes (oxygenates) are used as detergents, plasticizers, lubricant bases and personal care products,[20,21] while alkenes can be used as high-value bulk chemical products, such as surfactants, lubricants, plasticizers or polymers, in which the presence of a C=C double bond is highly beneficial for the chemical functionality.[21]

Table 7.1 Comparison of activity and selectivity of Mo and W carbides and noble metals for isomerization (Isom.), hydrodeoxygenation (HDO) and hydrogenation (HYN) reactions. TOF=Turnover frequency, Conv.=Conversion

Reac.	Carbide	Activity	Select.	Compared to:	Activity	Select.	Reac. Conditions	Ref
Isom.	**W_2C**	TOF: 10×10^{-4} s^{-1}	Hydrogenolysis	**Ru/Al_2O_3**	TOF: 85×10^{-4} s^{-1}	Isomerization	216 °C, Neopentane, 95 kPa H_2	22
	WC	TOF: 300×10^{-4} s^{-1}	Hydrogenolysis					
	W_2C	Conv.: 12.9% TOF: 0.17 s^{-1}	Isomerization	**Pt/SiO_2**	Conv.: 10.5% TOF: 0.13 s^{-1}	Cyclization	350 °C, Heptane, 96 kPa H_2	10
	Mo_2C	Conv.: 15% TOF: 10000×10^{-10} mol g^{-1} s^{-1}	Isomerization	**Pt/β-zeolite**	Conv.: 8% TOF: 25000×10^{-10} mol g^{-1} s^{-1}	Isomerization	350 °C (Mo) & 250 °C (Pt), n-Heptane, 6.5 bar H_2	23
HDO	**Mo_2C/AC**	Conv. (0.5h): 30 mol% TOF: Pd>Ru>Mo_2C	Direct demethylation	**Pd/AC**	Conv. (0.5h): 95 mol%	HYN	330 °C, Guaiacol, 34 bar H_2	24
				Ru/AC	Conv. (0.5h): 98 mol%			
	Mo_2C/CNF	Conv. (1h): 73% TOF: 9.7 min^{-1}	HDO	**Pt/CNF**	Conv. (1h): 30% TOF: 4.3 min^{-1}	DCO	350 °C, stearic acid, 30 bar	*
	W_2C/CNF	Conv. (1h): 38 mol% TOF: 2.9 min^{-1}						
HYN	**Mo_2C/CNF**	TOF: 14 min^{-1}	C=C HYN + β-methylstyrene	**Pt/CNF**	TOF: 86 min^{-1}	C=C HYN	200 °C. cinnamaldehyde, 20 bar	* 25
	W_2C/CNF	TOF: 22 min^{-1}						
CO_2 Reduction	**Mo_2C**	Conv.: 8.7% TOF: 25.7 min^{-1}	CO:CH_4 14.5	**PtCo/CeO_2**	Conv.: 6.6% TOF: 14.6 min^{-1}	CO:CH_4 4.5	200 °C, CO_2	26
				PdCo/CeO_2	Conv.: 2.5% TOF: 5.6 min^{-1}	CO:CH_4 0.6		

*This work

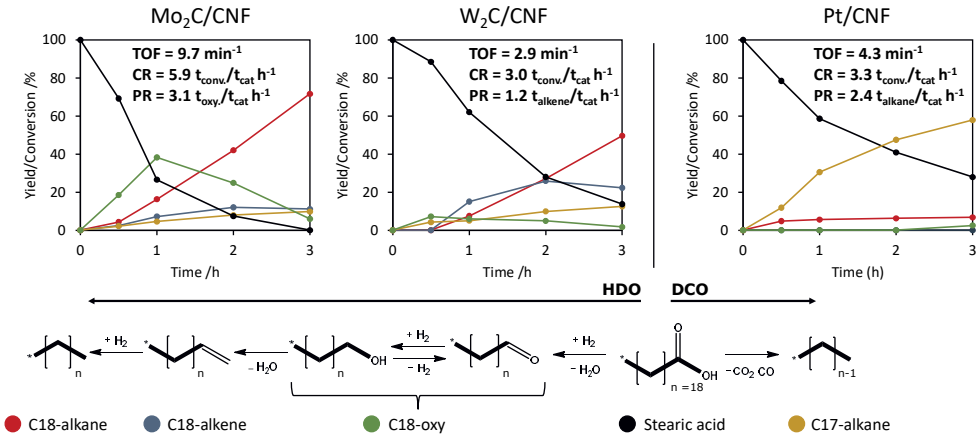

Figure 7.2 Pt versus Mo and W carbide catalysts in stearic acid conversion and product distribution in a batch reactor. [i] *Turnover frequency (TOF) is calculated from CO chemisorption after 1 h. Conversion and production rates (CR and PR) are based on the converted t stearic acid per t catalysts after 1 h.*

In addition, one should note that the DCO pathways do not require the consumption of hydrogen (H_2) to deoxygenate the fatty acid reactant. The oxygen is either removed from the fatty acid as carbon monoxide and water to yield an alkene in the case of decarbonylation or as carbon dioxide to yield an alkane in the decarboxylation pathway (see Figure 7.2). However, the use of H_2 during DCO hinders the formation of carbonaceous deposits (coke) on the catalytic metal surface sites. By contrast, the HDO requires H_2 for the formation of aldehyde and water in the first step of the HDO pathway.[27] This makes additional safety measures necessary and increases the process costs. Thus, whether the DCO or the HDO pathway is preferable from an economical/industrial point of view needs to be evaluated based on the higher carbon efficiency and lower greenhouse gas (CO_2) production of HDO and the lower hydrogen (H_2) consumption and higher product selectivity of DCO.[28,29]

In addition, it is also worth having a closer look into the activity of the Pt and carbide catalysts. The activity of a catalyst can be described by (1) the turnover frequency (TOF, the number of reactant molecules converted per accessible site per second or minute); (2) the turnover number (TON, the number of reactant molecules converted in the life time of the catalyst); (3) the conversion or production rate (CR or PR, the weight in tonnes of reactant converted or product produced per tonne catalyst per hour); or (4) the feedstock or reactant conversion (in percent). The latter is often used, but it is only valid when catalyst loading and reaction conditions

[i] The carbon nanofiber supported Mo (8.5wt%) and W (15wt%) carbides were prepared via carbothermal reduction (900 °C, β =5 °C/min, N_2 flow of 50 ml/min) and transferred to the reaction mixture under an inert atmosphere (glove box). The Pt supported catalyst (5wt%) was reduced in hydrogen (300 °C, β =5 °C/min, H_2 flow of 30 ml/min and N_2 flow of 50 ml/min). The hydrodeoxygenation conditions were: 250 mg catalyst, 2 g stearic acid, 350 °C, 50 ml solvent and 30 bar H_2. Details of catalyst preparation, testing and evaluation can be found in Chapter 3.

(concentration, time) are given to allow a reasonable comparison of catalysts.[30] In Figure 7.2 the activity of different catalysts can be evaluated by comparing the black lines. As can be seen the Mo carbide catalyst were more active than the Pt and W carbides and achieved full conversion of stearic acid after 3 h. For the W carbide and the Pt similar conversions rates of stearic acid under the given conditions were observed.

Additionally, the activity was also evaluated by means of TOF and PR/CR. The TOF is a measure for the activity of a catalyst. It is independent of the catalyst weight and loading if the dispersion stays the same and is often used in catalytic research.[31] Here, the TOF is based on the accessible (CO) sites of the catalyst. The Mo carbide (9.7 min^{-1}) showed the highest TOF in comparison with Pt (4.3 min^{-1}) and W carbide (2.9 min^{-1}). However, in contrast to the conversion the TOF-based activity showed higher rates for the Pt catalysts than for the W carbide catalysts. In order to put the conversion and productivity rates obtained into perspective of commercially applied heterogeneous catalysts in the manufacture of fuels, chemical intermediates and polymers, the PR was also calculated. Lange et al. stated that a minimal production rate of 0.1 $t_{product}/(t_{catalysts}\times h)$ is needed for a commercial application, otherwise the process might encounter economic difficulties.[32] All catalysts used here, Mo carbide, W carbide and Pt, seem to surpass the activity threshold, with rates of 5.9, 3.0 and 3.3 $t_{conv.}/(t_{catalysts}\times h)$, respectively. Also the PR based on the respective product of each catalyst passed these threshold, although it decreases to 3.1-1.4 $t_{product}/(t_{catalysts}\times h)$ due to the selectivity of the catalysts. These results indicate that the application of carbide catalysts is not limited by their conversion and productivity rates.

These results show that it is important to determine and compare the catalytic activity using different measure methods (e.g., TOF, PR and feedstock conversion level) to obtain a reasonable comparison of different catalysts. Nevertheless, instead of using expensive noble-metal catalysts this thesis focuses more on finding Mo and W carbide based catalysts with an interesting product selectivity – without compromising too heavily on the activity.[33] In order to increase productivity, one can easily increase the weight of transition metal catalysts used in the reaction, since these metals are less expensive than noble metals.[3] This thesis instead aims at providing a deeper understanding of the relationship between catalysts' properties and their performance.

Considering all this evidence, transition metal carbides are not simply replacements for noble metals. In many instances the reactivity and bonding of Mo and W carbides resemble that of noble metals. However, the analogy between these two materials does not extend to every aspect of catalytic behaviour. The carbides exhibit their own unique activity and selectivity. Consequently, this **unique catalytic behaviour of transition metal carbides leads to an interesting class of catalysts for the deoxygenation of biobased feedstock**.

2. Formation of oxycarbides - What does the active site of carbides really look like?

The selectivities of Mo and W carbides described above often arise from the modification of the catalytic surface by oxygen, resulting in acid (the surface oxygen sites) and metal-like (the carbides) sites.[34] The metal-like properties show a catalytic behaviour (e.g., hydrogenation) similar to that of noble metal catalysts, whereas it is suggested that the acidic sites are responsible for the selective C-O cleavage, which distinguishes the carbides from noble metals.[9] This is exemplified in the work of Ribeiro et al.,[17,22,35] who studied bifunctional tungsten based catalysts. In their catalysts metallic sites (W carbides) were present, and the acidic sites were introduced through modification of the carbide surface by oxygen (passivation by an oxygen treatment after carburisation). The bifunctional tungsten carbide obtained in this way isomerizes C5–C7 alkanes via a sequence of dehydrogenation (metal sites needed), methyl shift (acidic sites needed) and hydrogenation (metal sites needed), as evidenced by using terminal isotopic enrichment in n-heptane.[13]. In contrast, noble metal catalysts perform C5 hydrogenolysis.[22,35] Moreover, Sullivan et al. investigated the acid functionality on Mo and W catalysts.[36-39] The authors showed that for the isopropanol dehydration over metal carbides (β-Mo_2C, α-Mo_2C, W_2C and WC), the dehydration rates increases by an order of magnitude for all catalysts when adding oxygen to the feeds.[37,39]

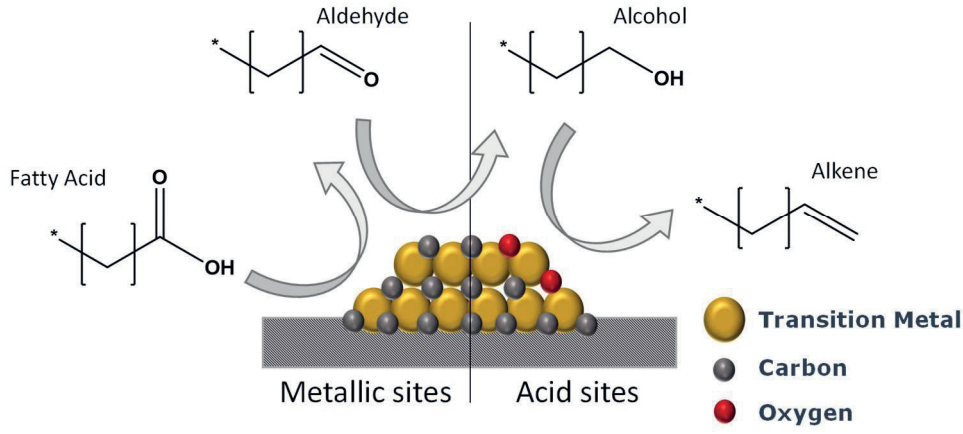

Figure 7.3 Proposed reaction network for fatty acid deoxygenation over metallic and acid Mo or W carbide sites

Also for the HDO reaction over Mo and W carbide catalysts it has often been reported that both hydrogenation and dehydration reactions can occur, which indicates the presence of metallic and acidic sites.[27,38,40-43] For instance, in the hydrodeoxygenation of stearic acid over CNF supported Mo and W carbides, Stellwagen et al.[27] observed that the initial formation of the aldehyde is the result of a metal-mediated C-O hydrogenolysis reaction. The next step is a metal-catalyzed

hydrogenation of the aldehyde to the alcohol, which is then dehydrated over an acidic site to form the alkene (see Figure 7.3). Finally, the alkene can undergo hydrogenation to form the alkane. Interestingly, the acid-catalysed dehydration was claimed to be easier over the acid sites present in tungsten carbide catalysts than over those in molybdenum carbide, resulting in higher alkene yields over tungsten carbide. The acidic sites in molybdenum carbide seem to be less able to effect dehydration, yielding higher concentrations of C18-oxygenates as intermediate products. The differences in nature between the acidic sites of tungsten carbide and molybdenum carbide were attributed to the more oxophilic nature of tungsten, which is more likely to generate stronger or more numerous acid sites than molybdenum. Please note that in the study of Stellwagen et al. the acid sites were most likely introduced during the short exposure of the catalyst to air while it was transferred from the synthesis reactor to the catalytic testing reactor. Thus, the carbides hold a potential for performing bifunctional (acidic and metallic) catalysis if the carbide is exposed to a suitable oxygen source.

In Chapters 2 and 3 this is extended to bimetallic MoW carbides, where it is shown that Mo_2C and Mo rich bimetallic carbides are capable of converting stearic acid to a high concentration of oxygenates and that W_2C and W rich bimetallic catalysts yield high concentrations of alkenes. Thus, also in these cases the monometallic and bimetallic carbides based on tungsten contain acid sites that dehydrate the alcohol to the alkene. However, in contrast to the abovementioned studies, where the oxygen was introduced on the carbide surface via exposure to air or oxygen (i.e., passivation, either during transfer or by O_2 cofeeding), the carbide catalysts used in this study were transferred under nitrogen (via glove box) and, thus, **the carbide catalysts investigated here had not been in contact with air or oxygen.** Therefore, these acid sites presumably originate from the in situ generation of O*-Me_2C,[44] i.e., surface oxides that are formed when the catalyst is exposed to oxygen from the reactant or to water formed during the HDO reaction. This explanation is consistent with the absence of acid sites, revealed by NH3 TPD, on freshly carburized carbide catalysts, as described in Chapter 3. In order to avoid confusion about the terms “oxide”, “oxycarbide” and “oxide layer,” each of these terms as used in this thesis is defined in Figure 7.4. An oxide does not contain any carbon atoms. The oxide layer covers the whole surface of the carbide nanoparticle and is formed by e.g. passivation. The oxycarbides are isolated oxide sites on the carbide surface, which can thus not be detected by bulk techniques like XRD or XANES.

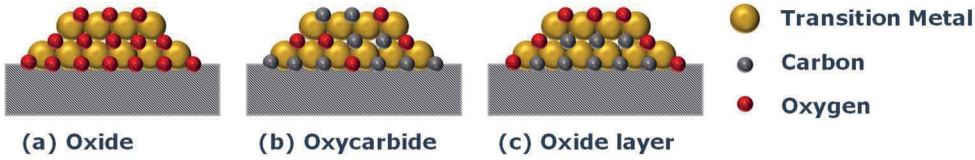

Figure 7.4 Definitions of oxide, oxycarbide and oxide layer

A similar hypothesis regarding the in situ generation of acid sites by water was made by Mortensen et al.[40] The authors studied the stability of ZrO_2 supported Mo_2C catalysts for phenol and 1-octanol HDO in a flow reactor and observed significant catalyst deactivation. The researchers attributed the observed deactivation to the oxidation of the carbide by water, which is formed as a byproduct of the deoxygenation reactions. However, none of the characterization tests used indicated the formation of an intermediate molybdenum oxycarbide phase. To support their hypothesis, Mortenson et al. cofed water in the stability experiments. They found that the presence of water in the feed resulted in faster deactivation due to the formation of a MoO_2 phase. In addition, DFT calculations showed that water can dissociate into H* and OH* (* represents an adsorption site), where the OH* can further dissociate into O* and H* on the Mo carbide surface.[44-46] This is supported by the work of Namiki et al.,[47] who studied the dissociation of water on an Al_2O_3 supported Mo carbide surface during the water-gas shift reaction (WGS). It was found that H_2O dissociated because H_2, $^{13}C^{18}O$, $^{13}C^{18}O_2$ and $^{13}C^{18}O^{16}O$ were formed after the injection of $H_2{}^{18}O$ into the $^{13}C^{16}O$ stream, which most likely resulted in an oxidized carbide surface.

These studies provide evidence of how dynamic the surface composition and the catalytic function of these carbide catalysts are under reaction conditions involving oxygen molecules. Subsequent characterization of the catalysts does not capture the dynamics of the catalyst surface under the reaction conditions. Therefore, assessing the composition of the surface present under reaction conditions under in situ or operando conditions is necessary.[48] These operando or in situ, surface-sensitive experiments are technically challenging for vapor-phase reactions but even more so for liquid-phase reactions as used in this thesis. However, some studies have attempted to establish the surface composition under operando conditions. In the following the different techniques of in situ or operando, surface-sensitive experiments for accessing the oxygen adsorption on the Mo carbide phase are described and compared with existing studies:

(1) In situ/operando XPS: The conventional XPS instrument operates under ultra-high vacuum conditions, which limit the characterization of catalysts in the presence of gases or liquids. However, new types of XPS apparatuses have recently emerged that allow in situ measurements of catalysts in gaseous environments in

the millibar range[48] and even up to several bars (2.5 bars).[49,50] For instance, Murugappan et al.[51] used operando near-ambient pressure XPS (NAP-XPS) to probe the nature of active sites on MoO_3, Mo_2C and passivated Mo_2C catalysts during the HDO of anisole at 320 °C with a H_2 pressure of ≤1 mbar. Although the authors attempted to minimize air exposure, an oxidized layer on the Mo_2C was found prior to the measurements. The reduction of the carbide catalysts (H_2 flow, 320 °C) decreased the oxide layer on the surface layer but did not eliminate it. The NAP-XPS experiments revealed that the surface of fresh Mo_2C is predominantly carbidic in nature (~85% Mo^{2+}) throughout the reaction. However, some oxidic characteristics (~15% total of Mo^{4+}, Mo^{5+} and Mo^{6+}) were present too. It was demonstrated that for passivated Mo_2C more than 80% of the Mo was present in oxidation states higher than 2, and only 20% of the Mo was in the Mo^{2+} oxidation state. Moreover, the Mo in the molybdenum oxide used switched between Mo^{5+} and Mo^{6+} during anisole HDO, which indicates the role of redox chemistry in the HDO reaction. This study clearly shows that operando XPS can be used to probe the oxidation state of the active sites of carbide catalysts during HDO. An advantage of this technique is that it can be used for both bulk and supported carbide catalysts.

(2) In situ chemical titration: Chen et al.[52] and Sullivan et al.[9,37,38] demonstrated the use of in situ chemical titration methods for determining acid catalysis sites. With this method probe molecules such as oxygen, water and methanol are added as cofeed to the pure feed to identify and quantify the acid sites in a reaction. The oxygen cofeed introduces O* sites on the carbide surface and increases the acid site density.

Chen et al. used these technique for the reaction of a benzene/toluene mixture over bulk Mo_2C. A cofeed of methanol or water was added to the vapor-phase hydrogenation reaction and led to a shift towards more acid-site selectivity. Sulivan et al.[37] demonstrated the development of Brønsted acidity on Mo_2C catalysts with the introduction of an O_2 cofeed by selective Brønsted acid titration during isopropanol dehydration, using 2,6-di-tert-butylpyridine (DTBP) at varying acid-site densities. The selective DTBP titration directly demonstrates the presence of Brønsted acid sites on O* modified carbides.

In addition, the extensive review of Sullivan et al.[9] highlights the critical importance of in situ chemical transient and chemical titration studies for assessing the site requirements in carbide materials.[9] To the best of our knowledge, titration studies of supported catalysts have not been undertaken yet. The probe molecule (e.g.,

water or oxygen) might also be adsorbed on the (carbon) support and thus hampering the titration measurements.

(3) In situ/operando surface-sensitive diffuse reflectance infrared Fourier transform spectroscopy (DRIFTS) and Raman spectroscopy: In situ spectroscopy methods have been developed to establish the surface sites of the a catalyst under working conditions.[53,54] Schaidle et al.[55] used in situ DRIFTS (in combination with XPS and DFT calculations) to probe the surface chemistry of Mo_2C the deoxygenation of acetic acid . The Mo_2C surface was found to remain partially oxidized following pretreatment and under reaction conditions, potentially existing as an oxycarbide, and this partially oxidized surface possessed metal-like H adsorption sites, oxygen vacancy sites (exposed Mo sites), and acidic sites.

No study using surface-sensitive Raman spectroscopy or attenuated total reflectance infrared spectroscopy (ATR/FT-IR) to probe the surface chemistry of Mo or W carbide catalysts has been found, although the latter one mentioned would be beneficial as it can be conducted in the liquid phase.[56] It should be noted that these spectroscopy analyses have not received much attention for carbon supported catalysts due to the high background adsorption of the carbon especially for high surface area graphitic carbons.

In summary, the two coexisting functionalities of carbide catalysts, i.e. metallic hydrogenation and acidic dehydration make the carbides excellent deoxygenation catalysts. The acid sites are the result of some form of oxygen adsorption on the carbide surface, which can either be directly introduced after carburization by exposure to air (passivation) or can originate from the in situ generation of O^*-Me_2C species when the catalyst is exposed to the oxygen of the reactant or the water formed. To assess the composition of the surface present under the reaction conditions, in situ surface-sensitive experiments such as XPS and titration are required and must be further developed to explore the active phase of these materials.

3. Influence of mixing W and Mo carbides on catalytic performance and challenges regarding their synthesis

In order to arrive at a certain (desired) catalytic performance, the required (1) nature, (2) density and (3) accessibility of the active sites in the catalyst needs to be realized. These three aspects can be controlled during the catalyst preperation.[57] In the case of the carbon nanofibers (CNF)-supported carbide catalysts used in this study, the nature of the active sites is determined by the

composition and size of the nanoparticles, the density of sites depends on the metal loading, and the accessibility calls upon control of the porosities of the CNF support and the active phase.

For CNF supported tungsten and molybdenum carbides it was shown in chapter 2 and also by other researchers[58] that the crystal structures of the produced phases and the nanoparticle size differ depending on the synthesis method. A cubic carbide (MeC_{1-x}) phase with 3–4 nm nanoparticles was obtained when using the temperature-programmed reduction (TPR) method, while a hexagonal phase (Me_2C) with 4–5 nm nanoparticles was found when using the carbothermal reduction (CR) method. The TPR-synthesized carbides showed higher activity for the hydrodeoxygenation of fatty acids. This higher activity was related to their cubic crystal structure, their particle size, or a combined effect. These results highlight that the nature of the catalyst's preparation has a great impact on the characteristics of the active site and this, in turn, on the catalytic performance.

An issue related to the carbide preparation is the necessary high temperature during the carburization step. Both the TPR and the CR synthesis require careful thermal treatments (e.g., ramp and isotherm) at high carburization temperatures (600–700 °C and 900 °C, respectively). In comparison, noble metal like Pt require lower temperatures, i.e., they are reduced at ~200–300 °C. Therefore, new alternative routes that do not require high temperatures while giving good control over the catalyst properties are desired.

Solution chemistry methods have been applied in which the transition metal precursor and the carbon precursor interact at molecular level.[59] This usually permits lower treatment temperatures and shorter preparation times. For example, Zeng et al.[60] reported the room-temperature reduction of molybdenum and tungsten halides with $LiBEt_3H$, which results in the formation of Mo_2C and W_2C colloids. Unfortunately, this method has not been used for supported nanoparticles yet. Another method to decrease the synthesis temperature is the addition of another metal. This is exemplified in Chapter 2, where it is shown that the addition of Mo to the W carbide lowered the carburization temperature. Similar results have been found by Mehdad et al.[61] who demonstrated that the presence of both niobium and molybdenum salts caused the carburization to occur at lower temperatures in comparison with the synthesis of the pure metal carbides. However, the addition of a second metal can change the catalytic performance, which might not be desired.

One of the main objectives of this thesis was to prepare and characterize supported bimetallic (MoW) carbides. The challenge here is to synthesize a single-phase mixed metal carbide. In Chapter 2, CNF-supported mixed MoW carbides were prepared via **co-impregnation** by

dissolving both the Mo and W salts in water. After impregnation the catalysts were dried at 110 °C and then carburized using the TPR or the CR method. Though both synthesis methods resulted in different crystal structures and nanoparticle sizes. On the nanoscale level all bimetallic catalysts (Mo:W bulk ratios of 1:3, 1:1 and 3:1) showed MoW compositions that are on average close to those of the bulk ratios. This was proven by analysing the synthesis of the carbide via TGA, TPD-MS and XRD and their nanoparticle composition with TEM-EDX, XANES and EXAFS. From the TEM-EDX measurements it was gained that at single-particle level the Mo:W ratio varies, indicating that mixed-phase nanoparticles with heterogeneous composition were formed (see Figure 7.5B). Possibly the precursor salts already form a heterogeneous MoW salt complex during the co-impregnation and drying process. Besides the formation of a heterogeneously mixed phase, two metals can also form homogenously mixed alloys, core-shell alloys or segregated particles (Figure 7.5).[62] In the following, the different preparation methods for supported and bulk bimetallic carbide catalysts and their predicted mixing patterns are discussed and compared with the literature:

(1) **Co-impregnation (supported catalysts):** Co-impregnation is a widely reported method for the synthesis of bimetallic metal catalysts and was also used during this thesis. Here, both metal salts are solved in, e.g., water or ethanol and impregnated in one step onto the support. Additionally, the pH of the aqueous salt solution can be adjusted to ensure better mixing of the metal salts. In this synthesis process homogenously mixed alloyed, heterogeneous mixed alloyed or segregated nanoparticles can be formed.[63] Fu et al.[64] used (wet) co-impregnation for the preparation of MoW carbides. The two metal salts were dissolved in ethanol and the carbon support was added to the solution, stirred and dried in a rotary evaporator. Due to the XRD and EDS results, the author stated that it is highly likely that the obtained nanoparticles consist of "atomically mixed", i.e. homogenously mixed, MoW carbides instead of discrete Mo and W carbides nanoparticles.

(2) **Sequential-impregnation (supported catalysts)**: With this method two or more separate solutions containing different metal salts are prepared and impregnated subsequently. The consecutive deposition of a metal onto another metal nanoparticle can lead to a core-shell structure.[65,66] No example for bimetallic carbides was found, but Pt modified with Mo carbide synthesized by co-impregnation do from Pt/Mo_2C core-shell particles.[67] On the other hand, co-impregnation can also result in segregated particles as has been shown for AgAu bimetallics.[65]

(3) **Co-precipitation (bulk and supported catalysts)**: The first step of this method is to change the pH of the aqueous solution containing the two precursor salts. This change

leads to a simultaneous precipitation of both metals.[2] The obtained particles might be homogenously mixed but can also be enriched in one or the other metal or even be monometallic.[63] Leclercq et al. [68] used this method for the preparation of bulk MoW carbides. Hydrochloride was added dropwise to an ammonium paratungstate and ammonium heptamolybdate solution. After 6 h a precipitate was formed, which was then dried and carburized in the addition of carbon source at 1520 °C. XPS analysis of the mixed MoW carbides shows an accumulation of Mo on the carbide surface. However, the author did not attribute this surface enrichment to the precipitation but to a surface modification occurring during the passivation treatment of the carburization.

(4) **Physical Mixing (bulk catalysts)**: With this method bimetallic oxide precursors are prepared by solid-state fusion of two monometallic oxides. The two monometallics are ground together using mortar and pestle. Ethanol was added to achieve better dispersion. The ground salts are then compressed to remove boundaries between the particles. This method has been used, for instance, to prepare bulk bimetallic NbMo carbide.[69] Depending on the Nb:Mo salt ratio, a homogenous or heterogeneous mixture was formed.

(5) **Freeze drying (bulk catalysts)**: With the freeze drying method, two salts containing the metals are dissolved in water and flash frozen by dropping them into liquid nitrogen.[2] Using this technique Mehdad et al.[70] were able to synthesize single-phase MoW metal carbides.

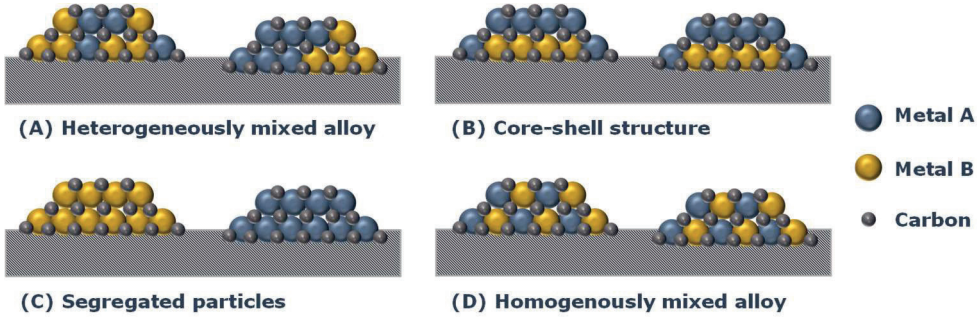

Figure 7.5 Schematic presentation of possible mixing patterns of supported bimetallic nanoparticles. (A) heterogeneously mixed alloy, (B) core-shell structure, (C) segregated particles and (D) homogenously mixed alloy

It should be taken into account that also the drying and carburization process can influence the overall composition of the metal carbides. This possibility was also mentioned by Leclercq et al.,[68] who attributed the surface enrichment of molybdenum to the passivation treatment during carburization.

The addition of a second metal is a strategy to improve the activity, selectivity and stability of a catalyst.[71-74] Fu et al.[64] and Tran et al.[75-77] have shown that the addition of W to Mo carbide enhances the catalytic performance for the electrocatalytic hydrogen evolution reaction and the hydrodeoxygenation of guaiacol and canola oil, respectively. In contrast, the CNF-supported bimetallic MoW used in this thesis does not show an enhanced activity for the hydrodeoxygenation of stearic acid. The carbide catalysts show an activity that lies between that of the monometallic carbides, of which the Mo carbide is more active than W carbide (see Figure 7.2). With respect to selectivity a similar trend was observed: Mixed carbides with higher Mo:W ratio (3:1) reach higher yields of aldehydes and alcohols, while carbides with a lower Mo:W ratio (1:3) yield high concentrations of alkenes.

This section highlights the importance of controlled-synthesis methods for (mixed) carbides to direct physical and chemical parameters. Depending on the method used, the resulting active sites will differ and tune the performance. For this reason it is important to investigate different preparation methods and their influence on the structure and performance of the catalysts to understand this relationship. In addition, more effort should be directed to exploring preparation methods that are efficient and economically feasible.

4. Stability of transition metal carbides

Catalysts are often losing their activity over time, especially in liquid-phase reactions.[78-80] For this reason it is highly important to evaluate the stability of the catalysts during the reaction to understand the deactivation mechanism and to possibly improve the catalytic stability. Commonly, four pathways of catalyst deactivation are defined, i.g., (a) blocking of the active site (e.g. by coke deposition), (b) crystallite growth, (c) leaching and (d) oxidation.[58]

Also in this thesis catalyst deactivation was observed in both the HDO of stearic acid (Chapter 2) and the HYN of cinnamaldehyde (Chapter 4 and 5) reactions. However, due to the nature of the batch reactor, it was challenging to find the cause of this deactivation since multiple subsequent experiments needed to be run, which made it difficult to reuse the catalyst for a second reaction. For this reason, the stability of Mo carbide catalysts in cinnamaldehyde HYN was studied in a plug-flow reactor (Chapter 5). Two different catalysts with different particle sizes (3 nm and 4.5 nm) were synthesized. The carbide particle size was varied by altering the distribution of the metal precursor over the carbon nanofiber support. Interestingly, the Mo carbide catalyst with larger particles is more stable for the hydrogenation reaction of cinnamaldehyde (0.4% deactivation within 40 h), while the smaller particles readily deactivate (63% deactivation within

40 h). The deactivation was attributed to the adsorption of reactant and/or product that block the active site of the catalysts and to particle growth.

Deactivation due to particle growth is irreversible and detrimental in the long term. There are two major routes that lead to particle growth: (a) coalescence (or particle diffusion) and (b) Ostwald ripening (Figure 7.6).[81] [82] During coalescence, two smaller particles merge to form a bigger one or a bigger particle develops from species moving over the surface of the support. This process is also often reported as sintering. The second mechanism, Ostwald ripening, is based on interparticle migration. Molecules or atoms dissolve into solution or evaporate into the gas phase and precipitate onto a larger particle. The increase in particle size of the Mo carbides in the hydrogenation reaction has been explained by the Ostwald ripening mechanism based on the fact that small quantities of Mo were found to leach into the reaction solution. Further investigations are required to prove this and to understand the exact mechanism of Ostwald ripening for carbide nanoparticles, e.g., to determine if the carbon and Mo dissolve separately or combinedly. In situ TEM is a tool for observing particle growth, although the liquids and gases used for the reaction are incompatible with the high-vacuum environment required for TEM measurements.[83] Nevertheless, advancements in the in situ TEM techniques made it possible to conduct particle growth studies under conditions approaching reaction conditions (albeit limited in pressure) and to determine the particle growth route. For instance, Simonsen et al.[84] studied the Ostwald ripening in Pt/SiO_2 model catalysts at temperatures up to 650 °C under 10 mbar air pressure. In a similar way Luo et al.[85] observed particle migration and coalescence for Pt supported on carbon nanotubes exposed to O_2 and H_2O gas, at 0.01 mbar and 100 °C.

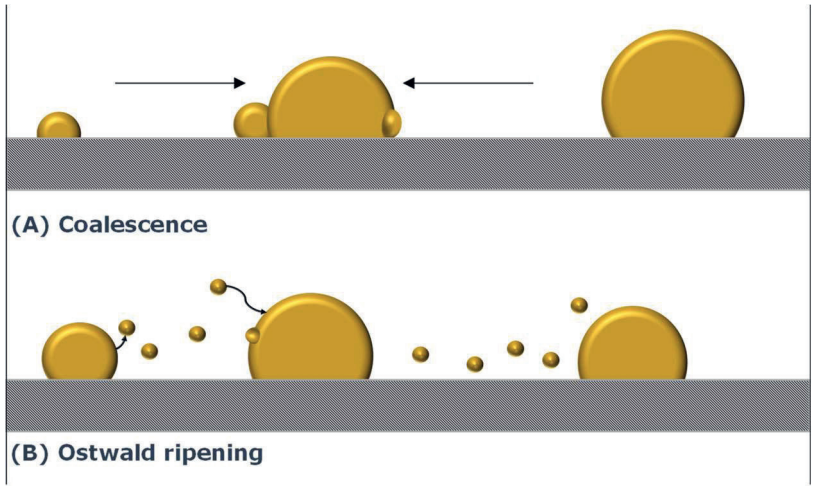

Figure 7.6 Particle growth mechanisms: (A) coalescence and (B) Ostwald ripening

In summary, carbide catalysts are prone to deactivation in liquid phase reactions, with particle growth being one of the main deactivation mechanisms. However, the exact mechanism of particle growth of Mo and W carbides has not been assessed. Nevertheless, this thesis shows in the case of hydrogenation of cinnamaldehyde that Mo carbide nanoparticles of 4–5 nm are significantly more stable than those of 3–4 nm.

Summary and recommendations

Transition metal carbide catalysts can play an important role for the realization of at least two of the twelve principles of green chemistry.[86,87] One of those two is principle 9, which is the "general use of catalysis" to reduce the amount of waste often generated when using stoichiometric reagents and to increase the energy efficiency of the reaction. In this respect Mo and W carbide materials belong to an interesting class of catalysts as they are efficient and selective catalysts based on abundant elements. The other principle is "the use of renewable feedstocks" (principle 7). We have shown that carbide materials are efficient catalysts for biomass conversion reactions, such as HYN and HDO. Thus, carbide catalysts could play an important role in the shift from a fossil-based chemical industry to a more sustainable, bio-based industry by using renewable biomass as raw material.

However, no major industrial application of Mo and W carbide catalysts has been developed yet.[1] Since the seminal work of Boudart and Levi, many successes regarding the preparation, utilization and understanding of the catalytic behaviour of molybdenum and tungsten carbide have been achieved, although there is still a significant amount of work to be done to apply these carbides for HYN and HDO reactions on a larger scale.[88] In the following, three recommendations regarding further fundamental and applied research are presented.

(1) The development of **a controlled-synthesis method** for monometallic and mixed carbide is required to control physical and chemical parameters, like particle size, surface structure and crystalline structure. Further investigations in this area will advance the understanding of the structure-performance relationship. Additionally, preparation methods that are both efficient and economically feasible (e.g., lower carburization temperatures) should be explored to meet the requirements for industrial applications.

(2) The development of **more in situ/operando characterization** techniques, like spectroscopic and imaging techniques, is recommended for exploring the active phase under reaction conditions. Especially, the development of in situ surface-sensitive experiments might be beneficial for the understanding of bifunctional properties of the acid and metallic sites.

(3) **The stability and recyclability** of carbide catalysts has been studied on model reactions, whereas tests **on the pilot-scale** for primary potential applications, e.g., hydrogenation and hydrodeoxygenation reactions, for long-term operation have to the best of our knowledge not been carried out. These tests would be valuable for the commercialization of carbide catalysts.

Concluding remarks

This thesis targeted the development of Mo, W and bimetallic MoW carbide catalysts for hydrodeoxygenation and hydrogenation reactions in biomass feedstock conversion. New insights into the preparation and characteristics of Mo, W and MoW transition metal carbides were gained, which led to a better understanding of the relationship between the catalysts' properties and their performances. Especially with regard to the preparation**,** the characteristics (Chapter 2) and the behaviour (Chapter 3) of bimetallic MoW carbides, this thesis achieved a deeper insight. In **Chapter 2**, the synthesis of carbon nanofiber-supported, mixed MoW carbides via CR and TPR methods was investigated. It was found that, irrespective of the synthesis method used, all bimetallic catalysts (Mo:W bulk ratios of 1:3, 1:1 and 3:1) show compositions on the nanoscale level that are close to those of the bulk ratios. However, the crystal structure and the particle size depend on the synthesis method. A cubic carbide (MeC_{1-x}) phase with 3–4 nm nanoparticles was obtained when using the TPR method, while a hexagonal (Me_2C) phase with 4–5 nm nanoparticles was found when using the CR method. The activity of these bimetallic carbides synthesized via TPR method is higher than that of the CR-synthesized bimetallic carbides. These results indicate that both the crystal structure and particle size have an impact on the catalytic performance. In **Chapter 3**, the catalytic selectivity of the bimetallic carbides was investigated. Both the monometallic W and Mo carbides and the bimetallic MoW carbides (with different ratios) prefer the HDO pathway over the DCO pathway. The Mo:W ratio was found to shift the intermediate product yield towards either oxygenates or alkenes in the HDO pathway. The more Mo rich samples deliver a higher yield of intermediate oxygenates, while the more W rich samples result in higher yields of alkene intermediate. The behaviour of the 1:1 MoW carbide was found to be similar to a physical mixture of monometallic Mo and W carbides.

In addition, **Chapter 4** dealt with the potential of carbon supported Mo and W carbides for replacing Pt for the hydrogenation of cinnamaldehyde. The carbide catalysts, like Pt, favour the hydrogenation of the C=C bond to produce hydrocinnamaldehyde, especially at higher reaction temperatures, although the carbides are slightly less active. In **Chapter 5**, the utilization of tungsten and molybdenum carbide catalysts for the HYN of cinnamaldehyde in a plug flow reactor was reported for the first time. The obtained results will broaden the understanding and, thus,

the commercial usability of the carbide catalysts. It was demonstrated that Mo carbide with larger nanoparticle sizes are more stable in the cinnamaldehyde hydrogenation. The increase in stability for larger particles was shown to be due to an improved resistance against particle growth and site blocking of carbonaceous species.

In **Chapter 6** we argue that molybdenum and tungsten carbide hold great potential for the catalytic conversions of future feedstocks due to their ability to remain active in the presence of impurities in the feedstock. Based on thermodynamic arguments carbide catalysts might change the nature of their active site when used in the presence of S and N impurities during the processing of crude oil or renewable feedstock. However, they can remain catalytically active since the sulfide and nitride phases also possess activity for the same type of reactions. This distinguishes them from noble metal catalysts which quickly deactivate in the presence of sulfur or nitrogen containing compounds.

Hence, this thesis contributed to a deeper understanding of carbide catalyst preparation, characterization and performance. The improved insight can help to advance the application of more abundant and sustainable catalysts for the use in biomass upgrading reactions and to meet the principles of green chemistry.

References

(1) Lloyd, L. Handbook of industrial catalysts. *Springer* **2006**, DOI:10.1007/978-0-387-49962-8 10.1007/978-0-387-49962-8.

(2) Mehdad, A. Mixed metal carbides: understanding the synthesis, surface properties and catalytic activities. **2015**.

(3) Bullock, R. M.; Chen, J. G.; Gagliardi, L.; Chirik, P. J.; Farha, O. K.; Hendon, C. H.; Jones, C. W.; Keith, J. A.; Klosin, J.; Minteer, S. D. Using nature's blueprint to expand catalysis with Earth-abundant metals. *Science* **2020,** *369* (6505), eabc3183.

(4) Führer, M.; van Haasterecht, T.; Bitter, J. Molybdenum and tungsten carbides can shine too. *Catalysis Science & Technology* **2020**.

(5) Feng, J. P.; Liu, J. J.; Tang, M. X.; Zhou, L. G.; Zhang, X. Y.; Wen, X. D.; Ge, H.; Li, D. B.; Li, X. K. Effect of sulfur-carbon interaction on sulfur poisoning of Ni/Al2O3 catalysts for hydrogenation. *Int. J. Hydrog. Energy* **2017,** *42* (10), 6727.

(6) Lott, P.; Eck, M.; Doronkin, D. E.; Zimina, A.; Tischer, S.; Popescu, R.; Belin, S.; Briois, V.; Casapu, M.; Grunwaldt, J.-D. Understanding Sulfur Poisoning of Bimetallic Pd-Pt Methane Oxidation Catalysts and their Regeneration. *Applied Catalysis B: Environmental* **2020**, 119244.

(7) Mancino, G.; Cimino, S.; Lisi, L. Sulphur poisoning of alumina supported Rh catalyst during dry reforming of methane. *Catal Today* **2016,** *277*, 126.

(8) Furimsky, E. Metal carbides and nitrides as potential catalysts for hydroprocessing. *Applied Catalysis A: General* **2003,** *240* (1–2), 1.

(9) Sullivan, M. M.; Chen, C. J.; Bhan, A. Catalytic deoxygenation on transition metal carbide catalysts. *Catalysis Science and Technology* **2016,** *6* (3), 602.

(10) Iglesia, E.; Baumgartner, J. E.; Ribeiro, F. H.; Boudart, M. Bifunctional Reactions of Alkanes on Tungsten Carbides Modified by Chemisorbed Oxygen. *Journal of Catalysis* **1991,** *131* (2), 523.

(11) Szymanska-Kolasa, A.; Lewandowski, M.; Sayag, C.; Brodzki, D.; Djega-Mariadassou, G. Comparison between tungsten carbide and molybdenum carbide for the hydrodenitrogenation of carbazole. *Catal Today* **2007,** *119* (1-4), 35.

(12) Wang, H.; Liu, S.; Smith, K. J. Understanding selectivity changes during hydrodesulfurization of dibenzothiophene on Mo2C/carbon catalysts. *Journal of Catalysis* **2019,** *369*, 427.

(13) Akopyan, A. V.; Polikarpova, P. D.; Forofontova, O. I.; Levin, I. S.; Mnatsakanyan, R. A.; Davtyan, D. A.; Zurnachyan, A. R.; Anisimov, A. V.; Karakhanov, E. A. Hydrogenation of Alkenes on Molybdenum and Tungsten Carbides. *Theor. Found. Chem. Eng.* **2020,** *54* (5), 1045.

(14) Kumar, A.; Phadke, S.; Bhan, A. Acetic acid hydrodeoxygenation on molybdenum carbide catalysts. *Catalysis Science and Technology* **2018,** *8* (11), 2938.

(15) Levy, R. B.; Boudart, M. Platinum-Like Behavior of Tungsten Carbide in Surface Catalysis. *Science* **1973,** *181* (4099), 547.

(16) Sinfelt, J. H.; Yates, D. J. C. Effect of Carbiding on the Hydrogenolysis Activity of Molybdenum. *Nature Physical Science* **1971,** *229* (1), 27.

(17) Iglesia, E.; Ribeiro, F. H.; Boudart, M.; Baumgartner, J. E. Synthesis, Characterization, and Catalytic Properties of Clean and Oxygen-Modified Tungsten Carbides. *Catal Today* **1992,** *15* (2), 307.

(18) Oyama, S. Preparation and catalytic properties of transition metal carbides and nitrides. *Catal Today* **1992,** *15* (2), 179.

(19) Chen, J. G. Carbide and nitride overlayers on early transition metal surfaces: preparation, characterization, and reactivities. *Chemical reviews* **1996,** *96* (4), 1477.

(20) Munkajohnpong, P.; Kesornpun, C.; Buttranon, S.; Jaroensuk, J.; Weeranoppanant, N.; Chaiyen, P. Fatty alcohol production: an opportunity of bioprocess. *Biofuels, Bioproducts and Biorefining* **2020,** *14* (5), 986.

(21) Biermann, U.; Bornscheuer, U.; Meier, M. A.; Metzger, J. O.; Schäfer, H. J. Oils and fats as renewable raw materials in chemistry. *Angewandte Chemie International Edition* **2011,** *50* (17), 3854.

(22) Ribeiro, F. H.; Betta, R. A. D.; Boudart, M.; Baumgartner, J.; Iglesia, E. Reactions of Neopentane, Methylcyclohexane, and 3,3-Dimethylpentane on Tungsten Carbides - the Effect of Surface Oxygen on Reaction Pathways. *Journal of Catalysis* **1991,** *130* (1), 86.

(23) Blekkan, E. A.; Pham-Huu, C.; Ledoux, M. J.; Guille, J. Isomerization of n-Heptane on an Oxygen-Modified Molybdenum Carbide Catalyst. *Industrial and Engineering Chemistry Research* **1994,** *33* (7), 1657.

(24) Liu, S. D.; Wang, H. Y.; Smith, K. J.; Kim, C. S. Hydrodeoxygenation of 2-Methoxyphenol over Ru, Pd, and Mo2C Catalysts Supported on Carbon. *Energy & Fuels* **2017,** *31* (6), 6378.

(25) Führer, M.; van Haasterecht, T.; Bitter, J. H. Cinnamaldehyde hydrogenation over carbon supported molybdenum and tungsten carbide catalysts. *Chem Commun* **2022**, DOI:10.1039/D2CC05322E 10.1039/D2CC05322E.

(26) Porosoff, M. D.; Yang, X.; Boscoboinik, J. A.; Chen, J. G. Molybdenum carbide as alternative catalysts to precious metals for highly selective reduction of CO<inf>2</inf>to CO. *Angewandte Chemie - International Edition* **2014,** *53* (26), 6705.

(27) Stellwagen, D. R.; Bitter, J. H. Structure–performance relations of molybdenum-and tungsten carbide catalysts for deoxygenation. *Green Chemistry* **2015,** *17* (1), 582.

(28) Seber, G.; Malina, R.; Pearlson, M. N.; Olcay, H.; Hileman, J. I.; Barrett, S. R. Environmental and economic assessment of producing hydroprocessed jet and diesel fuel from waste oils and tallow. *Biomass and Bioenergy* **2014,** *67*, 108.

(29) Donnis, B.; Egeberg, R. G.; Blom, P.; Knudsen, K. G. Hydroprocessing of bio-oils and oxygenates to hydrocarbons. Understanding the reaction routes. *Topics in Catalysis* **2009,** *52* (3), 229.

(30) Macedo, L. S., Wageningen University and Research, 2019.

(31) Kozuch, S.; Martin, J. M.; ACS Publications, 2012; Vol. 2.
(32) Lange, J.-P. Fuels and chemicals manufacturing; guidelines for understanding and minimizing the production costs. *Cattech* **2001,** *5* (2), 82.
(33) Fuhrer, M.; van Haasterecht, T.; Bitter, H. Cinnamaldehyde hydrogenation over carbon supported molybdenum and tungsten carbide catalysts. *Chem Commun* **2022**, DOI:10.1039/D2CC05322E 10.1039/D2CC05322E.
(34) Liu, N.; Rykov, S.; Chen, J. A comparative surface science study of carbide and oxycarbide: the effect of oxygen modification on the surface reactivity of C/W (1 1 1). *Surf Sci* **2001,** *487* (1-3), 107.
(35) Ribeiro, F. H.; Boudart, M.; Dallabetta, R. A.; Iglesia, E. Catalytic Reactions of Normal-Alkanes on Beta-W2c and Wc - the Effect of Surface Oxygen on Reaction Pathways. *Journal of Catalysis* **1991,** *130* (2), 498.
(36) Sullivan, M. M.; Bhan, A. Effects of oxygen coverage on rates and selectivity of propane-CO2 reactions on molybdenum carbide. *Journal of Catalysis* **2018,** *357*, 195.
(37) Sullivan, M. M.; Bhan, A. Acid site densities and reactivity of oxygen-modified transition metal carbide catalysts. *Journal of Catalysis* **2016,** *344*, 53.
(38) Sullivan, M. M.; Bhan, A. Acetone Hydrodeoxygenation over Bifunctional Metallic–Acidic Molybdenum Carbide Catalysts. *ACS Catalysis* **2016,** *6* (2), 1145.
(39) Sullivan, M. M.; Held, J. T.; Bhan, A. Structure and site evolution of molybdenum carbide catalysts upon exposure to oxygen. *Journal of Catalysis* **2015,** *326*, 82.
(40) Mortensen, P. M.; de Carvalho, H. W. P.; Grunwaldt, J.-D.; Jensen, P. A.; Jensen, A. D. Activity and stability of Mo2C/ZrO2 as catalyst for hydrodeoxygenation of mixtures of phenol and 1-octanol. *Journal of Catalysis* **2015,** *328*, 208.
(41) Jongerius, A. L.; Gosselink, R. W.; Dijkstra, J.; Bitter, J. H.; Bruijnincx, P. C. A.; Weckhuysen, B. M. Carbon Nanofiber Supported Transition-Metal Carbide Catalysts for the Hydrodeoxygenation of Guaiacol. *ChemCatChem* **2013,** *5* (10), 2964.
(42) Chen, C. J.; Bhan, A. Mo2C Modification by CO2, H2O, and O-2: Effects of Oxygen Content and Oxygen Source on Rates and Selectivity of m-Cresol Hydrodeoxygenation. *Acs Catalysis* **2017,** *7* (2), 1113.
(43) Jongerius, A. L.; Bruijnincx, P. C. A.; Weckhuysen, B. M. Liquid-phase reforming and hydrodeoxygenation as a two-step route to aromatics from lignin. *Green Chemistry* **2013,** *15* (11), 3049.
(44) Liu, P.; Rodriguez, J. A. Water-Gas-Shift Reaction on Molybdenum Carbide Surfaces: Essential Role of the Oxycarbide. *The Journal of Physical Chemistry B* **2006,** *110* (39), 19418.
(45) Medford, A. J.; Vojvodic, A.; Studt, F.; Abild-Pedersen, F.; Norskov, J. K. Elementary steps of syngas reactions on Mo2C(0 0 1): Adsorption thermochemistry and bond dissociation. *Journal of Catalysis* **2012,** *290*, 108.
(46) Tominaga, H.; Nagai, M. Density functional theory of water– gas shift reaction on molybdenum carbide. *The Journal of Physical Chemistry B* **2005,** *109* (43), 20415.
(47) Namiki, T.; Yamashita, S.; Tominaga, H.; Nagai, M. Dissociation of CO and H2O during water–gas shift reaction on carburized Mo/Al2O3 catalyst. *Applied Catalysis A: General* **2011,** *398* (1), 155.
(48) Zhong, L.; Chen, D.; Zafeiratos, S. A mini review of in situ near-ambient pressure XPS studies on non-noble, late transition metal catalysts. *Catalysis Science & Technology* **2019,** *9* (15), 3851.
(49) Amann, P.; Degerman, D.; Lee, M.-T.; Alexander, J. D.; Shipilin, M.; Wang, H.-Y.; Cavalca, F.; Weston, M.; Gladh, J.; Blom, M. A high-pressure x-ray photoelectron spectroscopy instrument for studies of industrially relevant catalytic reactions at pressures of several bars. *Review of Scientific Instruments* **2019,** *90* (10), 103102.
(50) Kalha, C.; Fernando, N. K.; Bhatt, P.; Johansson, F. O.; Lindblad, A.; Rensmo, H.; Medina, L. Z.; Lindblad, R.; Siol, S.; Jeurgens, L. P. Hard x-ray photoelectron spectroscopy: a snapshot of the state-of-the-art in 2020. *Journal of Physics: Condensed Matter* **2021,** *33* (23), 233001.
(51) Murugappan, K.; Anderson, E. M.; Teschner, D.; Jones, T. E.; Skorupska, K.; Román-Leshkov, Y. Operando NAP-XPS unveils differences in MoO3 and Mo2C during hydrodeoxygenation. *Nature Catalysis* **2018,** *1* (12), 960.
(52) Chen, C. J.; Lee, W. S.; Bhan, A. Mo2/C catalyzed vapor phase hydrodeoxygenation of lignin-derived phenolic compound mixtures to aromatics under ambient pressure. *Applied Catalysis A: General* **2016,** *510*, 42.
(53) Urakawa, A.; Maeda, N.; Baiker, A. Space-and Time-Resolved Combined DRIFT and Raman Spectroscopy: Monitoring Dynamic Surface and Bulk Processes during NOx Storage Reduction. *Angewandte Chemie* **2008,** *120* (48), 9396.
(54) Kale, M. J.; Christopher, P. Utilizing quantitative in situ FTIR spectroscopy to identify well-coordinated Pt atoms as the active site for CO oxidation on Al2O3-supported Pt catalysts. *ACS Catalysis* **2016,** *6* (8), 5599.
(55) Schaidle, J. A.; Blackburn, J.; Farberow, C. A.; Nash, C.; Steirer, K. X.; Clark, J.; Robichaud, D. J.; Ruddy, D. A. Experimental and Computational Investigation of Acetic Acid Deoxygenation over Oxophilic Molybdenum Carbide: Surface Chemistry and Active Site Identity. *ACS Catalysis* **2016,** *6* (2), 1181.
(56) Huber, G. W.; Shabaker, J. W.; Evans, S. T.; Dumesic, J. A. Aqueous-phase reforming of ethylene glycol over supported Pt and Pd bimetallic catalysts. *Applied Catalysis B: Environmental* **2006,** *62* (3-4), 226.
(57) Hanefeld, U.; Lefferts, L. *Catalysis: An integrated textbook for students*; John Wiley & Sons, 2018.
(58) Macedo, L. S.; Stellwagen, D. R.; da Silva, V. T.; Bitter, J. H. Stability of Transition-metal Carbides in Liquid Phase Reactions Relevant for Biomass-Based Conversion. *Chemcatchem* **2015,** *7* (18), 2816.
(59) Liu, X.; Pajares, A.; Matienzo, D. D. C.; de la Piscina, P. R.; Homs, N. Preparation and characterization of bulk MoXC catalysts and their use in the reverse water-gas shift reaction. *Catal Today* **2020,** *356*, 384.
(60) Zeng, D.; Hampden-Smith, M. J. Room-temperature synthesis of molybdenum and tungsten carbides, Mo2C and W2C, via chemical reduction methods. *Chemistry of Materials* **1992,** *4* (5), 968.
(61) Mehdad, A.; Jentoft, R. E.; Jentoft, F. C. Single-phase mixed molybdenum-niobium carbides: Synthesis, characterization and multifunctional catalytic behavior in toluene conversion. *Journal of catalysis* **2017,** *351*, 161.
(62) de Jong, K. P. *Synthesis of solid catalysts*; John Wiley & Sons, 2009.
(63) Hermans, S. In *Atomically-Precise Methods for Synthesis of Solid Catalysts*; Royal Society of Chemistry, 2014.

(64) Fu, Q.; Peng, B. X.; Masa, J.; Chen, Y. T.; Xia, W.; Schuhmann, W.; Muhler, M. Synergistic Effect of Molybdenum and Tungsten in Highly Mixed Carbide Nanoparticles as Effective Catalysts in the Hydrogen Evolution Reaction under Alkaline and Acidic Conditions. *Chemelectrochem* **2020,** *7* (4), 983.
(65) Loza, K.; Heggen, M.; Epple, M. Synthesis, structure, properties, and applications of bimetallic nanoparticles of noble metals. *Advanced functional materials* **2020,** *30* (21), 1909260.
(66) Romero-Sáez, M.; Dongil, A.; Benito, N.; Espinoza-González, R.; Escalona, N.; Gracia, F. CO2 methanation over nickel-ZrO2 catalyst supported on carbon nanotubes: A comparison between two impregnation strategies. *Applied Catalysis B: Environmental* **2018,** *237*, 817.
(67) Kelly, T. G.; Lee, K. X.; Chen, J. G. Pt-modified molybdenum carbide for the hydrogen evolution reaction: From model surfaces to powder electrocatalysts. *Journal of Power Sources* **2014,** *271*, 76.
(68) Leclercq, L.; Provost, M.; Pastor, H.; Grimblot, J.; Hardy, A. M.; Gengembre, L.; Leclercq, G. Catalytic properties of transition metal carbides: I. Preparation and physical characterization of bulk mixed carbides of molybdenum and tungsten. *Journal of Catalysis* **1989,** *117* (2), 371.
(69) Yu, C. C.; Ramanathan, S.; Dhandapani, B.; Chen, J. G.; Oyama, S. T. Bimetallic Nb−Mo Carbide Hydroprocessing Catalysts: Synthesis, Characterization, and Activity Studies. *The Journal of Physical Chemistry B* **1997,** *101* (4), 512.
(70) Mehdad, A.; Jentoft, R. E.; Jentoft, F. C. Single-phase mixed molybdenum-tungsten carbides: Synthesis, characterization and catalytic activity for toluene conversion. *Catal Today* **2019,** *323*, 112.
(71) Gao, L.; Liu, J.; Long, H.; Wang, P.; Yu, H. One-step calcination synthesis of WC-Mo2C heterojunction nanoparticles as novel H2-production cocatalysts for enhanced photocatalytic activity of TiO2. *Catalysis Science and Technology* **2021,** *11* (22), 7307.
(72) Duan, Y.; Yu, Z.-Y.; Yang, L.; Zheng, L.-R.; Zhang, C.-T.; Yang, X.-T.; Gao, F.-Y.; Zhang, X.-L.; Yu, X.; Liu, R. Bimetallic nickel-molybdenum/tungsten nanoalloys for high-efficiency hydrogen oxidation catalysis in alkaline electrolytes. *Nature communications* **2020,** *11* (1), 1.
(73) Robinson, A.; Ferguson, G. A.; Gallagher, J. R.; Cheah, S.; Beckham, G. T.; Schaidle, J. A.; Hensley, J. E.; Medlin, J. W. Enhanced Hydrodeoxygenation of m-Cresol over Bimetallic Pt–Mo Catalysts through an Oxophilic Metal-Induced Tautomerization Pathway. *ACS Catalysis* **2016,** *6* (7), 4356.
(74) Han, C. W.; Majumdar, P.; Marinero, E. E.; Aguilar-Tapia, A.; Zanella, R.; Greeley, J.; Ortalan, V. Highly stable bimetallic AuIr/TiO2 catalyst: physical origins of the intrinsic high stability against sintering. *Nano Letters* **2015,** *15* (12), 8141.
(75) Tran, C. C.; Hang, Y. L.; Garcia-Perez, M.; Kaliaguine, S. Synergistic effect of Mo-W carbides on selective hydrodeoxygenation of guaiacol to oxygen-free aromatic hydrocarbons. *Catalysis Science & Technology* **2019,** *9* (6), 1387.
(76) Tran, C.-C.; Akmach, D.; Kaliaguine, S. Hydrodeoxygenation of vegetable oils over biochar supported bimetallic carbides for producing renewable diesel under mild conditions. *Green Chemistry* **2020**.
(77) Tran, C.-C.; Mohan, O.; Banerjee, A.; Mushrif, S. H.; Kaliaguine, S. A Combined Experimental and DFT Investigation of Selective Hydrodeoxygenation of Guaiacol over Bimetallic Carbides. *Energy & Fuels* **2020,** *34* (12), 16265.
(78) Besson, M.; Gallezot, P. Deactivation of metal catalysts in liquid phase organic reactions. *Catal Today* **2003,** *81* (4), 547.
(79) van Haasterecht, T.; Ludding, C. C. I.; de Jong, K. P.; Bitter, J. H. Stability and activity of carbon nanofiber-supported catalysts in the aqueous phase reforming of ethylene glycol. *Journal of Energy Chemistry* **2013,** *22* (2), 257.
(80) Sádaba, I.; Granados, M. L.; Riisager, A.; Taarning, E. Deactivation of solid catalysts in liquid media: the case of leaching of active sites in biomass conversion reactions. *Green Chemistry* **2015,** *17* (8), 4133.
(81) van Haasterecht, T.; Swart, M.; de Jong, K. P.; Bitter, J. H. Effect of initial nickel particle size on stability of nickel catalysts for aqueous phase reforming. *Journal of Energy Chemistry* **2016,** *25* (2), 289.
(82) Van Haasterecht, T.; Ludding, C.; De Jong, K.; Bitter, J. Toward stable nickel catalysts for aqueous phase reforming of biomass-derived feedstock under reducing and alkaline conditions. *Journal of Catalysis* **2014,** *319*, 27.
(83) Madoud, N. The Stability of Supported Gold Catalysts. **2018**.
(84) Simonsen, S. B.; Chorkendorff, I.; Dahl, S.; Skoglundh, M.; Sehested, J.; Helveg, S. Ostwald ripening in a Pt/SiO2 model catalyst studied by in situ TEM. *Journal of catalysis* **2011,** *281* (1), 147.
(85) Luo, L.; Engelhard, M. H.; Shao, Y.; Wang, C. Revealing the Dynamics of Platinum Nanoparticle Catalysts on Carbon in Oxygen and Water Using Environmental TEM. *ACS Catalysis* **2017,** *7* (11), 7658.
(86) Anastas, P. T.; Warner, J. C. *Green Chemistry: Theory and Practice*; Oxford University Press, 1998.
(87) Anastas, P. T.; Kirchhoff, M. M. Origins, current status, and future challenges of green chemistry. *Accounts Chem. Res.* **2002,** *35* (9), 686.
(88) Deng, Y. C.; Ge, Y. Z.; Xu, M.; Yu, Q. L.; Xiao, D. Q.; Yao, S. Y.; Ma, D. Molybdenum Carbide: Controlling the Geometric and Electronic Structure of Noble Metals for the Activation of O-H and C-H Bonds. *Accounts Chem. Res.* **2019,** *52* (12), 3372.

Summary

Molybdenum and tungsten carbides can catalyse a wide range of reactions that are typically catalysed by noble metals such as platinum. For example, Mo and W carbides are viable catalysts for the hydrodeoxygenation of fatty acids and the hydrogenation of cinnamaldehyde, as shown here in this thesis. Despite the great potential of transition metal carbides, these carbides currently make up only a small group of catalysts. This is most likely due to their limited stability, their cumbersome preparation, and the lack of understanding of the relationship between properties and their performance. This thesis provides insights into the preparation and characteristics of Mo, W and MoW transition metal carbides which led to a deeper understanding of the relationship between catalysts properties and their performances.

Chapter 1 provides a general introduction to molybdenum and tungsten carbide as viable replacements for noble metals for biomass upgrading reactions. First, the advantages of carbide catalysts over noble metals are summarized: the abundance of Mo and W, the tolerance of carbides against S and N impurities in the feedstock and their catalytic activity for hydrogen transfer reactions. In addition, an overview of the different preparation and characterisation techniques of Mo and W carbides is given. Finally, the advantages and disadvantages of batch versus plug flow reactors were discussed with respect to the reusability and stability of the carbides.

Supported transition metal carbides like tungsten and molybdenum carbides are efficient catalysts for decarboxylation/decarbonylation and hydrodeoxygenation of triglyceride-based feedstock to alkanes and alkenes. Interestingly, when comparing supported W-carbide to supported Mo-carbide catalysts the former ones were more selective (>50%) towards alkenes, while the latter were more active but less selective to the (at that time) desired alkenes. In **Chapter 2 & 3**, we established to which extent we can combine the properties of both W-carbide and Mo carbide by using mixed MoW-carbides. However, for this, we first need to investigate to which extent we can mix these carbides.

In **Chapter 2** we investigated the synthesis and characterisation of supported bimetallic MoW carbide catalysts. Two different synthesis methods (temperature-programmed reduction and carbothermal reduction) were used to synthesise a series of bimetallic MoW catalysts with different Mo and W ratios (Mo:W bulk ratios of 1:3, 1:1 and 3:1). We found that both synthesis methods resulted in mixed bimetallic (MoW) carbide phases. Irrespective of the synthesis method, all bimetallic catalysts show compositions on the nanoscale level that are close to those

of the bulk ratios. The crystalline phases and the particle size differ depending on the synthesis method. A cubic carbide (MeC_{1-x}) phase with smaller particles (3-4 nm) was obtained when using the temperature-programmed reduction method whereas a hexagonal phase (Me_2C) with larger nanoparticles (4-5 nm) was obtained when using the carbothermal reduction method for all Mo:W ratio (1:3, 1:1 and 3:1). The TPR-synthesized carbides showed higher activity for the hydrodeoxygenation of fatty acids. This higher activity of the TPR samples was tentatively related to the cubic crystal structure, particle size or a combination of those two effects.

In **Chapter 3**, we studied the catalytic performance of MoW mixed metal carbides in the stearic acid deoxygenation. It was shown that the Mo:W ratio in bimetallic carbide can steer the product yield towards either aldehydes, alcohols, alkenes or alkanes. The mixed carbides with a higher Mo/W ratio (3:1) reached higher yields towards aldehydes and alcohols, while the carbides with a lower Mo/W (1:3) ratio yielded high concentrations of alkenes. The intrinsic activity (turnover frequency (TOF)) of the catalysts was both assessed based on H_2 and CO density site chemisorption. The TOF_{H2} relates linearly with the Mo/W ratio while the TOF_{CO} did not show a relevant relationship. Therefore, H_2-chemisorption is suggested as the preferred way to assess the intrinsic activities of these catalysts.

Although molybdenum and tungsten carbides have been shown to be active for hydrogenation reactions, their potential for chemoselective hydrogenations has not been often studied. Selective hydrogenations are often exemplified by cinnamaldehyde hydrogenation towards either unsaturated alcohols (cinnamyl alcohol) or saturated aldehydes (hydrocinnamaldehyde) primarily with noble metal catalysts. In **Chapter 4**, the potential of carbon-supported Mo and W carbides to replace Pt is shown for the hydrogenation of cinnamaldehyde**.** The carbide catalysts and Pt, both favour the hydrogenation of the C=C bond to produce the saturated aldehydes, although the carbides were less active. The main difference between Pt and the carbide was the high selectivity towards β -methylstyrene with the carbide catalysts.

Motivated by these findings we investigated in **Chapter 5** the stability of Mo carbides during the hydrogenation reaction in a plug flow reactor. It was demonstrated that the carbide nanoparticle size is a critical factor for the stability in the cinnamaldehyde hydrogenation. The Mo carbide with larger nanoparticles (4-5 nm) showed enhanced stability, in comparison to the Mo catalysts with smaller nanoparticles (3-4 nm). The deactivation of the catalysts was ascribed to particle growth and site blocking by a carbonaceous species.

Chapter 6 is a perspective in which we argue that molybdenum and tungsten carbides hold great potential, as replacements for noble metals, for future catalytic conversions due to their

capability/ability to remain active in the presence of impurities/poisons in the feedstock. Especially N and S impurities, found in fossil-based feed and to a certain extent also in new renewable feedstocks (such as biomass), might convert the carbides to their respective nitrides or sulphides. These phases are catalytic active for similar reactions as the carbides and do not lead to complete catalyst deactivation as likely for noble metals. To unlock the full potential of the carbide-based catalysts studies focusing on real feedstock and on the role of hetero atoms during the processing of fossil and novel feedstock are required though.

Chapter 7 provides a general discussion of the most important achievements that are outlined within this thesis. Special attention is given to suggestions for future research e.g. to develop controlled-synthesis methods and more *in situ/operando* characterisation (to establish oxycarbide surfaces) and to focus on the stability of carbide catalysts.

Acknowledgement

The past four years of my research at the Biobased Chemistry and Technology (BCT) group here in Wageningen have been a great experience. I have learned to be an independent researcher and to value the work and expertise of others. Writing this thesis would not have been possible without the support, inspiration and help of people whom I had the privilege to work with and whom I'd like to thank. And of course, this starts with my (co-)promotors.

Harry, first of all, I would like to thank you for giving me the opportunity to do a PhD in your group and having the trust in a biotechnologist to finish a PhD in heterogeneous catalysis. Your enthusiasm about carbide catalysis is contagious and motivated me through the last 4 years. What I value most is your open attitude, your optimism and your ability to see the bigger picture. Your door was always open, when I was asking 'Do you have 2 min?', although you would know that it would actually take at least 10 min. Thank you also for giving me the opportunity to present my work at multiple (inter)national conferences. I enjoyed our times in Spain, Brazil and New York.

Tomas, you have introduced me to the world of heterogenous catalysis as a master student and I am very glad you did so. Your knowledge in catalysis and your technical skills are truly impressive. You have guided me through this PhD and many of your great ideas have been applied in my thesis. I enjoyed working with you and I am very proud that we were able to build the continuous flow reactor. Thank you for your engagement in my research, your inspiration and your support!

Thanks again to my two favourite 'Knakkers', it was a pleasure to work with you! 😉

The trips to the synchrotron in Brazil have been exciting and a great experience. Thank you, **Cristiane** and **Dean**, for your help and involvement in my research to gather as many results as possible in a short time. These results would not have been analyzed without the help of **Moniek** and **Edwin**. Moniek, thank you for your patience in guiding me through the XANES/EXAFS calculations. Edwin, I truly appreciate your help, our fruitful discussions about carbides and above all, your dry sense of humour. Working with you has not only been productive, but also fun.

Thank also to my (other) co-authors, **Petra, Johan, Emil** and **Tiny** who helped me out with essential measurements/analyses. Your scientific input led to this success.

In addition, I would like to thank the BCT staff. **Danielle**, thank you for all the help with all the organizational and administrative tasks! I appreciate very much your help and patience with our PhD trip. Great thanks to **Susan**, who always helped me with GC and other lab issues. Your magic hands have simplified many things for me. Thank you also for the organization of many events and your participation and support in the Veluweloop! Thanks, **Nadine** for making sure that the chemicals were available, and that the lab was well-organized. **Elinor**, thank you for often initiating the coffee, tea, lemonade or lunch breaks at BCT. Our (scientific) conversions are unforgettable for me. I also want to thank you for your guidance in supervising students and teaching the biobased refinery practicals. **Costas** and **Akbar**, thank you for the nice conversions and for joining the PhD trip to France. It was great to have you both with us. Thank you, **Guanna**, for your kindness and interest in carbide catalysis and your (and Raghavendra's) patience to explain me the basics of DFT calculations.

My dear office mates, **Eleni & Ivo**! I must admit I liked our 'hidden' office a lot, although the heating did not work properly - your kindness helped making it bearable. Eleni, thank you for the good time in our igloo. It was always a pleasure to sit next to you, talk about graph design, sample colors or shoes we would like to buy and to grape a 'good' coffee. I am looking forward to the next concert with you! Ivo, I very much appreciated our nice talks and discussions. Sharing the pleasure of catalysts, carbon supports and TEM imaging with my office mate is definitely something I already miss. I also miss our snack breaks, although I must admit, that I prefer the cinnamon roll and Oreo cookies above celery…

I owe my colleagues at BCT a big thank you who all contributed in one way or another to this thesis. **Matthijs**, I enjoyed our discussions about science and other topics. I am looking very much towards our next visit and to see and taste your growing wine and beer brewery. **Torin, Raghavendra** and **Dmit**ry, it was a pleasure to work with you and to organize the PhD trip with you, guys. I like to think back to Lyon: a glass of Côtes du Rhône in a Bouchon restaurant and smiling into the happy faces of **Freek** and **Roel** (thank you too!). Or the lovely train and bus trips to Université Paris-Saclay –unforgettable. Thanks, **Maggi, Mingming, Yufan** and **Chenqiang**, to guide us to this super delicious restaurant in Paris. Many thanks also to the great Oleosome group, **Umay, Lorenz** and **Ma**! I had a great time at BCT. Thank you for all the nice moments!

I also want to thank all my former colleagues: **Nazila**, many thanks for your help in the lab and our various valuable discussions on (Pt or carbide) catalysis. These led me to many great ideas, which are now implemented in this thesis and our papers. Thank you also for supporting me during my trip to the synchrotron! **Laura** and **Simha**, thank you for the nice talks and support at work, the great dinners, the BCT PhD party and the drinks at the Zaaier! **Thiago**, it was great to

have a carbide soulmate with whom I could discuss the carbide catalysts in every detail. It was also a pleasure to visit **Luana** in Delft together with you- a memorable evening. **Roxani, Tim, Frits and Gerben**, thanks for the fruitful discussions and help with e.g. chemisorption or the autoclave. **Tim**, thank you for getting fries at our Friday's lunch – I appreciated it.

This research was not possible without the help of my BSc and MSc students: **Koen, Merijn, Ruben, Sumeyye, Norwin, Krishna, Jos and Kai-Ching**. You all have contributed to this research. All the hard work, great results and new insights we got from your work have been taken into account in my thesis. Many thanks for that! It was a great pleasure working with such enthusiastic students as you all were. I was/am lucky and proud of you.

Fortunately, I was surrounded by amazing friends during the last years. Starting off with **Rebecca**: you are a wonderful friend. I liked our coffee/tea breaks at Axis X, the runs on Wednesdays after our exhausting VALG meetings, the vacation to Montpellier and of cause our game nights. Thank you for the great support you have been! **Bas** and **Pascal**, I am glad that we have become friends. We spent quite some time together hiking, running, playing games, etc. Thank you for these nice distractions. **Margo** and **Katharina**, thank you both for the effective and nice writing weeks! Thanks also to the **Wageningen Réunions** (Mirka, Sophie, Lara, Ute & Marian)! Our weekends together in any German city have always been a nice distraction. **Lei**, dank je wel voor alle leuke activiteiten die wij de afgelopen jaren hebben ondernomen. Het is heel fijn om zo een vrienden als jou te hebben, die zo goed kan luisteren en ondersteunen maar waar ik ook veel me kan lachen en feesten. **Irene** (en Henk-Jan), bedankt voor jullie gastvrijheid op jullie mooie boerderij tijdens mijn vele bezoeken in Groningen. Ook op musical vlakte had ik altijd genoeg afleiding; dank aan de **'Harde Kern'** en **'Malac Banda'** voor de leuke repetities en optredens maar vooral voor de ontzettend gezellige en grappige momenten samen. In het eerste jaar van mijn PhD woonde ik nog op **Huyze Goudheerlijk** in de Taarthorst, en het was een fijn en gezellig huisje. Dank jullie wel voor jullie support.

Auch bei meinen lieben Freunden aus Deutschland möchte ich mich bedanken. Unsere **David Gerät** Gruppe ist und bleibt doch eine ganz besondere Freundschaft. Insbesondere möchte ich mich bei **Leonie** und **Miri** für eure Unterstützung bedanken, eure Besuche und eure Anrufe. Ich bin unglaublich dankbar für unsere langjährige und innige Freundschaft. **Patricia, Harald, Martina, Hung, Gitta und Betty,** ihr kennt mich jetzt schon ziemlich lang und ich finde es echt wahnsinnig lieb, dass ihr mich so unterstützt und euch so für mich interessiert. Ich freue mich sehr, dass ihr bei der PhD-Verteidigung und Feier dabei seid! Danke auch an **Leonie und Dominik** für das cover! A book is first judged by its cover!

I gratefully acknowledge my two paranimfen. Dear **Cynthia**, since the VLAG week I realized that I have won a very special friend. I love to talk to you, I very much appreciate your opinion and your honest friendship. You always took time for me and motivated me at times I was getting frustrated. Our various activities, e.g. dinners, concerts and hikes, deepened our friendship and mutual confidence. Thank you for everything! **Sanne**, my dearest (ex)-housemate! It was truly a pleasure for me to live with such a lovely person as you are. As well as a friend you were a huge support during my PhD. Almost every day we would exchange our daily experiences at our cozy bar, what did go wrong or well. I very much appreciated these moments as you were always able to encourage me due to you big hard and great optimism. Our sportive exercises, movie nights and shopping tours were a nice way for me to reset my brain. Thank you for your companionship!

I would also like to thank my family. **Wolfgang und Anja**, lieben Dank für eure Unterstützung und die tollen Skiurlaube, wo ich mich immer gerne anschließe. Auch lieben Dank an meine liebe **Omi**, die mich mit ihrer Liebe und ihrem wahnsinnigen Stolz auf ihre Enkel immer unterstützte. Ook mijn Nederlandse familie (vooral aan **Lida, Ada** en **Nell**) wil ik graag bedanken voor de steun en liefde van de afgelopen jaren (en mijn hele leven). Thanks also to my dearest brother, **Maxim,** for the all the support and the prove reading! Also for all the great, funny moments we have when spending time together. I missed you here the last year in Wageningen, but I am very happy that you are willing to come all the way from Madagascar to join my defense. A special thanks goes out to my **parents**. I am very lucky to have such lovely parent who always are there for me. Mama, Papa, thank you for all the support and love I got from you!

About the author

Marlene Führer was born in August 1993 in Frankfurt a. M., Germany. She finished high school in 2013 at the Albert-Einstein-Gymnasium, Schwalbach am Taunus after which she moved to Wageningen to study Biotechnology at the Wageningen University. During her BSc studies, she attended one semester, as an Erasmus exchange student, at Lund University after which she conducted her BSc thesis at the Organic Chemistry group of Wageningen University. She obtained her Bachelor of Science degree in 2016. She then continued her studies in Biotechnology at Wageningen University and obtained her Master title in 2018. As part of her Master program, she performed an internship in the Green Chemistry group of Prof. James Clark at the University of York, United Kingdom. Her master thesis research was performed in the Biobased Chemistry and Technology group at Wageningen University. The title of her master thesis was "Carbohydrate Oxidation by Platinum on Activated Carbon: Altering the Catalytic Performance by Changing the Surface Chemistry of the Support". The research was performed under the supervision of dr.ir. Tomas van Haasterecht and prof.dr. Harry Bitter. Under the same supervision and in the same research group, she started her PhD research on "Transition Metal Carbides for Biomass Upgrading" in 2018. The most important results of this work are presented in this dissertation.

In January 2023 she will start her first job as Project Leader at Avantium in Amsterdam.

List of Publications

This thesis

Führer, M., van Haasterecht, T., & Bitter, J. H. (2020). Molybdenum and tungsten carbides can shine too. Catalysis Science & Technology, 10(18), 6089-6097.

Führer, M., van Haasterecht, T., & Bitter, H. (2022). Cinnamaldehyde hydrogenation over carbon supported molybdenum and tungsten carbide catalysts. Chemical Communications, 58(98), 13608-13611.

Führer, M., van Haasterecht, T., E.J.J. de Boed, P. E. de Jongh & Bitter, J. H. (2022). Synthesis and Characterization of Supported Mixed MoW Carbide Catalysts. The Journal of Physical Chemistry C *(accepted)*

Führer, M., van Haasterecht, T., & Bitter, J. H. (2023). Catalytic performance of carbon-supported mixed MoW carbides for the deoxygenation of stearic acid. Catalysis Today, 418, 114108

Führer, M., Fan, KC., van Haasterecht, T., & Bitter, J. H. (2022). Particle size effect on the stability of carbon nanofiber supported Mo carbide catalysts in the hydrogenation of cinnamaldehyde. *(Manuscript in preparation)*

Other publications

Führer, M., van Haasterecht, T., Masoud, N., Barrett, D. H., Verhoeven, T., Hensen, E., Tromp, M., Rodella, C. B. & Bitter, H. (2022). The Synergetic Effect of Support-oxygen Groups and Pt Particle Size in the Oxidation of α-D-glucose: A Proximity Effect in Adsorption. ChemCatChem, 14(19), e202200493.

Masoud, N., Clement, V., van Haasterecht, T., **Führer, M**., Hofmann, J. P., & Bitter, J. H. (2022). Shedding Light on Solid Sorbents: Evaluation of Supported Potassium Carbonate Particle Size and Its Effect on CO2 Capture from Air. Industrial & Engineering Chemistry Research, 61(38), 14211-14221.

Overview of completed training activities

Conferences, Symposia and discipline courses

NIOK	Schiermonnikoog, The Netherlands	2018
NCCC Conference[1]	Noordwijkerhout, The Netherlands	2019
CHAIN Conference[2]	Veldhoven, The Netherlands	2019
NCCC Conference[2]	Noordwijkerhout, The Netherlands	2020
ICEC2020 Conference[2]	Online	2020
TEM/SEM operation course	Wageningen, The Netherlands	2018-2019
NCCC Conference[2]	Online	2021
NCCC Conference[2]	Noordwijkerhout, The Netherlands	2022
NAM27[2]	New York, The United States	2022
CarboCat Conference[2]	Zaragoza, Spain	2022
CHAIN Conference[1]	Veldhoven, The Netherlands	2022

General courses

Teaching and supervising Thesis students	Wageningen, The Netherlands	2019
Scientific Publishing	Wageningen, The Netherlands	2019
Scientific Writing	Wageningen, The Netherlands	2019
Vlag Week	Baarlo, The Netherlands	2019
Presenting with impact	Wageningen, The Netherlands	2020
Scientific Artwork, Data visualization and Infographics with Adobe Illustrator	Wageningen, The Netherlands	2020
VLAG council coaching session	Wageningen, The Netherlands	2021
Career perspective (planning on taking)	Wageningen, The Netherlands	2021

Others

Preparation of research proposal	Wageningen, The Netherlands	2018
VLAG council	Wageningen, The Netherlands	2018-2021
Discussion meetings (Catalysis meeting, Group meeting, PhD meeting)	Wageningen, The Netherlands	2018-2022
Advanced Organic Chemistry	Wageningen, The Netherlands	2019
Organisation of the PhD study trip to France	Wageningen, The Netherlands	2019-2021
PhD study trip	Lyon & Paris, France	2022

[1]Poster presentation [2]Oral presentation

The research described in this thesis was financially supported by Dutch Research Council (NWO, 729.004.022) and São Paulo Research Foundation (FAPESP, 2017/50261-1).

Financial support from Wageningen University for printing this thesis is gratefully acknowledged.

Cover design by Leonie Specht and Dominik Keller

Printed by Proefschriftmaken